THUNDERSTORM LIGHTNING AND RADAR CHARACTERISTICS: INSIGHTS ON ELECTRIFICATION AND SEVERE WEATHER FORECASTING

A Dissertation

by

SCOTT MICHAEL STEIGER

Submitted to the Office of Graduate Studies of
Texas A&M University
in partial fulfillment of the requirements for the degree of

DOCTOR OF PHILOSOPHY

December 2005

Major Subject: Atmospheric Sciences

THUNDERSTORM LIGHTNING AND RADAR CHARACTERISTICS: INSIGHTS ON ELECTRIFICATION AND SEVERE WEATHER FORECASTING

A Dissertation

by

SCOTT MICHAEL STEIGER

Submitted to the Office of Graduate Studies of
Texas A&M University
in partial fulfillment of the requirements for the degree of

DOCTOR OF PHILOSOPHY

Approved by:

Chair of Committee,	Richard E. Orville
Committee Members,	Larry D. Carey
	John Nielsen-Gammon
	Fuqing Zhang
	George Kattawar
	Donald R. MacGorman
Head of Department,	Richard E. Orville

December 2005

Major Subject: Atmospheric Sciences

ABSTRACT

Thunderstorm Lightning and Radar Characteristics: Insights on Electrification and Severe Weather Forecasting. (December 2005)

Scott Michael Steiger, B.S., State University of New York at Oswego;

M.S., Texas A&M University

Chair of Advisory Committee: Dr. Richard E. Orville

Total lightning mapping, along with radar and NLDN cloud-to-ground lightning data, can be used to diagnose the severity of a storm. Analysis of the 13 October 2001 supercell event (Dallas-Fort Worth, Texas), some supercells of which were tornadic, shows that LDAR II lightning source heights (quartile, median, and 95th percentile heights) increased as the storms intensified. Most of the total lightning occurred where reflectivity cores extended upwards and within regions of reflectivity gradient rather than in reflectivity cores. A total lightning hole was associated with an intense, non-tornadic supercell on 6 April 2003. This feature was nonexistent from all supercells analyzed during the 13 October case.

During tornadogenesis, the radar and LDAR II data indicated updraft weakening. The height of the 30 dBZ radar top began to descend approximately 10 minutes (2 volume scans) before tornado touchdown in one storm. Total lightning and CG flash rates decreased by up to a factor of 5 to a minimum during an F2 tornado touchdown associated with this storm. LDAR II source heights all showed descent by 2-4 km

during a 25 minute period prior to and during this tornado touchdown. This drastic trend of decreasing source heights was observed in two tornadic storms prior to and during tornado touchdown, but did not occur in non-tornadic supercells, suggesting that these parameters can be useful to forecasters. These observations agree with tornadogenesis theory that an updraft weakens and the mesocyclone can become divided (composed of both updraft and downdraft) when a storm becomes tornadic.

LDAR II source density contours were comma-shaped in association with severe wind events within mesoscale convective systems (MCSs) on 13 October 2001 and 27 May 2002. This signature is similar to the radar reflectivity bow echo. Consistent relationships between severe weather, radar and lightning storm characteristics (i.e., lightning heights) were not found for cells within MCSs as was the case for supercells. Cell interactions within MCSs are believed to weaken these relationships as reflectivity and lightning from nearby storms contaminate the cells of interest. It is also more difficult to clearly define a cell within an MCS.

DEDICATION

To Mom, Dad, and Christine…

To Olivia Rose and Macy Alexander…

To all my family and friends…

To Stephanie, my love and my life! Thank you!

"Remember, George: no man is a failure who has friends."

ACKNOWLEDGMENTS

While I was in the middle of working on my master's thesis I made a decision not to continue on for the Ph.D. However, after I completed it I thought what the heck, that wasn't so bad, let's keep going! I owe Dr. Orville a lot of gratitude for offering me the chance to do more research with him. I couldn't have asked anything more from him in being my mentor: he truly helped me become an independent thinker. He loosened the chains and let me develop a research plan on my own. I really appreciate that now as I prepare to be a professor! Speaking of my career choice, I thank him so much for supporting my move to SUNY Oswego, my Alma Mater, to teach while still working on my dissertation. He knew this offer was a dream come true for me, and he continued to mentor me from afar – answering my questions via e-mail and phone, sending me to conferences, and allowing me to conduct research at Texas A&M during the summers. Thank you so much Dr. Orville!

I wrote this dissertation, but several of the ideas presented here began within the minds of my committee members: Dr. Carey, Dr. Nielsen-Gammon, Dr. MacGorman, Dr. Zhang, and Dr. Kattawar. Your advice helped to make this project so much more fruitful and I greatly appreciate all the hours you spent writing corrections and meeting with me (and contending with all my e-mails!)!

The meteorology faculty at SUNY Oswego has been so supportive of my dual role as graduate student and instructor. Dr. Stamm: thank you for giving me the opportunity to come back and for looking out for me so that I would have at least a few

hours a day to work on my dissertation. Dr. Ballentine: you have been a great role model to me, both when I was your student and now as your colleague and friend. Dr. Skubis: you are such an awesome teacher – someone for me to aspire to become like!

Of course I couldn't have gotten this far without my family and friends – ya'll are truly the best! One friend, Brandon Ely, deserves special recognition. Brandon and I met several years ago at SUNY Oswego. He is such a supportive person – Brandon is the type of person who truly cares about others, often stopping whatever he is in the middle of doing to help someone else. I am proud to be his colleague and his friend. Thanks, Brandon!

Stephanie – WOW! You are truly a wonderful person! You have been in my corner rooting for me from day one! Thank you for all the things you have done for me! Finally you get to know me without the dissertation on my mind. You are so patient, so kind, and so beautiful!

TABLE OF CONTENTS

Page

INTRODUCTION

Lightning can be used with radar observations to characterize thunderstorms and to warn people of imminent severe weather. Combined, these two data sets form a strong foundation for the short term forecasting of convective weather. Also, relationships between radar and lightning characteristics give insight into how a thunderstorm's dynamics and electrification processes operate. The advent of the WSR-88D nationwide (U. S.) radar system, the National Lightning Detection Network (NLDN), and 3-dimensional lightning mapping systems (here the Lightning Detection and Ranging Dallas-Fort Worth (LDAR II) network is used) allows scientists to dissect thunderstorms and explore relationships between observables.

Electrical characteristics of storms, both severe and non-severe, have been documented over the past couple of decades (MacGorman and Rust 1998 give a thorough review on pp. 192-286), and have been related to the storm's radar characteristics. The studies mentioned by MacGorman and Rust used such tools as the NLDN, lightning mapping techniques, WSR-88D and research radars (some polarimetric). Using the same three types of observations (NLDN cloud-to-ground (CG), total (intracloud (IC) and CG) lightning mapper LDAR II, and DFW WSR-88D radar data), the spatial and temporal development of the three major convective storm modes observed in the U. S. plains states will be examined: isolated non-severe thunderstorms, mesoscale convective systems (MCSs), and supercell thunderstorms.

This dissertation follows the style of *Monthly Weather Review*.

Total (intracloud (IC) and cloud-to-ground (CG)) lightning data are more informative than CG data alone because the first lightning discharge in a thunderstorm is typically IC and a high percentage (typically well over 50%) of flashes in a storm are IC. Hence, having both LDAR II and NLDN data give a comprehensive overview of a thunderstorm's electrical activity. A key characteristic used in this study is the height of lightning activity and this has been related to storm evolution and intensity. MacGorman et al. (1981) show that lightning activity tends to concentrate in layers, often in a bimodal height distribution. An experiment conducted by Williams et al. (1985) shows that discharge propagation occurs in regions of maximum space charge density (lightning "seeks out" regions of charge). The above two results suggest that total lightning detection by such instruments as the LDAR II can map out the main charge regions in a thunderstorm. It will be shown that the altitude of these inferred charge regions is controlled by a thunderstorm's main updraft.

TOTAL LIGHTNING SIGNATURES OF SUPERCELL THUNDERSTORM INTENSITY

1. Introduction

The most comprehensive work detailing the electrical structure of isolated storms and mesoscale convective systems (MCSs) is discussed by Stolzenburg et al. (1998a, b, c), and reveals a more complex charge structure than the classic tripole (see Fig. 3.2, MacGorman and Rust 1998). Within convective updrafts, the basic charge structure has four charge regions, alternating in polarity, and the lowest is positive. The main negative and positive charge regions are within the middle-upper levels, with weaker charge regions near the base and top of the thunderstorms. Outside updrafts there are typically at least six charge regions, alternating in polarity, with the lowest again being positive. Among the three storm types examined (MCS, supercell, and isolated New Mexican convection), there are differences in the heights and temperatures at which the four charge regions are found in updrafts. The charge regions are higher in altitude when the balloon ascent rate (a proxy for updraft strength) is greater. Hence, charge regions detected by VHF networks like LDAR II (Rison et al. 1999, Coleman et al. 2000, Bruning et al. 2002, Detwiler et al. 2002, and Wiens et al. 2002) are expected to ascend when a thunderstorm's updraft intensifies.

Supercells are prolific lightning producers, and some studies suggest they may have unique lightning characteristics that may help predict the severe weather that can accompany them. MacGorman et al. (1989) found that the ground stroke rate and flash multiplicity (number of strokes per flash) increased after the tornadic stage of a storm

ended. The ground flash rate was negatively correlated with cyclonic shear. However, there was a strong correlation between intracloud (IC) flash rate and cyclonic shear at 1.5 km altitude. To explain this, MacGorman et al. propose the elevated charge region hypothesis: As a storm's updraft intensifies, the main negative charge region is lifted and brought closer to the main positive charge region typically located higher in the storm, and IC flashes become more frequent and cloud-to-ground (CG) flash rates decrease; when the updraft weakens, CG flash rates increase as the lower negative charge region descends. Charge regions have been shown to become elevated in a simulated supercell updraft (Ziegler et al. 2003). MacGorman and Nielsen (1991) showed the opposite relationship for CG flash rates in the "Edmond storm:" as low-level cyclonic shear initially increased, negative CG lightning flash rates also increased. It is clear that robust relationships between storm dynamics, severe weather, and lightning activity (especially CG) have not been found. The major purpose of this study is to better understand how we can use total lightning information in determining storm intensity and to observe if storm cell lightning characteristics can be used to predict severe weather at the ground. Comparisons between charge region heights (revealed by lightning mapping), IC and CG flash rates, IC:CG ratios, and radar characteristics are made to test the hypothesis that lightning characteristics are directly related to storm strength.

Lightning "jumps" (total flash rate increasing rapidly; Williams et al. 1999) and "holes" (areas of weak lightning density values surrounded by an annulus of larger values; Krehbiel et al. 2000) have been noted in severe thunderstorms. Preliminary

results from the north Alabama LMA network (McCaul et al. 2002) show lightning jumps prior to tornadogenesis, and lightning holes co-located with a bounded weak echo region in the updraft in tornadic storms, while being absent in nontornadic supercells. A tornadic storm analyzed by Wiens et al. (2003) had total lightning rates approaching 300 flashes per minute (only IC for the first 2 hours of the storm). Mathematical analysis by Baker et al. (1995) shows that total flash rate ~ w^6, where w is storm updraft speed. Hence, lightning jumps can be proxies for increases in updraft strength.

Cloud-to-ground lightning polarity also has been examined as a forecaster's tool in predicting severe weather in supercells. Reap and MacGorman (1989) show that tornadoes and large hail are more probable in storms having a high density of positive ground flashes. Branick and Doswell (1992) have suggested that whether or not a storm may have a high percentage of positive CG lightning may depend on storm type (low-precipitation (LP) versus high-precipitation (HP) supercells), which is ultimately controlled by the regional environment (i.e., a difference in tropospheric moisture content). On 13 March 1990, tornadic storms from northern Oklahoma northward into Kansas and Nebraska produced an unusually high percentage of positive CG flashes, whereas those in central and southern Oklahoma produced mainly negative flashes. 63% of warm season (April-September) severe storm reports (large hail and tornado) are associated with predominantly negative CG lightning producing storms (> 90% -CG) in the southern plains of the U. S., while only 11% of the reports are associated with predominantly positive storms (> 50% +CG) (Carey et al. 2003b). In contrast, severe storms in the northern plains are better characterized by positive CG lightning (43%

storm reports predominantly positive and only 28% predominantly negative). Carey and Rutledge (2003) show that for severe storms near Dallas-Ft. Worth (DFW), only 10% of the CG lightning they produce is positive as opposed to 40-50% for northern plains severe storms. Carey et al. (2003b) attribute this geographical distinction to storms moving through high-θ_e gradients in the U. S. northern plains, which accelerate updrafts resulting in higher values of supercooled liquid water content aloft and positive charging of precipitation particles (Saunders 1993). Since this study is focused on the DFW area (southern plains), it is expected that the relationships between positive CG lightning and severe weather will be rare. Indeed, Carey and Rutledge (2003) show differences in CG characteristics between severe and non-severe storms are less clear in southern plains compared to northern plains storms (i.e., the difference in mean %+CG lightning values between severe and non-severe is < 5% near DFW and > 30% in northern Nebraska using their figs. 6 and 7).

The evolution of CG lightning in relation to significant tornadoes is well-documented by Seimon (1993) and Perez et al. (1997). The Plainfield F5 tornado in 1990 had 91% +CG lightning during development, CG flash rate reduction coinciding with mesocyclone development (in agreement with the elevated charge region hypothesis of MacGorman et al. 1989), a reversal from dominant positive (well over 50%) to dominant negative CG lightning at the time of tornado touchdown, and weakening +CG currents before the polarity reversal and strengthening –CG currents after (Fig. 7, Seimon 1993). The change in the dominant polarity of ground flashes in this storm corresponds with changes in the occurrence of large hail and a transition from

classic to HP supercell characteristics (MacGorman and Burgess 1994). In contrast, positive CG lightning flash rate and percentage of CG lightning being positive in the Spencer supercell of 30 May 1998 began to increase dramatically during tornadogenesis and continued to rise while the storm was wreaking F4 damage (Carey et al. 2003a). Perez et al. (1997) show that out of 42 F4/F5 tornadoes, 31 (74%) have a peak CG rate preceding tornado formation (an average of 17 minutes before touchdown), 6 (14%) have polarity reversals from positive to negative, and 20 (48%) storms show a decrease in CG activity coincident with tornado touchdown. Relations between CG flash rates, polarity, and tornado development vary widely (Bluestein and MacGorman 1998). In terms of radar characteristics examined by MacGorman and Burgess (1994), both the vertically-integrated liquid (VIL) water and storm height peaked during domination by positive ground flashes in one storm. The same regional effects on ground flash polarity discussed by Branick and Doswell (1992) are found in their study. In general, storms dominated by positive ground flashes frequently produce tornadoes or large hail, but tornadoes and large hail also can occur in storms dominated by negative ground flashes. Hence, the probability of detection (POD) using CG polarity to predict severe weather is expected to be small.

In comparing lightning in a supercell to a multicell storm, Ray et al. (1987) show the following: 1) lightning tends to be downshear of the main updraft (with weak echo region) and reflectivity core in the supercell while in the multicell storm it is concentrated in the updraft and reflectivity core, and 2) the distribution of lightning with height is unimodal with a peak at approximately 8 km (-30°C environmental

temperature) in the supercell while for the multicell it is bimodal, with peaks at 6 and 11 km (-10°C and -40°C, respectively). From their observations, Ray et al. conclude that the magnitudes and vertical shear of the environmental wind are key parameters in lightning location (as shown by the distribution of VHF impulses) relative to severe storm structure. The lightning data from the LDAR II overlaid on radar reflectivity data for the supercell storms in this study will be shown to test the conclusions regarding the spatial patterns discussed by Ray et al.

A mesoscale convective system (MCS) moved through the Dallas-Fort Worth, TX area late on 12 October to early 13 October 2001. Embedded in this system were several supercells, a few of which were severe, producing strong F2 tornadoes and large hail. Intense, isolated supercells (non-tornadic, but with large hail) occurred near Dallas on 6 April 2003. These events provide an excellent opportunity to compare severe storm reports, radar and lightning data from the NLDN and LDAR II to test the hypothesis that there are spatial/temporal signatures in the lightning data that are related to storm intensity and can assist in predicting severe weather.

2. Data and methodology

The radar data used in this study were from the Dallas-Fort Worth WSR-88D (KFWS), obtained from the National Climatic Data Center (NCDC). To analyze the collected data initially, the WDSS-II (Warning Decision Support System-Integrated Information) software (Hondl 2003) provided by the National Severe Storms Laboratory (NSSL) was used. This software has algorithms that identify, track (Storm Cell Identification and Tracking (SCIT) algorithm, Johnson et al. 1998), and quantitatively

describe the state of storm cells (Hail Detection Algorithm (HDA), Witt et al. 1998, and Mesocyclone Detection Algorithm (MDA), Stumpf et al. 1998). The Dallas-Fort Worth (FWD) sounding was used to obtain temperature level data to import into the HDA. Storm cells, and hence lightning data, were analyzed only within a range of 30 to 100 km from the KFWS radar site due to the cone of silence and beam elevation effects (lowest tilt beam is above the melting level at far ranges, and this causes systematic error in the HDA), and the poor resolution and detection efficiency of the LDAR II instrument beyond 150 km from the network center (see Fig. 1). Note that the radar is approximately 45 km to the southwest of the LDAR II network center. Radar data were also converted from a polar to a Cartesian grid space using the REORDER software (Oye and Case 1995). The horizontal and vertical grid spacings were set at 1.0 and 0.5 km, respectively. In this way, lightning (LDAR II source points, CG flash locations) were overlaid on radar reflectivity values for comparisons between the two data sets.

Cummins et al. (2000) describe three lightning detection technologies and location methods that employ networks of radiation-field sensors. The technologies are segregated by frequency ranges of operation: very low frequency (VLF), low frequency (LF), and very high frequency (VHF). Each has its own advantages. Breakdown and ionization processes (leaders and streamers) emit strongly in the VHF, while high currents which occur in previously ionized channels (CG return strokes) have their most powerful emissions in the LF and VLF ranges. Hence, CG lightning detection utilizes the lower frequency ranges while IC mapping uses the VHF band.

The cloud-to-ground (CG) lightning data used in this study were from the National Lightning Detection Network (NLDN). These data were obtained from Vaisala, Inc., Tucson, AZ. The network consists of 106 sensors across the U. S. (Orville and Huffines 1999). The NLDN was given an upgrade in 1994 (Cummins et al. 1998). This upgrade included a combination of improved accuracy from combined technology (IMPACT) and time-of-arrival (TOA) sensors. The upgrade resulted in improving the median location accuracy to 500 m and the expected flash detection efficiency to ~85% for events with peak currents above 5 kA. The NLDN underwent another upgrade in 2002-3 (during the study period) so Cummins et al. documents the NLDN "as it existed in 2001" (Murphy 2005, personal communication). The CG lightning characteristics that were analyzed from these data include: negative and positive flash density, percent positive flashes, median peak current for both polarity flashes, and mean multiplicity for each polarity.

Total lightning flash data over the Dallas-Fort Worth area were from the VHF lightning mapping instrumentation known as the Lightning Detection and Ranging (LDAR II) network operated and maintained by Vaisala, Inc (it is assumed the instrument detects both IC and portions of CG flashes, hence *total* flashes were detected). Because VHF impulses are of short duration and have line-of-sight propagation, they are shown as point sources located in three dimensions (thousands of which can comprise a single flash). The LDAR II uses the time-of-arrival (TOA) technique described by Rakov and Uman (2003, pp. 562-565). This network is composed of 7 sensors with 20 to 30 km baselines centered on the Dallas-Fort Worth

International Airport (Fig. 1). The regional LDAR II network accurately maps lightning flashes in 3-dimensions within approximately 150 km of the center of the network, degrading in performance with increasing range (Demetriades et al. 2001, Carey et al. 2005). The expected lightning *flash* detection efficiency is typically greater than 95% within 30 km (the interior of the network) from the DFW Airport, and greater than 90% out to a range of 100 km (see Fig. 2). Significantly less detection efficiencies were estimated at these ranges for 6 April 2003 (only 6 sensors were operable as shown in Fig. 3). The contours were off-center (more rapid decrease in DE to the southwest) in figure 3 because the two northeastern sensors were weakest in gain and threshold (Murphy 2005, personal communication). Expected 3-dimensional location accuracy for individual pulses of radiation is between 100 and 200 m within the interior of the network and better than 2 km to a range of 150 km (Carey et al. 2005). LDAR II VHF sources were grouped into flashes according to temporal and spatial restrictions using an IDL (Interactive Data Language) program provided by Dr. Gary Huffines. It is a modified version of an algorithm created by NASA. The constraints used to determine if a source point was part of a flash were: a maximum of 3 s for the duration of the flash, maximum time lag of 0.5 s between points in a flash, maximum time delay of 0.03 s between points in a flash branch, and adjacent points must be within 5 km of each other to be considered part of the same flash (see Appendix A for details and sensitivity tests on this algorithm).

There are a few drawbacks to using a system like the LDAR II for lightning detection. Its limited useful range is one of them, owing to VHF signal attenuation, loss

of below-horizon VHF sources (due to line-of-sight propagation), and increasing location errors at far ground ranges (Boccippio et al. 2000). Comparatively few sources are observed from CG processes because of how IC and CG channels radiate differently (CG strokes radiate as long antennas/lower frequency than the short breakdown processes associated with IC flashes; Cummins et al. 2000). The total source density is thus dominated by the in-cloud portion of total lightning flashes. VHF TOA lightning detection systems like LDAR II detect more sources from lightning traveling through positive charge regions than negative charge regions because negative polarity breakdown into positive charge regions is noisier (because more intermittent pulses) at radio frequencies (RF) than positive breakdown into negative charge regions (Rison et al. 1999).

To compare the lightning and radar characteristics of storm cells, lightning data (CG and total) within 5, 10, and 20 km horizontal distance of the radar-defined cell or mesocyclone (cell/mesocyclone locations given by WDSS-II) was analyzed for each radar volume scan (interval approximately 5 minutes). The 10 km results mostly will be shown as most lightning from the storms of interest were contained within this distance without contamination from nearby storms. This resulted in cylindrical volumes of total lightning data from LDAR II. The radar and lightning characteristics analyzed included: storm cell maximum reflectivity, maximum reflectivity height, radar top (maximum height of the 30 dBZ contour), severe hail index (SHI), vertically integrated liquid (VIL), low-level mesocyclone diameter, mesocyclone strength index (MSI), lower quartile, median, 95^{th} percentile (defined as the lightning-based storm top), and peak

height of LDAR II sources, number of modes (peaks) in the height distribution of sources, normalized peak value of sources, half-peak thickness of the main peak in sources, total number of sources within the cylindrical volume, number of flashes from sources (total flash rate), and the IC:CG ratio. To calculate the number of flashes from sources, the flash grouping algorithm was run using the selected sources (i.e., all sources detected within 10 km of a cell). This procedure can overestimate flash rates as two or more branches of a flash which initiated outside the radius can be separated as two flashes in this circular region. A more preferable method may be to calculate the flash origins using a larger domain (i.e., 60 x 60 km box centered on the cell) and then summing the number of origins within 10 km of the cell location. Sensitivity tests showed for one case (13 October tornadic) the flash rates were inflated using the first method compared to the second method, but trends were similar. An advantage to the method for calculating cell flash rates used here is that it requires less computer processing time. Refer to Johnson et al. (1998), Witt et al. (1998), and Stumpf et al. (1998) for how the storm cell radar characteristics were calculated. The VIL and SHI are determined by vertically integrating the reflectivity throughout the whole depth and above the melting level of the storm, respectively. The MSI is a measure of mesocyclone rotation; the algorithm vertically integrates rotation strength ranks from all levels sampled of the cell, which is then normalized by the depth of the mesocyclone.

To obtain a four-dimensional (x, y, z, and t) representation of a storm's radar and lightning structure the following projections of the data were produced on a single plot: time-height, x distance-height, y distance-height, and x-y distance (see Fig. 4). The x

and y distances represent the directions west-east and south-north, respectively in the plots. LDAR II source density was computed at 1 km resolution in all spatial dimensions, and the time-height panels were constructed using 5 s time resolution. Source data were plotted within a 60 x 60 x 20 km volume (most lightning was detected within 20 km of sea level) centered horizontally on the storm. Projections were taken onto the horizontal and vertical planes and plotted as two-dimensional source densities.

The radar reflectivity vertical and horizontal projections were constructed using a similar method, but the values shown are the mean reflectivity for each cuboid. The mean reflectivity values were conditional in that only points in the cuboids that had reflectivity values above 0 dBZ were used. For the horizontal projections only points above the melting level were used to calculate the mean reflectivity. This was done to test the idea that lightning production is highly dependent on the existence of hydrometeors above the melting level in a thunderstorm.

The total lightning (LDAR II) and radar reflectivity history following a storm cell will be shown in a time-height display (i.e., Fig. 19). For each radar volume scan, the mean reflectivity of a storm was calculated for each height at 0.5 km intervals. Only values within 20 km in horizontal distance of the storm cell location, determined from WDSS-II, were used to calculate the mean reflectivity at each height for each volume scan. Contours of the total number of LDAR II sources in each 1 km height interval within 20 km horizontal distance of the storm cell for each radar volume scan interval were overlaid on the radar data. A volume scan interval for this data was approximately 5 minutes.

3. Lightning and radar reflectivity overlays of supercell thunderstorms

a. Total lightning and radar reflectivity

1) 13 OCTOBER 2001

Figure 4 shows projections of the total lightning source density and mean reflectivity of a supercell on 13 October 2001. The LDAR II and WSR-88D data shown were from the time period 001537 to 002034 UTC (time convention hhmmss). The height of maximum lightning activity remained constant near 10 km MSL during the 5 minute period shown (see time-height panel). The plan view radar structure shows large reflectivity gradients, especially on the southwest side of the supercell, and the shape of the 55 dBZ contour (which encompasses the hail report) is suggestive of a hook, two classic signatures of a mature supercell. The reflectivity contours tilted downshear (00 UTC proximity sounding at FWD indicated southwesterly wind shear) in the west-east vertical projection. Reflectivity values greater than 40 dBZ extended higher than 10 km MSL (above the -40°C isotherm). Both vertical projections indicate reflectivity maxima (55 dBZ) aloft above the hail report. The hail report in the height-y projection was within a weak reflectivity echo region.

The greatest LDAR II source density values in all projections were within areas of reflectivity gradient. The areas of maximum lightning activity in the vertical projections were above where the reflectivity core extended upward at x, y position (-62, 55 km). The source density maximum in the plan view was 5 km to the east of the maximum 40 dBZ echo height (12 km MSL) located at (-64, 56) (Fig. 5), which infers the location of the strongest updraft, ideal for charge separation and lightning. The

peaks in the vertical distributions of lightning sources and flash origins were at 10 km and 11 km MSL, respectively. 3846 sources comprising 220 flashes were included in this plot (an average of 17 sources per flash).

Note the lack of lightning activity in the rear part of the storm (southwest side in Fig. 4). Note the absence of any activity just southwest of the hail report, where the mean reflectivity was over 55 dBZ! The majority of lightning activity occurred most likely between the main updraft and the forward flank downdraft of the supercell according to the above interpretations of figures 4 and 5 (see Lemon and Doswell (1979) for locations of vertical drafts in an ideal mature supercell).

This supercell produced a strong F2 tornado (NCDC 2001) between 010010 and 010507 UTC (Fig. 6). There was more lightning activity (more sources) at lower-levels (below 5 km MSL) than 40 minutes earlier (Fig. 4), indicating the storm possibly had weakened (weaker updrafts can lead to lower charge regions). This also could be a result from the storm being 30 km closer to the center of the LDAR II network (effect of less source attenuation closer to the network). However, the reflectivity structure of the supercell shows that it had weakened as well. The reflectivity did not extend upward as high as earlier; the 40 dBZ contour in the vertical projections extended only to about 7 km MSL as opposed to being above 10 km in figure 4. Another indication that this was a weaker storm than earlier was that the maximum mean reflectivity (plan view) in the cell was a small area of 50-55 dBZ, while figure 4 shows a larger area of greater than 55 dBZ.

The mean reflectivity tilted downshear once again, and the maximum LDAR II source density was above the reflectivity upward protrusion at x = -17 km in the x-height projection (Fig. 6). The peak number of sources was located at 10 km MSL (above the -40°C isotherm), and there were two peaks in the height histogram of flash origins: 4 km (near the melting level) and 10 km MSL. The vertical projections show the lower origin peak was associated with another storm in the southeastern portion of the plan view. There were 9159 sources that comprised 196 flashes in this plot (about 47 sources per flash).

The tornado's path was in the rear flank of the supercell (see plan view of Fig. 6). The tornado was reported to occur throughout this volume scan time interval, and there were no abrupt changes in the altitude of maximum lightning activity according to the time-height panel. A hook was apparent in the mean reflectivity (observe the 35 dBZ contour at (-25, 72)). The WDSS-II indicated mesocyclone was within the hook region, along with the tornado path. As in figure 4, notice that most of the lightning activity in the plan view occurred in areas of reflectivity gradient downshear of the storm.

2) 6 APRIL 2003

Three intense, isolated supercells moved through the Dallas-Ft. Worth region early on 6 April 2003. A supercell, which produced 5 cm diameter hail (SPC 2003), is shown in figure 7. As first documented by Murphy and Demetriades (2005) for this storm, the most striking feature in the plan view is that of a "lightning hole" (a source density minimum surrounded by greater source density values) located at (41, 51 km) 5 km to the northwest of the radar-indicated mesocyclone. This hole was a persistent

feature for at least an hour of the storm's lifetime (from 0330 to 0430 UTC 6 April). Source density values were over a factor of 5 less in the hole compared to the large density annulus surrounding it. An asymmetry was apparent: the largest source density values were in the southern half of the annulus. The mean reflectivity does not show the same pattern. An enhanced reflectivity contour (> 55 dBZ) had a sideways-S shape (also noted by Murphy and Demetriades). The lightning hole was near the western notch in this reflectivity pattern.

Maximum LDAR II source density values in figure 7 were located above where the reflectivity contours extended upwards as with the 13 October 2001 supercells (compare Figs. 4 and 7). Figure 8 shows that the maximum source density was collocated with the greatest 40 dBZ echo height (near the mesocyclone location at (46, 47 km)). The 8 and 10 km MSL 40 dBZ height contours have a similar shape as the largest source density contour. The source density contours sloped downward to the west and north of the storm in the vertical projections, following the reflectivity contours. The lightning layer was thickest near the center of the storm in the south-north vertical projection (at y = 47 km), gradually becoming thinner farther to the north. There was one peak in the vertical distribution of source density, located at 8 km MSL. The reflectivity field indicated a similar tilt to the storm's core in the downshear direction as shown for the 13 October 2001 supercells, revealing the effect of strong environmental vertical wind shear.

Figure 9 shows the same storm discussed above, but approximately 30 minutes before that shown in figure 7. The lightning hole was not as distinct; its diameter was

1.5 km compared to the 4 km diameter hole shown in figure 7. A weak source density region, analogous to the weak echo region (WER) in reflectivity data sometimes present in strong supercells (Weisman and Klemp 1986), is shown in the west-east vertical projection of figure 9. This feature was located in a region of enhanced reflectivity aloft (> 55 dBZ) at x, z = (17, 6 km). This location was consistent with that of the mesocyclone indicated in the plan view at (15, 46). The lightning hole was associated with a circular area of large mean reflectivity values (> 55 dBZ) in the plan view (note large source density was also located in > 55 dBZ region). The largest source densities were once again in the southern and eastern parts of the annulus surrounding the hole (asymmetric).

b. Total and CG lightning

1) 13 OCTOBER 2001

Several times during the 13 October 2001 supercell event, two centers of negative cloud-to-ground (CG) lightning activity were associated with a single supercell. Figure 10 shows the LDAR II source density and negative CG lightning distributions for the tornadic supercell discussed above, one radar volume scan prior to the storm shown in figure 6 (65 km from the LDAR II network center). 296 flashes, 40 of which were –CG flashes, are included in this plot. The maximum in total lightning source density (> 27 sources km^{-2} $(5\ minutes)^{-1}$) occurred 7 km north of the mesocyclone at this time. Two –CG flash density maxima (each had values > 0.18 flashes km^{-2} $(5\ minutes)^{-1}$) were located in the front (east) and rear (west) flanks of the storm. The maximum value at (-25, 81) (front flank) was well-associated with the source density maximum. The rear

flank –CG density maximum at (-35, 76) was in an area of significantly lower source density indicating that total lightning activity was not a good indicator of -CG lightning flashes. The two centers of –CG lightning activity were most distinct immediately prior to the tornado report associated with this storm at 0100 UTC.

Figure 11 shows two centers of –CG lightning activity (values > 0.22 flashes km^{-2} $(5\ minutes)^{-1}$) associated with a second tornadic supercell which occurred on 13 October 2001. The source density was significantly weaker than in figure 10 due to the storm being much farther away from the LDAR II network (119 km). Interestingly, the two –CG maxima feature was most distinct again prior to a tornado touchdown (at 0315 UTC).

This signature in –CG flash density was not related to the total lightning structure (LDAR II source density). Another occurrence of two centers of –CG lightning activity occurred with a different supercell (non-tornadic) on 13 October 2001 and exhibited two LDAR II source density maxima associated with each –CG flash density maximum. The vertical source structure had one peak in source density in all cases examined that showed this signature.

2) 6 APRIL 2003

Two distinct, strong –CG flash density maxima also occurred within supercells during several volume scans from the 6 April 2003 event. Negative CG flash density values exceeded 0.22 flashes km^{-2} $(5\ minutes)^{-1}$ to the west and northeast of a lightning hole in figure 12. Based on their positions relative to the mesocyclone and mean storm

reflectivity (not shown), these features were likely located within the rear and forward flank downdrafts of the supercell.

c. CG lightning and radar reflectivity

1) 13 OCTOBER 2001

Two storms with very different radar reflectivity and –CG flash density structure are shown in figure 13. The more intense storm with respect to reflectivity was located at (1, 98 km) and had a maximum –CG flash density of 0.08 flashes km^{-2} (5 minutes)$^{-1}$. A very weak (reflectivity) storm cell located at (27, 76), however, had very impressive values of –CG flash density (0.24 flashes km^{-2} (5 minutes)$^{-1}$). Its maximum reflectivity was 35-40 dBZ, and had very limited vertical extent when compared to the cell at (1, 98). The storm cell which produced relatively few –CG flashes had an elevated reflectivity core (see 50 dBZ contour in the x-height projection), while the greater –CG flash density storm had its maximum reflectivity at the ground. The weaker storm had a lower charge region as indicated by LDAR II source density (not shown) which contributed to enhancing the –CG rates with this storm (supporting the MacGorman et al. (1989) hypothesis).

An intense supercell producing high percent positive CG lightning is shown in figure 14. Mean reflectivity values greater than 40 dBZ extended above 12 km (well above the -40°C level). The enhanced areas of high percent positive CG lightning were located on the edges of the reflectivity structure of this supercell. The area of greater than 60% +CG lightning at (10, -94 km) was associated with the reflectivity-indicated storm anvil at 11 km MSL in the x-height projection (see 35 dBZ appendage above near

x = 10 km). The two other regions of elevated %+CG lightning at (-3, -84) and (-16, -94) were also associated with reflectivity-indicated anvils in the height-y and x-height projections, respectively. A less significant maximum of 30% +CG lightning was associated with higher reflectivity values near the mesocyclone where the +CG flash density (not shown) was 0.16 flashes km^{-2} $(5\ minutes)^{-1}$ (the +CG flash density values within the other %+CG anomalies were: 0.04 flashes km^{-2} at (10, -94) and (-16, -94) and 0.16 flashes km^{-2} at (-3, -84)). The distribution of +CG flash density (not shown) had a similar pattern as with the %+CG values shown in figure 14.

2) 6 APRIL 2003

A classic radar structure of an intense supercell, the bounded weak echo region (BWER; Weisman and Klemp 1986) was observed within the 6 April 2003 storm (position (27, 52 km) in Fig. 15). The mean reflectivity field in the south-north vertical projection shows a band of values greater than 55 dBZ originating at the ground at y = 56 km. The enhanced reflectivity extended upward and then curved southward above the mesocyclone located at y = 49 km. The 50 dBZ contour made a complete half-circle above this location. A BWER was also apparent in the west-east vertical projection with an area of weaker reflectivity (< 50 dBZ) bounded at 3 km MSL. This BWER was shallow and its reflectivity deficit (about 10 dBZ) small because these are vertical projections, not cross sections (as in Fig. 15.5c in Weisman and Klemp 1986), of mean reflectivity in the supercell. This storm cell had the most intense radar-derived characteristics as determined by the WDSS-II software (using the SCIT, HDA, and

MDA) with maximum reflectivity values greater than 70 dBZ and severe hail indices (SHI) approaching 1000. An intense updraft is required to produce these signatures.

Two –CG flash density maxima were associated with this supercell, as discussed for a different volume scan in subsection 3b2. The –CG density absolute maximum (> 0.22 flashes km^{-2} (5 $minutes)^{-1}$) was associated with the BWER and hence the main updraft as shown in both vertical projections.

4. Time series of radar and lightning characteristics during tornadic supercells

Several different "lightning heights" were computed to diagnose the intensity of the supercell. As was shown in figures 4-9, the areas of maximum total lightning activity were approximately above where reflectivity extended upward, representative of a strong updraft. The source density contours were also at relatively higher altitudes at these locations in the vertical projections. Comparing the vertical projections of figures 4 and 6 also shows the altitudes of the source density contours were higher in the more intense storm (Fig. 4). Hence, a plausible hypothesis is that lightning heights can be used to diagnose storm intensity. These were calculated by finding the 95^{th} percentile (lightning-based storm top), peak, median, and lower quartile height of all LDAR II sources located within 10 km of the radar-defined mesocyclone for each radar volume scan time interval. Figure 16 reaffirms that the tornadic storm discussed in subsection 3a reached its peak intensity (Ltop height 15 km, peak height 12 km, median height 12 km, and lower quartile height 11 km MSL) about 12 minutes prior to the report of the first tornado (F2) touchdown at 0050 UTC. Descent in the heights began at 0043 UTC (note: times are referenced to the nearest minute) and they reached a minimum during the

second tornado (F2) at 0108 UTC. The two severe hail reports (0015 and 0144 UTC) occurred when the storm cell was relatively intense (lightning heights greater – implied stronger updraft), and this agrees with the storm structure shown in figure 4.

To test the idea that the storm was weakening during tornadogenesis, the radar-derived storm cell and mesocyclone diagnostics given in WDSS-II were examined. Figures 17 and 18 show that most radar characteristics decreased to minimum values during the tornadoes. Radar top peaked at 12 km MSL about 7 minutes before the first tornado and decreased to a minimum of 6 km during the middle of the second tornado. This characteristic had more variation than the lightning top during the first 35 minutes shown. The severe hail index (SHI), which is an integration of the reflectivity above the melting level, reached an absolute maximum near 0018 UTC, more than 30 minutes before the first tornado was reported, followed by a secondary maximum at 0038 UTC, and then decreased to a value near 0 during the second tornado. The VIL and MSI followed a similar trend, reaching minimum values during the second tornado report. The mesocyclone diameter and MSI were near minimum values during the same time. This is contradictory to conservation of angular momentum arguments: as the mesocyclone becomes more compact, the rotational velocity should increase.

The significant updraft weakening of the storm during tornadogenesis is clearer in figure 19. The vertical extent of mean reflectivity peaked at 0043 UTC, about 7 minutes or over 1 volume scan before the first tornado touchdown. The height of the 30 dBZ contour was 13 km, and descended to 7 km MSL during the second tornado associated with this supercell (0108 UTC). The height of maximum LDAR II source

density (denoted by the 800 sources km^{-1} (5 minutes)$^{-1}$ contour) had a trend similar to the radar contours and also reached a minimum during the second tornado. There was a secondary intensification to the storm's updraft apparent at 0122 UTC, preceding a severe hail report at 0145 UTC. The area of > 55 dBZ reflectivity below 3 km at 0122 UTC was a measurement error (mean reflectivity values were near 75 dBZ associated with this storm – these had no time continuity with measurements before and after this time). Note the elevated reflectivity maximum of 50-55 dBZ at 5 km MSL at the time of the hail report at 0015 UTC and its descent to the ground by 0022 UTC.

The most intense lightning flash rates of this supercell also occurred before the tornado reports (Fig. 20). Shortly before the first tornado, the total (IC and CG) flash rate peaked at 200 flashes per approximate 5 minute volume scan (at 0048 UTC), and the –CG flash rate reached a maximum value of 60 flashes (5 minutes)$^{-1}$ (at 0038 UTC). Both rates decreased before and during the tornadoes to a minimum that was 20% or less of the peak values during the second F2 tornado. The IC:CG values were near 10 in the initial stage of the storm, decreased to a minimum the same time the –CG flash rate peaked (0038 UTC), reached a maximum value of 25 during the second F2 tornado (the total and -CG flash rates were 5 minutes out of phase in their minimum values), and then were steady near 10 throughout the remainder of the period. The percentage of +CG flashes was also at a minimum during the second tornado and remained small thereafter.

A second, separate tornadic (F1) supercell which occurred on 13 October 2001 was examined to see if these relationships between inferred updraft strength (lightning heights) and tornado occurrence were consistent. Figure 21 shows once again that the

lightning heights had their maximum values before tornado touchdown. The lightning top peaked at 17.5 km MSL by 0301 UTC, approximately 14 minutes prior to the report. This value was higher than the maximum lightning top for the previous tornadic storm, partially because this storm was farther from the network (see Appendix B regarding range effects on LDAR II source heights). The lightning top was nearly steady in the period before descent. The other lightning heights (lower quartile, median, and peak heights) show an interesting signature between 0227 and 0306 UTC. These lower lightning heights had cyclic characteristics, with maxima near 0237 and 0306 UTC and a minimum value at 0252 UTC. The 30 minute period of this cycle is consistent with pulsing in storm updraft strength. After the tornado, all heights continued to descend as the storm weakened (indicated by cell radar characteristics, not shown).

The second tornadic storm's vertical radar structure indicated a more intense storm prior to the tornado report (Fig. 22). The 45 dBZ contour reached its highest extent of 6.5 km MSL near 0256 UTC, approximately 20 minutes before the tornado touchdown. The storm was going through a slow collapse phase during tornadogenesis, consistent with the findings for the tornadic storm in figure 19. The height of maximum source density followed a similar trend, decreasing during and after the tornado. The increased source density at 0252 UTC near 5 km MSL was well associated with an upward growth of reflectivity greater than 45 dBZ. This feature is related to the minimum in the lower lightning height cycle discussed above. The minimum in lower lightning heights at 0252 UTC was associated with strengthening of the updraft as inferred from the upward growth of reflectivity.

Negative CG rates during the second tornadic storm (figure 23) peaked near 75 flashes (5 minutes)$^{-1}$ at 0237 UTC and decreased to 0 by 0401 UTC. The peak –CG rate occurred more than 30 minutes prior to tornado touchdown, consistent with the trends for the first tornadic storm. Total flash rate, however, showed a steady increase to near 200 flashes (5 minutes)$^{-1}$ well after the tornado. There was no rapid decrease in total flash rate associated with the tornado as in the earlier tornadic storm. The percentage of positive CG flashes increased preceding the tornado, and attained a relative maximum of 40% 6 minutes after the tornado. Percent positive values reached 100% at 0401 UTC, but this included only 2 +CG flashes. The behavior in IC:CG ratio was also different for this storm compared to the previous tornadic storm. The ratio was lower (< 5) preceding and during the tornado, but then increased rapidly to near 60 at 0406 UTC, well after the tornado and when figure 22 indicated a weaker storm cell. Note the CG rate was near 0 at this time (much smaller than earlier in the storm), contributing to such a large ratio.

5. Relationships between lightning and radar characteristics

The previous results indicate that storm radar reflectivity and lightning characteristics are related. This section uses correlation analysis to test the hypothesis that if radar characteristics indicate a storm's updraft is becoming more intense, there is a corresponding signal in the lightning characteristics. The support of this hypothesis indicates that storm dynamics, microphysics, and electrification are related and that lightning can be used to diagnose and predict storm evolution, an idea that has been tested by many lightning researchers (i.e., MacGorman et al. 1989, Carey and Rutledge 1998, Harlin et al. 2000, Lang and Rutledge 2002, MacGorman et al. 2002). This study

is different from the aforementioned ones in that it uses cell characteristics from WDSS-II and uses LDAR II source heights as a measure of storm updraft strength.

Correlations between lightning and radar characteristics calculated for each volume scan during a supercell (first tornadic storm discussed, which occurred between 000436 and 015933 UTC 13 October 2001) are shown in Table 1. The lightning-based storm top (Ltop) was statistically significantly correlated with the radar measures of storm strength. The VIL-Ltop correlation coefficient was the largest at 0.82 while the Ltop correlation with maximum reflectivity height was the smallest (0.44). The number of flashes determined from the source data (flash rate) was also positively correlated with these measures, and its highest r value was with VIL (0.66). The relationship between maximum reflectivity height and the flash rate was the weakest with $r = 0.13$. The mesocyclone strength index (MSI) was statistically significantly positively correlated with both LDAR II characteristics shown (nfl, Ltop). Hence, the hypothesis that the lightning characteristics used in this study can indicate storm strength is supported.

To test the sensitivity of these relationships, the same correlations were repeated using different radii (5 and 20 km) to calculate the lightning statistics (not shown). All correlations shown in Table 1 were positive for the other radii, and the majority of them were statistically significant. Once again the VIL-Ltop correlation was the strongest for both the 5 and 20 km analysis radii. The weaker correlations involved maximum reflectivity and maximum reflectivity height.

Surprisingly, the SHI-nfl correlation (r = 0.34) was less than that between VIL and the total flash rate (r = 0.66). One might expect that SHI should be better correlated with total flash rate as it is a measure of the reflectivity only above the melting level while VIL represents an integration of reflectivity throughout the whole storm depth. However, such was not the case. Similar correlation analysis for the second tornadic storm discussed (occurred between 022418 and 042305 UTC) was consistent with the above results, except all the correlations between the radar characteristics and the flash rate were not statistically significant (r values < 0.1).

6. Non-tornadic supercell characteristic trends

a. 13 October 2001

To observe if the above signatures associated with the 13 October 2001 tornadic supercells may have been unique to a tornadic storm, radar and lightning data were analyzed from a non-tornadic supercell from the same day (from 005015 to 015437 UTC). The lightning heights show a general upward trend during this period (Fig. 24). The lightning storm top was 12.5 km MSL at 0053 UTC, and reached a maximum value at 0142 UTC of 14.5 km.

The mean reflectivity history of the non-tornadic supercell shows an increase in the vertical extent of the storm to a maximum at 0132 UTC (Fig. 25). The maximum height of the 30 dBZ contour increased from 10 km at 0102 UTC to higher than 14 km MSL at 0132 UTC. There was a corresponding increase in the height of the maximum LDAR II source density (3200 sources km^{-1} (5 minutes)$^{-1}$ contour), but the trend was not as drastic as with the tornadic storms shown in figures 19 and 22.

Surprisingly, the maximum source density shown in figure 25 (6400 sources km^{-1} (5 minutes)$^{-1}$) occurred at 0102 UTC when the radar reflectivity contours were at lower altitudes (indicative of weaker updraft than at 0132 UTC). Comparing figures 19, 22, and 25 shows that the maximum contoured source densities were greater for the non-tornadic supercell (6400 vs. 1600 sources). This was likely because the non-tornadic storm shown in figure 25 traversed closer to the LDAR II network than the tornadic supercells (mean distance from the network throughout each storm's lifetime = 91 km for the tornadic storms, 39 km for the non-tornadic storm; see Appendix B).

b. 6 April 2003

The hail-producing (non-tornadic) supercell of 6 April 2003 had no significant variations in the lightning heights, unlike those for the tornadic storms shown in figures 16 and 21. Figure 26 shows the lightning top (95th percentile source height) remained near 11 km MSL for the hour analyzed. A signature was not associated with the hail report at 0414 UTC. The lower heights (quartile, median, and peak heights) show some minor changes, with maximum lower quartile and peak heights (8, 9 km MSL, respectively) near the time of the hail report. LDAR II source data within 20 km of the mesocyclone were used to calculate the characteristics shown in figure 26 because the mesocyclone location given by WDSS-II was typically on the south side of the storm and a significant fraction of the data would have been missed if a radius of 10 km was used as in figure 16. This storm was also well-isolated from other storms, minimizing contamination.

The vertical extent (as shown by the radar reflectivity distribution) of the 6 April storm and altitude of maximum source density was nearly constant throughout its lifetime (Fig. 27). Regions of smaller mean reflectivity values (< 50 dBZ) occurred below 3 km MSL at 0338, 0353, and 0413 UTC. These were signatures of the weak echo region (i.e., Fig. 15). The maximum thickness bounded by the 6400 sources km^{-1} $(5\ minutes)^{-1}$ contour (2 km) occurred approximately 10 minutes before the weak echo region signatures at 0353 and 0413 UTC.

7. Discussion and conclusions

The horizontal projections in figures 4-9 show that most lightning occurs where there exists gradients of mean cold cloud (above melting level) radar reflectivity. Examining data within the layer where most of the lightning occurred in figure 4 (between 8 and 12 km MSL; not shown) also shows that most of the sources were in reflectivity gradient within that layer. Rust et al. (1982) and Proctor (1991) show lightning origins occur at the edges of high radar reflectivity precipitation cores, where reflectivity and vertical velocity horizontal gradients are large. Dye et al. (1986) explain why lightning is unlikely to originate within a strong reflectivity core: the particle interactions responsible for charge separation and ultimately lightning initiation occur in an updraft, but at the core of the updraft where speeds at 7 km altitude are generally at least 10 to 15 m s^{-1} even the largest particles would be carried upward. Greatest charge separation occurs where there are horizontal gradients in vertical velocity (where typically lighter positively-charged ice crystals are lofted to form a higher positive charge center while heavier negatively-charged graupel particles descend to form a

lower negative charge region and a strong electric field develops between the two) and gradients in radar reflectivity may be used as a proxy for vertical velocity gradients. Mean reflectivity maxima in the aforementioned plan views of supercells indicate the main updraft regions of the storms, and are likely on the edges of maximum updraft speeds (refer to the cross-sections of reflectivity and storm updraft location in an ideal supercell in Fig. 15.5 in Weisman and Klemp 1986). Reflectivity gradient develops within the updraft and downdraft interface. Hence, lightning activity is greater where gradients in reflectivity occur, and the observations from this study support this hypothesis.

The maximum LDAR II source density values in the vertical projections of figures 4-9 are located in reflectivity gradient above where the reflectivity contours protrude vertically. The plan views in figures 5 and 8 show the maximum source density is within 5 km of the maximum 40 dBZ echo height. These areas are indicative of strong updrafts that increase charge separation processes and elevate precipitation particles and their associated charge. The area of maximum source density is thickest (largest vertical distance enclosed by a source density contour) within and above these reflectivity upward bulges in the vertical projections indicating more charging within a thicker layer and/or the merging of multiple charge layers by a strong updraft.

Only the 6 April 2003 supercell exhibited the total lightning holes (Figs. 7-9, 12) as discussed by Krehbiel et al. (2000), McCaul et al. (2002) and Wiens et al. (2002). The lightning hole is associated with large values of mean reflectivity in this study (the collocation with large reflectivity values occurred for all the volume scans analyzed).

Murphy and Demetriades (2005) explain that storms with intense updrafts and large hail, such as the 6 April supercell, can develop a condition within the updraft region unfavorable to non-inductive charge separation and hence, lightning. In this condition, the graupel and hail particles become heavily coated with liquid water (wet growth), decreasing the number of effective rebounding collisions which can lead to charge separation (Saunders and Brooks 1992 show charge transfer values are insignificant during wet growth). High reflectivity values can also be associated with relatively low concentrations of large hail particles, a condition also unfavorable to non-inductive charging (reduced total surface area) and lightning. The lightning hole was also collocated with significant reflectivity within the 2-6 and 6-10 km MSL layers of the storm. The diameter of the lightning holes in figures 7 and 9 are consistent with typical thunderstorm updrafts (1-10 km; Weisman and Klemp 1986). The weak source density region in the vertical projection of figure 9 is in the vicinity of the radar-detected mesocyclone, which also supports the hypothesis that the lightning hole is created by an intense updraft. The lightning hole and the maximum 40 dBZ echo height in figure 8 are not collocated, inconsistent with the above hypothesis (this may be the result of storm tilting). Examining total (0-20 km MSL) and low-level lightning (0-6, 0-10 km) from the 13 October 2001 supercells did not reveal a lightning hole as described above, perhaps because the tornadic storms in this case were greater than 65 km from the network center and a significant amount of lightning went undetected due to the rapid decrease in LDAR II source detection efficiency with range (the 6 April supercells were within 25 km from the network). Analyzing the total lightning from the 13 October

tornadic storms with shorter integration times (2 minutes) did not show a lightning hole signature either (holes may appear when shorter integration times are used as the effect of storm advection is reduced). Hence, lightning holes are not ubiquitous features of supercell storms, except for the ones with intense updrafts and/or that are close to the network.

Figure 6 shows a weak lightning hook at (-22, 78 km) and that most lightning is downshear of the mesocyclone (Fig. 4 also shows this). Ray et al. (1987) also show that lightning tended to be downshear of the main updraft and reflectivity core in a supercell. Charge is clearly being advected on the precipitation particles when there is significant wind shear (as is the case with supercell environments). The double maxima in –CG flash density observed in the supercells prior to the reported tornado touchdowns (Figs. 10 and 11) and within the 6 April supercell case (Figs. 12 and 15) is a new finding in this study. They are located in regions of the supercell where areas of downdraft may be expected based on the Lemon and Doswell (1979) supercell model. The –CG density maxima shown in figures 10 and 11 were associated with areas of relative maximum mean reflectivity (not shown). Lower elevation charge regions associated with the downdraft regions of these storms can enhance CG lightning production. An exception to these observations and hypothesis is shown in figure 15; maximum -CG flash density is associated with the bounded weak echo region (BWER, an updraft signature).

The peaks in the height histograms of LDAR II sources (Figs. 4-12), which are hypothesized to be the locations of major positive charge regions, are located at environmental temperatures near or below -40°C. Particle charging likely occurred a

few km below this level, with the lighter ice crystals (typically positively charged after collisions with graupel; Saunders 1993) ascending to form a reservoir of positive charge near the -40°C isotherm level. Figures 4-6, 9-10, and 12 also show that the distributions of flash *origins* peak on the edges of source peaks. Electric fields are at maximum values *between* oppositely charged regions. Lightning is initiated where the electric field is the strongest (MacGorman and Rust 1998, p. 203). If it is assumed that the main negative charge region is located at the minima in the source height distributions (since positive breakdown into negative charge regions is not well-detected by VHF TOA systems (Rison et al. 1999)), the observations support the hypothesis that the source peaks represent positive charge regions as the maxima in the number of flash origins is located between oppositely charged regions. However, the flash origin peaks in figures 7 and 11 are also where the source peaks are located, contrary to this hypothesis.

The lightning heights (lower quartile, median, 95th percentile, and peak heights) calculated with the LDAR II data are useful indicators of storm updraft strength. Figures 16-18 show that when radar storm cell characteristics, such as the radar top, SHI, and VIL, indicate a stronger storm, the lightning heights are higher. The radar top has two maxima at 0043 and 0122 UTC, near the same times as when the lightning heights are at their highest. As a storm's updraft intensifies, precipitation particles are lofted higher, especially the lighter ice crystals that are typically charged positively (Saunders 1993). Hence, the radar top and LDAR II sources, which show where positive charge is in the storm, are at higher altitudes. Stolzenburg et al. (1998a, b, c) show by more direct means (electric field meter balloons) that charge regions are higher in altitude when the

balloon ascent rate (a proxy for updraft strength) is larger. Changes in the altitude of VHF sources (which can map positive charge regions) are associated with the updraft core (Dotzek et al. 2001). Significant lightning height fluctuations did not occur during the hour shown for the 6 April 2003 case (Fig. 26) because the storm was in a quasi-steady intense state. It formed and decayed outside the analysis time.

Table 1 also supports the hypothesis that the lightning characteristics calculated in this study can be used as indicators of changes in storm intensity. Maximum reflectivity, maximum reflectivity height, radar top, SHI, VIL, and MSI show statistically significant positive correlations with the lightning parameters shown (95^{th} percentile source height and total flash rate) for a tornadic supercell. These results agree with those of Mazur et al. (1986), who show a storm's maximum flash rate typically occurs when the height of the storm core has peaked. The advantages of the characteristics calculated from LDAR II data are that the time and spatial resolution of the lightning data are better than WSR-88D data (these characteristics can be calculated for every minute of the storm's lifetime as opposed to the 5-6 minutes required for a radar volume scan).

The lightning and radar characteristics shown in figures 16-22 show a significant weakening in each tornadic supercell prior to and during the reported tornado touchdowns. Lightning heights show significant descent and radar characteristics like the SHI peak well-before the tornado touchdowns. Most of these indicators have their absolute minimum values during the second tornado in figure 16, rated F2. Figures 19 and 22 clearly show each tornadic storm is going through a collapse phase during

tornadogenesis. Both –CG and total flash rates peaked prior to the F2 tornado and decreased by at least a factor of 5 to a minimum during the tornado in figure 20. Similar behavior in the –CG rate is observed for the second tornadic storm analyzed in figure 23 (agrees with the results from Perez et al. 1997), but the total flash rate trend is different (it is believed a cell merger and/or split process affected this result). Comparing the plan views of figures 4 and 6, the WDSS-II indicated mesocyclone becomes more separated from the total lightning activity during the tornadic stage of this storm. This may explain why the flash rates decreased substantially as only lightning data within 10 km of the mesocyclone was chosen to calculate the characteristics. However, a similar analysis was conducted as shown in figure 20 using data within 20 km of the mesocyclone and found similar results. Recent studies show the rates of VHF emissions and total flashes tend to increase prior to tornado occurrence (Williams et al. 1999, MacGorman et al. 2002). A dramatic decrease in total flash rate has been observed near the same time as tornado touchdown and bounded weak echo region collapse in some Florida storms (Sharp 2005). Tornadoes occur during or shortly *after* updraft surges inferred from lightning in these studies.

Lemon and Doswell (1979) explain that tornado touchdown occurs when the updraft of an intense supercell weakens in magnitude and extent and the downdraft (rear flank) of the storm intensifies. The mesocyclone becomes divided between updraft and downdraft. This theory is supported by the observations in this study: most lightning and radar characteristics indicate the storm is indeed weakening (updraft decreasing intensity and/or downdraft overtaking the storm) while the tornadoes are on the ground

in both tornadic storms examined. Conversely, the Lemon and Doswell theory combined with these observations support the hypothesis the altitude of lightning activity as shown by the LDAR II source heights is related to the thunderstorm's updraft. Caution must be taken in that there can be errors in the timing and location of the reported tornadoes. The non-tornadic supercells examined in this study show a gradual increase or no significant change in lightning heights throughout the period shown for each storm (Figs. 24 and 26). The lightning and radar trends shown for the tornadic storms are more abrupt and at least appear to be related to tornadogenesis.

A comparison of figures 16 and 20 shows that the lightning heights, total flash rate, and –CG flash rate are near maximum values at similar times (near 0038 UTC). The IC:CG ratio is at a minimum at this time (less than 5). The lightning heights in this study have been shown to be indicators of storm updraft intensity. MacGorman et al. (1989) suggest that as a storm's updraft intensifies, IC flash rate increases and CG flash rate decreases as oppositely charged regions are brought closer to each other higher in the storm producing higher electric fields there. Thus, the observation that total flash rate increases with updraft strength as indicated by the lightning heights appears to support this hypothesis. A minimum IC:CG ratio at 0038 UTC, however, does not support the elevated charge region hypothesis proposed by MacGorman et al. Table 2 shows that as lightning storm top increases, the IC:CG ratio decreases for the two tornadic storms examined in this study (Ltop-rat r values are statistically significantly negative at the $p = 0.1$ level). However, the correlation coefficient between these two variables for the 6 April 2003 intense supercell is 0.34 (0.46 for the 20 km radius

analysis). Surprisingly, the total and CG flash rates are both negatively correlated with the lightning storm top (r = -0.33, -0.29, respectively) in this case. The strong positive correlations (statistically significant at the p = 0.1 level) between lightning top and the thickness of the primary source peak (all cases in Table 2) suggest that as an updraft intensifies, charge layers merge together and are revealed as one, thick charge region at the 1 km height resolution used in this study. Figure 13 shows support for the elevated charge region hypothesis as the weaker storm has significantly higher amounts of CG lightning. The enhanced reflectivity below 6 km at 0252 UTC in figure 22 is concurrent with a strong storm updraft (inferred from the large vertical extent of the storm's reflectivity structure) and large –CG flash rates (Fig. 23). Low-level enhanced reflectivity values, not necessarily updraft strength, is a better predictor of -CG lightning in these two cases. The differing conclusions drawn from the above results show more research needs to be done to study if there are certain *situations* the elevated charge region hypothesis can be applied to a severe storm (as suggested by MacGorman and Nielsen 1991). The observation that lightning heights ascend as a storm intensifies shows that charge is elevated by stronger updrafts. The relationship between elevated charge and IC:CG ratios remains unclear. As discussed earlier, the charge regions detected by the LDAR II instrument are most likely positively charged, and the MacGorman et al. hypothesis claims the negative charge region is lifted in a stronger updraft. The modeling study by Ziegler and MacGorman (1994) shows that in a strong supercellular updraft, *both* the main negative and positive charge regions are elevated (see their Fig. 7). Hence, it is assumed that an elevated positive charge region, as

detected by the LDAR II system, indicates an elevated negative charge region in the storm.

Enhanced positive cloud-to-ground (CG) lightning activity is not located in a persistent region with respect to the supercell structures in this study. Figure 14 supports the hypothesis that anvils are an origin of positive CG flashes as %+CG maxima are located underneath the radar-detected anvils. Large +CG density values (> 0.14 flashes km^{-2} (5 minutes)$^{-1}$) also occur near the mesocyclone, in areas of high reflectivity, with similar frequency as the pattern shown in figure 14. Positive CG flash densities increase substantially when radar signatures indicate an updraft undergoing intensification in two cases (first tornadic storm analyzed and the 13 October 2001 non-tornadic storm; not shown). The time series shown in figures 18 and 20 indicate maxima in %+CG values near the times (0017 and 0127 UTC) when the SHI has elevated values. The correlation coefficient between SHI and %+CG for the first tornadic storm is 0.4 (statistically significant). This r value is -0.25 for the second tornadic storm, but the coefficient between SHI and +CG flash density is 0.5. SHI is a proxy for hail development in a storm. Hence, a relationship between hail formation and +CG lightning exists in these two storms, which agrees with the results shown in Wiens et al. (2003). The hail reports also occur when %+CG values are greater, near 20% (Fig. 20). During hail development the storm's updraft is intense, and enhanced supercooled liquid water values might increase positive charging at lower storm levels which increase +CG flash production (MacGorman et al. 2002).

The %+CG value is at an absolute minimum (near 0%) during the F2 tornado in figure 20. Percent +CG values increase during tornadogenesis and reach a maximum after the tornado report in figure 23, agreeing with the results from Carey et al. (2003a). Carey et al. attribute this behavior to a merging process between a supercell and a squall line. The tornadic storm analyzed in figure 23 also possibly went through a merger process with nearby cells during the time %+CG was increasing. Figure 22 shows this storm to be weakening during the same time the %+CG values are increasing (Fig. 23); the storm in Carey et al. strengthened during the period of increasing %+CG values.

Overall, the first tornadic storm analyzed (000436-015933 UTC 13 October 2001) has 12% of its CG flashes lower positive charge to ground and an average +CG flash density of 0.009 flashes km^{-2} (5 minutes)$^{-1}$ (the statistics here were calculated each volume scan of the storm's lifetime using data within 10 km of the mesocyclone). The tornadic storm occurring between 022418 and 042305 UTC 13 October 2001 has 21%+CG flashes and an average +CG density of 0.025 flashes km^{-2} (5 minutes)$^{-1}$. Surprisingly, the 13 October 2001 non-tornadic supercell analyzed has the largest overall %+CG value at 29%. The large %+CG storm being non-severe is contrary to the model typically used in the northern plains of the United States, where storms with a high fraction of positive CG flashes frequently have severe weather associated with them (Carey and Rutledge 2003). This agrees with the expectations expressed in the Introduction that a relationship between severe weather and CG polarity is difficult to observe since southern plains thunderstorms were analyzed in this study (Carey and Rutledge). Using a large sample of supercells (all storms having a mesocyclone rank ≥ 5

and hence classified as supercells by the mesocyclone detection algorithm (Stumpf et al. 1998) in the WDSS-II software during the 13 October 2001 event), the percentage and average density of +CG flashes is 22% and 0.022 flashes km^{-2} (5 minutes)$^{-1}$.

Total lightning (IC+CG) characteristics, especially lightning height information and flash rates, have been shown to be useful in diagnosing supercell intensity. Used in conjunction with radar data, researchers and forecasters will have a better understanding of thunderstorm morphology and its relation to the occurrence of severe weather (tornado, large hail) at the ground. The advantages of volumetric LDAR II source data include higher temporal and spatial resolutions (especially at far ranges) compared to WSR-88D radar data. The National Weather Service in Birmingham, AL has successfully used source data at 2 minute resolution in their warning operations (Goodman 2005, personal communication). Future research will include calculating the total lightning characteristics used in this study every two minutes to observe if warning times can be increased compared to when using radar data alone. The lower limit for the time interval used for calculating total lightning characteristics requires further testing to determine the proper sampling of storms (i.e., can characteristics be calculated every 30 s? Probably not as only a few flashes occur in this interval assuming a typical storm flash rate of 10 min^{-1}). LDAR II data is useful for these purposes within 150 km from the network; beyond this distance range and altitude errors have significant effects (Appendix B). LDAR II source density is not very useful to compare storm intensity at different ranges as the number of detected sources decreases rapidly with distance from the network (Appendix B).

TOTAL LIGHTNING SIGNATURES OF MESOSCALE CONVECTIVE SYSTEM INTENSITY

1. Introduction

A mesoscale convective system (MCS) is "a group of storms that interacts with and modifies the environment and subsequent storm evolution in such a way that it produces a long-lived storm system having dimensions much larger than individual storms" (MacGorman and Rust 1998, p. 258). Houze et al. (1990) gives a thorough description of the reflectivity structure of MCSs. There are three classic structures: 1) leading line of deep convection with symmetrically placed trailing stratiform, 2) leading line of deep convection with asymmetrically placed trailing stratiform (usually displaced to the north in the Northern Hemisphere), and 3) chaotic, unclassifiable mass of convective and stratiform rain. Certain identifiable lightning patterns have been associated with these MCS types as different dynamics operate in the stratiform and convective regions. Severe weather (large hail, damaging winds, and tornadoes) occasionally accompanies these systems (mainly in the leading convective line). Lightning has been shown to be a useful indicator of imminent severe weather in supercellular convection (previous section), and it is a major purpose of this study to show lightning's utility in diagnosing and predicting intense thunderstorms within MCSs.

Schuur et al. (1991), Stolzenburg et al. (1994), and Stolzenburg et al. (1998a) document the electrical charge structure of MCSs, within both the convective and stratiform regions (see fig. 9 in Stolzenburg et al. (1998a) for a conceptual model based

on their observations). They propose that two processes are responsible for charge structure in the stratiform region: growth of mixed-phase precipitation particles and subsequent local charging in the stratiform region (in-situ), and advection of charged particles from the convective portion of the system back (storm relative) into the stratiform region.

The convective portion of an MCS analyzed by Carey et al. (2005) exhibits a bimodal height distribution of lightning activity (source peaks at 4.5 km (3°C) and 9.5 km MSL (-35°C)) while the stratiform region has three peaks (4.5, 6, and 9 km MSL). These peaks are thought to be regions of positive charge as the total lightning instrument used by Carey et al. (LDAR II; same as the one used here) detects more radiation from lightning propagating through positive than negative space charge (Rison et al. 1999). The more complex charge structure outside convection agrees with the results from Stolzenburg et al. (1998a). Radar reflectivity and lightning source density contours slant downward behind the convective line into the stratiform region (Carey et al.). The excellent agreement between snow trajectories and the slanted path of VHF sources into the stratiform region strongly supports the charge advection mechanism thought to be partly responsible for charging the stratiform regions of MCSs. Carey et al. caution, however, that in-situ charging cannot be disregarded as charge advection does not explain the entire charge structure of the stratiform region in the MCS they analyzed. It is very likely both charging mechanisms are active in the stratiform region of MCSs, and support is shown for this hypothesis in this study.

As a new cell in an MCS grows and its reflectivity increases, the flash density maximum moves toward the rear of the cell, eventually merging with lightning in older cells. As cells age, the length of the flashes they produce become longer (Mazur and Rust 1983). McCormick et al. (2002) show an increase in the number of LDAR II flash origins along the back edge of the convective region of a squall line, in the leading edge of the stratiform region, and in the enhanced reflectivity "bridge" in the transition zone that connects the convective and stratiform regions. There are relatively few LDAR II flashes associated with the leading edge of the convective line and in the stratiform region. LDAR II flashes begin in regions of moderate reflectivity (< 45 dBZ) above convective cores at altitudes mostly > 5 km MSL, and LDAR II sources are at higher altitudes above enhanced reflectivity aloft (indicative of a strong updraft) (McCormick et al. 2002, McCormick 2003). LDAR II source densities in the convective line of the MCS discussed in Carey et al. (2005) are well correlated with reflectivity enhancements. These data can also help resolve the issue of where flashes in the stratiform region are initiated and how they propagate (MacGorman and Rust 1998, pp. 280-281). The relationship between reflectivity and lightning will be examined and compared to these previous results.

In MCSs, peak ground flash rates tend to occur later than reports of severe weather (Goodman and MacGorman 1986). Cloud-to-ground (CG) flash rates lag echo volume aloft (which is related to updraft strength (Carey and Rutledge 1996)) and total flash activity in MCSs by 30 minutes (McCormick 2003). A bipole pattern, the spatial separation between regions of concentrated positive and negative ground flashes, has

been noticed in some MCS cases (Orville et al. 1988). Negative ground flashes in MCSs are usually associated with the convective region (MacGorman and Rust 1998, p. 275) while the positive ground flashes concentrate in the stratiform region when a bipole is observed. The average peak +CG current in the stratiform region (43 kA) is greater than double the mean peak positive current in the convective region (20 kA) of an MCS studied by McCormick (2003) (Petersen and Rutledge (1992) and MacGorman and Morgenstern (1998) show similar results, but their were some exceptions). The charge regions are more expansive in the stratiform region and may provide more charge to a CG flash to produce a larger current (Petersen and Rutledge). Sometimes, the convective cells are dominated by positive CG flashes. Typically the storm that is dominated by +CGs occurs early in the lifetime of the MCS, and is on the southern end of the convective region, where most severe weather is reported (MacGorman and Rust 1998, p. 278).

Mazur and Rust (1983) show that in one storm the number of cloud flashes is 40 times the number of ground flashes. In contrast to this observation and expectations from the MacGorman et al. (1989) elevated charge region hypothesis, McCormick (2003) shows intracloud to cloud-to-ground (IC:CG) flash ratios are at relative minimum values (near 12.7) when cells in the 13 October 2001 MCS are most intense. Another MCS analyzed by McCormick has a mean IC:CG ratio of 7 and its stratiform region has greater IC:CG ratios than the convective region.

Unlike many of the aforementioned studies, this study mostly shows *individual* storm cell analysis (radar reflectivity and lightning) of three mesoscale convective

systems (13 October 2001, 27 May 2002, and 16 June 2002) using methods similar to those in the first section. The life cycle of MCS storm cells is examined. The radar and lightning cell characteristics are related to storm intensity and severe weather occurrence. Certain identifiable patterns in the total (IC+CG) lightning behavior are shown that can be used to infer storm dynamics (i.e., a lightning bow). A comparison between the lightning and reflectivity structures of the convective and stratiform regions of MCSs is shown to observe how the dynamics, microphysics, and electrification differ between these two portions of the systems.

2. Data and methodology

Three data sets were used in this study: Dallas-Fort Worth WSR-88D (KFWS) radar data, National Lightning Detection Network (NLDN) cloud-to-ground (CG) lightning data, and Lightning Detection and Ranging II (LDAR II) total lightning data. Analysis was focused on individual convective storm cells within mesoscale convective systems (MCSs). Severe storm reports were obtained from NCDC (2001, 2002ab). I also examined the total MCS structure to compare results with previous studies (i.e., Carey et al. 2005). Partitioning convective and stratiform MCS regions was done subjectively by examining the horizontal and vertical radar structure of an MCS. Convective regions were defined as having large values of mean reflectivity (> 40 dBZ) and reflectivity gradient and having reflectivity contours that extended upward.

The CG and total (intracloud (IC) and CG) lightning data were from the NLDN and the LDAR II network, respectively, and were obtained from Vaisala, Inc., Tucson, AZ. Both of these networks are described in more detail in the first section. The CG

lightning characteristics analyzed from these data were: negative and positive flash density, percent positive flashes, median peak current for both polarity flashes, and mean multiplicity for each polarity. The LDAR II source density (number of sources per unit area per unit time interval) was analyzed in horizontal and vertical projections as described in the first section of this study. The Huffines flash grouping algorithm (first section) organized sources into flashes. The total lightning characteristics calculated for each storm cell (using LDAR II data within 5, 10, and 20 km of the radar-indicated cell location (see below)) included: lower quartile, median, 95th percentile (defined as the lightning-based storm top), and peak heights of LDAR II source density, number of modes (peaks) in the height distribution of sources, normalized peak value of sources, half-peak thickness of the main peak in sources, total number of sources within the cylindrical volume, number of flashes from sources (total flash rate), and the IC:CG ratio. LDAR II flash detection efficiency maps for the 27 May 2002 and 16 June 2002 case studies are shown in figures 28 and 29. The detection efficiency distributions for the 13 October 2001 and 27 June 2001 events are shown in the first section, figure 2.

The radar data to be used in this study were from the Dallas-Fort Worth WSR-88D (KFWS) radar, obtained from the NCDC. As in the first section, the Warning Decision Support System-Integrated Information (WDSS-II) software (Hondl 2003) was used to determine cell location and characteristics. The radar top (maximum height of the 30 dBZ contour), severe hail index (SHI), and vertically integrated liquid (VIL) were used to diagnose storm intensity and were correlated to the CG and total lightning

characteristics. The radar data were converted to a Cartesian grid for contouring reflectivity and overlaying lightning data.

Four-dimensional and time-height representations (first section, Figs. 4 and 19) of the radar reflectivity and lightning data for individual storm cells within MCSs were produced. The first section details the procedures for creating these plots. For the next subsection, the storm cell most closely associated (in time and space) with a severe wind report was chosen. The selected cell was tracked by using WDSS-II for its lifetime before and after the report. The cell lifetimes shown in figures 34, 38-40, 42-44, and 47-48 are determined from when SCIT first identified the cell of interest (first assigned a cell identification number) to when the cell was no longer identified by that particular identification number. This does not necessarily coincide with the cell dissipating completely; this is one of the errors in using the SCIT algorithm. Also, cell lifetimes were sometimes prematurely ended in the analysis because the cell's location exited the analysis domain (30 to 100 km range from the radar; see first section, Data and methodology). This occurred for the 27 May 2002 case. Unlike the majority of the supercells analyzed in the first section, the MCS cells were not isolated. Hence, it was more likely that radar and lightning data from other cells infiltrated the analysis radius of the cell of interest. When this contamination appeared significant, the cell lightning characteristics were calculated using data within smaller radii (5 or 10 km) of the WDSS-II cell location.

3. Lightning and radar reflectivity signatures associated with MCS high wind events

a. 13 October 2001

Figure 30 shows the mean reflectivity and total lightning structure of a storm cell that was part of a leading-line, trailing stratiform (LLTS) MCS 14 minutes prior to a high wind report (26.8 m s^{-1}) associated with this cell. The storm was at the northern end of an asymmetric system (Houze et al. 1990). 21971 LDAR II sources comprised 546 flashes in this plot, an average of 40 sources per flash. All vertical projections show that the source density was concentrated in three levels: 4 km (above the melting level), 9 km, and 11 km MSL (T < -40°C). There were several density maxima within these levels (especially in the x-height projection) indicating a more complex charge structure in the horizontal. Distinct multimodal vertical distributions of source density were observed when cells in this study were within 50 km of the LDAR II network center (this cell was 20 km from the network); beyond this distance distributions were unimodal. The LDAR II may have difficulty detecting the lower part of multimodal distributions beyond 50 km (see Appendix C). The enhanced source density values observed near 10 km MSL between x = 6 and 24 km in the x-height projection mapped the anvil region of the storm. As in the first section, the source density maxima were above near where the reflectivity contours extended upward (at x, y location 33, 57 km) indicative of where the main storm updraft was located (they are not as well collocated in the height-y projection). Figure 31 confirms this as the source density maxima in the

plan view (located at (35, 66), (31, 58), and (42, 45)) were within 40 dBZ echo height gradient near echo height maxima.

The reflectivity and lightning structure observed with this storm in the horizontal projection was comma-shaped (this radar reflectivity pattern is associated with strong downdraft winds (Przybylinski 1995)). The cell center location (indicated with an asterisk in Fig. 30) was within the comma head. Enhanced lightning activity (> 23 sources km^{-2} (5 minutes)$^{-1}$) was collocated with areas of large mean reflectivity (> 40 dBZ). Doppler radial wind velocity was strong outbound 5-10 km south-southeast of the comma head (approximately 30 m s^{-1} (storm-relative radial velocity 14 m s^{-1}) at the lowest tilt) (Fig. 32). The precipitation was moving outbound at all vertical levels sampled by the radar (the cell was located 64 km to the northeast of the KFWS radar). The storm-relative radial velocity in the northern portion of the comma head (not shown) at the lowest tilt was inbound at -4 m s^{-1}. This radial velocity pattern partially explains the comma shape to the reflectivity and total lightning storm structure observed in figure 30.

The wind report associated with this storm cell occurred at 0214 UTC. According to figure 33, the wind report's time and/or location was inaccurate as it was nearly 15 km to the west of the apex in the reflectivity and lightning comma-shaped structures (near the apex is where the strongest surface winds are expected in these storms (Przybylinski 1995)). The high wind event likely occurred several minutes earlier than the report. A multimodal source density distribution continued to be observed in this storm, with peaks at 4 and 12 km MSL. 42073 sources comprised 389

flashes, an average of 108 sources per flash. As with figure 30, there were three maxima in flash origins at heights of 4, 9, and 12 km MSL. There were two locations in the x-height projection where the reflectivity contours extended upward (at x = 42 and 53 km associated with the main cell and new cells developing to the southeast of it, respectively). The two horizontal layers of maximum source density were connected by vertical segments of enhanced source density at these locations. There was a wide area (> 30 km) of relatively weak electrical activity extending behind this storm to the west.

The time-height history of the reflectivity and total lightning structure of this storm is shown in figure 34. Only data within 10 km were selected to reduce contamination from nearby cells. Most of the cell's reflectivity contours had their highest extent at 0202 UTC. The 30 dBZ contour was at 14 km MSL at this time. Before this time period, the maximum source density was bimodal with values greater than 1600 and 3200 sources km^{-1} (5 minutes)$^{-1}$ centered near 5 km and 12 km MSL, respectively. The upper lightning layer was thicker (compare the vertical distances between the 1600 sources km^{-1} (5 minutes)$^{-1}$ contours in each layer) than the lower one. After 0202 UTC, there was only one distinct maximum in source density located at 12 km (1600 sources km^{-1} (5 minutes)$^{-1}$) and a weak signature of a lower mode at 5 km MSL (800 sources km^{-1} (5 minutes)$^{-1}$). The altitudes of both of these lightning layers remained constant throughout the lifetime of this cell (1 hour). The wind report occurred while the altitudes of the upper reflectivity contours were in descent. The severe wind occurred while the reflectivity data show the storm was at maximum intensity or while it

was weakening (it is difficult to diagnose this with better accuracy due to the possible timing error in the wind report discussed above).

A peak in negative CG flash rate occurred approximately 10 minutes before the 13 October 2001 wind report (not shown). Figure 35 shows –CG flash densities were greater than 0.22 flashes km^{-2} (5 minutes)$^{-1}$ near the center of the storm (at 37, 58) during the time of peak –CG activity. This area of large –CG flash density coincided with an area of large source density values (> 86 sources km^{-2} (5 minutes)$^{-1}$). The –CG maximum also was located where the vertical projections indicate a bimodal vertical distribution of sources (centered at (40, 60)). A hypothesis for this relationship is discussed in Appendix C.

b. 27 May 2002

The convection on 27 May 2002 was an unorganized mass of thunderstorms with stratiform rain and some significant breaks in precipitation. One of these storms produced a severe wind report of 26.4 m s^{-1} between 2014 and 2026 UTC. Figure 36 shows the reflectivity and total lightning structure for a volume scan during this period. As with the 13 October 2001 wind event, the LDAR II source density had a bow-shaped appearance in the plan view. A large area of mean reflectivity values greater than 55 dBZ in a south-north orientation was 5 km to the west of the enhanced lightning activity. There were two weak echo notches on the backside of this storm (which propagated eastward) at positions y = -24 and -15 km, but the overall reflectivity pattern was straight (no bow echo). The high wind report was adjacent to the northern weak echo notch.

Even though the histogram in figure 36 indicates 2 levels of maximum lightning activity at 10 and 12 km MSL, the central area of the storm cell exhibited an unimodal source density height distribution in the vertical projections (as expected since it was 86 km from the LDAR II network (Appendix C)). The maximum number of flash origins was at 9 km MSL, below the source maximum. 2910 total sources and 228 flashes were included in this plot. This resulted in an average of 13 sources per flash, significantly less than the average number of sources per flash for the 13 October 2001 cells (Figs. 30 and 33). This was most likely due to the 27 May 2002 storm's distance from the LDAR II network center, being more than double what it was for the storms shown in figures 30 and 33 (Appendix B discusses how source detection efficiency rapidly decreases with distance decreasing the number of sources per flash). The radar data indicated the 27 May 2002 storm to be more intense than the 13 October 2001 cells; maximum contoured reflectivity values were greater than 55 dBZ in figure 36, while in figures 30 and 33 these values were between 45 and 50 dBZ.

A bow echo in the horizontal reflectivity structure of the storm (Fig. 37) developed approximately 10 minutes after the wind report shown in figure 36. The total lightning pattern continued to have a bow shape, but it was asymmetrical with maximum source densities within the reflectivity gradient on the northern end at (-28, -19). Smaller values of source density (9-14 sources km^{-2} (5 minutes)$^{-1}$) extended south from this maximum. A feature of both figures 36 and 37 was the significant tilting of the main reflectivity core eastward with height in the x-height projections. Maximum lightning activity topped the reflectivity cores observed in the west-east vertical

projections in figures 36 and 37. Note how the source density maximum increased altitude in the height-y projection approaching y = -20 km (the location of the reflectivity core) from either side in figure 37. As in the first section, the lightning layer was elevated in the vicinity of the main storm updraft. The thickness of the layer decreased as the distance from the storm center increased. The regions of relatively thin lightning activity in the vertical projections likely show where the storm anvil was located.

The 27 May 2002 storm intensified before it produced severe surface winds. Low-level mean reflectivity values increased from 50 to greater than 55 dBZ at 1941 UTC (Fig. 38). Maximum reflectivity values between 50-55 dBZ extended to the ground and values greater than 55 dBZ were present near 5 km MSL during the high wind event. The upper reflectivity contours also increased altitude preceding and during the severe weather report (the 30 dBZ contour increased from 8 km at 1921 UTC to over 13 km MSL at 2035 UTC; most of this increase was attained 30 minutes before the event). Total lightning activity was unimodal, centered near 10 km MSL (-40°C) throughout the period. Maximum source densities (> 400 sources km^{-1} (5 minutes)$^{-1}$) at this altitude occurred during the middle of the report (at 2021 UTC) and was sustained for approximately 10 minutes after the event. Before 1936 UTC there were no sources detected in this storm below 5 km MSL, while after this time there was some lightning detected below this level (the minimum contour interval is 1 source km^{-1} (5 minutes)$^{-1}$). This occurred just before the development of areas of reflectivity greater than 55 dBZ between 2 and 5 km MSL and descent of 50-55 dBZ to the ground. The storm was also

propagating closer to the LDAR II network center during its lifetime (between 118 and 76 km range), and this may have resulted in the detection of more low-level sources (Appendix B).

Total lightning and –CG flash rates increased to maximum values of 190 and 50 flashes (5 minutes)$^{-1}$, respectively, during the 27 May high wind report (Fig. 39). Negative CG rates significantly increased about 10 minutes after the development of the low-level maximum reflectivity at 1941 UTC shown in figure 38. Total flash rate reached a relative maximum value of greater than 130 flashes (5 minutes)$^{-1}$ at 1951 UTC, about 10 minutes prior to the first significant –CG flash rate relative maximum. Total and –CG flash rates both decreased to relative minimum values at 2006 UTC (approximately 8 minutes prior to the wind event) before achieving absolute maximum values during the wind report. This minimum was partly due to a shift in the areas of large lightning density (LDAR II source and –CG flash) farther away from the radar-indicated cell location (not shown). The IC:CG ratio for the cell had relative maxima at 1951 and 2035 UTC and was nearly an absolute minimum during the wind event. The large –CG flash rates during the wind report contributed to the low IC:CG ratios (< 5) at this time. Positive CG flash rate and percent positive values were small throughout this storm's lifetime.

Lightning heights (95th percentile (lightning top), median, lower quartile, and peak source heights) are shown to be useful indicators of supercell strength in the first section. Figure 40 shows the evolution of these heights for the 27 May 2002 MCS cell. The lightning top was near 11 km MSL at 1916 UTC and then quickly lifted to over 13

km during the next volume scan. It then decreased to 12 km by 1946 before reaching a maximum altitude near 14 km MSL at 2001 UTC, 13 minutes before the high wind report. The lightning top remained elevated during the first half of the wind report, and then decreased to near 12 km MSL after the report. The other lightning heights (which were lower in elevation and are likely related to the updraft strength at lower-levels in the storm) followed a similar pattern, except they did not ascend at the initial stage of the storm. They decreased steadily until 1946 UTC and then ascended until peaking at 2006 UTC (8 minutes before the wind report). These trends did not have changes as drastic as those found with some supercells (i.e., first section, Fig. 16).

c. 16 June 2002

The 16 June 2002 MCS was a well-developed LLTS squall line, and the system's radar and total lightning characteristics are discussed by Carey et al. (2005). The cell analyzed in figure 41 was at the southern end of this system. The system produced severe straight line winds (27.7 m s^{-1}) during the time shown. The cell was part of a convective region which extended in a southwest-northeast orientation.

LDAR II source density values were significantly less than those associated with the other cells examined in this study, partially due to this storm's distance of 108 km west-southwest from the LDAR II network center (Fig. 29 shows a rapid decrease in flash DE in this region; see Appendix B for more details regarding range effects). Larger source density values (near 16 sources km^{-2} (5 minutes)$^{-1}$) were located at the northeastern section of the plot; these storms had similar mean reflectivity values as the cell being examined, but were closer to the LDAR II network centered at (25, 35 km).

Enhanced source densities (4-5 sources km^{-2} (5 minutes)$^{-1}$) were also associated with the northeastern quadrant (at -75, 20) of the analyzed storm. The reflectivity field in the plan view shows a significant weak echo notch less than 5 km to the northwest of the cell location shown by the asterisk. The wind report is located 14 km to the north-northeast from this feature in an area of weaker mean reflectivity (30 dBZ) also near another notch that almost extends through the line, suggesting the wind event may have occurred earlier than the report.

As in previous cases, maximum source density was above where reflectivity contours extended upward at x = -74 and -55 km in the x-height projection. However, the reflectivity bulge at y = 5 km had smaller source densities associated with it. There were 13 sources per flash (2475 sources and 185 flashes). Both source density and the number of flash origins peaked at 10 km MSL.

The wind report occurred while total flash rate was increasing and near a minimum in –CG flash rate (15 flashes (5 minutes)$^{-1}$) (Fig. 42). The –CG flash rate reached an absolute maximum at 0448 UTC, approximately 7 minutes (about 1 volume scan) prior to the wind event. The –CG flash rate had a steady decline later in the storm's lifetime (between 0518 and 0557 UTC). The total flash rate had two maxima, 60 and 50 flashes (5 minutes)$^{-1}$, at 0503 and 0538 UTC, respectively. These peaks had no relationship with the severe weather as they occurred after the report. Notice how the IC:CG ratios are very low (< 3) throughout the period (the number of –CG flashes outnumbered the total flashes between 0443 to 0453 and 0513 to 0528 UTC resulting in IC:CG ratios < 0); this was the result of the storm being greater than 100 km from the

LDAR II network. The number of sources and total flashes determined from the source data were not representative of the storm's lightning production as source detection efficiency is very small at this range (Carey et al. 2005, Appendix C shows relative detection efficiencies < 5% beyond 100 km range from the network). The total flash rate trends are also suspect as the storm was just coming into the range of the network and the initial large increase in total flash rate may be an artifact of this. Positive CG lightning production was insignificant as +CG flash rates and percent positive values were less than 3 flashes (5 minutes)$^{-1}$ and 8%, respectively.

The lightning-based storm top was at a relative minimum near 13 km MSL during the high wind report (Fig. 43). The lower quartile and median heights were also at relative minima near this time. After relative maxima in the heights at 0503 UTC, these values generally decreased until the end of the storm. The lightning top had variations of only 2 km during the cell's lifetime. The minima in all the lightning heights during the wind report and toward the later stages of the storm imply a weaker storm during those time intervals; -CG flash rate trends (Fig. 42) agree with this interpretation. The trend in the cell's radar top (Fig. 44) was similar to the lightning top. It had a minimum value (7 km MSL) at 0458 UTC near the time of the wind report. The radar top reached maximum altitudes at the same times as the lightning top shown in figure 43 (0503 and 0528 UTC).

4. Isolated, non-severe thunderstorm merger

The total lightning and mean reflectivity structure of two non-severe thunderstorms which occurred on 27 June 2001 is shown in figure 45. These cells

merged during their evolution. In comparison to the storms discussed in the previous subsection, these cells were isolated and not part of a large storm system. Each cell had an associated mean reflectivity and LDAR II source density maximum in the plan view. A developing cell to the northwest at (86, -9 km) had a maximum reflectivity value of 20 dBZ, was shallow in vertical extent, and had no lightning associated with it. The maximum lightning activity occurred downshear (south) of the reflectivity maxima, clearly in regions of reflectivity gradient. The cell located at x = 94 km had an elevated reflectivity core in the x-height projection, an indication of an ordinary thunderstorm in its mature stage (Byers and Braham 1949). The source density maxima occurred near 9 km MSL (immediately below the -40°C level) above each reflectivity core in the vertical projections. An increase in lightning activity is observed during the 6 minute period shown in the time-height panel, indicating the storms were strengthening. 705 sources and 56 flashes were associated with these two cells, an average of 13 sources per flash.

The two cells completely merged by 2115 UTC, approximately 24 minutes after the storms shown in figure 45. Figure 46 shows one core of reflectivity maximum and one area of large source density at (99, -19), south of the radar-inferred storm center. A region of > 13 sources km^{-2} (6 minutes)$^{-1}$ northeast of the source density absolute maximum was associated with the remnants of the eastern cell shown in figure 45. An anvil has developed with this storm, extending downshear of the storm center (see 10 dBZ contour in the plan view). The reflectivity gradient is large upshear (north) of the storm, where there was little lightning activity. Lower values of source density associated with the thunderstorm anvil extended 15 km south of the cell. As with figure

45, the maximum lightning activity was above where the reflectivity contours had the greatest vertical extent near the storm center. The maximum source density tilted downward following the reflectivity contours east of the storm in the west-east projection. The total number of sources increased dramatically from 705 to 1934 sources in figures 45 and 46, respectively. The total flash rate increased to 180 while the number of sources per flash decreased to 11 during this time period. The distance from the network center remained nearly constant between the time periods shown (86 and 89 km). Hence, the source detection efficiency was constant and the source density was a good indicator of storm intensity. The lightning activity significantly increased during and after the merger process.

The 27 June 2001 storm system reached its greatest vertical extent by 2118 UTC, suggesting it was most intense at this time (Fig. 47). This occurred immediately after the storm had merged as shown in figure 46. The 35 dBZ contour was near 10 km MSL for the first 4 volume scans; it rapidly increased to 13 km by 2118 UTC and then descended to near 10 km MSL again after 2130 UTC. The source density in figure 47 also indicated a more intense storm later in the period (after 2124 UTC) as these values increased to greater than 400 sources km^{-1} (6 minutes)$^{-1}$. The total flash rate shows a similar trend (Fig. 48). Total flash rate peaked at greater than 170 flashes (6 minutes)$^{-1}$ by 2118 UTC. CG flash rates (both negative and positive) had relatively small values (< 10 flashes (6 minutes)$^{-1}$) and showed little variation. Percent positive CG values increased during the second half of the storm, but +CG rates were quite small (3 or less +CG flashes (6 minutes)$^{-1}$); hence, the %+CG trends were not significant.

5. Lightning and radar reflectivity structures in convective and stratiform MCS regions

Convective and stratiform areas of an MCS are diagnosed subjectively in this section; convective regions are defined as having large values of mean reflectivity (> 40 dBZ) and reflectivity gradient and having reflectivity contours that extend upward. Enhanced LDAR II source densities were collocated with maxima in mean reflectivity within the 13 October 2001 mesoscale convective system (Fig. 49). The source density maxima identified intense storm cells (convection). The most intense cells were oriented in a south-north line along x = 40 km (see plan view and x-height projection). Reflectivity contours had a distinct upward protrusion at this position, and large source density values through most of the depth of the storm were associated with this feature in a vertical bimodal distribution. The source density contours attained higher altitudes at this position, and then extended downward to the west (rear) of the main line of thunderstorms into the stratiform region of the MCS. This corresponds very well with the lightning pattern in the line-normal vertical cross section of an LLTS squall line shown by Carey et al. (2005) (see their Fig. 3). Another bulge upward in the reflectivity contours occurred near x = 5 km in the west-east vertical projection. This was associated with a strong cell located at (5, -40) in the southern portion of the MCS. The southern and northern portions of the MCS were more complex than in the central portion; to the north were remnants of supercellular convection that produced a tornado over an hour before the time shown, while to the south two cells with mean reflectivity values in the plan view > 40 dBZ were oriented in a west-east direction. The anvil

extended 40 km behind the southern part of the system in the x-height projection and had minimal source density values west of the x = -10 km position.

There were two peaks of source density at 4 and 10 km MSL in figure 49 (near 0 and -40°C). Three peaks of flash origins occurred at 4, 8, and 11 km MSL. The two upper origin peaks were adjacent to the main source peak (above and below) and corresponded to regions of IC flash initiation while the origin peak at 4 km MSL was most likely associated with CG lightning production. More than 113000 LDAR II sources and 1355 flashes comprised this system, an average of 83 sources per flash while it was near the center of the LDAR II network.

Total lightning activity extended ahead (to the east) of the system according to the x-height and plan view panels of figure 49. Weak lightning activity (1-6 sources km^{-2} $(5\ minutes)^{-1}$) was approximately 20 km east of the main convective line between y = 0 and 50 km in areas of mean reflectivity between 10 to 20 dBZ (plan view). This feature was present in several of the analyzed volume scans during the lifetime of this system. Weak lightning activity also expanded westward into the stratiform region (mean reflectivity values 10-25 dBZ) after the convective cells had developed. The plan view of figure 49 is approximately centered on the LDAR II network at (25, 35 km). The cells farther from the center of the network (to the north and south) were of similar strength according to the projections of mean reflectivity (values and vertical extent), but had significantly different total lightning distributions, especially in the vertical projections. The source density distributions became unimodal as distance from the network increased, while the closer cells had distinct bimodal appearances. This effect

will be further discussed in Appendix C. Also, the altitudes of the lower-level source density contours systematically increased with distance from the center of the plot, especially in the south-north vertical projection. There was less low-level lightning activity detected at these greater ranges. This is the result of an instrument effect and is discussed in Appendix B.

Negative CG flashes were collocated with areas of convection (Fig. 50). Negative CG lightning activity was nearly nonexistent in the stratiform region of the MCS. Figures 49 and 50 show source density maxima were better collocated with large reflectivity values than –CG flash density partially because higher spatial resolution (1 vs. 5 km for CG density) was used to plot the source density values. The reflectivity "bridge" discussed by McCormick et al. (2002) is observed extending to the west-northwest from the convective line at y = 35 km. Enhanced source densities were associated with this feature (Fig. 49), but CG activity did not occur within the reflectivity bridge during this time period. The reflectivity bridge became wider at 0304 UTC, and 2 +CG flashes were produced within this region (not shown). The +CG flash density was also closely associated with portions of the convective region of the MCS (Fig. 51). Positive CG flash density values exceeded 0.18 flashes km^{-2} (5 minutes)$^{-1}$ within the intense storm cell at (45, 90). This cell's maximum mean reflectivity in the plan view was greater than 50 dBZ, and its large vertical development (the 35 dBZ contour was above 13 km MSL in both vertical projections) indicated this was an intense storm. Surprisingly, there were no severe storm reports associated with this storm near this time. Unlike the source density in figure 49, -/+CG activity was nonexistent behind

(west) and ahead (east) of the system. The above overall MCS lightning patterns persisted while the system was within 100 km range of the LDAR II network.

The lightning top, median, and peak source heights had little variation throughout the 13 October 2001 MCS lifetime (Fig. 52). The 95th percentile source height was between 13 and 14 km MSL. The variations in lightning top were significantly less than those shown for the 27 May 2002 storm (Fig. 40) and the supercells discussed in the first section. The only lightning height that changed significantly during the 2.5 hour period shown was the lower quartile height. It was near 9 km at 0122 UTC, then decreased to 6.5 km MSL at 0152 UTC. The lower quartile height returned to near 9 km MSL by 0302 UTC and remained at this altitude until the end of the period. The lower quartile height minimum occurred during the same time period when there was a significant lower region of large source density values (i.e., Fig. 49) and a strong bimodal height distribution signature was present.

Total flash rates were between 1200 and 1500 flashes (5 minutes)$^{-1}$ until 0307 UTC and then decreased rapidly to values less than 1000 flashes (5 minutes)$^{-1}$ after this time (Fig. 53). Negative CG flash rates were near 300 flashes (5 minutes)$^{-1}$ during the earlier stages (first 1.5 hours) of the system and then decreased significantly concurrently with the total flash rate. Portions of the MCS exited the analysis domain (200 by 200 km box centered on the LDAR II network) after 0312 UTC and this was the reason for the significant decrease in flash rates near this time. The total and –CG flash rates had similar trends throughout the period shown; there were relative maxima in both at 0127, near 0222, and near 0307 UTC, and both rates had relative minima near 0202,

0237, and 0302 UTC. Percent +CG values were between 10 and 20%, and the IC:CG ratio had small variations between 2 and 4 during this system's lifetime.

Figure 54 shows the system's –CG median peak current was larger than its +CG counterpart. Negative current values were between 16 and 18 kA while +CG currents were between 12 and 14 kA. Approximately 31% (13%) of the time periods (32 total) analyzed had –CG (+CG) maximum peak currents greater than or equal to 100 kA. Only –CG mean multiplicity (number of strokes per flash) shows significant variation in figure 54. Two –CG flash multiplicity maxima (3.0 and 3.3) occurred at 0237 and 0356 UTC.

6. Discussion and conclusions

As in the first section, this study examined total lightning behavior in addition to radar reflectivity data to discover repeatable signatures used to diagnose thunderstorm intensity and forecast severe weather. The majority of the severe weather associated with the cells in the mesoscale convective systems (MCSs) in this study was in the form of straight-line wind damage.

The most significant severe weather signature found in this study is the development of a lightning comma-shape/bow structure in the LDAR II plan view source density prior to (over 10 minutes in the 13 October 2001 case) and during severe wind reports (Figs. 30-31, 33, 35-37). This structure is quite similar to the radar-detected bow echo, which is associated with strong downbursts (Przybylinski 1995). Two hypotheses explain the bow feature in source density: 1) new thunderstorm cells develop along the bowing gust front, initiating lightning in an orientation similar to the

front, and 2) the strong winds advect charged cloud and precipitation particles ahead of the parent wind-producing thunderstorm and lightning propagates into these advected charge regions. The KFWS radar detected two altitudes (near 4 and 12 km MSL in Fig. 32) of strong outbound radial velocity values (30 m s^{-1} (storm-relative radial velocity 14 m s^{-1})) in the 13 October 2001 severe thunderstorm which are near two source peak heights in figure 30 (see histogram). The low-level velocity maxima is likely associated with the severe surface wind report while the upper one is likely storm top outflow (environmental winds were greater than 38 m s^{-1} from the southwest). The strong winds at these levels likely advected the charge regions identified by the source peaks in figure 30 and played a role in the plan view source density pattern. Examining several radar volume scans before and after the time period shown in figure 30 shows the initiation of a new cell at the apex in the reflectivity structure (the point where the reflectivity contours are most curved) initiated at 015437 UTC (one volume scan before that shown in Fig. 30). The mean reflectivity maximum (45 dBZ) at (41, 50) in figure 30 indicates this cell. The first hypothesis discussed above is supported by these observations; the strong low-level winds initiated a new cell which, in conjunction with the original cell, developed a total lightning comma-shape pattern as observed in figures 30, 33, and 35. This lightning pattern persisted for several volume scan time intervals (over 20 minutes).

Most of the lightning occurred in the upper-levels (above 6 km MSL) of the 27 May 2002 storm (Fig. 36). The low-level lightning was not detected because the storm was approximately 90 km from the LDAR II network (Appendix B discusses the range effects on low-level lightning detection by the LDAR II instrument). In contrast to the

13 October 2001 storm, there is only one reflectivity maximum elongated along a south-north axis in the plan view. Most of the total lightning activity is ahead (to the east) of the storm reflectivity core. The tilt of the reflectivity core in the west-east vertical projection of figure 36 indicates the cloud and precipitation particles were being advected by the environmental winds. The winds were from the west-southwest at 26 m s^{-1} near 10 km MSL according to the 1200 UTC 27 May 2002 FWD proximity sounding (storm-relative environmental winds were west-southwest at 10 m s^{-1}). This explains why the maximum LDAR II source densities are to the east of the storm core as the charge region centered at 10 km MSL was also advected on the cloud/precipitation particles at this level (supports second hypothesis above), but this does not explain the bow shape. Storm advection during the volume scan time interval can also partially explain the storm tilt: by the time the radar beam sampled the upper-levels of the storm, it propagated several km downstream (to the east) of where the radar sampled the storm during its first elevation scan. The storm shown in figures 36 and 37 developed as a series of cells from north to south. A new cell developed to the south (less than 5 km) of the original cell of this storm at 200813 UTC (not shown), followed by the development of a new cell to its south by 202303 UTC. Each one of these cells developed a bow structure in the source density and had associated reflectivity bow echoes or weak echo notches within the rear portion of the system. Inbound radial velocity values near -20 m s^{-1} (storm-relative radial velocity -5 m s^{-1}) indicate rear inflow occurred within these cells.

The evolution of lightning characteristics calculated within 10 km of the radar-identified storm cell must be examined with caution. Unlike the supercells examined in the first section, MCS cells are difficult to isolate. Hence, lightning from a nearby cell may contaminate the volume surrounding the cell of interest. The 10 km analysis radius was chosen because the 20 km radius ring frequently contained lightning from a nearby cell while the 5 km radius ring did not include a significant fraction of lightning associated with the storm. Tracking the 13 October 2001 and 27 May 2002 severe wind producing thunderstorms (Figs. 30 and 36) using WDSS-II also shows that most of the radar reflectivity of a storm is contained within 10 km of the cell location without significant contamination from other cells. MCS cells develop discretely (i.e., along gust fronts) near other cells, and the cell tracking shown by the WDSS-II software (using the SCIT algorithm; Johnson et al. 1998) is likely to have some error in cell identification.

A consistent relationship between the radar reflectivity and lightning characteristics of storm cells within an MCS and the severe weather they produce could not be found. Figure 34 shows that the vertical extent of the 13 October 2001 storm (denoted by the maximum heights of the reflectivity contours) began to decrease about 12 minutes prior to the wind report. However, the 27 May 2002 storm's wind event occurred while the storm intensified (vertical extent increased in figure 38). Note how the heights of maximum LDAR II source density remained constant throughout each storm's lifetime in figures 34 and 38, significantly different from the behavior observed during the lifetimes of tornadic supercells in the first section. Lightning flash rates (total

and CG) also had varying relations to severe weather. Consistent with the decreasing trend in the vertical extent of the 13 October 2001 storm, total, negative and positive CG flash rates decreased during the high wind report (not shown). However, total and –CG flash rates increased to maximum values during the high wind report on 27 May 2002 (Fig. 39). The increasing trend in total flash rate during the 27 May 2002 storm is partially due to the storm propagating closer to the LDAR II network with time from 118 to 76 km range (see Appendix B for range effects on source and total flash rates), but the large decrease in flash rates after the wind report in figure 39 shows this range effect is not significant enough to mask true flash rate trends (otherwise the rate would continue increasing as the storm moves closer). If the hypothesis that flash rates are a good measure of storm intensity is valid, the strong relationship between reflectivity development and lightning flash rates between figures 38 and 39 also supports that these trends are true. The total and –CG flash rates have opposite trends near the time of the 16 June 2002 high wind report (Fig. 42): total flash rate increases while the –CG rate decreases. This storm had nearby cells contaminating the lightning analysis and there was a large distance between the cell and wind report (Fig. 41) indicating there was a possible error in its association with the report. Lightning characteristics are good indicators of storm intensity if the MCS cells are isolated (no other cells within 10 km) as in the 27 May 2002 case. Percent positive values were quite small in all cases (< 10%) and the trends have no relation with severe weather.

The inconsistent relationships between storm cell radar and lightning characteristics with severe wind reports can further be explained by the dynamics

responsible for these strong surface winds. Bow-echo reflectivity structures and their associated winds (observed on 13 October and 27 May) are thought to be more the result of system processes, not necessarily directly related to individual convective cell downdrafts. The development of a rear inflow jet (see Wakimoto 2001 for an excellent review on the dynamics of MCS high wind events) that interacts with the convective downdrafts of a line of cells produces severe winds at the surface associated with bow echoes (and lightning source density bows). The cell characteristics calculated in this study (for the cells closest in time and space to the wind reports) may not be good indicators of how the storm system (composed of several cells) is evolving that is responsible for the severe winds. Hence, weak relations are expected between individual cell characteristics and MCS severe wind events.

Consistent with the findings of Mazur et al. (1986) and the first section (supercells), where reflectivity contours extend upward, the layer height and values of maximum source density are greater (see Figs. 30-31, 33, 36-37, 46, 49). These features indicate where the main storm updraft is located. A vertical bridge of enhanced source density connects the bimodal distribution of sources in figures 30, 31, and 33. The strong updraft at this location enhanced charging and hence lightning development within the vertical column encompassing the updraft. The height-y projection of figure 37 shows the maximum source density layer is at a higher altitude within the storm core (at y = -27 km) relative to the altitude of the lightning layer extending to the north of the core. To test the idea that the altitude of lightning activity can be used to infer storm strength, linear correlation coefficients between the lightning heights (lower quartile,

median, peak, and 95th percentile source altitudes (lightning top)) and a radar measure of storm intensity (radar top; maximum height of the storm 30 dBZ echo contour) were calculated. The correlation plot between radar top and lightning top is shown in figure 55 for the 27 May 2002 storm. The correlation coefficient is 0.19 (the r-squared value of 0.04 is shown), but it is not statistically significant at the p = 0.05 level. The 13 October 2001 MCS cell has a more significant correlation coefficient of 0.41 between these two variables (Fig. 56). Surprisingly, the correlation coefficients for the 27 May 2002 storm between radar top and the other lightning heights (lower quartile, median, and peak heights; not shown) are negative (r values near -0.40). The same coefficients for the 13 October 2001 storm are positive, except for the radar top – lower quartile source height coefficient. These results weakly support the hypothesis that lightning altitude is a measure of storm cell intensity within an MCS (in contrast, similar analysis for supercells in the first section (Table 1) strongly supports this hypothesis).

Two thunderstorm cells merged to become a more intense cell on 27 June 2001 (Figs. 45-48). The horizontal and vertical extent of lightning activity (shown by the LDAR II source density) increase during the 24 minute period between figures 45 and 46. The reflectivity structure also indicates a more intense storm by 2118 UTC: the altitudes of the upper reflectivity contours increase after the two cells completely merge (Fig. 47) and the maximum reflectivity increases from 40 to greater than 50 dBZ in the plan view (compare Figs. 45 and 46). The total flash rate also peaks after the merger (Fig. 48). The plan views of figures 45 and 46 indicate that most lightning activity (maximum source density) is downshear of the reflectivity cores (shear vector between

300 and 850 mb is from the north). Carey et al. (2003a) show storm intensification coincident with a supercell merging with a squall line approaching from the west. Storm echo heights significantly increased and a violent tornado developed in association with this cell merging process. A hypothesis for a more intense storm (with respect to radar reflectivity and lightning) resulting from a cell merger consistent with the above results is that the amount of precipitation particles aloft increases per unit volume of the storm. This increases collisions and coalescence of particles, increasing their size, and hence increasing the radar reflectivity factor and charge separation/lightning within a storm. Other studies have noticed storm intensification during cell merging and have hypothesized reduced dry air entrainment into the core updraft (Westcott 1984), deeper and stronger cold pools from the combined downdrafts of the merged system, and an ice seeding effect (new updrafts penetrating an ice crystal layer from older convection leading to more collisions and charge separation) to explain their observations (Carey and Rutledge 2000).

Carey et al. (2005) and Dotzek et al. (2005) discuss the reflectivity and total lightning structure of squall lines which occurred on 7-8 April 2002 and 16 June 2002, respectively, near Dallas-Fort Worth using similar data sets as in this study. As with the 13 October 2001 system analyzed here, these were leading-line, trailing stratiform (LLTS) MCSs. An individual cell that was associated with a severe wind report from the 16 June 2002 system is analyzed in subsection 3c. This presents an ideal situation to compare results between squall lines from different dates (and seasons) which used the same instrumentation (LDAR II and KFWS WSR-88D).

Radar reflectivity and lightning characteristics of the complete 13 October 2001 squall line (in contrast to the individual cell analysis) have many similarities to the results from Carey et al. (2005) and Dotzek et al. (2005). LDAR II source density is well associated with radar reflectivity in figure 49 (also shown by McCormick 2003 for this case). Source density and mean reflectivity contours slope downward behind (to the west of) the convective line (the region in the west-east vertical projection of Fig. 49 where reflectivity contours have a maximum upward extent defines the convective line). Carey et al. interpret this observation to support the charge advection hypothesis for stratiform region charging (Rutledge and MacGorman 1988). The in-situ charging mechanism, however, can not be rejected (Rutledge et al. 1990 and Carey et al.). The lightning bipole (separated regions of concentrated negative and positive CG flashes in the convective and stratiform regions of an MCS, respectively; Orville et al. 1988) is nonexistent during the 13 October 2001 case. Figures 50 and 51 show that both polarity flashes mostly occur within convection (this was true for each volume scan during the analyzed system lifetime); hence, separate analysis of convective and stratiform CG characteristics was not performed. Large values of +CG flash density are associated with a strong convective cell (35 dBZ reflectivity contour extends above 13 km MSL) in figure 51. The cell's position on the northern end of the squall line is unusual as strong storms dominated by +CGs typically occur on the southern end (MacGorman and Rust 1998, p. 278). This cell had strong updrafts which produced large liquid water contents that could lead to the growth and positive charging of graupel particles (Saunders 1993)

in the low-levels of the storm and enhanced +CG lightning production (e.g., Williams 2001).

The weak IC lightning activity to the east of the 13 October 2001 system is associated with the forward anvil of the squall line (Fig. 49). Even though CG flashes are not associated with this feature, it shows that the cloud is electrified 20 km ahead of the storm. This has an important implication for warning people of dangerous weather as lightning *could* propagate to the ground from the anvil well ahead of the system, and is also dangerous to nearby flying aircraft.

Lightning signatures related to storm cell intensity within MCSs include larger LDAR II source density and higher total flash rates as cells strengthen, thicker and elevated lightning layers associated with inferred updraft regions, and source density comma-shape/bow structures associated with high wind reports. Other cases need to be examined to test if these signatures are common with these storms and can be used by forecasters. The lightning characteristics calculated within 10 km of an MCS cell show some skill in determining storm intensity and relations with severe weather. They are not as useful as with supercells (first section) likely because these cells are not well-isolated and interact with nearby cells. MCS cells also discretely develop and radar algorithms (SCIT) have difficulties in tracking them. However, analyzing trends in individual thunderstorm cell characteristics show more variation than total system characteristics (compare Figs. 39 and 53). If total lightning data will be used to diagnose/predict intensity changes and severe weather occurrence, it is recommended to use cell analysis. Future research should focus on how to better isolate lightning with a

particular storm cell (i.e., isolate lightning flashes whose *origins* are within 10 km of a cell as opposed to determining flashes using all sources within that radius).

CORRELATION ANALYSIS BETWEEN STORM CHARACTERISTICS

The first and second major sections have shown support for the hypothesis that storm lightning characteristics are related to the storm's dynamics (i.e., updraft strength and flash rate are directly related). The strength of a thunderstorm's updraft was inferred from radar characteristics such as maximum reflectivity and storm top. Whereas correlations do not show cause and effect, this section tests the significance of certain relationships between storm characteristics (lightning and radar) determined in the first and second sections. Table 3 shows the correlation coefficients between several radar and lightning parameters for five different storm events; these events occurred in different seasons and were of differing storm types (supercells, squall line, and isolated cells). Consistently significant correlations across these events strongly support the reliability in using a particular relationship to predict storm characteristics.

Lightning and radar data were from the LDAR II instrument, NLDN, and KFWS WSR-88D radar (see first section, Data and methodology for more details). The strongest and weakest (with maximum reflectivity above 45 dBZ) storm cells were chosen from each volume scan during each event shown in Table 3 using the WDSS-II software (Hondl 2003) to obtain an appreciable sample size (> 50 samples in each event). Specific cells were not tracked in this section as in previous sections (though some cells were repeatedly sampled if they were the strongest cell over several volume scans for example); this is more of a random sample. Storm cells were ranked according to strength by WDSS-II using reflectivity and radial velocity characteristics. Table 3 shows radar characteristics associated with these cells that were recorded and lightning

characteristics that were calculated using data within a 10 km radius of the storm (or mesocyclone; 13 October supercell case) location given by WDSS-II and over the duration of a volume scan (approximately 5 minutes). Linear correlation coefficients were then calculated between the storm characteristics. To test the significance of these correlations (reject the null hypothesis r = 0), the t-statistic (Neter and Wasserman 1974) was calculated:

$$t = \frac{r * \sqrt{(n - 2)}}{\sqrt{(1 - r^2)}}, \quad (1)$$

$$df = n - rp - 2, \quad (2)$$

where r is the correlation coefficient, n is the sample size (number of pairs), df is the number of degrees of freedom, and rp is the number of cells which occurred more than once (repeats) in the sample. Equation (2) was recommended by Preston (2004, personal communication) as a best estimate for the number of independent measurements.

The following correlations were of consistent sign (all positive/all negative) with each case in Table 3: neg-nmul, Ltop-thick1, Ltop-dist, rtop-nfl, shi-nfl, vil-nfl, vil-dens, shi-dens, and shi-pos. The lightning top is shown in the first section to be a good measure of thunderstorm updraft strength (Table 1). LDAR II source density maps charge layers, especially positive charge regions (Rison et al. 1999). The thickness of a LDAR II source-defined charge region (thick1) was determined using the height histogram of source density and calculating the distance between the half-peak points of the major peak. As an updraft intensifies, the distance between thunderstorm charge regions decreases and multiple charge layers appear as one thick charging zone at the

low vertical resolution used in this study (1 km). The positive correlations between the lightning top and inferred charge region thickness (statistically significant for the 13 October 2001 supercell and 27 June 2001 isolated cell) support this hypothesis. The greater Ltop-thick1 coefficients were calculated for isolated convection (r = 0.50 and 0.73 for the supercell and pulse storm events, respectively).

Significantly positive correlations between radar and lightning storm characteristics support the hypothesis that lightning is dependent on the dynamics and microphysics of thunderstorms. The severe hail index (SHI) and vertically integrated liquid water (VIL) are measures of the amount of precipitation mass above the melting level and through the whole depth of the storm, respectively (Witt et al. 1998, Johnson et al. 1998). Both are related to storm strength (stronger updrafts develop more and larger precipitation particles). Lightning parameters are expected to be better correlated with a storm cell's SHI value than with VIL because charge separation and lightning is strongly dependent on the presence of supercooled water and ice in a cloud (Williams 2001). The correlation coefficients calculated between the SHI and the total flash rate had similar values as between VIL and the flash rate for each case (i.e., r values for the 27 June case shi-nfl and vil-nfl were 0.78 and 0.83, respectively). Hence, the above hypothesis is not supported: SHI is not a *better* predictor of lightning than VIL. The coefficients were statistically significantly positive for all cases suggesting the total flash rate can be used to diagnose storm intensity. The correlation analysis for SHI and VIL related to CG flash density shows similar results as with the total flash rate. The SHI and VIL had maximum correlation coefficients with CG flash density for the 27 June case (r = 0.84

for the shi-dens and 0.81 for the vil-dens correlations). To better test the relationship between lightning frequency and ice, polarimetric radar (not available in this study) is favorable (i.e., precipitation ice mass and ice mass flux can be derived using this data).

Seventy percent (21 out of 30) of the correlation coefficients between storm characteristics in the 27 June case shown in Table 3 were statistically significant. Most coefficients had maximum magnitudes in this case; i.e., the coefficient between radar top and lightning storm top was 0.91 for 27 June, followed by 0.22 for the 13 October 2001 supercell case. Fifty-seven percent (17/30) of the supercell correlations were also statistically significant. Only 40% of the 13 October squall case correlations were statistically significant. Storm cell characteristics calculated in this study are more accurate in describing a cell that is more isolated, as in the 27 June pulse and 13 October supercell cases. Radar reflectivity and lightning contamination from nearby cells in the two squall and MCS cases resulted in more inaccurate calculations of these characteristics for a particular storm. Cell interactions (i.e., mergers) disrupted cell development which can result in weaker correlation coefficients between storm intensity measurands. Hence, the relationships shown in Table 3 are best applied to isolated convection events.

Is there a relationship between hail development and the polarity of CG flashes in thunderstorms? Several studies implicate CG polarity is related to storm intensity and severe weather (i.e., Reap and MacGorman 1989, Carey and Rutledge 2003, and Carey et al. 2003a, b). The correlation coefficients between the SHI and %+CG values present inconclusive evidence for hypotheses relating hail and +CG lightning. The coefficients

were weakly negative for all but the 27 June isolated storm case. The 27 June case had the most significant coefficient (r = 0.64), but didn't produce any severe weather. Fuquay (1982) shows weaker pulse storms (like the 27 June storm) have their most significant +CG flash rates during their decay, an observation inconsistent with the 27 June correlation (stronger (greater SHI) storms produced more +CG lightning). The coefficients between SHI and +CG flash density were more convincing (all positive and most statistically significant), but most samples contained few +CG flashes (< 5). In fairness to the above studies, strong relationships between CG polarity and severe weather mostly have occurred for storms in the U.S. northern plains and this study is focused on the southern plains (near Dallas, TX). Also, these previous studies concentrated on cases where storms were predominantly positive (> 50% +CG) and had significant positive flash densities for a significant fraction of their lifetimes, which none of the cases in this study had.

The coefficients between –(+)CG flash rate and –(+)median peak current were small (< 0.31) and varied in sign between the cases (Table 3). The electrical behavior of *some* of the MCSs in MacGorman and Morgenstern (1998) support the hypothesis that as a storm's CG flash rate increases the median current decreases because there is less charge available in the flash source region of the cloud. However, *most* of the MCSs in MacGorman and Morgenstern show flash rate and current to be independent of each other and the lack of significant negative correlations between these two variables in this study show storm electrical behavior is more complicated than the above hypothesis suggests.

The only statistically significant positive correlation between lightning top (an updraft proxy) and total flash rate was calculated for the 27 June case (r = 0.71). The Ltop-nfl coefficients associated with the other cases are not supportive of the hypothesis that lightning rates are strongly related to updraft speed (Baker et al. 1995) if the lightning top is accepted as a good updraft proxy (note, however, the weak rtop-Ltop coefficients except for the 27 June case). The correlation coefficients between radar top (another updraft proxy) and total flash rate are more convincing (all significantly positive except for the 16 June case). Storm interactions (discussed above) can partially explain the weaker coefficients with the non-isolated events. The correlation coefficient between the lightning top and IC:CG ratio for the 27 June case had a statistically significant value of 0.65. This observation supports the elevated charge region hypothesis of MacGorman et al. (1989): as a storm's updraft intensifies, the main negative charge region is uplifted and brought closer to the main positive charge region typically located higher in the storm, and IC flashes become more frequent and CG flash rates decrease. Two cases (13 October supercell and 16 June squall) had statistically significantly negative correlation coefficients (-0.54 and -0.59), however, which does not support the elevated charge region hypothesis.

SUMMARY

The utility of total lightning data in warning for severe weather is best summarized by meteorologists who have already used this data operationally: "Several correct warning decisions have been made due to data provided by the North Alabama Lightning Mapping Array, including decisions not to warn in several cases" (Bridenstine et al. 2005). Trends in lightning flash rate (especially total) and lightning altitude can serve as proxies for changes in updraft strength (and hence storm severity).

Total and -CG flash rates peaked approximately 10 minutes prior to tornado touchdown in two cases. Of course more tornadic cases with this total lightning data need to be examined to test how repeatable this observation is. These rates have been shown to be correlated with radar measures of updraft strength: the more vigorous an updraft becomes, the larger the flash rates. The elevated charge region hypothesis was not supported; IC:CG ratio values generally did not increase with storm updraft strength proxies (i.e., radar top). Possible errors with the flash algorithm (more testing needs to be done to see how realistic the values from these algorithms are) and poor source detection efficiency at ranges greater than 100 km can partially explain why this hypothesis was not supported. There was also no relationship between a storm's positive CG lightning production and severe weather as in previous studies (conducted mostly in the northern plains of the U.S. and examined high +CG flash density storms; neither condition applied to most of the storms in this study).

A distinct lightning hole associated with an intense supercellular updraft was apparent in one case (6 April 2003), but was not observed in any of the other severe

storm case studies. Hence, it may be a useful tool only with the most severe storms (like a hook echo). A feature associated with high wind events within squall lines was that of a lightning source density bow or comma-shape. This feature can be used much like the radar reflectivity bow echo in detecting storms capable of producing severe wind speeds. Detecting a lightning bow can add situational awareness to a forecasting environment, especially because total lightning density patterns can be examined more frequently than radar data (i.e., update a lightning plot every minute). The presence of a distinct couplet of –CG flash density in supercell thunderstorms was a new finding in this study. More cases should be examined to observe if this is a common feature of supercells (during some part of their lifetimes) and what it means to the dynamics of these storms.

Most of the analysis shows maximum lightning activity (LDAR II source density) within regions of reflectivity gradient. This supports the hypothesis that charge separation is greatest near the updraft/downdraft interfaces of storms (Dye et al. 1986). It was also shown that when storms merge, they can produce a more intense thunderstorm (based on radar and lightning characteristics).

The relationship between lightning characteristics and storm behavior (dynamics and microphysics) is a complex one. It is generally thought that as a storm intensifies (defined by updraft speed), flash production increases because more collisions of ice particles in the presence of supercooled water are likely leading to more charge separation. Unfortunately with this study, direct measurements of vertical wind speed within storms were not available. Radar properties, such as VIL and radar-defined storm top, were used as proxies for updraft strength. Future research with total lightning data

needs to include multiple-Doppler radar analysis of storms so vertical wind speed magnitudes can be deduced and related to lightning production.

The vertical distribution of LDAR II sources was mostly unimodal, but sometimes two distinct layers of lightning activity were present (i.e., 13 October squall line). It is speculated in Appendix C this was the result of an instrument effect (bimodal distributions were observed only within 50 km of the network center), but this effect does not explain unimodal distributions within 50 km from the network. Flash grouping algorithms also must be improved. Total flash rate trends appeared reasonable, but values were suspect, especially in high rate situations and when a storm was far from the network center (> 100 km). A significant reduction in source detection efficiency with range prohibits using these data for storm characterization at far ranges (see Figs. 2, 3, 28, and 29).

The most significant finding in this research was the use of storm cell lightning heights (i.e., 95^{th} percentile source altitude/lightning top) to diagnose changes in storm intensity. A relatively higher altitude of lightning activity given by lightning mappers like the LMA and LDAR II can serve as a proxy for thunderstorm updraft location and strength. Significant positive correlations between radar and lightning storm properties (i.e., radar and lightning top) support this claim. The altitude of the lightning layer in the vertical projections of LDAR II source density and mean reflectivity was higher where reflectivity protruded upward. Future research including a climatological survey of storm lightning heights (using different storm types, geographical regions, seasons, etc.) and correlating these characteristics to radar measures of storm intensity (i.e., radar top

as done in this study) will help to support/deny this hypothesis. Lightning height information is only available with *total* lightning networks and can be calculated faster (2 minute sampling intervals have been suggested by MacGorman 2005 and Goodman 2005, personal communication) than radar storm characteristics (i.e., it takes at least 5 minutes for VIL to be measured by radar and calculated).

REFERENCES

Baker, M. B., H. J. Christian, and J. Latham, 1995: A computational study of the relationships linking lightning frequency and other thundercloud parameters. *Quart. J. Roy. Meteor. Soc.*, **121**, 1525-1548.

Bluestein, H. B., and D. R. MacGorman, 1998: Evolution of cloud-to-ground lightning characteristics and storm structure in the Spearman, Texas tornadic supercells of 31 May 1990. *Mon. Wea. Rev.*, **126**, 1451-1467.

Boccippio, D. J., S. Heckman, and S. J. Goodman, 2000: A diagnostic analysis of the Kennedy Space Center LDAR network: 1. Data characteristics. *J. Geophys. Res.*, **106**, 4769-4786.

Branick, M. L., and C. A. Doswell III, 1992: An observation of the relationship between supercell structure and lightning ground-strike polarity. *Wea. Forecasting*, **7**, 143-149.

Bridenstine, P. V., C. B. Darden, J. Burks, and S. J. Goodman, 2005: The application of total lightning data in the warning decision making process. *Extended Abstracts*, *Conf. on Meteorological Applications of Lightning Data*, San Diego, CA, Amer. Meteor. Soc., CD preprints.

Bruning, E. C., D. Rust, D. R. MacGorman, P. R. Krehbiel, R. Thomas, W. Rison, T. Hamlin, and J. Harlin, 2002: Thunderstorm charge regions inferred from the vector electric field in combination with data from a lightning mapping array in STEPS. *Eos Trans. AGU*, **83**, Fall Meet. Suppl., Abstract A71B-0095.

Byers, H. R., and R. R. Braham, Jr., 1949: *The Thunderstorm*. Supt. of Documents, U.S. Government Printing Office, Washington, DC, 287 pp.

Carey, L. D., and S. A. Rutledge, 1996: A multiparameter radar case study of the microphysical and kinematic evolution of a lightning producing storm. *Meteorology and Atmospheric Physics*, **59**, 33-64.

Carey, L. D., and S. A. Rutledge, 1998: Electrical and multiparameter radar observations of a severe hailstorm. *J. Geophys. Res.*, **103**, 13979-14000.

Carey, L. D., and S. A. Rutledge, 2000: The relationship between precipitation and lightning in tropical island convection: A C-band polarimetric radar study. *Mon. Wea. Rev.*, **128**, 2687-2710.

Carey, L. D., and S. A. Rutledge, 2003: Characteristics of cloud-to-ground lightning in severe and nonsevere storms over the central United States from 1989-1998. *J. Geophys. Res.*, **108**, doi: 10.1029/2002JD002951.

Carey, L. D., W. A. Petersen, and S. A. Rutledge, 2003a: Evolution of cloud-to-ground lightning and storm structure in the Spencer, South Dakota, tornadic supercell of 30 May 1998. *Mon. Wea. Rev.*, **131**, 1811-1831.

Carey, L. D., S. A. Rutledge, and W. A. Petersen, 2003b: The relationship between severe storm reports and cloud-to-ground lightning polarity in the contiguous United States from 1989 to 1998. *Mon. Wea. Rev.*, **131**, 1211-1228.

Carey, L. D., M. J. Murphy, T. L. McCormick, and N. W. S. Demetriades, 2005: Lightning location relative to storm structure in a leading-line, trailing-stratiform

mesoscale convective system. *J. Geophys. Res.*, **110**, doi: 10.1029/2003JD004371.

Coleman, L., T. Marshall, M. Stolzenburg, P. Krehbiel, R. Thomas, and D. Shown, 2000: Comparison of thunderstorm charge location indicated by the lightning mapping array (LMA) and by balloon electric field soundings. *Eos Trans. AGU*, **81**, Fall Meet. Suppl., Abstract A52C-27.

Cummins, K. L., M. J. Murphy, E. A. Bardo, W. L. Hiscox, R. B. Pyle, and A. E. Pifer, 1998: A combined TOA/MDF technology upgrade of the U. S. National Lightning Detection Network. *J. Geophys. Res.*, **103**, 9035-9044.

Cummins, K. L., M. J. Murphy, and J. V. Tuel, 2000: Lightning detection methods and meteorological applications. Preprints, *4th International Symposium on Military Meteorology*, Malbork, Poland, 85-100.

Demetriades, N., M. J. Murphy, and K. L. Cummins, 2001: Cloud and cloud-to-ground lightning detection at LF and VHF: Early results from Global Atmospherics Dallas-Fort Worth LDAR II and IMPACT/ESP research networks. *Eos Trans. AGU*, **82**, Fall Meet. Suppl., Abstract AE21A-07.

Detwiler, A. G., J. H. Helsdon, D. V. Kliche, Q. Mo, and T. A. Warner, 2002: Lightning characteristics of two storms observed during STEPS. Preprints, *21st Severe Local Storms Conf.*, San Antonio, TX, Amer. Meteor. Soc., 311-314.

Dye, J. E., J. J. Jones, W. P. Winn, T. A. Cerni, B. Gardiner, D. Lamb, R. L. Pitter, J. Hallett, and C. P. R. Saunders, 1986: Early electrification and precipitation

development in a small, isolated Montana cumulonimbus. *J. Geophys. Res.*, **91**, 1231-1247.

Dotzek, N., H. Höller, C. Théry, and T. Fehr, 2001: Lightning evolution related to radar-derived microphysics in the 21 July 1998 EULINOX supercell storm. *Atmos. Res.*, **56**, 335-354.

Dotzek, N., R. M. Rabin, L. D. Carey, D. R. MacGorman, T. L. McCormick, N. W. Demetriades, M. J. Murphy, and R. L. Holle, 2005: Lightning activity related to satellite and radar observations of a mesoscale convective system over Texas on 7-8 April 2002. *Atmos. Res.*, in press.

Fuquay, D. M., 1982: Positive cloud-to-ground lightning in summer thunderstorms. *J. Geophys. Res.*, **87**, 7131-7140.

Goodman, S. J., and D. R. MacGorman, 1986: Cloud-to-ground lightning activity in mesoscale convective complexes. *Mon. Wea. Rev.*, **114**, 2320-2328.

Harlin, J. D., T. D. Hamlin, P. R. Krehbiel, R. J. Thomas, W. Rison, and D. Shown, 2000: LMA observations of tornadic storms during STEPS 2000. *Eos Trans. AGU*, **81**, Fall Meet. Suppl., Abstract A52C-25.

Hondl, K. D., 2003: Capabilities and components of the Warning Decision Support System - Integrated Information (WDSS-II). Preprints, *19th Conf. On Interactive Info. Processing Systems*, Long Beach, CA, Amer. Meteor. Soc., CD preprints.

Houze, R. A., Jr., B. F. Smull, and P. Dodge, 1990: Mesoscale organization of springtime rainstorms in Oklahoma. *Mon. Wea. Rev.*, **118**, 613-654.

Johnson, J. T., P. L. MacKeen, A. Witt, E. D. Mitchell, G. J. Stumpf, M. D. Eilts, and K. W. Thomas, 1998: The storm cell identification and tracking algorithm: An enhanced WSR-88D algorithm. *Wea. Forecasting*, **13**, 263-276.

Krehbiel, P. R., R. J. Thomas, W. Rison, T. Hamlin, J. Harlin, and M. Davis, 2000: GPS-based mapping system reveals lightning inside storms. *EOS*, **81**, 21-22, 25.

Lang, T. J., and S. A. Rutledge, 2002: Relationships between convective storm kinematics, precipitation, and lightning. *Mon. Wea. Rev.*, **130**, 2492-2506.

Lemon, L. R., and C. A. Doswell III, 1979: Severe thunderstorm evolution and mesocyclone structure as related to tornadogenesis. *Mon. Wea. Rev.*, **107**, 1184-1197.

MacGorman, D. R., and K. E. Nielsen, 1991: Cloud-to-ground lightning in a tornadic storm on 8 May 1986. *Mon. Wea. Rev.*, **119**, 1557-1574.

MacGorman, D. R., and D. W. Burgess, 1994: Positive cloud-to-ground lightning in tornadic storms and hailstorms. *Mon. Wea. Rev.*, **122**, 1671-1697.

MacGorman, D. R., and C. D. Morgenstern, 1998: Some characteristics of cloud-to-ground lightning in mesoscale convective systems. *J. Geophys. Res.*, **103**, 14011-14023.

MacGorman, D. R., and W. D. Rust, 1998: *The Electrical Nature of Storms*. Oxford University Press, 422 pp.

MacGorman, D. R., A. A. Few, and T. L. Leer, 1981: Layered lightning activity. *J. Geophys. Res.*, **86**, 9900-9010.

MacGorman, D. R., D. W. Burgess, V. Mazur, W. D. Rust, W. L. Taylor, and B. C. Johnson, 1989: Lightning rates relative to tornadic storm evolution on 22 May 1981. *J. Atmos. Sci.*, **46**, 221-250.

MacGorman, D., D. Rust, O. van der Velde, M. Askelson, P. Krehbiel, R. Thomas, B. Rison, T. Hamlin, and J. Harlin, 2002: Lightning relative to precipitation and tornadoes in a supercell storm during MEAPRS. Preprints, *21st Severe Local Storms Conf.*, San Antonio, TX, Amer. Meteor. Soc., 423-426.

Mansell, E. R., D. R. MacGorman, C. Ziegler, and J. M. Straka, 2002: Simulated three-dimensional branched lightning in a numerical thunderstorm model. *J. Geophys. Res.*, **107**, 10.1029/2000JD00244.

Mazur, V., and W. D. Rust, 1983: Lightning propagation and flash density in squall lines as determined with radar. *J. Geophys. Res.*, **88**, 1495-1502.

Mazur, V., W. D. Rust, and J. C. Gerlach, 1986: Evolution of lightning flash density and reflectivity structure in a multicell thunderstorm. *J. Geophys. Res.*, **91**, 8690-8700.

McCaul, E. W., J. Bailey, S. J. Goodman, R. Blakeslee, J. Hall, D. E. Buechler, and T. Bradshaw, 2002: Preliminary results from the North Alabama lightning mapping array. Preprints, *21st Severe Local Storms Conf.*, San Antonio, TX, Amer. Meteor. Soc., 427-430.

McCormick, T. L., 2003: Three-dimensional radar and total lightning characteristics of mesoscale convective systems. M.S. thesis, Dept. of Marine, Earth, and Atmospheric Sciences, North Carolina State University, 354 pp.

McCormick, T. L., L. D. Carey, M. J. Murphy, and N. W. Demetriades, 2002: Three-dimensional radar and total lightning characteristics of mesoscale convective systems. *Eos Trans. AGU*, **83**, Fall Meet. Suppl., Abstract A71B-0093.

Murphy, M. J., and N. W. S. Demetriades, 2005: An analysis of lightning holes in a DFW supercell storm using total lightning and radar information. *Extended Abstracts*, *Conf. on Meteorological Applications of Lightning Data*, San Diego, CA, Amer. Meteor. Soc., CD preprints.

NCDC, 2001: *Storm Data*. Vol. 43, No. 10, 174 pp. [Available from National Climatic Data Center, Federal Building, 151 Patton Ave., Asheville, NC 28801.]

NCDC, 2002a: *Storm Data*. Vol. 44, No. 5, 420 pp. [Available from National Climatic Data Center, Federal Building, 151 Patton Ave., Asheville, NC 28801.]

NCDC, 2002b: *Storm Data*. Vol. 44, No. 6, 354 pp. [Available from National Climatic Data Center, Federal Building, 151 Patton Ave., Asheville, NC 28801.]

Neter, J., and W. Wasserman, 1974: *Applied Linear Statistical Models: Regression, Analysis of Variance, and Experimental Designs*. Richard D. Irwin, Inc., 842 pp.

Orville, R. E., and G. R. Huffines, 1999: Lightning ground flash measurements over the contiguous United States: 1995-1997. *Mon. Wea. Rev.*, **127**, 2693-2703.

Orville, R. E., R. W. Henderson, and L. F. Bosart, 1988: Bipole patterns revealed by lightning locations in mesoscale storm systems. *Geophys. Res. Lett.*, **15**, 129-132.

Oye, D., and M. Case, 1995: *REORDER: A Program for Gridding Radar Data, Installation and Use Manual for the UNIX Version*. NCAR Atmospheric Technology Division, Boulder, CO, 19 pp.

Perez, A. H., L. J. Wicker, and R. E. Orville, 1997: Characteristics of cloud-to-ground lightning associated with violent tornadoes. *Wea. Forecasting*, **12**, 428-437.

Petersen, W. A., and S. A. Rutledge, 1992: Some characteristics of cloud-to-ground lightning in tropical Northern Australia. *J. Geophys. Res.*, **97**, 11553-11560.

Proctor, D. E., 1991: Regions where lightning flashes began. *J. Geophys. Res.*, **96**, 5099-5112.

Przybylinski, R. W., 1995: The bow echo: Observations, numerical simulations, and severe weather detection methods. *Wea. Forecasting*, **10**, 203-218.

Rakov, V. A., and M. A. Uman, 2003: *Lightning: Physics and Effects*. Cambridge University Press, 687 pp.

Ray, P. S., D. R. MacGorman, W. D. Rust, W. L. Taylor, and L. W. Rasmussen, 1987: Lightning location relative to storm structure in a supercell storm and a multicell storm. *J. Geophys. Res.*, **92**, 5713-5724.

Reap, R. M., and D. R. MacGorman, 1989: Cloud-to-ground lightning: Climatological characteristics and relationships to model fields, radar observations, and severe local storms. *Mon. Wea. Rev.*, **117**, 518-535.

Rison, W., R. J. Thomas, P. R. Krehbiel, T. Hamlin, and J. Harlin, 1999: A GPS-based three-dimensional lightning mapping system: Initial observations in Central New Mexico. *Geophys. Res. Lett.*, **26**, 3573-3576.

Rust, W. D., W. L. Taylor, and D. MacGorman, 1982: Preliminary study of lightning location relative to storm structure. *AIAA Journal*, **20**, 404-409.

Rutledge, S. A., and D. R. MacGorman, 1988: Cloud-to-ground lightning activity in the 10-11 June 1985 mesoscale convective system observed during the Oklahoma-Kansas PRE-STORM project. *Mon. Wea. Rev.*, **116**, 1393-1408.

Rutledge, S. A., C. Lu, and D. R. MacGorman, 1990: Positive cloud-to-ground lightning in mesoscale convective systems. *J. Atmos. Sci.*, **47**, 2085-2100.

Saunders, C. P. R., 1993: A review of thunderstorm electrification processes. *J. Appl. Meteor.*, **32**, 642-655.

Saunders, C. P. R., and I. M. Brooks, 1992: The effects of high liquid water content on thunderstorm charging. *J. Geophys. Res.*, **97**, 14671-14676.

Schuur, T. J., B. F. Smull, W. D. Rust, and T. C. Marshall, 1991: Electrical and kinematic structure of the stratiform precipitation region trailing an Oklahoma squall line. *J. Atmos. Sci.*, **48**, 825-841.

Seimon, A., 1993: Anomalous cloud-to-ground lightning in an F5-tornado-producing supercell thunderstorm on 28 August 1990. *Bull. Amer. Meteor. Soc.*, **74**, 189-203.

Sharp, D. W., 2005: Operational applications of lightning data at WFO Melbourne, FL: A 15-year retrospective. *Extended Abstracts*, *Conf. on Meteorological Applications of Lightning Data*, San Diego, CA, Amer. Meteor. Soc., CD preprints.

Stolzenburg, M., T. C. Marshall, W. D. Rust, and B. F. Smull, 1994: Horizontal distribution of electrical and meteorological conditions across the stratiform region of a mesoscale convective system. *Mon. Wea. Rev.*, **122**, 1777-1797.

Stolzenburg, M., W. D. Rust, B. F. Smull, and T. C. Marshall, 1998a: Electrical structure in thunderstorm convective regions, 1. Mesoscale convective systems. *J. Geophys. Res.*, **103**, 14059-14078.

Stolzenburg, M., W. D. Rust, and T. C. Marshall, 1998b: Electrical structure in thunderstorm convective regions, 2. Isolated storms. *J. Geophys. Res.*, **103**, 14079-14096.

Stolzenburg, M., W. D. Rust, and T. C. Marshall, 1998c: Electrical structure in thunderstorm convective regions, 3. Synthesis. *J. Geophys. Res.*, **103**, 14097-14108.

Storm Prediction Center, cited 2005: Storm reports. [Available on-line from http://spc.noaa.gov/climo/.]

Stumpf, G. J., A. Witt, E. D. Mitchell, P. L. Spencer, J. T. Johnson, M. D. Eilts, K. W. Thomas, and D. W. Burgess, 1998: The National Severe Storms Laboratory mesocyclone detection algorithm for the WSR-88D. *Wea. Forecasting*, **13**, 304-326.

Thomas, R. J., P. R. Krehbiel, W. Rison, T. Hamlin, J. Harlin, and D. Shown, 2001: Observations of VHF source powers radiated by lightning. *Geophys. Res. Lett.*, **28**, 143-146.

Thomas, R., P. Krehbiel, W. Rison, J. Harlin, T. Hamlin, and N. Campbell, 2003: The LMA flash algorithm. *Proc.*, *International Commission on Atmospheric Electricity*, Versailles, France, Available on CD.

Thomas, R. J., P. R. Krehbiel, W. Rison, S. J. Hunyady, W. P. Winn, T. Hamlin, and J. Harlin, 2004: Accuracy of the lightning mapping array. *J. Geophys. Res.*, **109**, doi: 10.1029/2004JD004549.

Wakimoto, R. M., 2001: Convectively driven high wind events. *Severe Convective Storms*, *Meteor. Monogr.*, No. 50, Amer. Meteor. Soc., 255-298.

Weisman, M. L., and J. B. Klemp, 1986: Characteristics of isolated convective storms. *Mesoscale Meteorology and Forecasting*, P. S. Ray, Ed., American Meteorological Society, 331-358.

Westcott, N., 1984: A historical perspective on cloud mergers. *Bull. Amer. Meteor. Soc.*, **65**, 219-226.

Wiens, K. C., S. A. Tessendorf, and S. A. Rutledge, 2002: June 29, 2000 STEPS supercell storm: Relationships between kinematics, microphysics, and lightning. Preprints, *21st Severe Local Storms Conf.*, San Antonio, TX, Amer. Meteor. Soc., 315-318.

Wiens, K. C., S. A. Tessendorf, and S. A. Rutledge, 2003: STEPS June 29, 2000 supercell: Observations of kinematic, microphysical, and electrical structure. *Proc.*, *International Commission on Atmospheric Electricity*, Versailles, France, Available on CD.

Williams, E. R., 2001: The electrification of severe storms. *Severe Convective Storms*, *Meteor. Monogr.*, No. 50, Amer. Meteor. Soc., 527-561.

Williams, E. R., C. M. Cooke, and K. A. Wright, 1985: Electrical discharge propagation in and around space charge clouds. *J. Geophys. Res.*, **90**, 6059-6070.

Williams, E. R., B. Boldi, A. Matlin, M. Weber, S. Hodanish, D. Sharp, S. Goodman, R. Raghavan, and D. Buechler, 1999: The behavior of total lightning activity in severe Florida thunderstorms. *Atmos. Res.*, **51**, 245-265.

Witt, A., M. D. Eilts, G. J. Stumpf, J. T. Johnson, E. D. Mitchell, and K. W. Thomas, 1998: An enhanced hail detection algorithm for the WSR-88D. *Wea. Forecasting*, **13**, 286-303.

Ziegler, C. L., and D. R. MacGorman, 1994: Observed lightning morphology relative to modeled space charge and electric field distributions in a tornadic storm. *J. Atmos. Sci.*, **51**, 833-851.

Ziegler, C. L., E. R. Mansell, D. R. MacGorman, and J. M. Straka, 2003: Electrification and lightning in a simulated supercell thunderstorm. *Proc.*, *International Commission on Atmospheric Electricity*, Versailles, France, Available on CD.

APPENDIX A

FLASH GROUPING ALGORITHM

The grouping of LDAR II sources into flashes is beneficial for two reasons: 1) most previous studies relating lightning to other thunderstorm characteristics use flash counts, not source counts, as a measure of lightning activity, and 2) flash detection efficiency falloff with range from the network is not as abrupt as with source detection efficiency (see Appendix B). These algorithms use spatial and temporal constraints in determining if a source is part of a flash based on the measured physical characteristics of typical flash length and propagation speed (MacGorman and Rust 1998, Ch. 5 details some of these measurements). Thomas et al. (2003) discuss a flash grouping algorithm they developed to be used on lightning mapping array (LMA) data. Their algorithm has shown success, but they caution that when flash rate is very large, the algorithm deteriorates in performance. Even though flash algorithms may be suspect in obtaining the true number of flashes in a given time interval, they have generally gained acceptance in showing the true *trends* of flash rates.

A modified version of the NASA flash algorithm was obtained for this study from Dr. Gary Huffines. It assigned each source to a flash and to a branch of that flash. The recommended spatial and temporal constraints used to determine flashes were: the analyzed source point must be within 5 km of a flash point to be considered part of that flash, maximum time interval between source points in a flash = 0.5 s, maximum duration of a flash = 3 s, and the maximum time delay between points in a branch = 0.03 s. Also, a flash had to be comprised of at least 3 sources. This algorithm accounted for

LDAR range errors (estimated to be 12% of the range from the network center) and an azimuthal error (1°) in determining flash points.

To test whether or not the algorithm used in this study was accurate in showing flash rate trends, total flash counts were calculated (using sources within 10 km of the mesocyclone) for the initial 10 radar volume scan intervals (5 minutes each) in the first 13 October 2001 tornadic storm discussed in the first section. Sensitivity tests were conducted in a manner similar to McCormick (2003). Eight algorithm runs in addition to the baseline run discussed above were conducted with the following constraints: 1) 3.0 km, 0.5 s, 3 s, 0.03 s, 2) 7.0 km, 0.5 s, 3 s, 0.03 s, 3) 5.0 km, 0.15 s, 3 s, 0.03 s, 4) 5.0 km, 0.85 s, 3 s, 0.03 s, 5) 5.0 km, 0.5 s, 2 s, 0.03 s, 6) 5.0 km, 0.5 s, 4 s, 0.03 s, 7) 5.0 km, 0.5 s, 3 s, 0.01 s, and 8) 5.0 km, 0.5 s, 3 s, 0.05 s. Each constraint was adjusted an equal increment to values below and above the baseline algorithm values.

Increasing the spatial constraint from 3 to 7 km decreased the number of calculated flashes by the algorithm (Fig. 57, panel a), as expected (more sources were assigned to a flash, which decreased the total flash rate). The trends were fairly consistent between the 3 algorithms with different spatial constraints. Adjusting the maximum time interval allowed between source points in a flash had the largest impact on the total flash rates and their trends (Fig 57, panel b), a different finding from that by McCormick (2003) who found no significant changes (note that she only adjusted these values by 0.15 s). Except for the initial increase in the flash rate between volumes 1 and 2, the trends were significantly different. The 0.15 s algorithm had its maximum value of near 400 flashes per volume scan (double the maximum baseline value) 2 volume

scans prior to the baseline algorithm's maximum flash rate. The flash rates during each volume in panel c of figure 57 were quite similar, but there were some discrepancies in the trends when adjusting the flash duration within the algorithm. Between volumes 6 and 8, the 2 s algorithm's flash rates increased, the baseline algorithm rates decreased, and the 4 s algorithm decreased then increased. Adjusting the maximum time delay between sources comprising a branch had no effect; the values and trends were the same. Examining the differences between the various algorithms using source points within different radii (5, 20 km) yielded similar results as above.

Figure 58 shows how IC:CG ratios were affected by using the various algorithms discussed above. The values and trends in the ratios were very similar between all cases. As with the total flash rate, the largest discrepancies arose from changing the maximum time interval between source points in a flash. Even though the IC:CG values were different in panel b of figure 58, the trends were the same. The 5 and 20 km radii analyses were consistent with the above results for IC:CG ratios.

The modified NASA flash grouping algorithm has shown robustness, especially with respect to trends in total flash rate and IC:CG ratio. The drastic differences in the number of flashes and the flash rate trend between algorithms which adjusted maximum time intervals between sources in a flash show more work is needed to improve this algorithm, and/or in the choice of values for the sensitivity tests (i.e., 0.85 s may be too long of a time interval allowed between sources in a flash as measured cloud flash durations are typically < 1 s (Rakov and Uman 2003, p. 325)).

APPENDIX B

LDAR II RANGE LIMITATIONS

As the distance between storms and the LDAR II network center increases, certain range effects on the total lightning data became apparent. When the tornadic supercell that occurred between 000436 and 015933 UTC 13 October 2001 was closer to the network in figure 6 (65 km from the network compared to 94 km for the storm in Fig. 4), more lightning was detected at lower levels. The maximum values of source density were larger in the closer storm in figure 25 (6400 sources km^{-1} (5 minutes)$^{-1}$) compared to figure 19 (1600 sources km^{-1} (5 minutes)$^{-1}$). This was not attributable to the storm in figure 25 being more intense than the storm shown in figure 19 because the radar characteristics indicated the storm with the lower maximum source density was stronger (i.e., larger values and heights of maximum reflectivity). There were also more sources per flash in the closer storm (47 sources per flash) shown in figure 6 compared to the more distant storm (17 sources per flash) shown in figure 4. The flashes could have been longer in the closer storm, but many storms were analyzed at different distances from the network and the same relationship was found. Hence, significantly more sources were detected in closer storms. An excellent example of the effect increasing distance from the network has on source detection efficiency is shown in figure 59. The center of the storm was 114 km from the network center. Negative CG flash densities were large, near 0.24 flashes km^{-2} (5 minutes)$^{-1}$, over the western portion of the figure. LDAR II source densities were small (1-2 sources km^{-2}) in this region, which was farther from the network center (located at (25, 35 km)) than where source

density was substantially higher over the northeastern section of the plot. Radar imagery (not shown) indicated similar intensity convection in the areas having large –CG density values in the southwest and northeast portions of the plot. Figure C3 in Carey et al. (2004) shows a rapid decrease in lightning source detection efficiency of the DFW LDAR II with range. The source density can not be used as an indicator of storm strength when comparing storms from different distances from the network.

Determining the number of flashes from the LDAR II source data mitigates the significant decrease in source detection efficiency with range. The correlation between total points detected within 10 km of a tornadic mesocyclone and the mesocyclone's distance from the network was -0.19 (Table 4). Negative correlations were calculated between these two variables for many other storm events from this study as well. The correlation coefficient between total flash rate and distance with this storm was 0.26, showing that the flash rate increased the farther the storm was from the network (between 57 and 101 km range). This indicated the storm was more intense when it was farther away from the network. The correlations between radar characteristics and distance agree with this interpretation (i.e., SHI-distance coefficient was statistically significant with a value of 0.84 in Table 4). The increase in the flash rate with distance may include an instrument/algorithm effect: a lower number of sources were detected with increasing range from the network and this may have a tendency to segregate sources from one flash into several flashes because the space and time criteria of the flash grouping algorithm were not met. To attempt to correct for this effect, the flash

grouping algorithm included a range error (equal to 12% of the range) that expanded the spatial area to include sources with a particular flash.

Boccippio et al. (2000) have shown that an altitude error exists with LDAR data. Using a large database from the KSC network, their figure 7 shows a systematic increase in the altitude of maximum source density with increasing range from the network (especially at ranges greater than 150 km). They explain this error is due to increasing radial location errors with distance from the network. Thomas et al. (2004) argue that "uncertainty in the elevation angle is the dominant factor in the source height values." The supercell in figure 16 steadily moved toward the LDAR II network center from 000436 (101 km range) to 015437 UTC (57 km range). The heights in figure 16 show descent until 0108 UTC, and then increase to a relative maximum height near 0122 UTC. The altitude error was not significant enough to mask the trends associated with the storm's intensity variations. This agrees with Boccippio et al.'s figure 7, which shows that large altitude errors (greater than 2 km) are not likely within 150 km from the network. It is recommended to not use lightning height information as an indicator of storm intensity beyond 150 km from the network. All lightning heights show a strong positive correlation with distance in Table 4, which may be a result of the systematic altitude error discussed in Boccippio et al. However, this supercell's radar characteristics were also strongly positively correlated with distance from the network (Table 4), indicating that the storm was most intense when at a greater range from the network. Hence, the lightning heights shown here were useful indicators of storm

updraft intensity (especially because of the observations mentioned above regarding the inability of systematic altitude errors to mask true storm intensity variations).

APPENDIX C

BIMODAL SOURCE DENSITY HEIGHT DISTRIBUTION

The storms shown in the first section and for the 27 June 2001 (Fig. 46), 27 May 2002 (Fig. 37) and 16 June 2002 (Fig. 41) cases analyzed in this study have unimodal vertical distributions of LDAR II source density. However, the 13 October 2001 MCS cells show a multimodal height distribution of LDAR II sources (Figs. 30, 31, 33-35). The time-height and vertical projections show two horizontally expansive layers connected by a vertical bridge of large values of lightning source density for the cell shown in figure 35. The upper layer (12 km MSL) had greater horizontal extent than the lower layer in both vertical projections. The x-height projection includes lightning from more than one storm (see cell with lightning hook in the plan view at (47, 47 km)). The cell at (47, 47) was at an earlier stage of development according to radar reflectivity data (not shown) than the main cell at (40, 60). Note how the cell at (47, 47) did not have a well developed lower layer of lightning activity – possibly a signature of a storm at an initial stage of development.

The height histogram in figure 35 indicates two levels of maximum lightning activity at 4 and 12 km MSL. The peak at 12 km occurred at an environmental temperature of well below -40°C, while the lower peak was slightly above the melting level. VHF TOA systems detect more radiation sources from positive charge regions (Rison et al. 1999). The distribution of sources in figure 35 reveals maxima where positive charge regions are typically observed by more direct means (electric field soundings; Stolzenburg et al. 1998a) and agree with charge separation theories based on

temperature and liquid water content in the cloud (Saunders 1993) (higher liquid water contents are assumed at lower levels near 0°C in the storm). Dotzek et al. (2001) also found a strong lower positive charge region near the melting level of storms.

Three maxima of flash origins (gray shaded) were located at 4, 9, and 12 km MSL in the histogram in figure 35. The lower-level and upper-level peaks of flash origins represent where the CG and IC flashes most likely initiated, respectively (the 9 km peak origin level was probably associated with normal polarity IC flashes). Negative CG flash density values were greater than 0.22 flashes km^{-2} (5 minutes)$^{-1}$ in three areas of the storm. Only one of these maxima of –CG flash density was well-associated with a maximum in LDAR II source density (the –CG density maximum at (37, 58)). Note that the developing storm at (47, 47), which did not have a well-developed lower (positive) charge region, had smaller –CG flash density values (near 0.08 flashes km^{-2} (5 minutes)$^{-1}$) than the mature storm at (40, 60). This agrees with observations from Mansell et al. (2002), who show a lower positive charge region is required for the initiation of –CG flashes.

The examined cells that exhibited a distinct multimodal height distribution of LDAR II sources occurred close to the network center (within 50 km). This behavior was observed in other storm types (supercells not discussed in this study) as well. Weaker power sources were associated with the lower-level source density peak compared to the upper peak (Fig. 60). The sources shown in figure 35 were used to construct this figure. The mean source powers below and above 7 km MSL were 50.6 and 59.2 dBm (decibels of milliwatts), respectively. The difference in these means is

statistically significant at the p = 0.01 level. Thomas et al. (2001) also show larger source powers detected in the upper parts of storms. Hence, the lower-level peak in a bimodal source density vertical distribution may be detected with lower efficiency (and may not be detected at all) the farther a storm is from the network because of the weaker power amplitudes associated with these sources. However, this hypothesis does not completely explain why there were several mature storms analyzed within 50 km of the network that did not exhibit multimodal characteristics. Meteorological storm conditions may be important in determining whether or not a storm has multimodal source density vertical distributions (i.e., Fig. 35 shows two storms at similar distances from the network center, but the developing storm had a unimodal distribution).

APPENDIX D

ACRONYMS

CG	Cloud-to-ground
dBZ	Decibels of Reflectivity
HAD	Hail Detection Algorithm
IC	Intracloud
IDL	Interactive Data Language
LDAR II	Lightning Detection and Ranging II
MCS	Mesoscale Convective System
MDA	Mesocyclone Detection Algorithm
MSI	Mesocyclone Strength Index
MSL	Mean Sea Level
NCDC	National Climatic Data Center
NLDN	National Lightning Detection Network
SCIT	Storm Cell Identification and Tracking algorithm
SHI	Severe Hail Index
TOA	Time-of-Arrival
UTC	Universal Coordinated Time
VIL	Vertically Integrated Liquid water
WDSS-II	Warning Decision Support System – Integrated Information
WSR-88D	Weather Surveillance Radar-1988 Doppler

APPENDIX E

ANALYSIS SOFTWARE

The multi-panel figures (i.e., Fig. 4) were created using the IDL (Interactive Data Language) program ldar_dens2.pro (p. 112), written by Brandon Ely and Scott Steiger. This program produced time-height, vertical, and horizontal projections of LDAR II source density. Radar reflectivity, cloud-to-ground (CG) lightning, and storm report data were overlaid on the source density using this program. Hist_plotstats.pro (not shown), a procedure called from ldar_dens2.pro, calculated the non-CG lightning statistics using data within a certain radius from the storm cell center (i.e., total flash rate, lightning top, etc.). Another called procedure, radar.pro (p. 124), calculated and overlaid mean, maximum, or cumulative reflectivity on the source density in the vertical and horizontal projections. Radar.pro was a modified version of the original program by the same name, written by Larry Belcher and Tracy McCormick while at North Carolina State University. Ldar_dens2.pro is a multi-task program and was used frequently to analyze the data for this study.

Other programs (not shown) called by ldar_dens2.pro include: cg.pro, flash_group2.pro, hist_plot.pro, plot_cg.pro, stateshp2.pro, countyshp2.pro, and tvcircle.pro. Cg.pro accessed the CG lightning data and created text files used to plot CG characteristics. It also calculated storm cell CG lightning characteristics (i.e., -CG flash rate, median peak currents, etc.). Flash_group2.pro is the flash grouping algorithm (originally written by NASA) used to find the number of flashes from LDAR II source data (see Appendix A). It was borrowed from Dr. Gary Huffines. Hist_plot.pro created

the histogram panel in figure 4. Plot_cg.pro used the text files created by cg.pro and overlaid CG characteristics on source density/radar data. Stateshp2.pro and countyshp2.pro were used to plot state and county outlines on the maps shown. Lastly, tvcircle.pro created the range rings for figure 1.

Figure 19 (and subsequent similar figures) was created using ldarradarth_plot2.pro (p. 127). This program plots a time-height history of a storm cell's mean radar reflectivity and LDAR II source density. It selects data from within a certain radius (5, 10, or 20 km) of a cell's location for each radar volume scan. The time series plots (i.e., Fig. 16) were created using time_series.pro (p. 132). Match_radarldar.pro (p. 139) is a program that created some of the results for the correlation analysis shown in Table 1 (the correlation coefficients between radar and LDAR II characteristics). These programs were written by Scott Steiger.

A semicolon marks where comments are located in IDL programming. Please see these comments for more information on each program.

```
PRO LDAR_DENS2

;Reads in a LDAR II data set from an ascii file and plots projections of
;source density for a selected time period and area centered on a cell/mesocyclone.
;Also determines cell lgh. statistics for sources within a certain range from the
;cell location (pk. ht., top, modes, norm. pk., median ht., etc.).
;
;Has capability to overlay CG, radar data, and severe storm reports.
;Can produce .gif or .eps image files
;
;Note: Must be at least two (for histogram) data points.
;
;Programmed by: Scott M. Steiger & Brandon L. Ely
;Created 24 June 2004 for automatic input file (version 2)
;Last update: 14 June 2005
;
;CALLS: cg.pro, flash_group2.pro, hist_plotstats.pro, hist_plot.pro, radar.pro, plot_cg.pro, stateshp2.pro,
; countyshp2.pro, and tvcircle.pro

COMPILE_OPT IDL2
CLOSE, /ALL

;Set up file paths
inpath='C:\My Documents\scotts\Dissertation\'
cases='011013supercase\overlaysT\'
outpathima=inpath+cases+'ldar-radarimagesm\'
outpathtex=inpath+cases+'ldartextm\'
;For CG analysis
outpathcgtex=inpath+cases+'cgtextm\'
outpathlgh=inpath+cases+'lghavgsm\'
;For Radar files
radardir=inpath+'Careyradar\20011013\KFWS20011013_'

freez=3.72; Ambient melting level in km (for radar.pro)
H20=6.76; -20C level
H40=9.59; -40C level

pi=3.14159265359

maxrec=2000000L; for reading data (see below)

; Define a user symbol to be a filled circle (for sensor plot)
A=FINDGEN(49)*(pi*2/49.0)
USERSYM, COS(A), SIN(A), /FILL

;Names of the States that you want county lines drawn for
countyname=['Texas','Oklahoma','Arkansas']
obpath='C:\shape_data\'
councol=0
clinthic=1.5
slinthic=3.0

;Get storm cell info. (times, locations, cell IDs)-change between cases
OPENR, lun, inpath+cases+'stormmesodata011013torn.txt', /GET_LUN
;Include tabs in fomt (why a5 not a4 sometimes)
fomt='(a4,i2,1x,i2,1x,f2.0,1x,i2,1x,i2,1x,f2.0,1x,i4,f6.1,i4,i4,a2,f6.1,f6.1,f6.1,f6.1,i2,1x,i2,1x,f2.0,1x,i2,1x,i2,1x,f2.0,1x,a1)'
;fomt='(a5,i2,1x,i2,1x,f2.0,1x,i2,1x,i2,1x,f2.0,1x,i4,f6.1,i4,i4,a1)';for non-storm report events
records={vol:'',st_hr:0,st_min:0,st_sec:0.0d,end_hr:0,end_min:0,end_sec:0.0d,azimu:0,range:0.0d, $
      mesoid:0,cellid:0,reportanswer:'',stxreport:0.0d,styreport:0.0d,ndxreport:0.0d, $
      ndyreport:0.0d,repst_hr:0,repst_min:0,repst_sec:0.0d,repend_hr:0,repend_min:0,repend_sec:0.0d,type:''}
;non-storm; mesoid=cellid in non-meso. cases:
;records={vol:'',st_hr:0,st_min:0,st_sec:0.0d,end_hr:0,end_min:0,end_sec:0.0d,azimu:0,range:0.0d,mesoid:0, $
;      cellid:0,reportanswer:''}
cell=REPLICATE(CREATE_STRUCT(records), maxrec); Create structures
ind1=0
WHILE NOT EOF(lun) DO BEGIN
```

```
  READF, lun, records, format=fomt
  cell[ind1]=records
  ind1=ind1+1
ENDWHILE; if doesn't exit loop correctly: make sure no spaces after last datum in file
FREE_LUN, lun
;Trims the structure array to the needed size
cell=cell[0:ind1-1]

;hour -> hour value for a given data point
;minu -> minute for a given data point
;sec -> second value for a given data point
;lat -> latitude value
;lon -> longitude value
;hght -> height value
;err -> error
;sens -> number of sensors

;Creates a structure to hold the information for the source points-
;CHANGE formats in flash_group2.pro if fmt changes!
;fmt='(i2,1x,i2,1x,i2,1x,i2,1x,i2,1x,f6.3,2x,f6.3,2x,f7.3,2x,f5.0,2x,f3.1,2x,i1)'; old cases
;fmt='(i2,1x,i2,1x,i2,1x,i2,1x,i2,1x,f12.9,2x,f6.3,2x,f7.3,2x,f5.0,2x,i1,2x,f3.1)'; new
;fmt='(i2,1x,i2,1x,i2,1x,i2,1x,i2,1x,f6.3,2x,f7.4,2x,f8.4,2x,f5.0)'; test Martin 16 April 2004 for 20011013
fmt='(i2,1x,i2,1x,i2,1x,i2,1x,i2,1x,f12.9,2x,f6.3,2x,f7.3,2x,f5.0)'; Nick's nanosecond data for 10/13 & 6/27
;fmt='(i2,1x,i2,1x,f9.6,3x,f7.4,2x,f8.4,4x,f5.0)'; 6 April 2003
;record={mon:0, day:0, year:0, hour:0, minu:0, sec:0.0d, lat:0.0d, lon:0.0d, $
;       hght:0.0d, err:0.0d, sens:0}; old cases
;record={mon:0, day:0, year:0, hour:0, minu:0, sec:0.0d, lat:0.0d, lon:0.0d, $
;     hght:0.0d, sens:0, err:0.0d}; new
record={mon:0, day:0, year:0, hour:0, minu:0, sec:0.0d, lat:0.0d, lon:0.0d, $
       hght:0.0d}; Nick's nano. data for 13 October & 27 June; test Martin 16 April
;record={hour:0, minu:0, sec:0.0d, lat:0.0d, lon:0.0d, hght:0.0d}; 6 April 2003
;Appended to record: juldat: julian dates of sources; (x/y)dist: x/y component distance of source from radar
;   (KFWS); cellgh(x/y)dif: x/y component distance between cell center and source; r: range of source from
;   cell center; (x/y): x/y component distance of source from LDAR center (DFW)
lghtng=REPLICATE(CREATE_STRUCT(record, 'juldat', 0.0d, 'xdist', 0.0d, 'ydist', 0.0d, $
  'cellghxdif', 0.0d, 'cellghydif', 0.0d, 'r', 0.0d, 'x', 0.0d, 'y', 0.0d), maxrec)

OPENR, lun, inpath+'DFWLDARII_011013at0000_13at0200.txt', /GET_LUN
;OPENR, lun, inpath+'200110130200-0210.filt5sen.nosen04.txt', /GET_LUN
ind=0
;While ind LT maxrec do begin
WHILE NOT EOF(lun) DO BEGIN
  READF, lun, record, format=fmt
  record2=CREATE_STRUCT(record, 'juldat', 0.0d, 'xdist', 0.0d, 'ydist', 0.0d, 'cellghxdif', 0.0d, $
        'cellghydif', 0.0d, 'r', 0.0d, 'x', 0.0d, 'y', 0.0d)
  lghtng[ind]=record2
  ind=ind+1
ENDWHILE
FREE_LUN, lun

lghtng=lghtng[0:ind-1]
;for 6 April 2003 case, use next 3 lines
;mon=4
;day=6; edit subprograms (i.e., flash algorithm)
;year=2003
lghtng.year=lghtng.year+2000
lghtng.hght=lghtng.hght/1000.0; km

;Calculates the julian day in seconds for each data point
lghtng.juldat=JULDAY(lghtng.mon, lghtng.day, lghtng.year, lghtng.hour, lghtng.minu, lghtng.sec)
;lghtng.juldat=JULDAY(mon, day, year, lghtng.hour, lghtng.minu, lghtng.sec); 6 April case

;Determines the min and max times available
;NOTE: Assumes increasing time order of data
min_jul=JULDAY(lghtng[0].mon, lghtng[0].day, lghtng[0].year, lghtng[0].hour, lghtng[0].minu, lghtng[0].sec)
max_jul=JULDAY(lghtng[ind-1].mon, lghtng[ind-1].day, lghtng[ind-1].year, lghtng[ind-1].hour, $
```

```
        lghtng[ind-1].minu, lghtng[ind-1].sec)
;min_jul=JULDAY(mon, day, year, lghtng[0].hour, lghtng[0].minu, lghtng[0].sec)
;max_jul=JULDAY(mon, day, year, lghtng[ind-1].hour, lghtng[ind-1].minu, lghtng[ind-1].sec)

;Sets up color table for plots
TVLCT, 255, 255, 255, 1; white
TVLCT, 0, 0, 0, 0; black
TVLCT, 204, 0, 204, 2; lt purple
TVLCT, 102, 0, 204, 3; dk purple
TVLCT, 51, 204, 204, 4; lt blue
TVLCT, 0, 51, 204, 5; med blue
TVLCT, 0, 153, 0, 6; green
TVLCT, 255, 255, 0, 7; yellow
TVLCT, 255, 102, 0, 8; orange
TVLCT, 255, 0, 0, 9; red
TVLCT, 128, 128, 128, 10; gray
TVLCT, r, g, b, /get

;Latitude and longitude of radar (KFWS):
rlat=32.5731
rlon=-97.3031
;LDAR center (DFW) latitude and longitude:
llat=32.902538
llon=-97.040176
; Define sensor locations
;llats=[32.902538, 33.134707, 32.985939, 32.840225, 32.693845, 32.824272, 33.055667]; latitudes for stations
;llons=[-97.040176, -97.017657, -96.764602, -96.853942, -97.044301, -97.340789, -97.231124]; longitudes
;n=N_ELEMENTS(llats)
;deltalati=FLTARR(n)
;deltalong=FLTARR(n)
;ys=FLTARR(n)
;xs=FLTARR(n)
;FOR i=0, n-1 DO BEGIN; Convert sensor lat/lon to x and y (from radar)
;  deltalati[i]=llats[i]-rlat
;  deltalong[i]=llons[i]-rlon
;  ys[i]=6370.*(deltalati[i]*!DTOR)
;  xs[i]=6370.*COS(0.5*(rlat+llats[i])*!DTOR)*(deltalong[i]*!DTOR)
;ENDFOR

;Create plot for each volume scan
FOR i=0, ind1-1 DO BEGIN; ind1-1

  ;for 6 April 2003 case, use to reset values
  ;mon=4
  ;day=6
  ;year=2003

  vol=STRCOMPRESS(cell[i].vol, /REMOVE_ALL)

  PRINT, ' '
  PRINT, 'Output for vol: ', vol
  PRINT, ' '

  reportanswer=STRCOMPRESS(cell[i].reportanswer, /REMOVE_ALL)
  ;Converts begin and end times of scan to julian format
  ;Note: be careful IF data on more than one day! (27 May case)
  ;Analysis begin time:
  st_jul=JULDAY(lghtng[0].mon, lghtng[0].day, lghtng[0].year, cell[i].st_hr, cell[i].st_min, cell[i].st_sec)
  end_jul=JULDAY(lghtng[0].mon, lghtng[0].day, lghtng[0].year, cell[i].end_hr, cell[i].end_min, cell[i].end_sec)
  ;st_jul=JULDAY(mon, day, year, cell[i].st_hr, cell[i].st_min, cell[i].st_sec); Analysis begin time for 4/6
  ;end_jul=JULDAY(mon, day, year, cell[i].end_hr, cell[i].end_min, cell[i].end_sec)
  IF reportanswer EQ 'y' THEN BEGIN; report begin and end times in julian
    repst_jul=JULDAY(lghtng[0].mon, lghtng[0].day, lghtng[0].year, cell[i].repst_hr, cell[i].repst_min, $
          cell[i].repst_sec)
    repend_jul=JULDAY(lghtng[0].mon, lghtng[0].day, lghtng[0].year, cell[i].repend_hr, cell[i].repend_min, $
          cell[i].repend_sec)
```

```
  ;repst_jul=JULDAY(mon, day, year, cell[i].repst_hr, cell[i].repst_min, cell[i].repst_sec)
  ;repend_jul=JULDAY(mon, day, year, cell[i].repend_hr, cell[i].repend_min, cell[i].repend_sec)
ENDIF

;Check if all data that you need is in current LDAR data file for the ith time period
IF end_jul GT max_jul THEN BEGIN
  PRINT, 'Out of time limits of LDAR data'
  BREAK
ENDIF

;Take out time interval of LDAR data
time_dex=WHERE((lghtng.juldat GE st_jul) AND (lghtng.juldat LE end_jul), time_count)
IF time_count LE 1 THEN BEGIN
  PRINT, 'Not enough valid points in area'
  GOTO, jump1
  PRINT, 'Check'
ENDIF

;Creates a structure with data points that lie within the time interval
lghtng2=REPLICATE(CREATE_STRUCT(record, 'juldat', 0.0d, 'xdist', 0.0d, 'ydist', 0.0d, 'cellghxdif', 0.0d, $
                'cellghydif', 0.0d, 'r', 0.0d, 'x', 0.0d, 'y', 0.0d), time_count)
lghtng2=lghtng[time_dex]

;Calculate source x and y distances from radar location.
deltalat=lghtng2.lat-rlat
deltalon=lghtng2.lon-rlon
lghtng2.xdist=6370.0*COS(0.5*(lghtng2.lat+rlat)*!DTOR)*(deltalon*!DTOR)
lghtng2.ydist=6370.0*(deltalat*!DTOR)
;Cell (x and y) location:
cellx=-cell[i].range*COS((pi/180.)*(270-cell[i].azimu))
celly=-cell[i].range*SIN((pi/180.)*(270-cell[i].azimu))
lghtng2.cellghxdif=ABS(lghtng2.xdist-cellx); x distance between source and cell
lghtng2.cellghydif=ABS(lghtng2.ydist-celly); y distance between source and cell

;Find cell range from center of network (DFW)
deltala=llat-rlat
deltalo=llon-rlon
xdfw=6370.0*COS(0.5*(rlat+llat)*!DTOR)*(deltalo*!DTOR)
ydfw=6370.0*(deltala*!DTOR)
xdiff=xdfw-cellx
ydiff=ydfw-celly
ldarrangetocell=SQRT(xdiff^2+ydiff^2)

;lghtng2.cellghxdif=ABS(lghtng2.xdist-xdfw); x distance between source and network (for when do system)
;lghtng2.cellghydif=ABS(lghtng2.ydist-ydfw); y distance between source and network

;For 60x60 km plots
miny=celly-30.0
maxy=celly+30.0
minx=cellx-30.0
maxx=cellx+30.0
;If centering on LDAR network
;miny=ydfw-100.0
;maxy=ydfw+100.0
;minx=xdfw-100.0
;maxx=xdfw+100.0

;Take out 60x60 km section of LDAR data centered on cell
xy_dex=WHERE((lghtng2.cellghxdif LE 30.0) AND (lghtng2.cellghydif LE 30.0), xy_count)
IF xy_count LE 1 THEN BEGIN
  PRINT, 'Not enough valid points in area'
  GOTO, jump1
  PRINT, 'Check'
endif

;Creates a structure with data points that lie within the x-y box and time interval
```

```
lghtng3=REPLICATE(CREATE_STRUCT(record, 'juldat', 0.0d, 'xdist', 0.0d, 'ydist', 0.0d, 'cellghxdif', 0.0d, $
            'cellghydif', 0.0d, 'r', 0.0d, 'x', 0.0d, 'y', 0.0d), xy_count)
lghtng3=lghtng2[xy_dex]

lghtng3.r=SQRT(lghtng3.cellghxdif^2+lghtng3.cellghydif^2); range of sources from cell/meso. in km

;Calculate source x and y distances from center of network (for flash alg.)
lghtng3.x=(lghtng3.xdist-xdfw)*1000.; to convert to m for flash algorithm
lghtng3.y=(lghtng3.ydist-ydfw)*1000.

st_hr=STRCOMPRESS(STRING(FIX(cell[i].st_hr)), /REMOVE_ALL)
st_min=STRCOMPRESS(STRING(FIX(cell[i].st_min)), /REMOVE_ALL)
st_sec=STRCOMPRESS(STRING(FIX(cell[i].st_sec)), /REMOVE_ALL)
end_hr=STRCOMPRESS(STRING(FIX(cell[i].end_hr)), /REMOVE_ALL)
end_min=STRCOMPRESS(STRING(FIX(cell[i].end_min)), /REMOVE_ALL)
end_sec=STRCOMPRESS(STRING(FIX(cell[i].end_sec)), /REMOVE_ALL)
IF STRLEN(st_hr) EQ 1 THEN st_hr='0'+st_hr
IF STRLEN(st_min) EQ 1 THEN st_min='0'+st_min
IF STRLEN(st_sec) EQ 1 THEN st_sec='0'+st_sec
IF STRLEN(end_hr) EQ 1 THEN end_hr='0'+end_hr
if STRLEN(end_min) EQ 1 THEN end_min='0'+end_min
if STRLEN(end_sec) EQ 1 THEN end_sec='0'+end_sec

year=STRCOMPRESS(STRING(lghtng[0].year-2000),/REMOVE_ALL)
;year=STRCOMPRESS(STRING(year-2000),/REMOVE_ALL); 6 April
IF STRLEN(year) EQ 1 THEN year='0'+year
mon=STRCOMPRESS(STRING(lghtng[0].mon),/REMOVE_ALL)
;mon=STRCOMPRESS(STRING(mon),/REMOVE_ALL)
IF STRLEN(mon) EQ 1 THEN mon='0'+mon
day=STRCOMPRESS(STRING(lghtng[0].day),/REMOVE_ALL); be wary when more than one day in analysis
;day=STRCOMPRESS(STRING(day),/REMOVE_ALL)
IF STRLEN(day) EQ 1 THEN day='0'+day

dates=[mon+'/'+day+'/'+year+' '+st_hr+':'+st_min+':'+st_sec, mon+'/'+day+'/'+year+' '+end_hr+':'+end_min+ $
      ':'+end_sec]

;CG lightning analysis - for plots (later in this program) and CG statistics - don't repeat in case studies
CG, dates, region=[miny, maxy, minx, maxx], outpathcgtex, outpathlgh, vol, cell[i].cellid, cell[i].mesoid, $
   cellx, celly, tot
;VERY IMPORTANT to make sure parameters are in same order in call and program!

;Height interval to analyze sources
minhght=0.
maxhght=20.
mnhght=STRCOMPRESS(STRING(FIX(minhght)), /REMOVE_ALL)
mxhght=STRCOMPRESS(STRING(FIX(maxhght)), /REMOVE_ALL)
IF STRLEN(mnhght) EQ 1 THEN mnhght='0'+mnhght
IF STRLEN(mxhght) EQ 1 THEN mxhght='0'+mxhght

ht_dex=WHERE((lghtng3.hght GE minhght) AND (lghtng3.hght LT maxhght), ht_count)
IF ht_count LE 1 THEN BEGIN
  PRINT, 'Not enough valid points in area'
  GOTO, jump1
  PRINT, 'Check'
ENDIF

;Determine LDAR stats. for different cell/meso. radii - may leave out for overlay plots
cellr=[20.0, 10.0, 5.0]
FOR k=0, 2 DO BEGIN
  cellra=STRCOMPRESS(STRING(FIX(cellr[k])), /REMOVE_ALL)
  IF STRLEN(cellra) EQ 1 THEN cellra='0'+cellra
  r_dex=WHERE((lghtng3[ht_dex].r LE cellr[k]), r_count)
  IF r_count LE 1 THEN BEGIN
    PRINT, 'Not enough valid points in area'
    BREAK
  ENDIF
```

```
  FLASH_GROUP2, lghtng3[ht_dex[r_dex]], inpath+cases+'flashalgresm\'+mnhght+'-'+mxhght+'km'+st_hr+st_min+ $
          st_sec+'_to_'+end_hr+end_min+end_sec+'v'+vol+'rad'+cellra+'.txt', $
          num_flashes=num_flashes, cellra=cellra
  totalCGs=tot[k]; total CGs within 20, 10, and 5 km (see cg.pro)
  IF totalCGs EQ 0 THEN BEGIN
    ICCGrat=-999.; to prevent Inf result
  ENDIF ELSE BEGIN
    ICCGrat=FLOAT(num_flashes-totalCGs)/totalCGs; IC:CG ratio
  ENDELSE
  OPENW, lun, outpathtex+'hthist'+mnhght+'-'+mxhght+'km'+st_hr+st_min+st_sec+'_to_'+end_hr+end_min $
          +end_sec+'v'+vol+'rad'+cellra+'.txt', /GET_LUN
  HIST_PLOTSTATS, lun, lghtng3[ht_dex[r_dex]].hght, binsize=1.0, normalize=1, minhght, maxhght, vol, $
      cell[i].cellid, cell[i].mesoid, ldarrangetocell, cellra, outpathlgh, num_flashes, ICCGrat
ENDFOR

;Run flash_group2 for 60x60 km box
FLASH_GROUP2, lghtng3[ht_dex], inpath+cases+'flashalgresm\'+mnhght+'-'+mxhght+'km'+st_hr+st_min+st_sec+ $
        '_to_'+end_hr+end_min+end_sec+'v'+vol+'30kmbox.txt', num_flashes=num_flashes, $
        originzs=originzs
;For squall system analysis:
;ICCGrat=FLOAT(num_flashes-tot)/tot; IC:CG ratio
;OPENW, lun, outpathtex+'hthist'+mnhght+'-'+mxhght+'km'+st_hr+st_min+st_sec+'_to_'+end_hr+end_min $
;          +end_sec+'v'+vol+'.txt', /get_lun
;cellra='box100'
;HIST_PLOTSTATS, lun, lghtng3[ht_dex].hght, binsize=1.0, normalize=1, minhght, maxhght, vol, $
;          cell[i].cellid, cell[i].mesoid, ldarrangetocell, cellra, outpathlgh, num_flashes, ICCGrat

;Time-Height density calculations
rest=(JULDAY(9, 14, 1976, 4, 29, 44.0)) - (JULDAY(9, 14, 1976, 4, 29, 39.0)) ;resolution=30s for 1 hr plots,
; =5s for 6 min plots
resh=1.0; km
nxth=LONG(ROUND((end_jul-st_jul)/rest))
nh=LONG(ROUND((maxhght-minhght)/resh))
cnt=FLTARR(nxth,nh)  ;all flash counts
OPENW, lun, outpathtex+'timht'+mnhght+'-'+mxhght+'km'+st_hr+st_min+st_sec+'_to_'+end_hr+end_min $
            +end_sec+'v'+vol+'_30kmbox.txt', /GET_LUN; 30km
;Based on Huffine's method
pind=LONG((lghtng3[ht_dex].juldat-st_jul)/rest)+LONG((lghtng3[ht_dex].hght-minhght)/resh)*nxth
cnt=HISTOGRAM(pind, min=0, max=nxth*nh-1, binsize=1, input=cnt)
cnt=FLOAT(REFORM(cnt, nxth, nh))

;Find the "area" of each grid element
area=rest*resh
;print, area ;- very small

;Find the flash densities
densth=FLTARR(nxth, nh)
densth=cnt/area

mindens=MIN(densth)
maxdens=MAX(densth)
kindex=WHERE(densth gt 0.0)
meandensth=MEAN(densth[kindex]); Conditional mean
PRINT, 'From ldar_dens2.pro: '
PRINT, 'meandens for th: ', meandensth

PRINTF, lun, minhght, maxhght, st_jul, end_jul
PRINTF, lun, nh, nxth, resh, rest, N_ELEMENTS(lghtng3[ht_dex])
PRINTF, lun, densth
FREE_LUN, lun

;X-Height calculations
res=1.0; km
nx=LONG(ROUND((maxx-minx)/res))
cnt=FLTARR(nx,nh)
OPENW, lun, outpathtex+'xh'+mnhght+'-'+mxhght+'km'+st_hr+st_min+st_sec+'_to_'+end_hr+end_min $
```

```
        +end_sec+'v'+vol+'_30kmbox.txt', /GET_LUN
pind=LONG((lghtng3[ht_dex].xdist-minx)/res)+LONG((lghtng3[ht_dex].hght-minhght)/resh)*nx
cnt=HISTOGRAM(pind, min=0, max=nx*nh-1, binsize=1, input=cnt)
cnt=FLOAT(REFORM(cnt, nx, nh))

;Find the area of each grid element
area=res*resh

;Find the flash densities
densxh=FLTARR(nx, nh)
densxh=cnt/area

mindens=MIN(densxh)
maxdens=MAX(densxh)
kindex=WHERE(densxh gt 0.0)
meandensxh=MEAN(densxh[kindex])
PRINT, 'meandens for xh:', meandensxh

PRINTF, lun, minhght, maxhght, minx, maxx
PRINTF, lun, nh, nx, resh, res, N_ELEMENTS(lghtng3[ht_dex])
PRINTF, lun, densxh
FREE_LUN, lun

;Height-Y calculations
ny=LONG(ROUND((maxy-miny)/res))
cnt=FLTARR(nh,ny)
OPENW, lun, outpathtex+'yh'+mnhght+'-'+mxhght+'km'+st_hr+st_min+st_sec+'_to_'+end_hr+end_min $
        +end_sec+'v'+vol+'_30kmbox.txt', /GET_LUN
pind=LONG((lghtng3[ht_dex].hght-minhght)/resh)+LONG((lghtng3[ht_dex].ydist-miny)/res)*nh
cnt=HISTOGRAM(pind, min=0, max=nh*ny-1, binsize=1, input=cnt)
cnt=FLOAT(REFORM(cnt, nh, ny))

;Find the area of each grid element
area=resh*res

;Find the flash densities
denshy=FLTARR(nh,ny)
denshy=cnt/area

mindens=MIN(denshy)
maxdens=MAX(denshy)
kindex=WHERE(denshy gt 0.0)
meandenshy=MEAN(denshy[kindex])
PRINT, 'meandens for hy:', meandenshy

PRINTF, lun, miny, maxy, minhght, maxhght
PRINTF, lun, ny, nh, res, resh, N_ELEMENTS(lghtng3[ht_dex])
PRINTF, lun, denshy
FREE_LUN, lun

;Plan view calculations
cnt=FLTARR(nx,ny)
OPENW, lun, outpathtex+'xy'+mnhght+'-'+mxhght+'km'+st_hr+st_min+st_sec+'_to_'+end_hr+end_min $
        +end_sec+'v'+vol+'_30kmbox.txt', /GET_LUN
pind=LONG((lghtng3[ht_dex].xdist-minx)/res)+LONG((lghtng3[ht_dex].ydist-miny)/res)*nx
cnt=HISTOGRAM(pind, min=0, max=nx*ny-1, binsize=1, input=cnt)
cnt=FLOAT(REFORM(cnt, nx, ny))

;Find the area of each grid element
area=res*res

;Find the flash densities (sources km^-2)
densxy=FLTARR(nx, ny)
densxy=cnt/area

mindens=MIN(densxy)
```

```
maxdens=MAX(densxy)
kindex=WHERE(densxy gt 0.0)
meandensxy=MEAN(densxy[kindex])
PRINT, 'Minplandens Maxplandens Meanplandens: ', mindens, maxdens, meandensxy

PRINTF, lun, miny, maxy, minx, maxx
PRINTF, lun, ny, nx, res, res, N_ELEMENTS(lghtng3[ht_dex])
PRINTF, lun, densxy
FREE_LUN, lun

PRINT, 'Distance from LDAR (km): '+STRTRIM(STRING(ROUND(ldarrangetocell)), 2)+'; Az., Range from KFWS: (' $
    +STRTRIM(STRING(ROUND(cell[i].azimu)), 2)+', '+STRTRIM(STRING(ROUND(cell[i].range)), 2)+ $
    ') for volume '+vol

hght=minhght+FINDGEN(nh)*resh+resh/2.0; height values for plots below

date_labels=LABEL_DATE(date_format=['%h%i%s%3']); for plot (time-height)

GOTO, jumpr; when not want radial plots
;Radial plot (radius vs. height density plot)-separate plot from above - take out for radar and cg overlays
post=outpathima+'ldar'+mnhght+'-'+mxhght+'km_'+st_hr+st_min+st_sec+'_to_'+end_hr+end_min $
          +end_sec+'v'+vol+'_radial_dens.eps'
;Setup the postscript device - place code before any plotting command
SET_PLOT, 'ps'
DEVICE, filename=post, xsize=4.9, ysize=6.5, /inches, /color, /Helvetica, $
  encapsulated=1, font_size=12.0, preview=0
!P.FONT=0

;An intricate way to determine the number of sources in each grid box with a changing delta-r to keep
;same volume
rad=FLTARR(100); Assuming not more than 100 radii intervals
dr=FLTARR(100); delta-r's
a0=78.53982; area for an initial circle of 5 km radius
ii=0
rad[ii]=0.0
dr[ii]=0.0
REPEAT BEGIN
  ii=ii+1
  rad[ii]=SQRT(ii*a0/pi); to keep integrating volumes the same as go out radially (totalling sources in
  ;same volumes)
  dr[ii]=rad[ii]-rad[ii-1]
ENDREP UNTIL dr[ii] LE 1.0; until the delta-r is 1 km (smallest radial resolution allowed)
maxr=MAX(rad)
nr=N_ELEMENTS(WHERE(rad gt 0.0))
hts=FINDGEN(nh+1)*resh+minhght
cnts=FLTARR(1)
FOR jj=1, nh DO BEGIN; heights
  FOR kk=1, nr DO BEGIN; radials
    ;Determine the number of sources in each grid box
    count=WHERE((lghtng3[ht_dex].r LT rad[kk]) AND (lghtng3[ht_dex].r GE rad[kk-1]) AND $
         (lghtng3[ht_dex].hght LT hts[jj]) AND (lghtng3[ht_dex].hght GE hts[jj-1]), cnt)
    IF jj EQ 1 AND kk EQ 1 THEN BEGIN
      cnts=cnt
    ENDIF ELSE BEGIN
      cnts=[cnts,cnt]
    ENDELSE
  ENDFOR
ENDFOR
cnts=FLOAT(REFORM(cnts, nr, nh))

OPENW, lun, outpathtex+'radial'+mnhght+'-'+mxhght+'km'+st_hr+st_min+st_sec+'_to_'+end_hr+end_min $
          +end_sec+'v'+vol+'.txt', /GET_LUN

;the volume of each grid element (constant)
volu=a0*resh
```

```
;find the flash densities
densrh = FLTARR(nr, nh)
densrh = cnts/volu

mindens=MIN(densrh)
maxdens=MAX(densrh)

PRINTF, lun, densrh
FREE_LUN, lun

;Contour the data
;set up rd and hght values
rd=FLTARR(nr)
FOR m=0, nr-1 DO BEGIN
  rd[m]=rad[m]+dr[m+1]/2.0
ENDFOR
lev=[0.001, 0.01, 0.1, 0.5, 1.0, 5.0, 10.0]
col=[2, 3, 4, 5, 6, 7, 8]
CONTOUR, densrh, rd, hght, levels=lev, c_colors=col, /fill, /closed, $
      xtitle='Range (km) from center of cell', ytitle='Height (km) MSL', xrange=[0.,maxr], $
      yrange=[minhght,maxhght], xstyle=1, ystyle=1, color=0, /noerase
DEVICE, /close_file, encapsulated=1
SET_PLOT, 'win'
!P.FONT=0
jumpr:

FOR j=0, 0 DO BEGIN; which cg chars. overlaying (j=0,2 implies doing 3 overlays with 3 different CG chars.)
;set j=0,0 for ldar-radar

  cgchar=['neg_','pos_','ppos','pmed','nmed','pmul','nmul']

  ;post=outpathima+'ldar'+mnhght+'-'+mxhght+'km_'+st_hr+st_min+st_sec+'_to_'+end_hr+end_min $
  ;              +end_sec+'v'+vol+'_30kmbox_'+cgchar[j]+'.eps'; for CG overlays
  post=outpathima+'ldar'+mnhght+'-'+mxhght+'km_'+st_hr+st_min+st_sec+'_to_'+end_hr+end_min $
              +end_sec+'v'+vol+'_30kmbox_dens.eps'; for radar-ldar overlays
  ; Setup the postscript device - place code before any plotting command
  SET_PLOT, 'ps'
  DEVICE, filename=post, xsize=8.0, ysize=9.0, /inches, /color, /Helvetica, $; ysize=8.0 for square
    encapsulated=1, font_size=12.0, preview=0
  !P.FONT=0

  ; PLOTS FREQUENCY VS. HEIGHT of LDAR II points
  OPENW, lun, outpathtex+'hthist'+mnhght+'-'+mxhght+'km'+st_hr+st_min+st_sec+'_to_'+end_hr+end_min $
               +end_sec+'v'+vol+'_30kmbox.txt', /GET_LUN; 'hthist2' for squall system
  OPENW, lun2, outpathtex+'hthistorigins'+mnhght+'-'+mxhght+'km'+st_hr+st_min+st_sec+'_to_'+end_hr+end_min $
               +end_sec+'v'+vol+'_30kmbox.txt', /GET_LUN
  HIST_PLOT, lun, lun2, lghtng3[ht_dex].hght, originzs, binsize=1.0, normalize=1, minhght, maxhght, freez, $
         H20, H40

  ;TIME VS. HEIGHT density plot

  ;Set up time values & contour the ldar data
  time=FINDGEN(nxth)*rest+st_jul+rest/2.0
  lev=[1.0 < 0.25*meandensth, 0.5*meandensth, 0.75*meandensth, meandensth, 1.25*meandensth, 1.5*meandensth, $
      2.0*meandensth, 4.0*meandensth]
  ;lev=[1.0 < 10000, 30000, 50000, 100000, 150000, 200000, 300000]
  col=[2, 3, 4, 5, 6, 7, 8, 9]
  CONTOUR, densth, time, hght, levels=lev, c_colors=col, /fill, /closed, position=[0.05,0.84,0.95,0.99], $
        xrange=[st_jul,end_jul], yrange=[minhght,maxhght], xcharsize=0.9, ycharsize=0.9, xstyle=1, $
        color=0, xtickformat='label_date', xticks=8, xticklen=0.07, /noerase

  ;Overlay storm reports
  IF reportanswer EQ 'y' THEN BEGIN
    type=cell[i].type
    ;Makes "report track"; use < or > to keep in plot area
    POLYFILL, [repst_jul > st_jul < end_jul, repend_jul < end_jul > st_jul, repend_jul < end_jul > st_jul, $
```

```
        repst_jul > st_jul < end_jul], [1.0, 1.0, 1.5, 1.5], 0, color=0
    XYOUTS, (repst_jul > st_jul), 2.0, type, charsize=1.0, charthick=2.0
  ENDIF

  ;X VS. HEIGHT density plot

  ;Set up x values & contour the data
  xd=FINDGEN(nx)*res+minx+res/2.0
  lev=[1.0 < 0.25*meandensxh, 0.5*meandensxh, 0.75*meandensxh, meandensxh, 1.25*meandensxh, 1.5*meandensxh, $
      2.0*meandensxh, 4.0*meandensxh]
  col=[2, 3, 4, 5, 6, 7, 8, 9]
  CONTOUR, densxh, xd, hght, levels=lev, c_colors=col, /fill, /closed, position=[0.05,0.67,0.75,0.795], $
        xrange=[minx,maxx], yrange=[minhght,maxhght], xcharsize=0.9, ycharsize=0.9, xstyle=1, color=0, $
        xticklen=0.1, /noerase

  ;Overlay storm reports
  IF reportanswer EQ 'y' THEN BEGIN
    stxreport=cell[i].stxreport
    ndxreport=cell[i].ndxreport
    POLYFILL, [stxreport > minx < maxx, ndxreport < maxx > minx, ndxreport < maxx > minx, $
         stxreport > minx < maxx], [1.0, 1.0, 1.5, 1.5], 0, color=0
    XYOUTS, (stxreport > minx < maxx), 2.0, type, charsize=1.0, charthick=2.0
  ENDIF

  ;Overlay radar data
  RADAR, radardir+st_hr+st_min+st_sec+'.cdf', 'DZ', 'y', [0.05,0.67,0.75,0.795], [minx,maxx], [miny,maxy], $
       zrange=[minhght,maxhght]

  ;Y VS. HEIGHT density plot

  ;Set up y values & contour the data
  yd=FINDGEN(ny)*res+miny+res/2.0
  lev=[1.0 < 0.25*meandenshy, 0.5*meandenshy, 0.75*meandenshy, meandenshy, 1.25*meandenshy, 1.5*meandenshy, $
      2.0*meandenshy, 4.0*meandenshy]
  col=[2, 3, 4, 5, 6, 7, 8, 9]
  CONTOUR, denshy, hght, yd, levels=lev, c_colors=col, /fill, /closed, position=[0.80,0.03,0.95,0.63], $
        xrange=[minhght,maxhght], yrange=[miny,maxy], xcharsize=0.9, ycharsize=0.9, ystyle=1, color=0, $
        yticklen=0.1, /noerase

  ;Overlay storm reports
  IF reportanswer EQ 'y' THEN BEGIN
    styreport=cell[i].styreport
    ndyreport=cell[i].ndyreport
    POLYFILL, [1.0, 1.0, 1.5, 1.5], [styreport > miny < maxy, ndyreport < maxy > miny, $
         ndyreport < maxy > miny, styreport > miny < maxy], 0, color=0
    XYOUTS, 2.0, (styreport > miny < maxy), type, charsize=1.0, charthick=2.0, orientation=270
  ENDIF

  ;Overlay radar data
  RADAR, radardir+st_hr+st_min+st_sec+'.cdf', 'DZ', 'x', [0.80,0.03,0.95,0.63], [minx,maxx], [miny,maxy], $
       zrange=[minhght, maxhght]

  ;PLAN VIEW density plot

  ;Contour the data
  lev=[1.0, ROUND(0.5*meandensxy+1.0), ROUND(0.75*meandensxy+2.0), ROUND(meandensxy+3.0), $
     ROUND(1.25*meandensxy+4.0), ROUND(1.5*meandensxy+5.0), ROUND(2.0*meandensxy+6.0), $
     ROUND(4.0*meandensxy+7.0)]; add 1,2,3,... to make sure interval not repeat
  slev=[STRCOMPRESS(STRING(1),/REMOVE_ALL),
STRCOMPRESS(STRING(ROUND(0.5*meandensxy+1.)),/REMOVE_ALL), $
       STRCOMPRESS(STRING(ROUND(0.75*meandensxy+2.)),/REMOVE_ALL), $
       STRCOMPRESS(STRING(ROUND(meandensxy+3.)),/REMOVE_ALL), $
       STRCOMPRESS(STRING(ROUND(1.25*meandensxy+4.)),/REMOVE_ALL), $
       STRCOMPRESS(STRING(ROUND(1.5*meandensxy+5.)),/REMOVE_ALL), $
       STRCOMPRESS(STRING(ROUND(2.0*meandensxy+6.)),/REMOVE_ALL), $
       STRCOMPRESS(STRING(ROUND(4.0*meandensxy+7.)),/REMOVE_ALL)]
```

```
col=[2, 3, 4, 5, 6, 7, 8, 9]
;lev=[1000000, 1000001, 1000002, 1000003, 1000004, 1000005, 1000006, 1000007]; for when just plot sensors
CONTOUR, densxy, xd, yd, levels=lev, c_colors=col, /fill, /closed, position=[0.05,0.03,0.75,0.63], $
     xrange=[minx,maxx], yrange=[miny,maxy], xcharsize=0.9, ycharsize=0.9, xstyle=1, ystyle=1, color=0, $
     /noerase; ;position=[0.1, 0.1, 0.9, 0.9],; for sensor plot; charsizes=2.0 for sensor plot

;Overlay CG chars.
;PLOT_CG, cgchar[j], vol, outpathcgtex
;pos_, neg_, ppos, nmed, nmul, pmed, pmul

;Overlay storm reports
IF reportanswer EQ 'y' THEN BEGIN
  POLYFILL, [stxreport > minx < maxx, ndxreport < maxx > minx, ndxreport < maxx > minx, $
       stxreport > minx < maxx], [styreport > miny < maxy, ndyreport < maxy > miny, $
       (ndyreport < maxy > miny)+0.5, (styreport > miny < maxy)+0.5], 0, color=0
  XYOUTS, (stxreport > minx < maxx), (styreport > miny < maxy)+1.0, type, charsize=1.0, charthick=2.0
ENDIF

;Overlay radar data
RADAR, radardir+st_hr+st_min+st_sec+'.cdf', 'DZ', 'z', [0.05,0.03,0.75,0.63], [minx,maxx], [miny,maxy], $
      zfr=[freez,maxhght];zfr=[freez,maxhght]

;Place the colorbar on the x-y part of chart; must change if do different size analysis box
;(i.e., not 60x60km)
POLYFILL, [cellx-29., cellx+29., cellx+29., cellx-29.], [celly-29., celly-29., celly-22., celly-22.], 0, $
       color=1
dx=6.0
dy=2.0
xbox=dx*[0,0,1,1]
ybox=dy*[0,1,1,0]
xref=cellx-FLOAT(N_ELEMENTS(lev))/2.0*dx
yref=celly-25.
FOR c = 0, N_ELEMENTS(lev)-1 DO BEGIN
  POLYFILL, xref+dx*c+xbox, yref+ybox, color=col[c]
  XYOUTS, xref+dx*c, yref-1.5*dy, slev[c], color=0, charsize=0.9
ENDFOR

;Colorbar for larger plot
;POLYFILL, [xdfw-99., xdfw+99., xdfw+99., xdfw-99.], [ydfw-99., ydfw-99., ydfw-89., ydfw-89.], 0, color=1
;dx=10.0
;dy=3.0
;xbox=dx*[0,0,1,1]
;ybox=dy*[0,1,1,0]
;xref=xdfw-FLOAT(N_ELEMENTS(lev))/2.0*dx
;yref=ydfw-94.
;FOR c = 0, N_ELEMENTS(lev)-1 DO BEGIN
;  POLYFILL, xref+dx*c+xbox, yref+ybox, color=col[c]
;  XYOUTS, xref+dx*c, yref-1.5*dy, slev[c], color=0, charsize=0.9
;ENDFOR

;Plot w/ block filling (Vaisala) - works, but not as "nice" as non-block filling (see test fig.)
;n_colors=7
;color_select=[2, 3, 4, 5, 6, 7, 8]
;density_level_incr=3.0d
;FOR p = 0, ny - 1 DO BEGIN
;  t=miny+DOUBLE(p)*res
;  tt=t+res
;  FOR q = 0, nx - 1 DO BEGIN
;     g=minx+DOUBLE(q)*res
;     gg=g+res
;     color_index=FIX(dens[q,p]/density_level_incr)
;     WHILE color_index GE n_colors DO color_index=color_index-n_colors
;     IF dens[q, p] GT 0.0d THEN $
;        POLYFILL, [g, gg, gg, g], [t, t, tt, tt], color=color_select[color_index]
;  ENDFOR
;ENDFOR
```

```
  ;Calls a subroutine that accesses the state line shapefile and plots the specified states
  snumb=N_ELEMENTS(countyname)
  FOR snumb=0, snumb-1 DO BEGIN
    STATESHP2, obpath, countyname, snumb, councol, slinthic
  ENDFOR

  ;Calls a subroutine that accesses the county line shapefile and plots the counties in the specified
  ;states; for when just plot sensors
  ;cnumb=N_ELEMENTS(countyname)
  ;FOR cnumb=0, cnumb-1 DO BEGIN
  ;  COUNTYSHP2, obpath, countyname, cnumb, councol, clinthic
  ;ENDFOR

  ;Plot sensor locations
  ;FOR s=0, n-1 DO BEGIN
  ;  PLOTS, xs[s], ys[s], psym=2, color=0, symsize=2.0; A-G
  ;ENDFOR

  ;Plot where center of cell/meso. is
  PLOTS, cellx, celly, psym=2, color=0, symsize=2.0

  ;Plot where DFW is (for sensor plot)
  ;XYOUTS, 0.0, 0.0, '  KFWS', color=0, charsize=1.0, charthick=1.5
  ;PLOTS, 0.0, 0.0, psym=8, color=0, symsize=2.0

  ;Range rings at 30 and 100 km (for study area plot)
  ;TVCIRCLE, 30.0, 0.0, 0.0, 0, /DATA, thick=2; 30 km
  ;TVCIRCLE, 100.0, 0.0, 0.0, 0, /DATA, thick=2; 100 km
  ;TVCIRCLE, 150.0, xdfw, ydfw, 0, /DATA, thick=8; 150 km around LDAR II

  DEVICE, /CLOSE_FILE, encapsulated=1
  SET_PLOT, 'win'
  !P.FONT=0

 ENDFOR

 jump1:

ENDFOR

STOP
END
```

```
;*******************************************************************************
; IDL PROGRAM: radar.pro
; USAGE: radar, ifile, (cut), var, dim, position, xrange, yrange, zrange=zrange, zfr=zfr
;
;   ARGUMENTS   ifile     Input:  String containing path/name to CDF file
;               cut       Input:  Level of analysis if used (then add in code from radarold)
;               var       Input:  Radar variable to be displayed
;               dim       Input:  plane to plot on (x, y, z) (slab)
;               position  Input:  plot position (normal coords.)
;               xrange    Input:  x range (LDAR box) for plots
;               yrange    Input:  y range
;               zrange    Input:  z range
;               zfr       Input:  z range for plan view calculations (above melting level)
;
;   CALLS       ncdf_read.pro
;               myconfill.pro
;               get_88d_info.pro
;               myconfillcolor.pro
;
;
;   ABSTRACT    This program reads in radar data from a netcdf file, which is
;       output to the IDL window. A ".png" is then created, which is then
;       converted into a ".gif" (using convert).  Alternatively, may create ".ps" file.
;       Modified to be called by ldar_dens2 and other pros. by Steiger.
;
;   AUTHOR:     Larry Belcher
;               NCSU
;               Raleigh, NC 27601
;
;
;   CREATED:    6/6/02
;
;   SAMPLE RUN: radar, 'C:\My Documents\scotts\Dissertation\Careyradar\KFWS20011013_010010.cdf', 'DZ', 'y', $
;         [0.05,0.03,0.75,0.63], [30, 90], [32.57, 92.57], zrange=[0.,20.]
;
;   MODIFIED:   Scott Steiger
;               Texas A&M University
;               6/29/04
;*******************************************************************************

PRO RADAR, ifile, var, dim, position, xrange, yrange, zrange=zrange, zfr=zfr
;For mean, max, cumu Z plots - no cut

;Get info about radar
rlevel=0.228; km MSL (KFWS)
radname=''
READS, ifile, radname, format='(56x, A4)'   ;Depends on what ifile "looks like"

;SET_PLOT, 'PS'  ;Postscript output
;DEVICE, /color, xoffset=0.254, yoffset=0.254, $
;     filename='C:\My Documents\scotts\Dissertation\Careyradar\test.ps'

;CALL NCDF_READ to read ".cdf" file
NCDF_READ,ifile,"DZ",info,dz
;NCDF_READ,ifile,"DR",info,dr
;NCDF_READ,ifile,"KD",info,kd
;NCDF_READ,ifile,"RH",info,rh
;NCDF_READ,ifile,"LD",info,ld
NCDF_READ,ifile,"base_time",info,real_time
NCDF_READ,ifile,"lat",info,lat
NCDF_READ,ifile,"lon",info,lon
NCDF_READ,ifile,"alt",info,zfirst
NCDF_READ,ifile,"x_spacing",info,xdelta
NCDF_READ,ifile,"y_spacing",info,ydelta
NCDF_READ,ifile,"z_spacing",info,zdelta
```

```
;Get Site info
GET_88D_INFO, radname, rlat, rlon

;Set up coordinate system
yfirst=TAN((lat-rlat)*0.01745329252)*6378.4
xfirst=TAN((lon-rlon)*0.01745329252)*6378.4
latadj=COS(lat*0.01745329252)
xfirst=xfirst*latadj
xfirst=FLOOR(xfirst+0.5)
yfirst=FLOOR(yfirst+0.5)
info.xdelta=FLOAT(xdelta)
info.ydelta=FLOAT(ydelta)
info.xfirst=FLOAT(xfirst)
info.yfirst=FLOAT(yfirst)
info.zfirst=FLOAT(zfirst+rlevel)
info.zdelta=FLOAT(zdelta)

;Get size info about the array
siz=SIZE(DZ)  ;Change for each variable

;Convert DZ to linear
Z=10^(DZ/10.)

;Set contour intervals
;IF (var EQ 'DZ') THEN levs=[100,200,300,400,500,600,700,800,900,1000,1100]; for cum. Z
IF (var EQ 'DZ') THEN BEGIN; Reflectivity
  ;levs=[10,20,30,40,50]
  ;slevs=['10','20','30','40','50 dBZ']
  levs=[10,20,25,30,35,40,45,50,55]
  slevs=['10','20','25','30','35','40','45','50','55 dBZ']
ENDIF
IF (var EQ 'DR') THEN levs=[-1.5,-1,-0.5,0,0.5,1,1.5,2,2.5,3,3.5]
IF (var EQ 'KD') THEN levs=[0.0,0.1,0.2,0.3,0.4,0.5,0.6,0.7,0.8,0.9,1.0]
IF (var EQ 'LD') THEN levs=[-30,-28,-26,-24,-22,-20,-18,-16,-14,-12,-10]
IF (var EQ 'RH') THEN levs=[0.9,0.91,0.92,0.93,0.94,0.95,0.96,0.97,0.98,0.99,1.0]

;***If change any variables in REORDER (spacing, first x (i.e., -150.0), etc.), may need to change below!
;For X-Y Plane:
IF dim EQ 'z' THEN BEGIN
  ;Determine 2-d projection of mean, max, and cumulative (integrated) DZ for each column
  meandz=FLTARR(siz[1], siz[2])
  maxdz=FLTARR(siz[1], siz[2])
  cumudz=FLTARR(siz[1], siz[2])
  rtop=FLTARR(siz[1], siz[2]); dBZ echo height
  FOR i=0, siz[1]-1 DO BEGIN
    FOR j=0, siz[2]-1 DO BEGIN
      m=WHERE(DZ[i,j,*] GT 0.0); So not average in any "missing" reflectivity; GT
      ;Only want above melting level:
      k=WHERE((m*zdelta+info.zfirst GE zfr[0]) AND (m*zdelta+info.zfirst LT zfr[1]))
      l=WHERE(DZ[i,j,*] GE 40.0); for rtop
      IF l[0] NE -1 THEN BEGIN; make sure there are points
        rtop[i,j]=MAX(l)*zdelta+info.zfirst
      ENDIF
      IF k[0] NE -1 THEN BEGIN
        meandz[i,j]=10.*ALOG10(MEAN(Z[i,j,m[k]])); average linearized values
        maxdz[i,j]=MAX(DZ[i,j,m[k]])
        cumudz[i,j]=TOTAL(Z[i,j,m[k]])
      ENDIF
    ENDFOR
  ENDFOR
  ;CALL MYCONFILL to do the contouring - change depending if want mean, max, cumu dz, or rtop
  ;MYCONFILLCOLOR, info, meandz, dim, levs, slevs, [2, 3, 4, 5, 6, 7, 8, 9, 1], xrange=xrange, yrange=yrange, $
  ;          position
  MYCONFILL, info, meandz, dim, levs ;[2.0, 4.0, 6.0, 8.0, 10.0, 12.0, 14.0, 16.0, 18.0]
  ;Use MYCONFILLCOLOR if want radar color-filled (i.e., radar-cg overlays)
  ;PRINT, 'radar test:'
```

```
  ;PRINT, DZ[239,114,*]
  ;PRINT, Z[239,114,*]
  ;PRINT, meandz[239,114]
ENDIF

;For X-Z Plane:
IF dim EQ 'y' THEN BEGIN
  ;Determine 2-d field of mean, max, and cumu DZ for each column
  meandz=FLTARR(siz[1], siz[3])
  maxdz=FLTARR(siz[1], siz[3])
  cumudz=FLTARR(siz[1], siz[3])
  FOR i=0, siz[1]-1 DO BEGIN
    FOR j=0, siz[3]-1 DO BEGIN
      m=WHERE(DZ[i,*,j] GT 0.0)
      ;Only want radar data in 60x60 km box (see ldar_dens2) (take out slab)
      k=WHERE((m*ydelta+yfirst GE yrange[0]) AND (m*ydelta+yfirst LT yrange[1]))
      IF k[0] NE -1 THEN BEGIN
        meandz[i,j]=10.*ALOG10(MEAN(Z[i,m[k],j]))
        maxdz[i,j]=MAX(DZ[i,m[k],j])
        cumudz[i,j]=TOTAL(Z[i,m[k],j])
      ENDIF
    ENDFOR
  ENDFOR
  ;MYCONFILLCOLOR, info, meandz, dim, levs, slevs, [2, 3, 4, 5, 6, 7, 8, 9, 1], xrange=xrange, zrange=zrange, $
  ;          position
  MYCONFILL, info, meandz, dim, levs
ENDIF

;For Y-Z Plane:
IF dim EQ 'x' THEN BEGIN
  ;Determine 2-d field of mean, max, and cumu DZ for each column
  meandz=FLTARR(siz[3], siz[2])
  maxdz=FLTARR(siz[3], siz[2])
  cumudz=FLTARR(siz[3], siz[2])
  FOR i=0, siz[2]-1 DO BEGIN
    FOR j=0, siz[3]-1 DO BEGIN
      m=WHERE(DZ[*,i,j] GT 0.0)
      k=WHERE((m*xdelta+xfirst GE xrange[0]) AND (m*xdelta+xfirst LT xrange[1]))
      IF k[0] NE -1 THEN BEGIN
        meandz[j,i]=10.*ALOG10(MEAN(Z[m[k],i,j]))
        maxdz[j,i]=MAX(DZ[m[k],i,j])
        cumudz[j,i]=TOTAL(Z[m[k],i,j])
      ENDIF
    ENDFOR
  ENDFOR
  ;MYCONFILLCOLOR, info, meandz, dim, levs, slevs, [2, 3, 4, 5, 6, 7, 8, 9, 1], yrange=yrange, zrange=zrange, $
  ;          position
  MYCONFILL, info, meandz, dim, levs
ENDIF

;STOP
END
```

```
PRO LDARRADARTH_PLOT2

;Plots a time-height display of a storm cell's radar and ldar source density history
;(within "radcut" km of cell center).
;Also overlays severe storm reports.
;
;Programmed by Scott M. Steiger 15 July 2004;
;Modified and slightly changed name from THLDARRADAR_PLOT 26 August 2004
;
;CALLS: ncdf_read.pro

COMPILE_OPT IDL2
CLOSE, /ALL
pi=3.1415926535

;Info about radar
rlevel=0.228; km MSL (KFWS)
radname='KFWS'

;Temperature levels (change between cases)
freez=3.5; Ambient melting level in km (for radar.pro)
H20=6.51
H40=9.1

radcut=10.0; radius cutoff in km
rcut=STRCOMPRESS(STRING(FIX(radcut)), /REMOVE_ALL)
IF STRLEN(rcut) EQ 1 THEN rcut='0'+rcut
minhght=0.; Height range
maxhght=20.; km
mnhght=STRCOMPRESS(STRING(FIX(minhght)), /REMOVE_ALL)
mxhght=STRCOMPRESS(STRING(FIX(maxhght)), /REMOVE_ALL)
IF STRLEN(mnhght) EQ 1 THEN mnhght='0'+mnhght
IF STRLEN(mxhght) EQ 1 THEN mxhght='0'+mxhght
resh=1.0; vertical resolution of ldar data in km
nh=ROUND((maxhght-minhght)/resh)

maxrec=100; for reading structure below

;Set up filepaths
inpath='C:\My Documents\scotts\Dissertation\'
cases='030406supercase\'
outpathima=inpath+cases+'ldarradar_time_imagesm\'; outpath for images
;For Radar files
radardir=inpath+'Careyradar\20030406\KFWS20030406_'; where radar netcdf files are located

mon=FIX(STRMID(cases, 2, 2))
day=FIX(STRMID(cases, 4, 2))
year=FIX('20'+STRMID(cases, 0, 2))

;Get storm cell info.-change between cases
;Storm data (times, locations, cell IDs); use '2' for 030406 case:
OPENR, lun, inpath+cases+'stormmesodata030406hail2.txt', /GET_LUN
fomt='(a5,i2,1x,i2,1x,f2.0,1x,i2,1x,i2,1x,f2.0,1x,i4,f6.1,i4,i4,a2,f6.1,f6.1,f6.1,f6.1,i2,1x,i2,1x,f2.0,1x,i2,1x,i2,1x,f2.0,1x,a1)'
;fomt='(a5,i2,1x,i2,1x,f2.0,1x,i2,1x,i2,1x,f2.0,1x,i4,f6.1,i4,i4,a1)'; for non-storm report events
;Included tabs in file above
records={vol:'',st_hr:0,st_min:0,st_sec:0.0d,end_hr:0,end_min:0,end_sec:0.0d,azimu:0,range:0.0d,mesoid:0, $
        cellid:0,reportanswer:'',stxreport:0.0d,styreport:0.0d,ndxreport:0.0d,ndyreport:0.0d,repst_hr:0, $
        repst_min:0,repst_sec:0.0d,repend_hr:0,repend_min:0,repend_sec:0.0d,type:''}
;records={vol:'',st_hr:0,st_min:0,st_sec:0.0d,end_hr:0,end_min:0,end_sec:0.0d,azimu:0,range:0.0d,mesoid:0, $
;      cellid:0,reportanswer:''}; non-storm
;mesoid=cellid in non-meso. cases
cell=REPLICATE(CREATE_STRUCT(records), maxrec); Create structures
ind1=0
WHILE NOT EOF(lun) DO BEGIN
  READF, lun, records, format=fomt
  cell[ind1]=records
```

```
  ind1=ind1+1
ENDWHILE; if doesn't exit loop correctly: make sure no spaces after last datum in file
FREE_LUN, lun
;Trims the structure array to the needed size
cell=cell[0:ind1-1]

st_jul=JULDAY(mon, day, year, cell.st_hr, cell.st_min, cell.st_sec); convert times to julian
;beware if more than one day!
end_jul=JULDAY(mon, day, year, cell.end_hr, cell.end_min, cell.end_sec)
voltime_jul=(st_jul+end_jul)/2.0 ; middle point of volume scan for plots
date_labels=LABEL_DATE(date_format=['%h%i%s%3']); plot time axis labels correctly

;Sets up color table for plots
TVLCT, 255, 255, 255, 1  ;white
TVLCT, 0, 0, 0, 0        ;black
TVLCT, 204, 0, 204, 2    ;lt purple
TVLCT, 102, 0, 204, 3    ;dk purple
TVLCT, 51, 204, 204, 4   ;lt blue
TVLCT, 0, 51, 204, 5     ;med blue
TVLCT, 0, 153, 0, 6      ;green
TVLCT, 255, 255, 0, 7    ;yellow
TVLCT, 255, 102, 0, 8    ;orange
TVLCT, 255, 0, 0, 9      ;red
TVLCT, 128, 128, 128, 10 ;gray
TVLCT, r, g, b, /GET

meandzs=FLTARR(1); for reflectivity calculations below

;Get total # of ldar sources info. for each volume scan (for ldar count calculations below)
; make sure ldar file has all volumes!
OPENR, lun, inpath+cases+'lghavgsm\ldarchars'+rcut+'km.txt', /GET_LUN; use *negs* files (see 020616 cases)
fmt='(a4,2x,i3,2x,i3,2x,f6.3,2x,f6.3,2x,f6.3,2x,i1,2x,f6.3,2x,f8.5,2x,f6.3,2x,i6,2x,f7.3,2x,f6.3,2x,f8.5,2x,f6.3,2x,i6,2x,f8.3)'
record={vol:'',cellid:0L,mesoid:0L,quart:0.0d,med:0.0d,top:0.0d,modes:0L,ht1:0.0d,normpk1:0.0d,thick1:0.0d, $
        totpts:0L,dist:0.0d,ht2:0.0d,normpk2:0.0d,thick2:0.0d,nfl:0L,rat:0.0d}
data=REPLICATE(CREATE_STRUCT(record), maxrec)
ind=0L
WHILE NOT EOF(lun) DO BEGIN
  READF, lun, record, format=fmt
  data[ind]=record
  ind=ind+1L
ENDWHILE
data=data[0:ind-1]
FREE_LUN, lun

post=outpathima+'ldarradarthrad'+rcut+'km.eps'; name of figure file
;Setup the postscript device - place code before any plotting command
SET_PLOT, 'ps'
DEVICE, filename=post, xsize=8.0, ysize=5.0, /inches, /color, /Helvetica, encapsulated=1, font_size=12.0, $
      preview=0
!P.FONT=0

;Loop through each volume scan to get ldar & radar data to plot cell history
; (within "radcut" km radial distance of each cell)
FOR i=0, ind1-1 DO BEGIN; ind1-1

  vol=STRCOMPRESS(cell[i].vol, /REMOVE_ALL); volume scan #
  PRINT, 'Output for vol: ', vol
  PRINT, ' '

  ;Cell x & y locations w.r.t. radar
  cellx=-cell[i].range*COS((pi/180.)*(270-cell[i].azimu))
  celly=-cell[i].range*SIN((pi/180.)*(270-cell[i].azimu))

  ; Start & end times of volume scan
  st_hr=STRCOMPRESS(STRING(FIX(cell[i].st_hr)), /REMOVE_ALL)
  st_min=STRCOMPRESS(STRING(FIX(cell[i].st_min)), /REMOVE_ALL)
```

```
st_sec=STRCOMPRESS(STRING(FIX(cell[i].st_sec)), /REMOVE_ALL)
end_hr=STRCOMPRESS(STRING(FIX(cell[i].end_hr)), /REMOVE_ALL)
end_min=STRCOMPRESS(STRING(FIX(cell[i].end_min)), /REMOVE_ALL)
end_sec=STRCOMPRESS(STRING(FIX(cell[i].end_sec)), /REMOVE_ALL)
IF STRLEN(st_hr) EQ 1 THEN st_hr='0'+st_hr
IF STRLEN(st_min) EQ 1 THEN st_min='0'+st_min
if STRLEN(st_sec) EQ 1 THEN st_sec='0'+st_sec
if STRLEN(end_hr) EQ 1 THEN end_hr='0'+end_hr
if STRLEN(end_min) EQ 1 THEN end_min='0'+end_min
if STRLEN(end_sec) EQ 1 THEN end_sec='0'+end_sec

;Get ldar data:
ldarfile=inpath+cases+'ldartextm\hthist'+mnhght+'-'+mxhght+'km'+st_hr+st_min+st_sec+'_to_'+ $
      end_hr+end_min+end_sec+'v'+vol+'rad'+rcut+'.txt'
;Get data from file
OPENR, lun, ldarfile, /GET_LUN
h=FLTARR(nh)
cnt=FLTARR(nh)
h0=0.0
cnt0=0.0; method from Bowman IDL book, p. 134
FOR j=0, nh-1 DO BEGIN
  READF, lun, h0, cnt0
  h[j]=h0
  cnt[j]=cnt0
ENDFOR
FREE_LUN, lun
cnt=ROUND(cnt*data[i].totpts); to convert to #of sources
IF i EQ 0 THEN BEGIN; if first pass...
  cnts=cnt
ENDIF ELSE BEGIN
  cnts=[cnts, cnt]
ENDELSE

;Get radar data:
ifile=radardir+st_hr+st_min+st_sec+'.cdf'
;CALL ncdf_read to read ".cdf" file
NCDF_READ,ifile,"DZ",info,dz
NCDF_READ,ifile,"lat",info,lat
NCDF_READ,ifile,"lon",info,lon
NCDF_READ,ifile,"alt",info,zfirst
NCDF_READ,ifile,"x_spacing",info,xdelta
NCDF_READ,ifile,"y_spacing",info,ydelta
NCDF_READ,ifile,"z_spacing",info,zdelta
;Get radar site info
GET_88D_INFO, radname, rlat, rlon
;Set up coordinate system
yfirst=TAN((lat-rlat)*0.01745329252)*6378.4
xfirst=TAN((lon-rlon)*0.01745329252)*6378.4
latadj=COS(lat*0.01745329252)
xfirst=xfirst*latadj
xfirst=FLOOR(xfirst+0.5)
yfirst=FLOOR(yfirst+0.5)
zfirst=zfirst+rlevel
;get size info about the array
siz = SIZE(DZ)
;Set up x and y axis values in cell-relative framework
x=xfirst+FINDGEN(siz[1])*xdelta-cellx
y=yfirst+FINDGEN(siz[2])*ydelta-celly
;Cycle through all x and y positions w.r.t. cell location and
; determine which are within "radcut" km of cell
xs=INTARR(1)
ys=INTARR(1)
ind2=0
FOR j=0, siz[1]-1 DO BEGIN
  FOR k=0, siz[2]-1 DO BEGIN
    rad=SQRT(x[j]^2+y[k]^2); radial distance of point to check from cell
```

```
    IF rad LE radcut THEN BEGIN; if point within distance of cell, count it and save position in array
     IF ind2 EQ 0 THEN BEGIN
       xs=j
       ys=k
     ENDIF ELSE BEGIN
       xs=[xs,j]
       ys=[ys,k]
     ENDELSE
     ind2=ind2+1
    ENDIF
   ENDFOR
  ENDFOR

  FOR j=0, siz[3]-1 DO BEGIN; for each height increment (i.e., every 0.5 km)
   ;Take out "slab" of reflectivity with array positions determined above
   js=INTARR(ind2)+j; to make sure properly paired in next line
   DBZ=DZ[xs, ys, js]; selected reflectivity field
   m=WHERE(DBZ GT 0)
   IF m[0] NE -1 THEN BEGIN
    DBZ=DBZ[m]
    Z=10^(DBZ/10.); Convert DBZ to linear units
    meandz=10.*ALOG10(MEAN(Z))
   ENDIF ELSE BEGIN
    meandz=0.0
   ENDELSE
   IF i EQ 0 AND j EQ 0 THEN BEGIN
    meandzs=meandz
   ENDIF ELSE BEGIN
    meandzs=[meandzs, meandz]
   ENDELSE
  ENDFOR

ENDFOR; to ind1-1

; Reform arrays into 2-D; see 8/26 notes to understand transpose
cnts=TRANSPOSE(FLOAT(REFORM(cnts, nh, ind1))); LDAR II data
meandzs=TRANSPOSE(FLOAT(REFORM(meandzs, siz[3], ind1))); assumes all radar files have same siz[3]

;Plot mean radar refl. vs. time
;Contour levels for radar refl. plots:
levs=[10,20,25,30,35,40,45,50,55]
slevs=['10','20','25','30','35','40','45','50','55 dBZ']
color=[2, 3, 4, 5, 6, 7, 8, 9, 1]
ht=zfirst+FINDGEN(siz[3])*zdelta; assumes all radar files have same characteristics (i.e, zdelta)
xticks=ROUND(N_ELEMENTS(voltime_jul)/5.); major tick intervals; want each tick mark (minor and major) to
; correspond to a volume time
;xticks=4
k=FINDGEN(xticks+1)*((N_ELEMENTS(voltime_jul)-1)/xticks); have actual volume times on x-axis evenly spaced
xminor=(N_ELEMENTS(voltime_jul)-1)/xticks
;xminor=5
CONTOUR, meandzs, voltime_jul, ht, levels=levs, c_colors=color, /fill, /closed, xrange=[voltime_jul[0], $
       voltime_jul[ind1-1]], yrange=[minhght,maxhght], xcharsize=0.9, ycharsize=0.9, xstyle=1, color=0, $
         xtitle='Time (UTC)', ytitle='Height (km) MSL', position=[0.10,0.1,0.90,0.8], $
         xtickformat='label_date', xticks=xticks, xtickv=voltime_jul[k], xminor=xminor, /noerase

;Place the colorbar above chart (for mean dz)
dx=0.08
dy=0.02
xbox=dx*[0,0,1,1]
ybox=dy*[0,1,1,0]
xref=0.5-FLOAT(N_ELEMENTS(levs))/2.0*dx
yref=0.85
FOR c=0, N_ELEMENTS(levs)-1 DO BEGIN
 POLYFILL, xref+dx*c+xbox, yref+ybox, color=color[c], /normal
 XYOUTS, xref+dx*c, yref-1.5*dy, slevs[c], color=0, charsize=0.9, /normal
ENDFOR
```

```
;calculate the source densities & plot
area=1.0*resh; 1 volume
dens=FLTARR(ind1, nh)
dens=cnts/area
;overplot source densities
lev=[1.0, 50.0, 100.0, 200.0, 400.0, 800.0, 1600.0, 3200.0, 6400.0]
hght=minhght+FINDGEN(nh)*resh+resh/2.0
CONTOUR, dens, voltime_jul, hght, c_colors=0, levels=lev, closed=1, c_labels=[1,0,1,0,1,0,1,0,1], /overplot, $
      color=0

;Overlay storm report bar(s)
s=WHERE(STRCOMPRESS(cell.reportanswer, /REMOVE_ALL) EQ 'y', stcount)
IF stcount GT 0 THEN BEGIN
  st_julrep=JULDAY(mon, day, year, cell[s].repst_hr, cell[s].repst_min, cell[s].repst_sec)
  nd_julrep=JULDAY(mon, day, year, cell[s].repend_hr, cell[s].repend_min, cell[s].repend_sec)
  type=cell[s].type
  FOR i=0, stcount-1 DO BEGIN
    POLYFILL, [st_julrep[i], nd_julrep[i], nd_julrep[i], st_julrep[i]], [1.0, 1.0, 1.5, 1.5], 0, color=0
    XYOUTS, st_julrep[i], 2.0, type[i], charsize=1.0, charthick=2.0
  ENDFOR
ENDIF

;Overlay Temp. level bars
twomin=(JULDAY(9, 14, 1976, 4, 29, 44.0))-(JULDAY(9, 14, 1976, 4, 27, 44.0)) ;2 minutes length for plot bar
XYOUTS, voltime_jul[ind1-1]+twomin, freez, '0 C', charsize=0.9
POLYFILL, [voltime_jul[ind1-1]-twomin, voltime_jul[ind1-1]+twomin, voltime_jul[ind1-1]+twomin, $
      voltime_jul[ind1-1]-twomin], [freez-0.2, freez-0.2, freez+0.2, freez+0.2], 0, color=0
XYOUTS, voltime_jul[ind1-1]+twomin, H20, '-20', charsize=0.9
POLYFILL, [voltime_jul[ind1-1]-twomin, voltime_jul[ind1-1]+twomin, voltime_jul[ind1-1]+twomin, $
      voltime_jul[ind1-1]-twomin], [H20-0.2, H20-0.2, H20+0.2, H20+0.2], 0, color=0
XYOUTS, voltime_jul[ind1-1]+twomin, H40, '-40', charsize=0.9
POLYFILL, [voltime_jul[ind1-1]-twomin, voltime_jul[ind1-1]+twomin, voltime_jul[ind1-1]+twomin, $
      voltime_jul[ind1-1]-twomin], [H40-0.2, H40-0.2, H40+0.2, H40+0.2], 0, color=0

DEVICE, /close_file, encapsulated=1
SET_PLOT, 'win'
!P.FONT=0

STOP
END
```

```
PRO TIME_SERIES

;Creates time series of ldar, radar, and cg chars. for a storm cell
; Document scaling factors!

COMPILE_OPT IDL2

CLOSE, /ALL

inpath='C:\My Documents\scotts\Dissertation\011013squallcase\overlaysystem\'
;Change between cases; also radar and storm filenames
;Place CG files in separate directory; Check 'check' when reading CG chars.; Create series directory
; Create radar file (check to uncomment meso. chars.)
radius='system'; 20, 10, 05 (km), whole MCS
mon=FIX(STRMID(inpath, 38, 2))
day=FIX(STRMID(inpath, 40, 2))
year=STRMID(inpath, 36, 2)
year=FIX('20'+year)

;Read in LDAR chars.
maxrec=200
OPENR, lun, inpath+'lghavgs\ldarchars'+radius+'km.txt', /GET_LUN; include where rat=neg. #
fmt='(a4,2x,i3,2x,i3,2x,f6.3,2x,f6.3,2x,f6.3,2x,f6.3,2x,i1,2x,f6.3,2x,f8.5,2x,f6.3,2x,i6,2x,f7.3,2x,f6.3,2x,f8.5,2x,f6.3,2x,i6,2x,f8.3)'
record={vol:'',cellid:0L,mesoid:0L,quart:0.0d,med:0.0d,top:0.0d,modes:0L,ht1:0.0d,normpk1:0.0d,thick1:0.0d, $
        totpts:0L,dist:0.0d,ht2:0.0d,normpk2:0.0d,thick2:0.0d,nfl:0L,rat:0.0d}
data=REPLICATE(CREATE_STRUCT(record), maxrec); Create structure
ind=0
WHILE NOT EOF(lun) DO BEGIN
  READF, lun, record, format=fmt; get data from file
  data[ind]=record; store data
  ind=ind+1
ENDWHILE
FREE_LUN, lun
data=data[0:ind-1]; trim data
data.vol=STRCOMPRESS(data.vol, /REMOVE_ALL)

;Read in Radar chars. - comment for MCS
;OPENR, lun, inpath+'radarstatswdss010627nosev.txt', /GET_LUN; Radar file
;fmt2='(a5, i4, i4, i3, f5.1, f5.1, f5.1, i5, i5, i4)'; Include tabs (why a5 not a4)
;record2={vol:'', mesoid:0L, cellid:0L, diam:0L, maxz:0.0d, maxzht:0.0d, rtop:0.0d, shi:0L, vil:0L, msi:0L}
;fmt2='(a5, i4, i4, f5.1, f5.1, f5.1, i5, i4)'    ;For non-mesocyclones
;record2={vol:'', mesoid:0L, cellid:0L, maxz:0.0d, maxzht:0.0d, rtop:0.0d, shi:0L, vil:0L}
;data2=REPLICATE(CREATE_STRUCT(record2), maxrec)
;ind2=0
;WHILE NOT EOF(lun) DO BEGIN
;  READF, lun, record2, format=fmt2
;  data2[ind2]=record2
;  ind2=ind2+1
;ENDWHILE
;FREE_LUN, lun
;data2=data2[0:ind2-1]

;Read in CG characteristics-loop through each CG char.
;Find all 8 CG files (all together in a separate directory)
filelist=FINDFILE(inpath+'cgavgs\*'+radius+'km.txt')
;cg_array is an array of structures to hold all CG chars.
cg_array=REPLICATE({vol:STRARR(maxrec), cellid:LONARR(maxrec), mesoid:LONARR(maxrec), cgchar:FLTARR(maxrec), $
          ind3:0L, check:''}, N_ELEMENTS(filelist))
FOR i=0, N_ELEMENTS(filelist)-1 DO BEGIN; Loop to read in all CG chars.
  OPENR, lun, filelist[i], /GET_LUN
  ;Check which CG char. reading in (may have to change this line between cases)
  check=STRMID(filelist[i], 74, 4)
  IF check EQ 'nmed' OR check EQ 'pmed' OR check EQ 'nmul' OR check EQ 'pmul' THEN BEGIN
    fmt3='(a4, 2x, i3, 2x, i3, 2x, f7.3, 2x, f7.3, 2x, f7.3, 2x, f7.3)'; set formats
    record3={vol:'', cellid:0L, mesoid:0L, cgchar:0.0, cgchar2:0.0, cgchar3:0.0, cgchar4:0.0}
    data3=REPLICATE(CREATE_STRUCT(record3), maxrec); create structure to hold data
```

```
  ENDIF
  IF check EQ 'ppos' THEN BEGIN
    fmt3='(a4, 2x, i3, 2x, i3, 2x, f8.4)'
    record3={vol:'', cellid:0L, mesoid:0L, cgchar:0.0}
    data3=REPLICATE(CREATE_STRUCT(record3), maxrec)
  ENDIF
  IF check EQ 'dens' OR check EQ 'pos_' OR check EQ 'neg_' THEN BEGIN
    fmt3='(a4, 2x, i3, 2x, i3, 2x, f10.7, 2x, f4.0)'
    ;Switched cgchar's to get #flashes as cgchar
    record3={vol:'', cellid:0L, mesoid:0L, cgchar2:0.0, cgchar:0.0}
    data3=REPLICATE(CREATE_STRUCT(record3), maxrec)
  ENDIF
  ind3=0L
  WHILE NOT EOF(lun) DO BEGIN
    READF, lun, record3, format=fmt3
    data3[ind3]=record3
    ind3=ind3+1L
  ENDWHILE
  FREE_LUN, lun
  vol=data3.vol; create radar volume number array
  cellid=data3.cellid; create cellid array
  mesoid=data3.mesoid; create mesoid array
  cgchar=data3.cgchar; create cgchar array
  ;Structure of all information about one CG char.
  cg_struct={vol:vol, cellid:cellid, mesoid:mesoid, cgchar:cgchar, ind3:ind3, check:check}
  cg_array[i]=cg_struct; Makes an array of all CG chars.
ENDFOR
neg=cg_array[WHERE(cg_array.check EQ 'neg_')]
;Need volumes to know corresponding times for CG chars. that not occur throughout entire period
negvol=STRCOMPRESS(neg.vol[0:neg.ind3-1], /REMOVE_ALL)
negfl=neg.cgchar[0:neg.ind3-1]; -CG flash rate
nmed=cg_array[WHERE(cg_array.check EQ 'nmed')]
nmedvol=STRCOMPRESS(nmed.vol[0:nmed.ind3-1], /REMOVE_ALL)
nmedfl=nmed.cgchar[0:nmed.ind3-1]; -CG median peak current
nmul=cg_array[WHERE(cg_array.check EQ 'nmul')]
nmulvol=STRCOMPRESS(nmul.vol[0:nmul.ind3-1], /REMOVE_ALL)
nmulfl=nmul.cgchar[0:nmul.ind3-1]; -CG mean flash multiplicity
pmed=cg_array[WHERE(cg_array.check EQ 'pmed')]; Comment out if no pmed file exists
pmedvol=STRCOMPRESS(pmed.vol[0:pmed.ind3-1], /REMOVE_ALL)
pmedfl=pmed.cgchar[0:pmed.ind3-1]; +CG median peak current
pmul=cg_array[WHERE(cg_array.check EQ 'pmul')]
pmulvol=STRCOMPRESS(pmul.vol[0:pmul.ind3-1], /REMOVE_ALL)
pmulfl=pmul.cgchar[0:pmul.ind3-1]; +CG mean multiplicity
pos=cg_array[WHERE(cg_array.check EQ 'pos_')]
posvol=STRCOMPRESS(pos.vol[0:pos.ind3-1], /REMOVE_ALL)
posfl=pos.cgchar[0:pos.ind3-1]; +CG flash rate
ppos=cg_array[WHERE(cg_array.check EQ 'ppos')]
pposvol=STRCOMPRESS(ppos.vol[0:ppos.ind3-1], /REMOVE_ALL)
pposfl=ppos.cgchar[0:ppos.ind3-1]; %+CG

;Get storm cell info.
OPENR, lun, inpath+'011013squallsysteminfo2.txt', /GET_LUN; Storm data (cell locations, etc.)
;Include tabs in fmt4
;fmt4='(a4,i2,1x,i2,1x,f2.0,1x,i2,1x,i2,1x,f2.0,1x,i4,f6.1,i4,i4,a2,f6.1,f6.1,f6.1,f6.1,i2,1x,i2,1x,f2.0,1x,i2,1x,i2,1x,f2.0,1x,a1)'
fmt4='(a5,i2,1x,i2,1x,f2.0,1x,i2,1x,i2,1x,f2.0,1x,i4,f6.1,i4,i4,a1)';for non-storm report events
;record4={vol:'',st_hr:0,st_min:0,st_sec:0.0,end_hr:0,end_min:0,end_sec:0.0,azimu:0,range:0.0,mesoid:0, $
;      cellid:0, reportanswer:'',stxreport:0.0,styreport:0.0,ndxreport:0.0,ndyreport:0.0,repst_hr:0, $
;      repst_min:0,repst_sec:0.0,repend_hr:0,repend_min:0,repend_sec:0.0,type:''}
record4={vol:'',st_hr:0,st_min:0,st_sec:0.0d,end_hr:0,end_min:0,end_sec:0.0d,azimu:0,range:0.0d,mesoid:0, $
      cellid:0,reportanswer:''}; non-storm; mesoid=cellid in non-meso. cases
cell=REPLICATE(CREATE_STRUCT(record4), maxrec)
ind4=0
WHILE NOT EOF(lun) DO BEGIN
  READF, lun, record4, format=fmt4
  cell[ind4]=record4
  ind4=ind4+1
```

```
ENDWHILE; if doesn't exit loop correctly: make sure no spaces after last datum in file
FREE_LUN, lun
cell=cell[0:ind4-1]
cell.vol=STRCOMPRESS(cell.vol, /REMOVE_ALL)

st_jul=JULDAY(mon, day, year, cell.st_hr, cell.st_min, cell.st_sec); Convert volume times to Julian
nd_jul=JULDAY(mon, day, year, cell.end_hr, cell.end_min, cell.end_sec)
voltime_jul=(st_jul+nd_jul)/2.0; middle point of volume scan for time axis

;date_labels=LABEL_DATE(date_format=['%h%i%s%3'])
date_labels=LABEL_DATE(date_format=['%h%i%s']); no decimal for seconds (w/ system)

;LDAR Heights time series plot
post=inpath+'series\ldarhtstime'+radius+'km.eps'; plot filename
; Setup the postscript device - place code before any plotting command
SET_PLOT, 'ps'
DEVICE, filename=post, xsize=8.0, ysize=5.0, /inches, /color, /Helvetica, encapsulated=1, font_size=12.0, $
      preview=0
!P.FONT=0

;Major tick intervals; want each tick mark (minor and major) to correspond to a volume time-check!
xticks=ROUND(N_ELEMENTS(voltime_jul)/5.)
;xticks=4
k=FINDGEN(xticks+1)*((N_ELEMENTS(voltime_jul)-1)/xticks); have actual volume times on x-axis evenly spaced
xminor=(N_ELEMENTS(voltime_jul)-1)/xticks
;xminor=5
PLOT, voltime_jul, data.quart, color=0, xstyle=1, xcharsize=1.3, ycharsize=1.3, yrange=[0.0, 20.0], $
    xticks=xticks, xtickv=voltime_jul[k], xminor=xminor, xrange=[st_jul[0],nd_jul[ind4-1]], $
    xtickformat='label_date', xtitle='Time (UTC)', ytitle='LDAR Hts. (km)', thick=3., /noerase
    ;, position=[0.10,0.10,0.90,0.80], $
OPLOT, voltime_jul, data.med, linestyle=1, thick=3.
OPLOT, voltime_jul, data.ht1, linestyle=2, thick=3.
OPLOT, voltime_jul, data.top, linestyle=3, thick=3.
;Key
XYOUTS, st_jul[0]+(0.02*(nd_jul[ind4-1]-st_jul[0])), 16.0, 'quart', charsize=1.3
OPLOT, [st_jul[0]+(0.12*(nd_jul[ind4-1]-st_jul[0])), st_jul[0]+(0.22*(nd_jul[ind4-1]-st_jul[0]))], $
      [16.0,16.0], linestyle=0, thick=3.
XYOUTS, st_jul[0]+(0.02*(nd_jul[ind4-1]-st_jul[0])), 17.0, 'med', charsize=1.3
OPLOT, [st_jul[0]+(0.12*(nd_jul[ind4-1]-st_jul[0])), st_jul[0]+(0.22*(nd_jul[ind4-1]-st_jul[0]))], $
      [17.0,17.0], linestyle=1, thick=3.
XYOUTS, st_jul[0]+(0.02*(nd_jul[ind4-1]-st_jul[0])), 18.0, 'ht1', charsize=1.3
OPLOT, [st_jul[0]+(0.12*(nd_jul[ind4-1]-st_jul[0])), st_jul[0]+(0.22*(nd_jul[ind4-1]-st_jul[0]))], $
      [18.0,18.0], linestyle=2, thick=3.
XYOUTS, st_jul[0]+(0.02*(nd_jul[ind4-1]-st_jul[0])), 19.0, 'top', charsize=1.3
OPLOT, [st_jul[0]+(0.12*(nd_jul[ind4-1]-st_jul[0])), st_jul[0]+(0.22*(nd_jul[ind4-1]-st_jul[0]))], $
      [19.0,19.0], linestyle=3, thick=3.

;Overlay storm reports
s=WHERE(STRCOMPRESS(cell.reportanswer, /REMOVE_ALL) EQ 'y', stcount)
IF stcount GT 0 THEN BEGIN
  st_julrep=JULDAY(mon, day, year, cell[s].repst_hr, cell[s].repst_min, cell[s].repst_sec)
  nd_julrep=JULDAY(mon, day, year, cell[s].repend_hr, cell[s].repend_min, cell[s].repend_sec)
  type=cell[s].type
  FOR i=0, stcount-1 DO BEGIN
    POLYFILL, [st_julrep[i], nd_julrep[i], nd_julrep[i], st_julrep[i]], [1.0, 1.0, 1.5, 1.5], 0, color=0
    XYOUTS, st_julrep[i], 2.0, type[i], charsize=1.3, charthick=2.0
  ENDFOR
ENDIF

DEVICE, /CLOSE_FILE, encapsulated=1
SET_PLOT, 'win'
!P.FONT=0

;LDAR other characteristics time series
post=inpath+'series\ldarothcharstime'+radius+'km.eps'
SET_PLOT, 'ps'
```

```
DEVICE, filename=post, xsize=8.0, ysize=5.0, /inches, /color, /Helvetica, encapsulated=1, font_size=12.0, $
      preview=0
!P.FONT=0

PLOT, voltime_jul, data.modes, color=0, xstyle=1, xcharsize=1.3, ycharsize=1.3, yrange=[0.0, 5.0], $
   xticks=xticks, xtickv=voltime_jul[k], xminor=xminor, xrange=[st_jul[0],nd_jul[ind4-1]], $
   xtickformat='label_date', xtitle='Time (UTC)', ytitle='LDAR Chars.', thick=3., /noerase
OPLOT, voltime_jul, data.normpk1, linestyle=1, thick=3.
OPLOT, voltime_jul, data.thick1, linestyle=2, thick=3.
OPLOT, voltime_jul, data.totpts/100000.0, linestyle=3, thick=3.
;Key
XYOUTS, st_jul[0]+(0.02*(nd_jul[ind4-1]-st_jul[0])), 4.0, 'modes', charsize=1.3
OPLOT, [st_jul[0]+(0.23*(nd_jul[ind4-1]-st_jul[0])), st_jul[0]+(0.33*(nd_jul[ind4-1]-st_jul[0]))], $
      [4.0, 4.0], linestyle=0, thick=3.
XYOUTS, st_jul[0]+(0.02*(nd_jul[ind4-1]-st_jul[0])), 4.25, 'normpk1', charsize=1.3
OPLOT, [st_jul[0]+(0.23*(nd_jul[ind4-1]-st_jul[0])), st_jul[0]+(0.33*(nd_jul[ind4-1]-st_jul[0]))], $
      [4.25, 4.25], linestyle=1, thick=3.
XYOUTS, st_jul[0]+(0.02*(nd_jul[ind4-1]-st_jul[0])), 4.5, 'thick1 (km)', charsize=1.3
OPLOT, [st_jul[0]+(0.23*(nd_jul[ind4-1]-st_jul[0])), st_jul[0]+(0.33*(nd_jul[ind4-1]-st_jul[0]))], $
      [4.5, 4.5], linestyle=2, thick=3.
XYOUTS, st_jul[0]+(0.02*(nd_jul[ind4-1]-st_jul[0])), 4.75, 'totpts/100000', charsize=1.3
OPLOT, [st_jul[0]+(0.23*(nd_jul[ind4-1]-st_jul[0])), st_jul[0]+(0.33*(nd_jul[ind4-1]-st_jul[0]))], $
      [4.75, 4.75], linestyle=3, thick=3.

;Overlay storm reports
IF stcount GT 0 THEN BEGIN
  FOR i=0, stcount-1 DO BEGIN
    POLYFILL, [st_julrep[i], nd_julrep[i], nd_julrep[i], st_julrep[i]], [1.1, 1.1, 1.2, 1.2], 0, color=0
    XYOUTS, st_julrep[i], 1.25, type[i], charsize=1.3, charthick=2.0
  ENDFOR
ENDIF

DEVICE, /CLOSE_FILE, encapsulated=1
SET_PLOT, 'win'
!P.FONT=0

goto, jump; when do MCS
;Radar chars. I time series
post=inpath+'series\radarcharstimeI.eps'
SET_PLOT, 'ps'
DEVICE, filename=post, xsize=8.0, ysize=5.0, /inches, /color, /Helvetica, encapsulated=1, font_size=12.0, $
      preview=0
!P.FONT=0

PLOT, voltime_jul, data2.maxzht, color=0, xstyle=1, xcharsize=1.3, ycharsize=1.3, yrange=[0.0, 20.0], $
   xticks=xticks, xtickv=voltime_jul[k], xminor=xminor, xrange=[st_jul[0],nd_jul[ind4-1]], $
   xtickformat='label_date', xtitle='Time (UTC)', ytitle='Radar Chars. (km)', thick=3., /noerase
OPLOT, voltime_jul, data2.rtop, linestyle=1, thick=3.
;OPLOT, voltime_jul, data2.diam, linestyle=2, thick=3.
;Key
XYOUTS, st_jul[0]+(0.02*(nd_jul[ind4-1]-st_jul[0])), 17.0, 'maxzht', charsize=1.3
OPLOT, [st_jul[0]+(0.12*(nd_jul[ind4-1]-st_jul[0])), st_jul[0]+(0.22*(nd_jul[ind4-1]-st_jul[0]))], $
      [17.0,17.0], linestyle=0, thick=3.
XYOUTS, st_jul[0]+(0.02*(nd_jul[ind4-1]-st_jul[0])), 18.0, 'rtop', charsize=1.3
OPLOT, [st_jul[0]+(0.12*(nd_jul[ind4-1]-st_jul[0])), st_jul[0]+(0.22*(nd_jul[ind4-1]-st_jul[0]))], $
      [18.0,18.0], linestyle=1, thick=3.
;XYOUTS, st_jul[0]+(0.02*(nd_jul[ind4-1]-st_jul[0])), 19.0, 'diam', charsize=1.3
;OPLOT, [st_jul[0]+(0.12*(nd_jul[ind4-1]-st_jul[0])), st_jul[0]+(0.22*(nd_jul[ind4-1]-st_jul[0]))], $
;     [19.0,19.0], linestyle=2, thick=3.

;Overlay storm reports
IF stcount GT 0 THEN BEGIN
  FOR i=0, stcount-1 DO BEGIN
    POLYFILL, [st_julrep[i], nd_julrep[i], nd_julrep[i], st_julrep[i]], [1.0, 1.0, 1.5, 1.5], 0, color=0
    XYOUTS, st_julrep[i], 2.0, type[i], charsize=1.3, charthick=2.0
  ENDFOR
```

```
ENDIF

DEVICE, /CLOSE_FILE, encapsulated=1
SET_PLOT, 'win'
!P.FONT=0

;Radar chars. II time series
post=inpath+'series\radarcharstimeII.eps'
SET_PLOT, 'ps'
DEVICE, filename=post, xsize=8.0, ysize=5.0, /inches, /color, /Helvetica, encapsulated=1, font_size=12.0, $
      preview=0
!P.FONT=0

PLOT, voltime_jul, data2.maxz, color=0, xstyle=1, xcharsize=1.3, ycharsize=1.3, yrange=[0.0, 150.0], $
   xticks=xticks, xtickv=voltime_jul[k], xminor=xminor, xrange=[st_jul[0],nd_jul[ind4-1]], $
   xtickformat='label_date', xtitle='Time (UTC)', ytitle='Radar Chars.', thick=3., /noerase
OPLOT, voltime_jul, data2.shi, linestyle=1, thick=3.
OPLOT, voltime_jul, data2.vil, linestyle=2, thick=3.
;OPLOT, voltime_jul, data2.msi/100.0, linestyle=3, thick=3.; /100 to fit on plot
;Key
XYOUTS, st_jul[0]+(0.02*(nd_jul[ind4-1]-st_jul[0])), 126.0, 'maxz', charsize=1.3
OPLOT, [st_jul[0]+(0.17*(nd_jul[ind4-1]-st_jul[0])), st_jul[0]+(0.27*(nd_jul[ind4-1]-st_jul[0]))], $
      [126.0,126.0], linestyle=0, thick=3.
XYOUTS, st_jul[0]+(0.02*(nd_jul[ind4-1]-st_jul[0])), 132.0, 'shi', charsize=1.3
OPLOT, [st_jul[0]+(0.17*(nd_jul[ind4-1]-st_jul[0])), st_jul[0]+(0.27*(nd_jul[ind4-1]-st_jul[0]))], $
      [132.0,132.0], linestyle=1, thick=3.
XYOUTS, st_jul[0]+(0.02*(nd_jul[ind4-1]-st_jul[0])), 138.0, 'vil', charsize=1.3
OPLOT, [st_jul[0]+(0.17*(nd_jul[ind4-1]-st_jul[0])), st_jul[0]+(0.27*(nd_jul[ind4-1]-st_jul[0]))], $
      [138.0,138.0], linestyle=2, thick=3.
;XYOUTS, st_jul[0]+(0.02*(nd_jul[ind4-1]-st_jul[0])), 144.0, 'msi/100', charsize=1.3
;OPLOT, [st_jul[0]+(0.17*(nd_jul[ind4-1]-st_jul[0])), st_jul[0]+(0.27*(nd_jul[ind4-1]-st_jul[0]))], $
;     [144.0,144.0], linestyle=3, thick=3.

;Overlay storm reports
IF stcount GT 0 THEN BEGIN
  FOR i=0, stcount-1 DO BEGIN
    POLYFILL, [st_julrep[i], nd_julrep[i], nd_julrep[i], st_julrep[i]], [1.0, 1.0, 3.0, 3.0], 0, color=0
    XYOUTS, st_julrep[i], 3.0, type[i], charsize=1.3, charthick=2.0
  ENDFOR
ENDIF

DEVICE, /CLOSE_FILE, encapsulated=1
SET_PLOT, 'win'
!P.FONT=0

;CG chars. I time series
jump: post=inpath+'series\cgcharstimeI'+radius+'km.eps'
SET_PLOT, 'ps'
DEVICE, filename=post, xsize=8.0, ysize=5.0, /inches, /color, /Helvetica, encapsulated=1, font_size=12.0, $
      preview=0
!P.FONT=0

;Determine which volumes have CG chars.
result=INTARR(N_ELEMENTS(negvol)); Create result array
FOR m=0, N_ELEMENTS(negvol)-1 DO BEGIN; Search all of negvol
  result[m]=WHERE(STRMATCH(cell.vol, negvol[m]) EQ 1); Indices of cell.vol where volumes match
ENDFOR
voltime_julneg=voltime_jul[result]; Corresponding times where there is CG data to plot

result=INTARR(N_ELEMENTS(posvol))
FOR m=0, N_ELEMENTS(posvol)-1 DO BEGIN
  result[m]=WHERE(STRMATCH(cell.vol, posvol[m]) EQ 1)
ENDFOR
voltime_julpos=voltime_jul[result]

result=INTARR(N_ELEMENTS(pposvol))
```

```
FOR m=0, N_ELEMENTS(pposvol)-1 DO BEGIN
  result[m]=WHERE(STRMATCH(cell.vol, pposvol[m]) EQ 1)
ENDFOR
voltime_julppos=voltime_jul[result]

;With multiple axes:
;PLOT, voltime_jul, data.rat, /nodata, ystyle=4, xtitle='Time (UTC)', color=0, xstyle=1, xcharsize=1.3, $
;     ycharsize=1.3, xticks=xticks, xtickv=voltime_jul[k], xminor=xminor, $
;     xrange=[st_jul[0],nd_jul[ind4-1]], xtickformat='label_date'
;AXIS, yaxis=0, yrange=[0.0, 100.0], /save, ytitle='CG Chars.'
;OPLOT, voltime_jul, data.rat, linestyle=0, thick=3.
;OPLOT, voltime_julppos, pposfl, linestyle=2, thick=3.
;OPLOT, voltime_julpos, posfl, linestyle=3, thick=3.
;OPLOT, voltime_julneg, negfl, linestyle=4, thick=3.

;AXIS, yaxis=1, yrange=[0.0, 200.0], /save, ytitle='# Total Flashes'
;OPLOT, voltime_jul, data.nfl, linestyle=1, thick=3.

;Without multiple axes (comment for when do multiple axes):
PLOT, voltime_jul, data.rat, color=0, xstyle=1, xcharsize=1.3, ycharsize=1.3, yrange=[0.0, 100.0], $
    xticks=xticks, xtickv=voltime_jul[k], xminor=xminor, xrange=[st_jul[0],nd_jul[ind4-1]], $
    xtickformat='label_date', xtitle='Time (UTC)', ytitle='CG Chars.', thick=3., /noerase
OPLOT, voltime_jul, data.nfl/20., linestyle=1, thick=3.
OPLOT, voltime_julppos, pposfl, linestyle=2, thick=3.
OPLOT, voltime_julpos, posfl/2., linestyle=3, thick=3.
OPLOT, voltime_julneg, negfl/6., linestyle=4, thick=3.

;Key - cut & paste before right axis generation when do multiple axes
XYOUTS, st_jul[0]+(0.02*(nd_jul[ind4-1]-st_jul[0])), 75., 'rat', charsize=1.3
OPLOT, [st_jul[0]+(0.17*(nd_jul[ind4-1]-st_jul[0])), st_jul[0]+(0.27*(nd_jul[ind4-1]-st_jul[0]))], $
      [75.,75.], linestyle=0, thick=3.
XYOUTS, st_jul[0]+(0.02*(nd_jul[ind4-1]-st_jul[0])), 80., 'nfl/20', charsize=1.3
OPLOT, [st_jul[0]+(0.17*(nd_jul[ind4-1]-st_jul[0])), st_jul[0]+(0.27*(nd_jul[ind4-1]-st_jul[0]))], $
      [80.,80.], linestyle=1, thick=3.
XYOUTS, st_jul[0]+(0.02*(nd_jul[ind4-1]-st_jul[0])), 85., 'ppos', charsize=1.3
OPLOT, [st_jul[0]+(0.17*(nd_jul[ind4-1]-st_jul[0])), st_jul[0]+(0.27*(nd_jul[ind4-1]-st_jul[0]))], $
      [85.,85.], linestyle=2, thick=3.
XYOUTS, st_jul[0]+(0.02*(nd_jul[ind4-1]-st_jul[0])), 90., 'pos/2', charsize=1.3
OPLOT, [st_jul[0]+(0.17*(nd_jul[ind4-1]-st_jul[0])), st_jul[0]+(0.27*(nd_jul[ind4-1]-st_jul[0]))], $
      [90.,90.], linestyle=3, thick=3.
XYOUTS, st_jul[0]+(0.02*(nd_jul[ind4-1]-st_jul[0])), 95., 'neg/6', charsize=1.3
OPLOT, [st_jul[0]+(0.17*(nd_jul[ind4-1]-st_jul[0])), st_jul[0]+(0.27*(nd_jul[ind4-1]-st_jul[0]))], $
      [95.,95.], linestyle=4, thick=3.

; Overlay storm reports - cut & paste for multiple axes too
IF stcount GT 0 THEN BEGIN
  FOR i=0, stcount-1 DO BEGIN
    POLYFILL, [st_julrep[i], nd_julrep[i], nd_julrep[i], st_julrep[i]], [1.0, 1.0, 2.0, 2.0], 0, color=0
    XYOUTS, st_julrep[i], 3.0, type[i], charsize=1.3, charthick=2.0
  ENDFOR
ENDIF

DEVICE, /CLOSE_FILE, encapsulated=1
SET_PLOT, 'win'
!P.FONT=0

;CG chars. II time series
post=inpath+'series\cgcharstimeII'+radius+'km.eps'
SET_PLOT, 'ps'
DEVICE, filename=post, xsize=8.0, ysize=5.0, /inches, /color, /Helvetica, encapsulated=1, font_size=12.0, $
      preview=0
!P.FONT=0

result=INTARR(N_ELEMENTS(nmedvol))
FOR m=0, N_ELEMENTS(nmedvol)-1 DO BEGIN
  result[m]=WHERE(STRMATCH(cell.vol, nmedvol[m]) EQ 1)
```

```
ENDFOR
voltime_julnmed=voltime_jul[result]

result=INTARR(N_ELEMENTS(pmedvol))
FOR m=0, N_ELEMENTS(pmedvol)-1 DO BEGIN
  result[m]=WHERE(STRMATCH(cell.vol, pmedvol[m]) EQ 1)
ENDFOR
voltime_julpmed=voltime_jul[result]

result=INTARR(N_ELEMENTS(nmulvol))
FOR m=0, N_ELEMENTS(nmulvol)-1 DO BEGIN
  result[m]=WHERE(STRMATCH(cell.vol, nmulvol[m]) EQ 1)
ENDFOR
voltime_julnmul=voltime_jul[result]

result=INTARR(N_ELEMENTS(pmulvol))
FOR m=0, N_ELEMENTS(pmulvol)-1 DO BEGIN
  result[m]=WHERE(STRMATCH(cell.vol, pmulvol[m]) EQ 1)
ENDFOR
voltime_julpmul=voltime_jul[result]

PLOT, voltime_julnmed, nmedfl, color=0, xstyle=1, xcharsize=1.3, ycharsize=1.3, yrange=[0.0, 40.0], $
    xticks=xticks, xtickv=voltime_jul[k], xminor=xminor, xrange=[st_jul[0],nd_jul[ind4-1]], $
    xtickformat='label_date', xtitle='Time (UTC)', ytitle='CG Chars.', thick=3., /noerase
OPLOT, voltime_julpmed, pmedfl, linestyle=1, thick=3.
OPLOT, voltime_julnmul, nmulfl*10.0, linestyle=2, thick=3.
OPLOT, voltime_julpmul, pmulfl*10.0, linestyle=3, thick=3.
;Key
XYOUTS, st_jul[0]+(0.02*(nd_jul[ind4-1]-st_jul[0])), 32.0, 'nmed', charsize=1.3
OPLOT, [st_jul[0]+(0.17*(nd_jul[ind4-1]-st_jul[0])), st_jul[0]+(0.27*(nd_jul[ind4-1]-st_jul[0]))], $
      [32.0,32.0], linestyle=0, thick=3.
XYOUTS, st_jul[0]+(0.02*(nd_jul[ind4-1]-st_jul[0])), 34.0, 'pmed', charsize=1.3
OPLOT, [st_jul[0]+(0.17*(nd_jul[ind4-1]-st_jul[0])), st_jul[0]+(0.27*(nd_jul[ind4-1]-st_jul[0]))], $
      [34.0,34.0], linestyle=1, thick=3.
XYOUTS, st_jul[0]+(0.02*(nd_jul[ind4-1]-st_jul[0])), 36.0, 'nmul*10', charsize=1.3
OPLOT, [st_jul[0]+(0.17*(nd_jul[ind4-1]-st_jul[0])), st_jul[0]+(0.27*(nd_jul[ind4-1]-st_jul[0]))], $
      [36.0,36.0], linestyle=2, thick=3.
XYOUTS, st_jul[0]+(0.02*(nd_jul[ind4-1]-st_jul[0])), 38.0, 'pmul*10', charsize=1.3
OPLOT, [st_jul[0]+(0.17*(nd_jul[ind4-1]-st_jul[0])), st_jul[0]+(0.27*(nd_jul[ind4-1]-st_jul[0]))], $
      [38.0,38.0], linestyle=3, thick=3.

; Overlay storm reports
IF stcount GT 0 THEN BEGIN
  FOR i=0, stcount-1 DO BEGIN
    POLYFILL, [st_julrep[i], nd_julrep[i], nd_julrep[i], st_julrep[i]], [1.0, 1.0, 2.0, 2.0], 0, color=0
    XYOUTS, st_julrep[i], 3.0, type[i], charsize=1.3, charthick=2.0
  ENDFOR
ENDIF

DEVICE, /CLOSE_FILE, encapsulated=1
SET_PLOT, 'win'
!P.FONT=0

CLOSE, /ALL

STOP
END
```

```
PRO MATCH_RADARLDAR

;Correlates RADAR to LDAR cell characteristics.  Creates scatter and residual plots.
;Written by Stephanie Tice and Scott Steiger 4 January 2004; Last update 30 September 2004
;Check file formats between cases (i.e., supercell diff. from others)!

COMPILE_OPT IDL2

CLOSE, /ALL; close all open files

;Only change these between cases
outfile='C:\My Documents\scotts\Dissertation\030406supercase\'
radius='05' ;20, 10, 05 (km) analysis radius

;Stats. file-heading only
OPENW, 8, outfile+'correlationsm\radar-ldarstats'+radius+'km.txt',/APPEND
PRINTF, 8, 'r^2', 'r', 't', 'df', format='(16x, a3, 5x, a1, 8x, a1, 9x, a2)
CLOSE, 8

maxrec = 400
OPENR, 11, outfile+'radarstatswdss030406hail2.txt'; radar characteristics file
;Radar file-remember to take out "H's", "W's", and "T's" appended on the volume numbers in radar files
; (severe time series cases)
OPENR, 12, outfile+'lghavgsm\ldarchars'+radius+'km.txt'; lightning chars. file
;Set up structures
fmt='(a5, i4, i4, i3, f5.1, f5.1, f5.1, i5, i5, i4)';radar file format; include tabs
fmt2='(a4,2x,i3,2x,i3,2x,f6.3,2x,f6.3,2x,f6.3,2x,i1,2x,f6.3,2x,f8.5,2x,f6.3,2x,i6,2x,f7.3,2x,f6.3,2x,f8.5,2x,f6.3,2x,i6,2x,f8.3)'
record={vol:'', mesoid:0L, cellid:0L, diam:0L, maxz:0.0d, maxzht:0.0d, rtop:0.0d, shi:0L, vil:0L, msi:0L}
record2={vol:'',cellid:0L,mesoid:0L,quart:0.0d,med:0.0d,top:0.0d,modes:0L,ht1:0.0d,normpk1:0.0d,thick1:0.0d, $
        totpts:0L,dist:0.0d,ht2:0.0d,normpk2:0.0d,thick2:0.0d,nfl:0L,rat:0.0d}
data=REPLICATE(CREATE_STRUCT(record), maxrec); create structures
data2=REPLICATE(CREATE_STRUCT(record2), maxrec)

;Read in data
ind=0L
WHILE NOT EOF(11) DO BEGIN
  READF, 11, record, format=fmt; get data from first file (radar)
  data[ind]=record; store data
  ind=ind+1L
ENDWHILE
data=data[0:ind-1]; trimming data to actual size
data.vol=STRCOMPRESS(data.vol, /REMOVE_ALL); remove all white spaces

ind=0L
WHILE NOT EOF(12) DO BEGIN
  READF, 12, record2, format=fmt2; get data from second file (ldar)
  data2[ind]=record2; store data
  ind=ind+1L
ENDWHILE
data2=data2[0:ind-1]; trimming data
data2=data2[WHERE(data2.rat GE 0.0)]; only use lines where IC:CG ratio a positive number
data2.vol=STRCOMPRESS(data2.vol, /REMOVE_ALL)

result=INTARR(N_ELEMENTS(data.vol)); create result array
FOR i=0, N_ELEMENTS(data.vol)-1 DO BEGIN; search all of data.vol
    result[i]=WHERE(STRMATCH(data2.vol, data[i].vol) EQ 1); indices of data2 where volumes match
    ;Do this because missing data for volume scans in one file but not the other sometimes
ENDFOR

;Radar chars. of matching volumes
diam=data[WHERE(result NE -1)].diam; comment out in non-supercell cases
maxz=data[WHERE(result NE -1)].maxz
maxzht=data[WHERE(result NE -1)].maxzht
rtop=data[WHERE(result NE -1)].rtop
shi=data[WHERE(result NE -1)].shi
vil=data[WHERE(result NE -1)].vil
```

```
msi=data[WHERE(result NE -1)].msi; comment out in non-supercell cases

n=N_ELEMENTS(WHERE(result NE -1))
new=INTARR(n); size of new is # of matching volumes
k=0
FOR j=0, N_ELEMENTS(data.vol)-1 DO BEGIN
   IF result[j] NE -1 THEN BEGIN; check if volumes match
      new[k]=result[j]; store indice of second file
      k=k+1
   ENDIF
ENDFOR

;LDAR chars. of matching volumes
quart=data2[new].quart
med=data2[new].med
top=data2[new].top
modes=data2[new].modes
ht1=data2[new].ht1
normpk1=data2[new].normpk1
thick1=data2[new].thick1
totpts=data2[new].totpts
dist=data2[new].dist
nfl=data2[new].nfl
rat=data2[new].rat
cellids=data2[new].cellid
mesoids=data2[new].mesoid

;Calculate # of degrees of freedom for statistics for non-time series
;repeats=0; number of cell repeats
;FOR z=0, n-1 DO BEGIN
;  IF N_ELEMENTS(WHERE(STRMATCH(STRING(cellids[0:z]), string(cellids[z])) EQ 1)) EQ 2 THEN $
;     repeats=repeats+1
;ENDFOR
;For mesos.
;FOR z=0, n-1 DO BEGIN
;  IF N_ELEMENTS(WHERE(STRMATCH(STRING(mesoids[0:z]), string(mesoids[z])) EQ 1)) EQ 2 THEN $
;     repeats=repeats+1
;ENDFOR
;df=n-repeats-2; degrees of freedom (decreased by the number of cells that occurred more than once)
; From Preston 2004

;Correlate Radar to LDAR data
radarchar=[diam, maxz, maxzht, rtop, shi, vil, msi]; include diam and msi when do mesos.
radarchartex=['diam', 'maxz', 'maxzht', 'rtop', 'shi', 'vil', 'msi']
;Axis titles:
radarchartitl=['Meso. Diam. (km)', 'Max. Z (dBZ)', 'Max. Z Ht. (km)', 'Radar Top (km)', 'SHI', 'VIL', 'MSI']

ldarchar=[quart, med, top, modes, ht1, normpk1, thick1, totpts, dist, nfl, rat]
ldarchartex=['quart', 'med', 'top', 'modes', 'ht1', 'normpk1', 'thick1', 'totpts', 'dist', 'nfl', 'rat']
ldarchartitl=['LDAR Quartile Ht. (km)', 'LDAR Median Ht. (km)', 'LDAR Top (km)', 'LDAR Modes', $
        'LDAR Peak Ht. (km)', 'LDAR Norm. Pk.', 'LDAR Thickness (km)', 'LDAR Total Points', $
        'Distance to LDAR Center (km)', '# Flashes', 'IC:CG']; axis titles

;Two loops to correlate each Radar to LDAR characteristic
FOR q=0, N_ELEMENTS(radarchartex)-1 DO BEGIN
  FOR p=0, N_ELEMENTS(ldarchartex)-1 DO BEGIN
    q1=q*n
    q2=(q+1)*n-1
    p1=p*n
    p2=(p+1)*n-1
    r_radldar=CORRELATE(radarchar[q1:q2], ldarchar[p1:p2], /DOUBLE); linear correlation coeff.
    r2_radldar=(r_radldar)^2; r-squared

    ;t-statistic to test significance of correlations (eqn. from Neter and Wasserman 1974)
    t_radldar=ABS((r_radldar*SQRT(n-2))/SQRT(1-r2_radldar))
```

```
;df for time series (comment out above one)
FOR i=1, n-1 DO BEGIN; see notes on MacGorman e-mail 24 April 2004
  x=CORRELATE(radarchar[q1:q2-i], radarchar[q1+i:q2], /DOUBLE)
  IF ABS(x) LT 0.1 THEN BREAK; data decorrelated
  IF FINITE(x) NE 1 THEN BREAK; if r Not-a-Number (NaN)
ENDFOR
decortime=FLOAT(i); "decorrelation time"
df1=n/decortime; "effective degrees of freedom" for first data (radar)
FOR i=1, n-1 DO BEGIN
  x=CORRELATE(ldarchar[p1:p2-i], ldarchar[p1+i:p2], /DOUBLE)
  IF ABS(x) LT 0.1 THEN BREAK
  IF FINITE(x) NE 1 THEN BREAK
ENDFOR
decortime=FLOAT(i)
df2=n/decortime
df=FIX(ROUND((df1+df2)/2.)); THE "degree of freedom"
;IF check_math() NE 0 THEN STOP; checking for math errors (if reach last iteration, x=NaN)

;Print statistics to a file
OPENW, 8, outfile+'correlationsm\radar-ldarstats'+radius+'km.txt', /APPEND
PRINTF, 8, radarchartex[q]+'-'+ldarchartex[p]+' ', r2_radldar, r_radldar, t_radldar, df, $
       format = '(a14, 2x, f6.4, 2x, f7.4, 2x, f8.4, 2x, i3)'
CLOSE, 8

;Scatter plots
xscale=21.0 ; cm
yscale=21.0
post=outfile+'correlationsm\'+radarchartex[q]+'-'+ldarchartex[p]+radius+'km.eps'
;Setup the postscript device - place code before any plotting command
SET_PLOT, 'ps'
DEVICE, filename=post, xsize=xscale, ysize=yscale, /Helvetica, $
      encapsulated=1, font_size=12.0, preview=0
!P.FONT=0
b=REGRESS(radarchar[q1:q2], ldarchar[p1:p2], const=a, /DOUBLE)
PLOT, radarchar[q1:q2], ldarchar[p1:p2], psym=1, xtitle=radarchartitl[q], ytitle=ldarchartitl[p], $
      xrange=[0.5*MIN(radarchar[q1:q2]), 1.5*MAX(radarchar[q1:q2])], yrange=[0.5*MIN(ldarchar[p1:p2]), $
      1.5*MAX(ldarchar[p1:p2])]
XYOUTS, 0.75, 0.15, 'r!u2!n = '+STRTRIM(STRING(r2_radldar), 2), /normal, charsize=1
XYOUTS, 0.75, 0.125, 't, df = '+STRTRIM(STRING(t_radldar), 2)+', '+STRTRIM(STRING(df),2), /normal, $
      charsize=1
;Overplot line
OPLOT, [!X.CRANGE[0], !X.CRANGE[1]], [a + b[0]*!X.CRANGE[0], a + b[0]*!X.CRANGE[1]]
DEVICE, /CLOSE
PRINT, 'Saving postscript to ' + post

;Create residuals
IF FINITE(a) NE 1 THEN GOTO, jump
y=a+b[0]*radarchar[q1:q2]
resids=ldarchar[p1:p2]-y
;Plot residuals by cellid/mesoid (for Preston 9/2004)
post=outfile+'correlationsm\'+radarchartex[q]+'-'+ldarchartex[p]+radius+'km_residuals.eps'
SET_PLOT, 'ps'
DEVICE, filename=post, xsize=xscale, ysize=yscale, /Helvetica, $
      encapsulated=1, font_size=12.0, preview = 0
!P.FONT = 0
PLOT, cellids, resids, psym=1, xtitle='Cell IDs', ytitle='Residuals'
OPLOT, [!X.CRANGE[0], !X.CRANGE[1]], [0,0]
DEVICE, /CLOSE
PRINT, 'Saving postscript to '+post
jump:

;Switch independent and dependent variables
post=outfile+'correlationsm\'+ldarchartex[p]+'-'+radarchartex[q]+radius+'km.eps'
SET_PLOT, 'ps'
DEVICE, filename=post, xsize=xscale, ysize=yscale, /Helvetica, $
      encapsulated=1, font_size=12.0, preview=0
```

```
    !P.FONT=0
    b=REGRESS(ldarchar[p1:p2], radarchar[q1:q2], const=a, /DOUBLE)
    PLOT, ldarchar[p1:p2], radarchar[q1:q2], psym=1, xtitle=ldarchartitl[p], ytitle=radarchartitl[q], $
          xrange=[0.5*MIN(ldarchar[p1:p2]), 1.5*MAX(ldarchar[p1:p2])], yrange=[0.5*MIN(radarchar[q1:q2]), $
          1.5*MAX(radarchar[q1:q2])]
    XYOUTS, 0.75, 0.15, 'r!u2!n = '+STRTRIM(STRING(r2_radldar), 2), /normal, charsize=1
    XYOUTS, 0.75, 0.125, 't, df = '+STRTRIM(STRING(t_radldar), 2)+', '+STRTRIM(STRING(df),2), /normal, $
          charsize=1
    ;Overplot line
    OPLOT, [!X.CRANGE[0], !X.CRANGE[1]], [a + b[0]*!X.CRANGE[0], a + b[0]*!X.CRANGE[1]]
    DEVICE, /CLOSE
    PRINT, 'Saving postscript to ' + post

    ;Create residuals
    IF FINITE(a) NE 1 THEN GOTO, jump1
    y=a+b[0]*ldarchar[p1:p2]
    resids=radarchar[q1:q2]-y
    ;Plot residuals by cellid/mesoid
    post=outfile+'correlationsm\'+ldarchartex[p]+'-'+radarchartex[q]+radius+'km_residuals.eps'
    SET_PLOT, 'ps'
    DEVICE, filename=post, xsize=xscale, ysize=yscale, /Helvetica, $
      encapsulated=1, font_size=12.0, preview=0
    !P.FONT=0
    PLOT, cellids, resids, psym=1, xtitle='Cell IDs', ytitle='Residuals'
    OPLOT, [!X.CRANGE[0], !X.CRANGE[1]], [0,0]
    DEVICE, /CLOSE
    PRINT, 'Saving postscript to '+post
    jump1:

  ENDFOR
  PRINT
ENDFOR

CLOSE, /ALL

STOP
END
```

APPENDIX F

TABLES

Table 1. Correlation analysis of radar and lightning characteristics for the first 13 October 2001 tornadic supercell discussed. The linear correlation coefficient is given by r, and the correlations that are statistically significant (sig) at the p = 0.05 level are marked by *. The characteristics shown include: maximum reflectivity (maxz), max. reflectivity height (maxzht), radar top (rtop), SHI, VIL, MSI, 95th percentile height of LDAR II sources (Ltop), and number of total flashes (flash rate; nfl). The LDAR II characteristics were calculated using data within 10 km of the mesocyclone.

	r^2	r	sig
maxz-Ltop	0.49	0.70	*
maxz-nfl	0.17	0.41	
maxzht-Ltop	0.19	0.44	*
maxzht-nfl	0.02	0.13	
rtop-Ltop	0.27	0.52	*
rtop-nfl	0.32	0.57	*
shi-Ltop	0.47	0.69	*
shi-nfl	0.11	0.34	
vil-Ltop	0.67	0.82	*
vil-nfl	0.44	0.66	*
msi-Ltop	0.32	0.57	*
msi-nfl	0.26	0.51	*

Table 2. Linear correlation coefficients between lightning characteristics for the first (T1r) and second (T2r) 13 October 2001 tornadic supercells and the 6 April 2003 hail producing supercell (Hr) discussed. The characteristics shown include: 95th percentile height of LDAR II sources (Ltop), IC:CG ratio (rat), number of total flashes (flash rate; nfl), CG flash density (dens), and half-peak thickness of the main peak in the source density height histogram (thick1). These characteristics were calculated using data within 10 km of the mesocyclones.

	T1r	T2r	Hr
Ltop-rat	-0.38	-0.71	0.34
Ltop-nfl	0.56	0.11	-0.33
Ltop-dens	0.61	0.84	-0.29
Ltop-thick1	0.62	0.29	0.63

Table 3. Linear correlation coefficients between lightning and radar characteristics for five cases (13 October 2001 supercells and squall line, 16 June 2002 squall line, 27 June 2001 pulse, and 27 May 2002 mesoscale convective system (MCS) storm cells). The lightning and radar characteristics include: -/+/total CG flash density (neg/pos/dens), %+CG (ppos), median peak -/+ CG current (nmed/pmed), mean -/+ CG flash multiplicity (nmul/pmul), lower quartile and 95th percentile LDAR II source heights (quart and Ltop), number of peaks in the height distribution of LDAR II sources (modes), half-peak thickness of the vertical LDAR II source peak (thick1), range from LDAR II network center (dist), total number of flashes (flash rate; nfl), IC:CG ratio (rat), maximum height of the 30 dBZ reflectivity contour (rtop), severe hail index (shi), and vertically integrated liquid water (vil). The lightning characteristics were calculated within 10 km of the storm cell location. The correlations that are significant at the p = 0.05 level are marked by *. NA (not available) = not enough points for calculation.

	13 Oct super	13 Oct squall	16 Jun squall	27 June pulse	27 May MCS
neg-nmed	0.26*	0.04	0.20	-0.14	-0.05
neg-nmul	0.04	0.06	0.24*	0.67*	0.24*
nmed-nmul	0.20	0.24*	0.17	-0.24	0.26*
pmed-pmul	0.06	-0.12	NA	-0.47	0.22
pos-pmed	-0.23	-0.21	0.25	-0.30	-0.27
pos-pmul	0.20	0.04	NA	-0.41	0.35
Ltop-dens	0.51*	-0.10	0.39*	0.62*	0.11
Ltop-nmed	-0.26*	-0.03	-0.23	0.33	0.09
Ltop-pmed	0.02	-0.08	NA	0.11	-0.73*
Ltop-pos	0.46*	0.11	-0.13	0.56*	0.13
Ltop-ppos	0.18	0.18	-0.57*	0.47*	-0.14
Ltop-modes	-0.16	0.06	0.22	-0.10	0.48*
quart-modes	-0.57*	-0.33*	-0.35*	-0.18	0.08
Ltop-thick1	0.50*	0.05	0.25	0.73*	0.15
Ltop-dist	0.82*	0.74*	0.62*	0.60*	0.26*
Ltop-nfl	0.00	-0.28*	0.17	0.71*	0.15
Ltop-rat	-0.54*	-0.01	-0.59*	0.65*	0.07
dist-nfl	-0.30*	-0.65*	-0.46*	0.83*	-0.24*
rtop-Ltop	0.22	-0.10	0.18	0.91*	0.21*
rtop-nfl	0.41*	0.73*	0.01	0.77*	0.40*
shi-Ltop	0.14	-0.12	0.20	0.59*	-0.02
shi-nfl	0.27*	0.67*	0.38*	0.78*	0.73*
shi-rat	-0.32*	-0.19	-0.07	0.49*	0.18*
vil-Ltop	0.11	-0.14	0.35*	0.73*	0.12
vil-nfl	0.33*	0.64*	0.40*	0.83*	0.65*
vil-rat	-0.37*	-0.21*	-0.31*	0.60*	0.07
vil-dens	0.48*	0.60*	0.70*	0.81*	0.70*
shi-dens	0.41*	0.56*	0.41*	0.84*	0.59*
shi-ppos	-0.10	-0.14	-0.14	0.64*	-0.16*
shi-pos	0.23*	0.36*	0.28*	0.88*	0.11

Table 4. Correlation analysis of radar and lightning characteristics with distance from the center of the LDAR II network (dist) for the first 13 October 2001 tornadic supercell analyzed in the first section. The linear correlation coefficient is given by r, and the correlations that are statistically significant (sig) at the p = 0.05 level are marked by *. The characteristics shown include: lower quartile (quart), median (med), 95th percentile (Ltop), and peak source density (ht1) heights of LDAR II sources, total number of sources (totpts), number of total flashes (flash rate; nfl), maximum reflectivity (maxz), max. reflectivity height (maxzht), radar top (rtop), SHI, and VIL. The LDAR II characteristics were calculated using data within 10 km of the mesocyclone.

	r^2	r	sig
quart-dist	0.43	0.66	*
med-dist	0.44	0.66	*
Ltop-dist	0.63	0.79	*
ht1-dist	0.21	0.45	
totpts-dist	0.04	-0.19	
nfl-dist	0.07	0.26	
maxz-dist	0.73	0.86	*
maxzht-dist	0.14	0.38	*
rtop-dist	0.16	0.40	*
shi-dist	0.71	0.84	*
vil-dist	0.51	0.72	

APPENDIX G

FIGURES

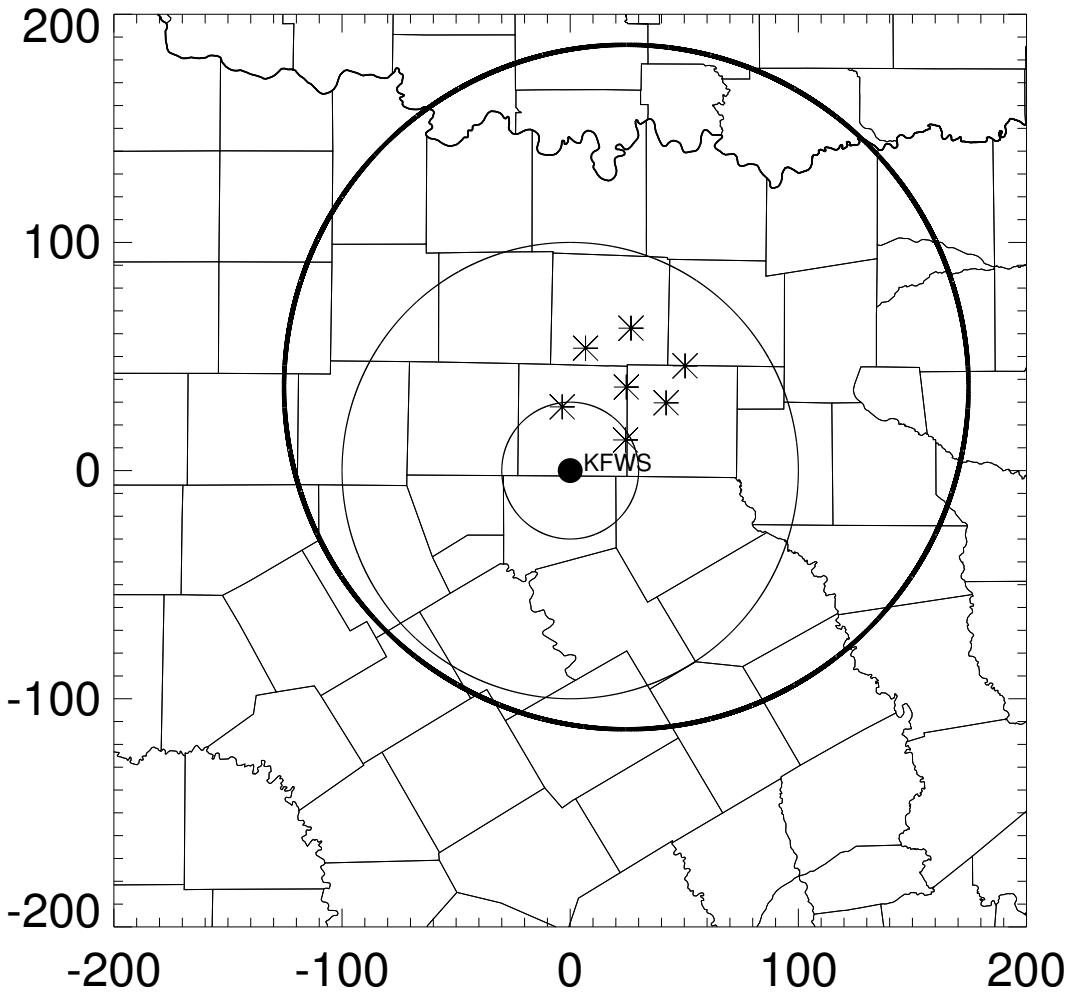

Figure 1. Locations of the Dallas-Ft. Worth LDAR II sites (asterisks) and WSR-88D radar (dot: KFWS). The x and y axes are labeled according to distance from the radar. The two concentric circles surrounding KFWS indicate the study domain (annulus between 30 and 100 km) while the larger, thicker circle denotes 150 km range from the LDAR II network center (at the DFW Airport). State and county outlines are also shown.

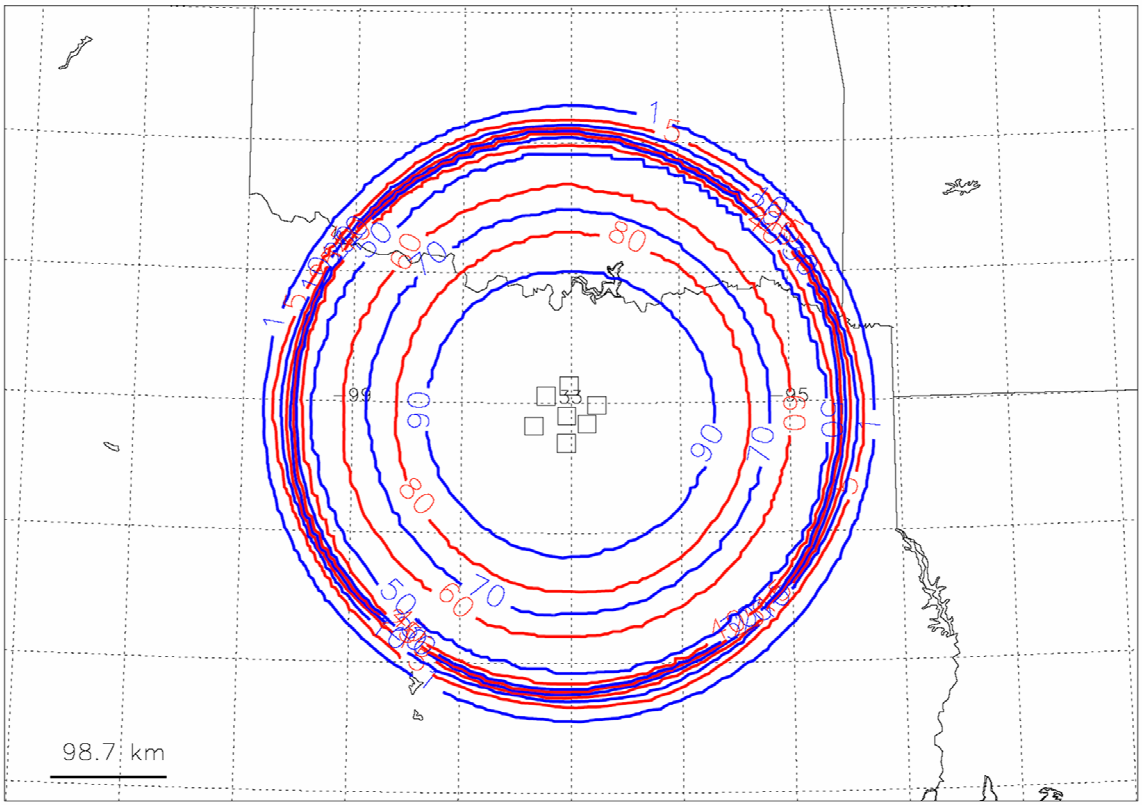

Figure 2. LDAR II flash detection efficiency (%) for the 13 October 2001 event. The 27 June 2001 event had a similar distribution. The seven sensors are shown as squares, centered on the DFW International Airport. Note how rapidly the efficiency decreases with range. State outlines of Texas, Oklahoma, Arkansas, and Louisiana are also shown. Figure provided by Martin Murphy, Vaisala, Inc.

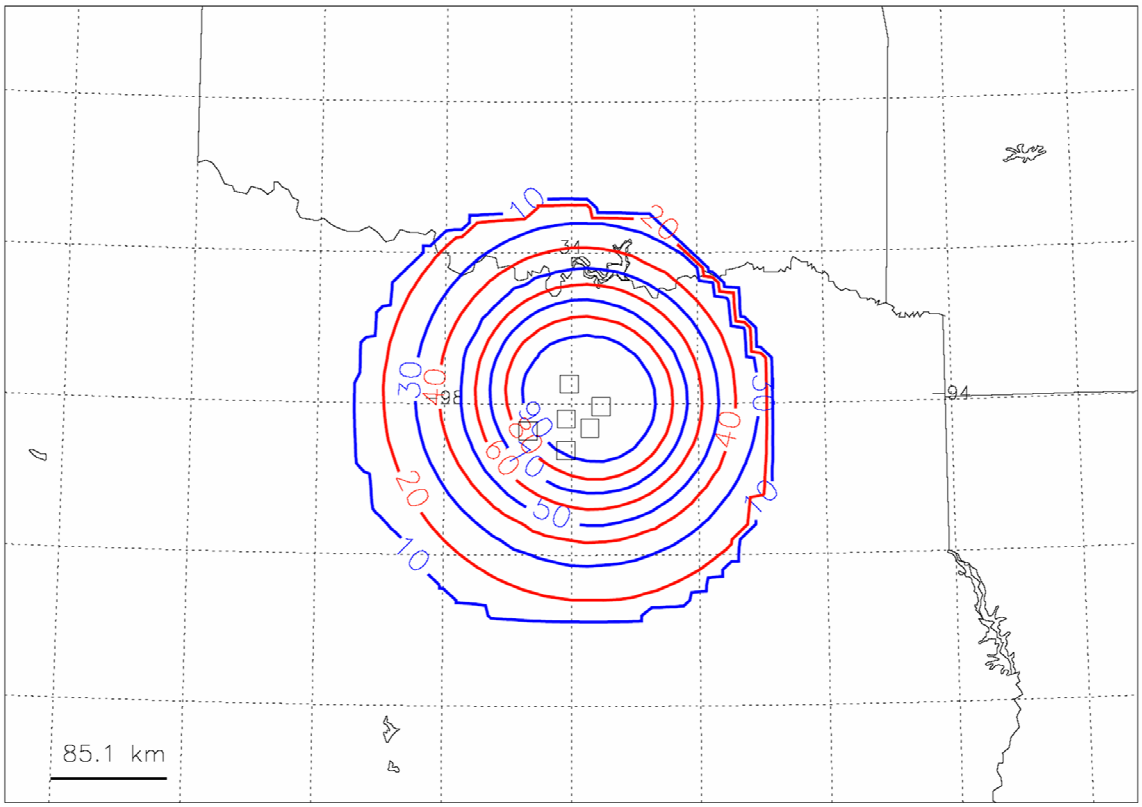

Figure 3. Same as figure 2, except for 6 April 2003.

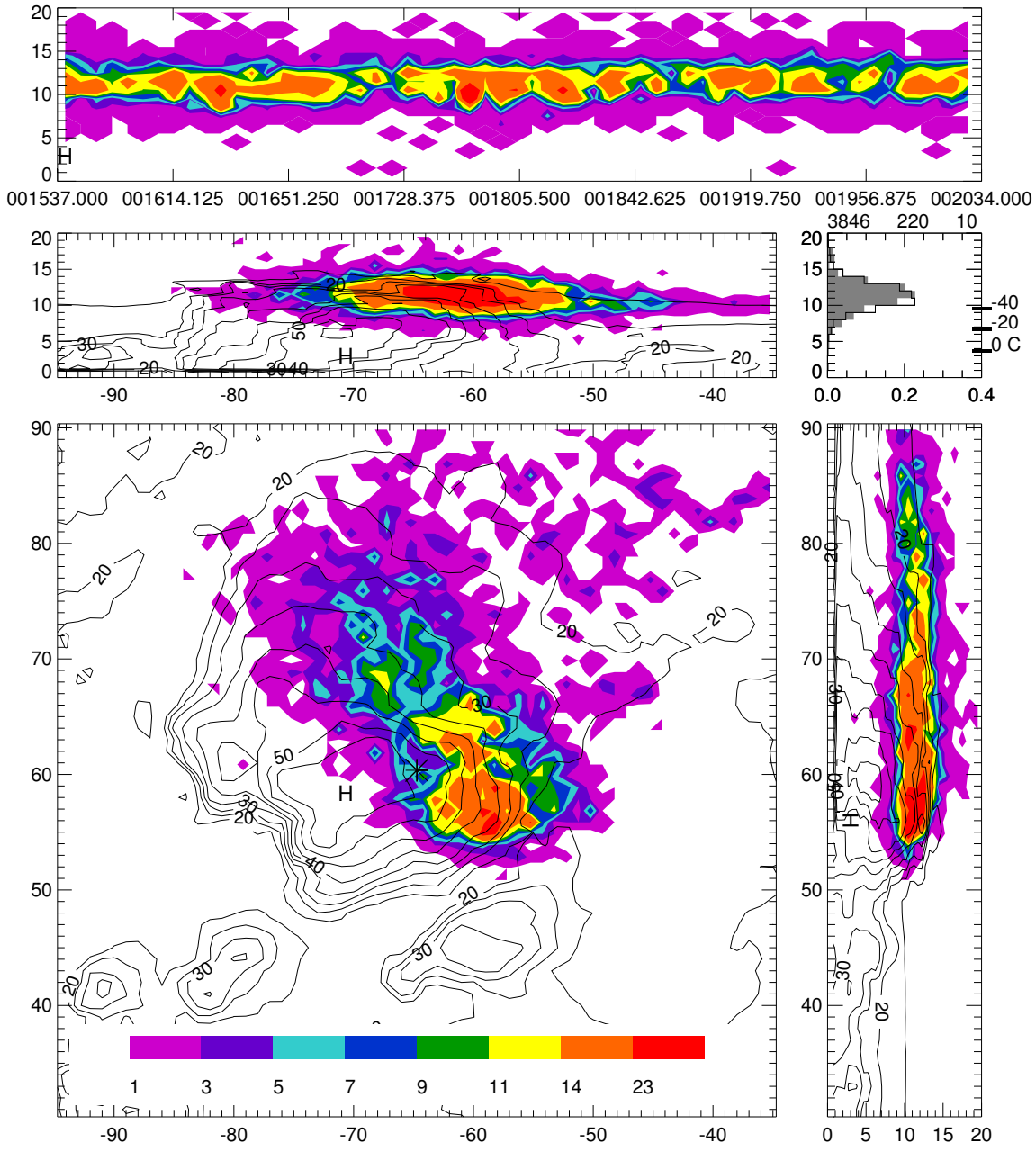

Figure 4. LDAR II source density and mean radar reflectivity of a supercell on 13 October 2001 (5 minute period). The uppermost panel shows the time (UTC) versus height display of lightning source density at 5 s and 1 km resolutions. The lower left panel shows the plan view projection of mean reflectivity (dBZ) overlaid on source density (color bar gives values in sources km^{-2}). The resolution of the LDAR II and radar data is 1 km. The asterisk is the location of the radar-detected mesocyclone (at -65, 61 km) by WDSS-II. The two panels which flank the horizontal projection are the vertical projections (x-height and height-y) of source density and mean reflectivity. The height resolution of the LDAR II data is 1 km and of the radar data 0.5 km. The color bar is not associated with these panels or the time-height panel. A normalized height histogram of the number of sources and flash origins (shaded) at 1 km intervals is plotted to the right of the x-height projection. Environmental temperature levels are plotted as bars, and the total number of sources, flashes, and peak source height (km) are given above the histogram. The "H" in the panels represents the time and location of a severe hail report. The axes are labeled as distances (x: west-east, y: south-north) from the KFWS radar (located at 0, 0) and in the vertical are heights in km MSL.

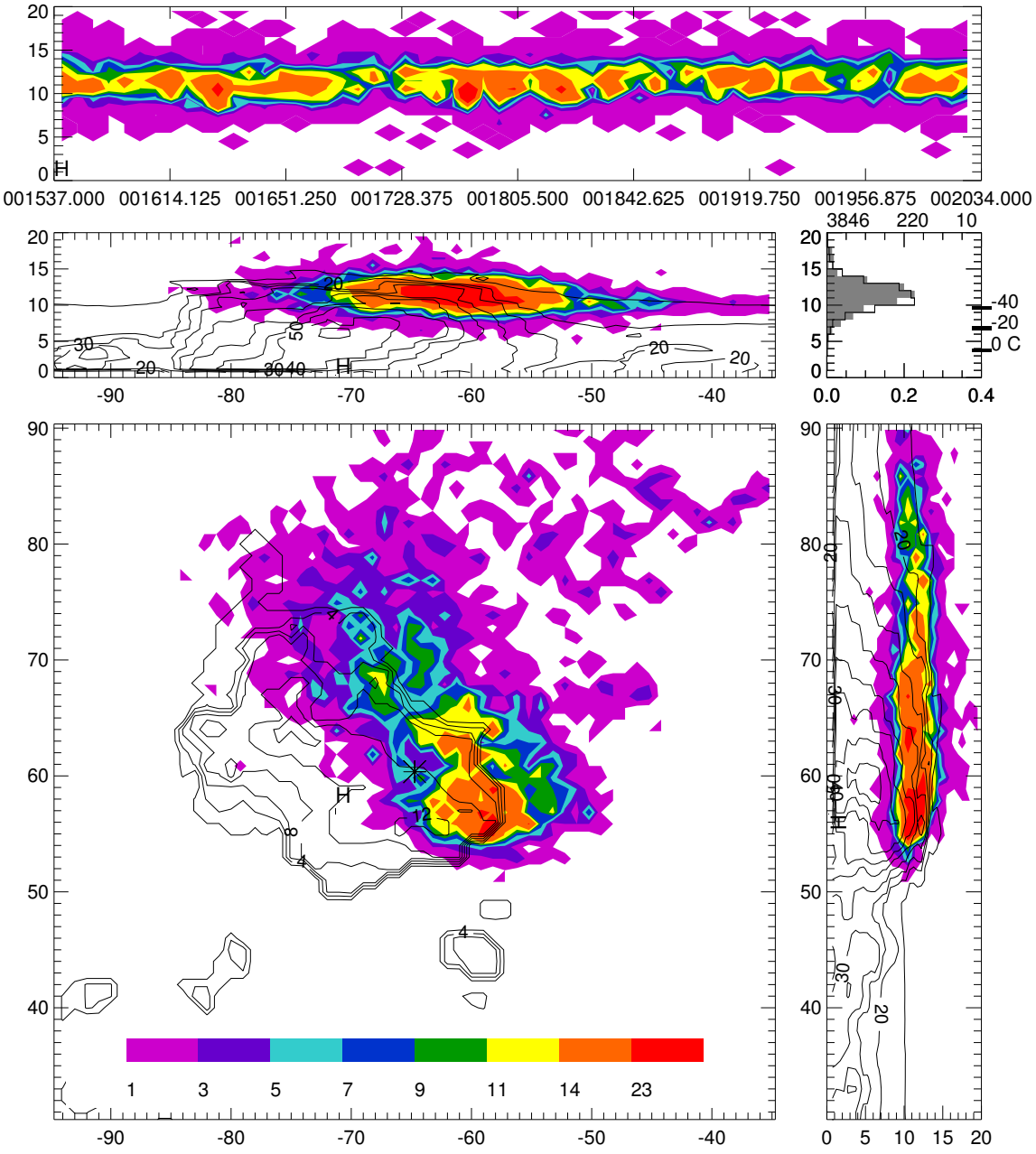

Figure 5. Same as figure 4, except the maximum 40 dBZ echo height (km) is overlaid on the source density in the plan view. The contour interval is 2 km.

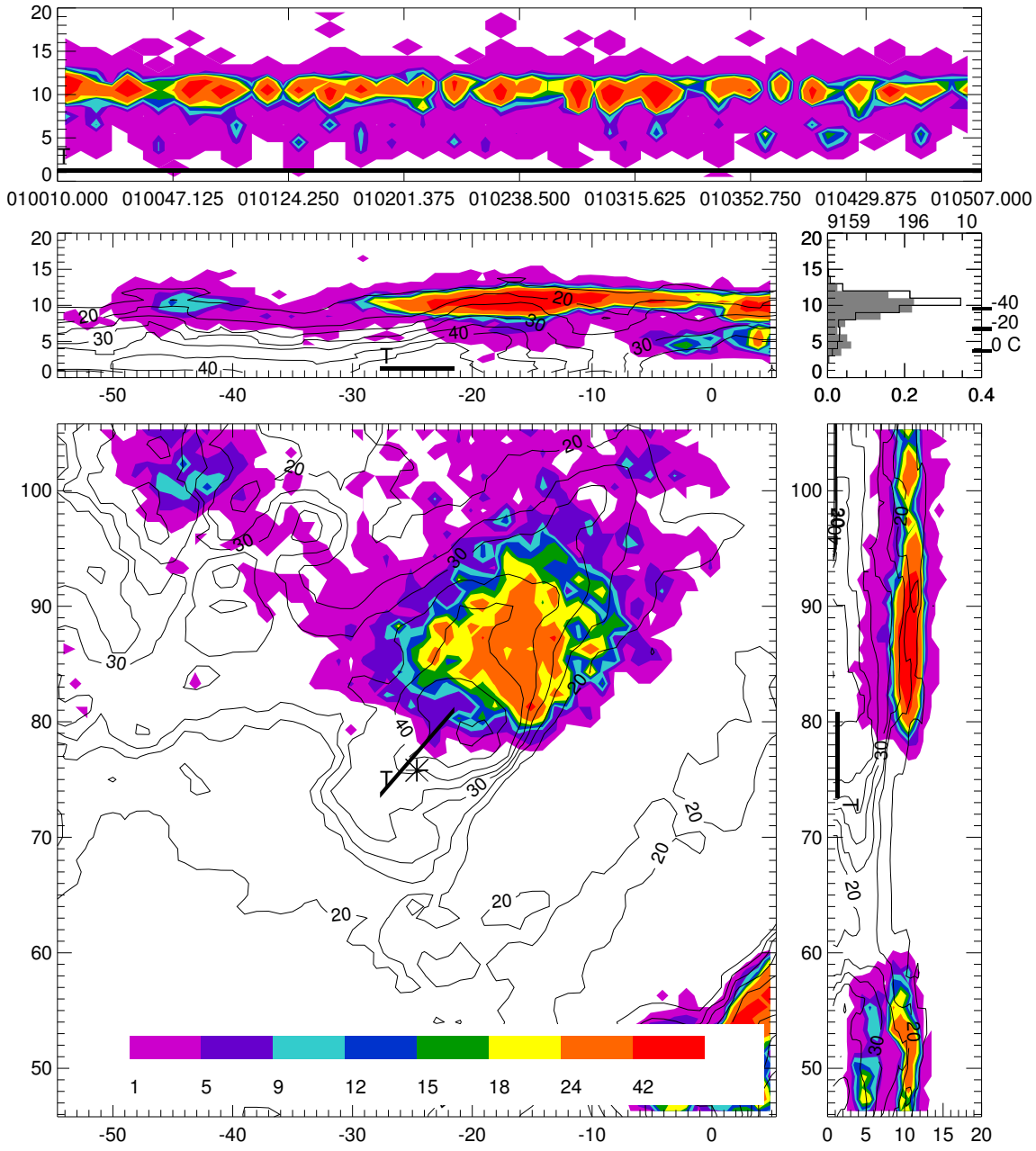

Figure 6. Same as figure 4, except for 010010 to 010507 UTC 13 October 2001 and "T" gives the location and track of a reported F2 tornado associated with this supercell. The location of the asterisk indicating the mesocyclone is (-24, 76).

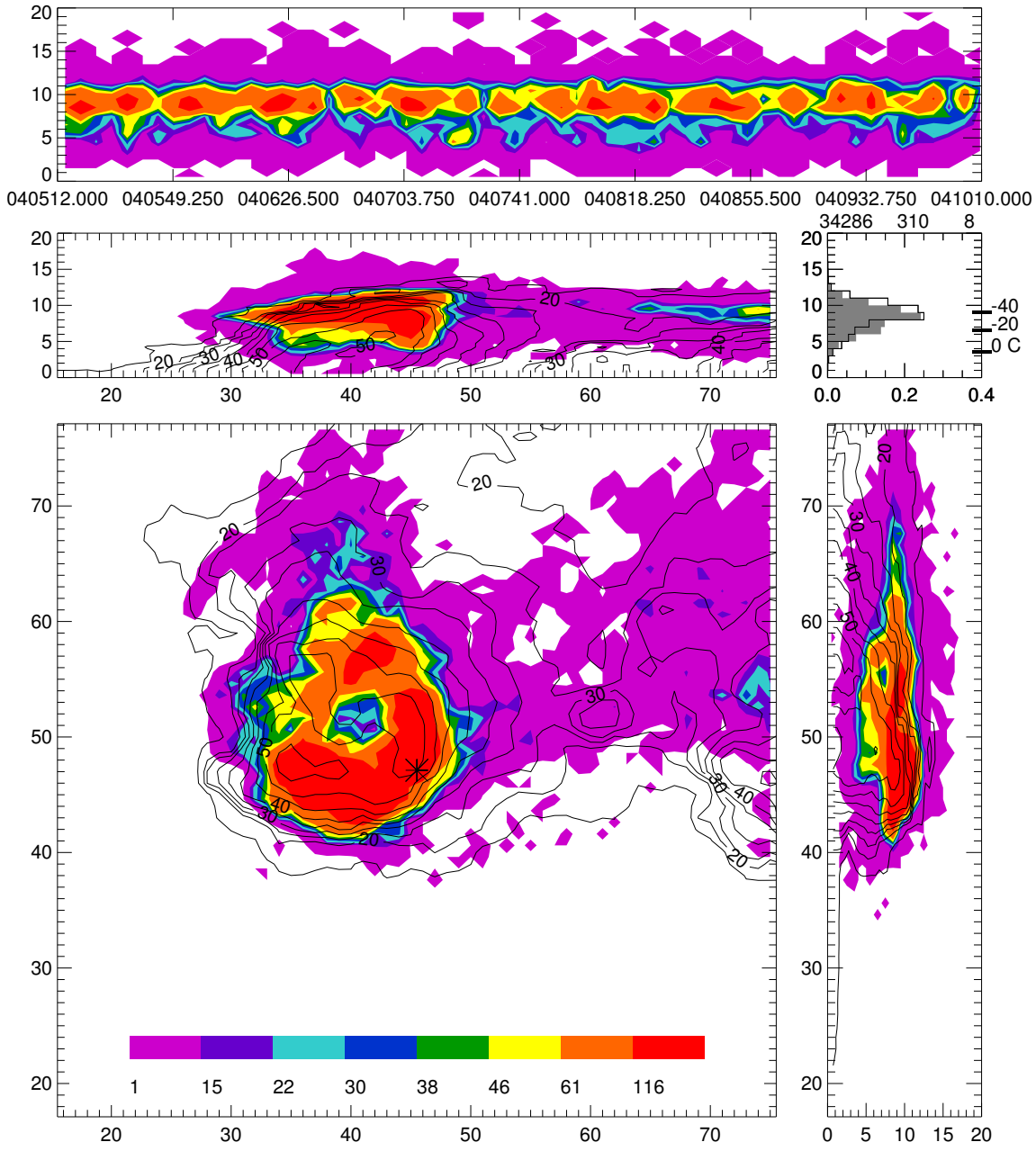

Figure 7. Same as figure 4, except for 040512 to 041010 UTC 6 April 2003. The location of the asterisk indicating the mesocyclone is (46, 47).

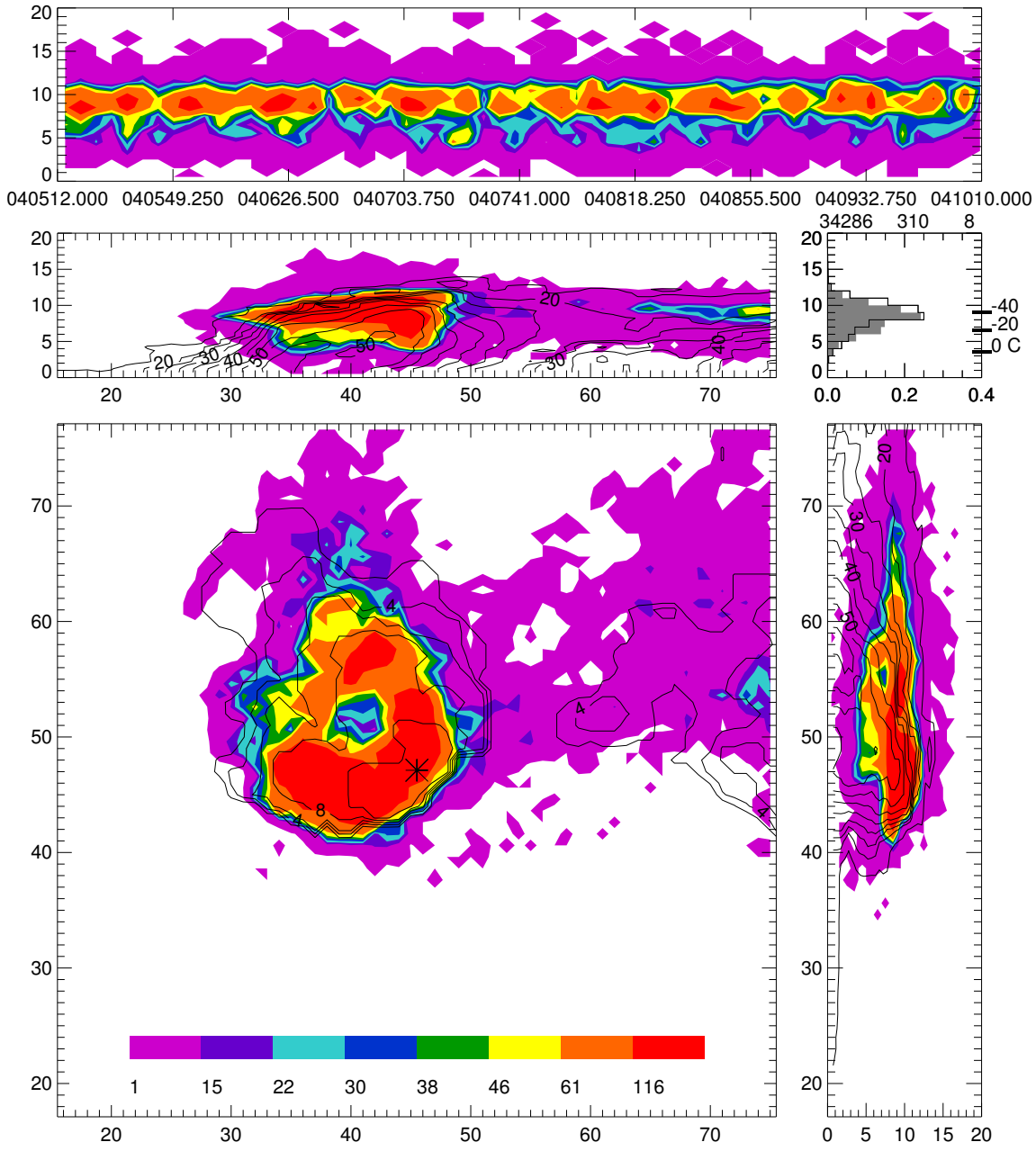

Figure 8. Same as figure 7, except the maximum 40 dBZ echo height (km) is overlaid on the source density in the plan view. The contour interval is 2 km.

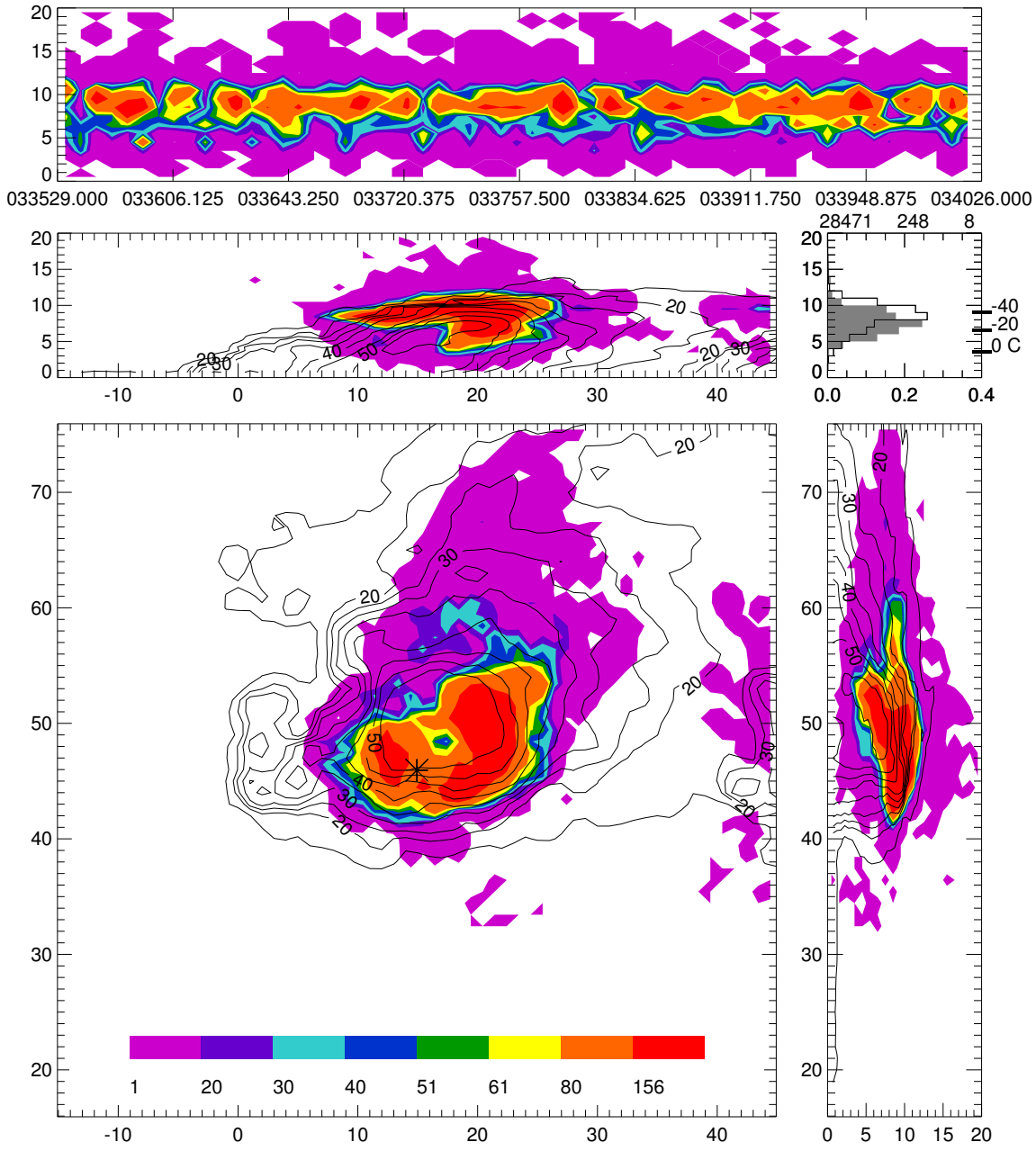

Figure 9. Same as figure 4, except for 033529 to 034026 UTC 6 April 2003. The location of the asterisk indicating the mesocyclone is (15, 46).

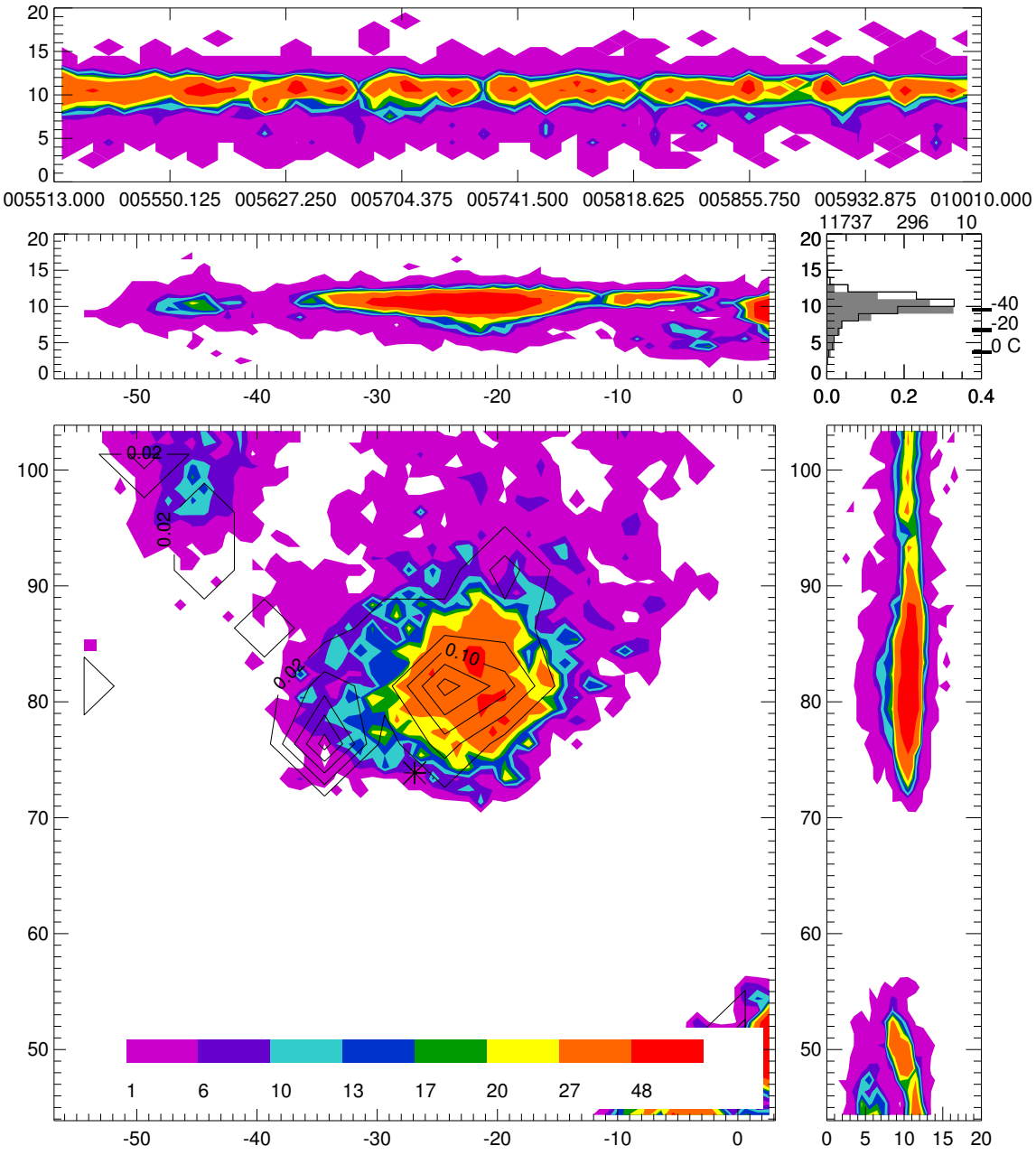

Figure 10. Same as figure 4, except for 005513 to 010010 UTC 13 October 2001 and instead of mean radar reflectivity, negative CG flash density is overlaid on the LDAR II source density in the plan view. The resolution of the CG data is 5 km and the contour interval is 0.04 flashes km^{-2}, starting at 0.02 and ending with 0.22 flashes km^{-2}. Note 1 flash per grid box (25 km^{2}) is 0.04 flashes km^{-2}. The location of the asterisk indicating the mesocyclone is (-27, 74).

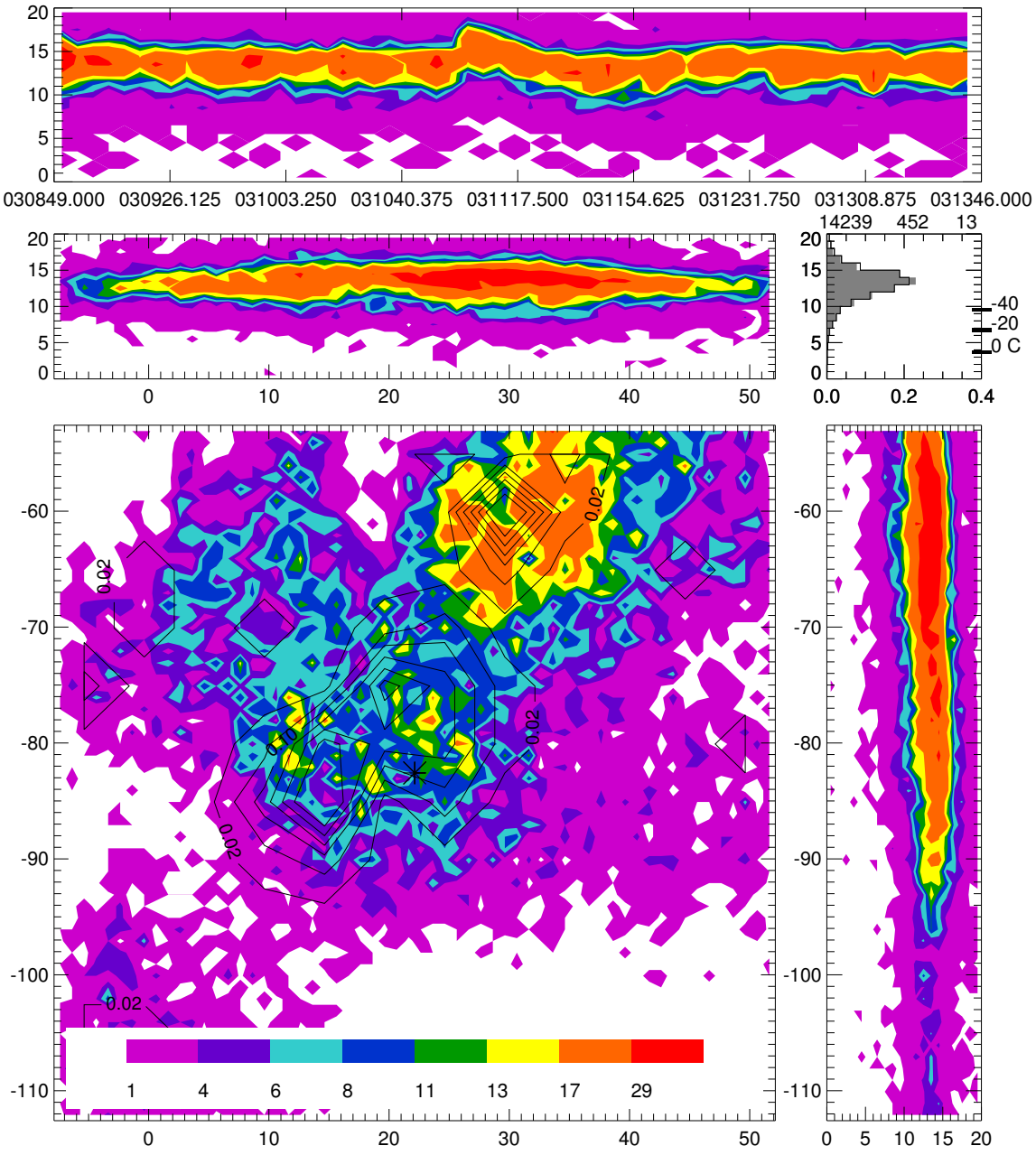

Figure 11. Same as figure 10, except for 030849 to 031346 UTC 13 October 2001. The location of the asterisk indicating the mesocyclone is (22, -77).

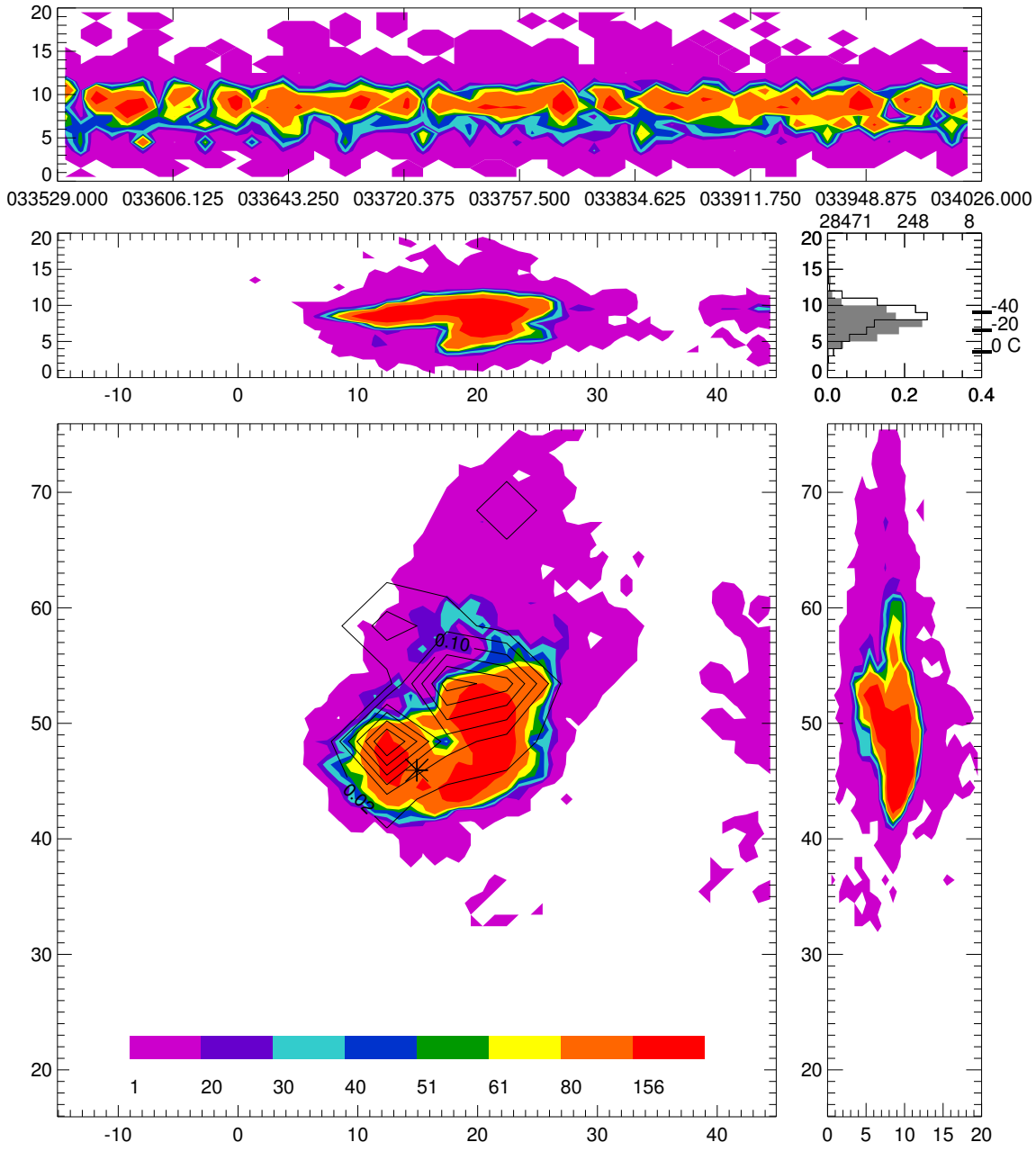

Figure 12. Same as figure 10, except for 033529 to 034026 UTC 6 April 2003. The location of the asterisk indicating the mesocyclone is (15, 46).

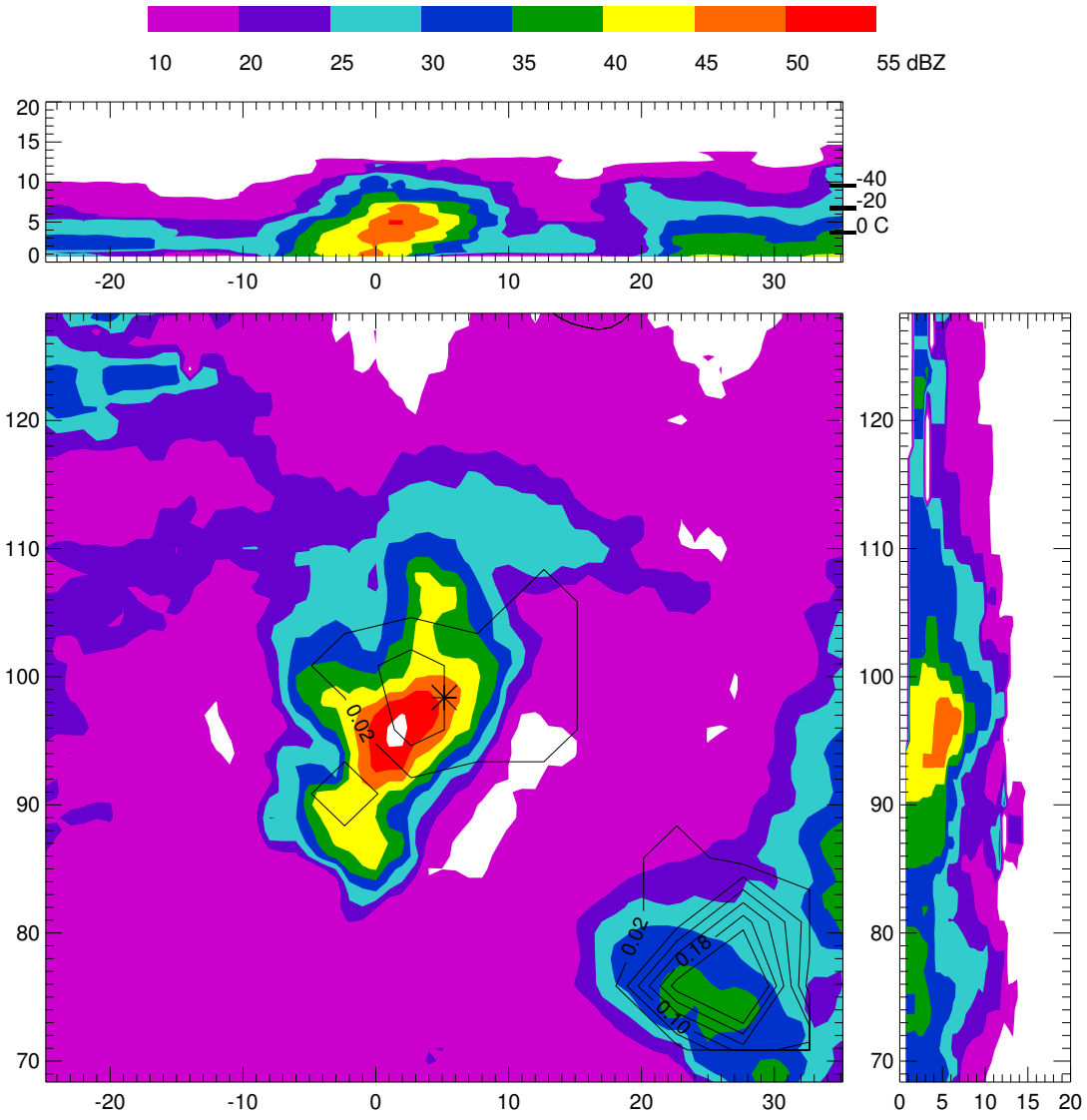

Figure 13. Mean reflectivity and –CG flash density for a pair of storm cells between 013449 and 013946 UTC 13 October 2001. The color bar (top) gives values of reflectivity in dBZ. The resolutions and contour intervals are the same for the radar and CG flash density as given in figures 4 and 10. Ambient temperature levels are given in the x-height projection. The location of the asterisk indicating the mesocyclone is (5, 98).

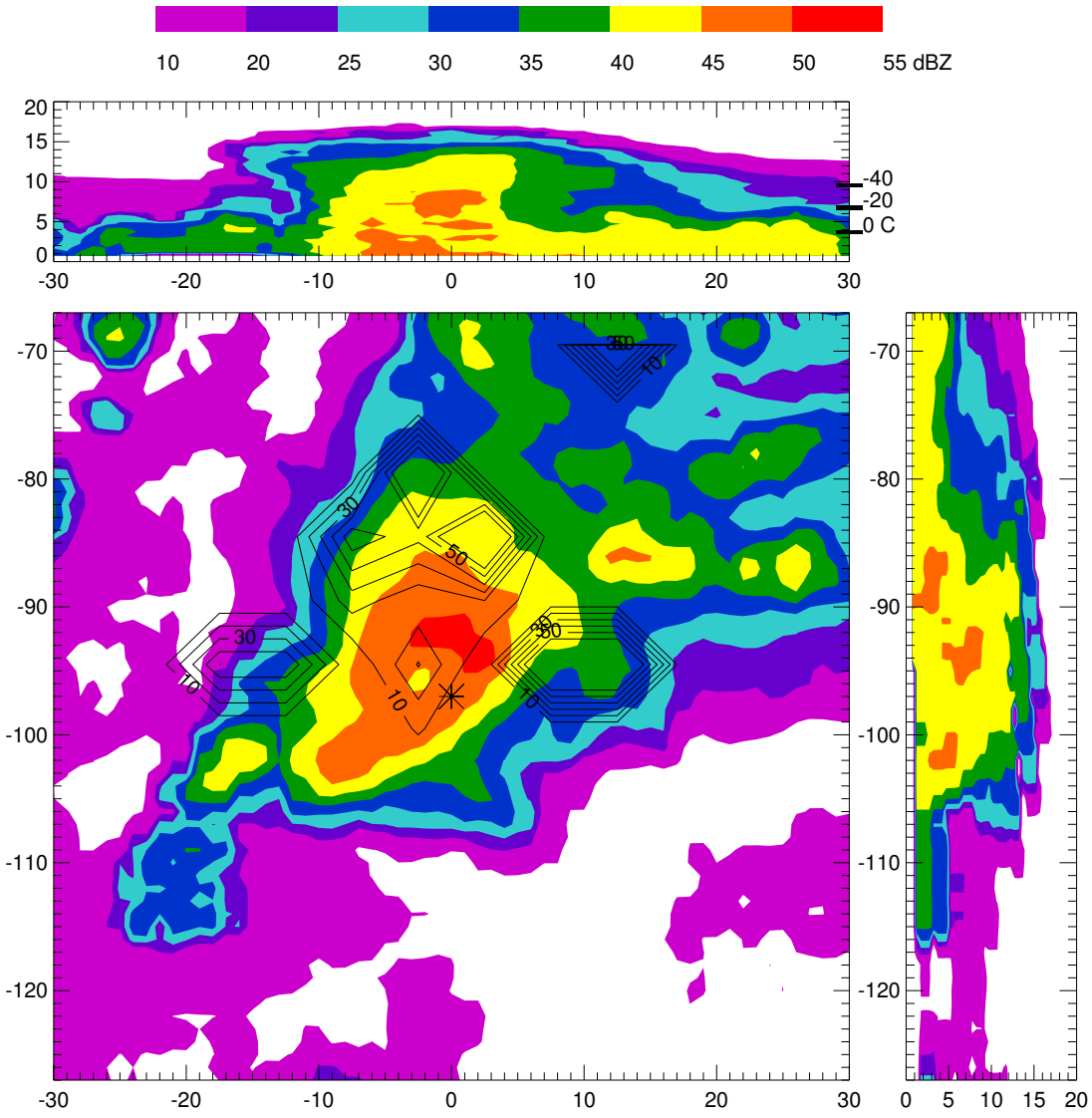

Figure 14. Mean reflectivity and percent positive CG lightning (contour interval 10%) for a supercell between 022914 and 023411 UTC 13 October 2001. The format is similar to that shown in figure 13. This storm produced an F1 tornado 45 minutes after the time shown. The location of the asterisk indicating the mesocyclone is (0, -97).

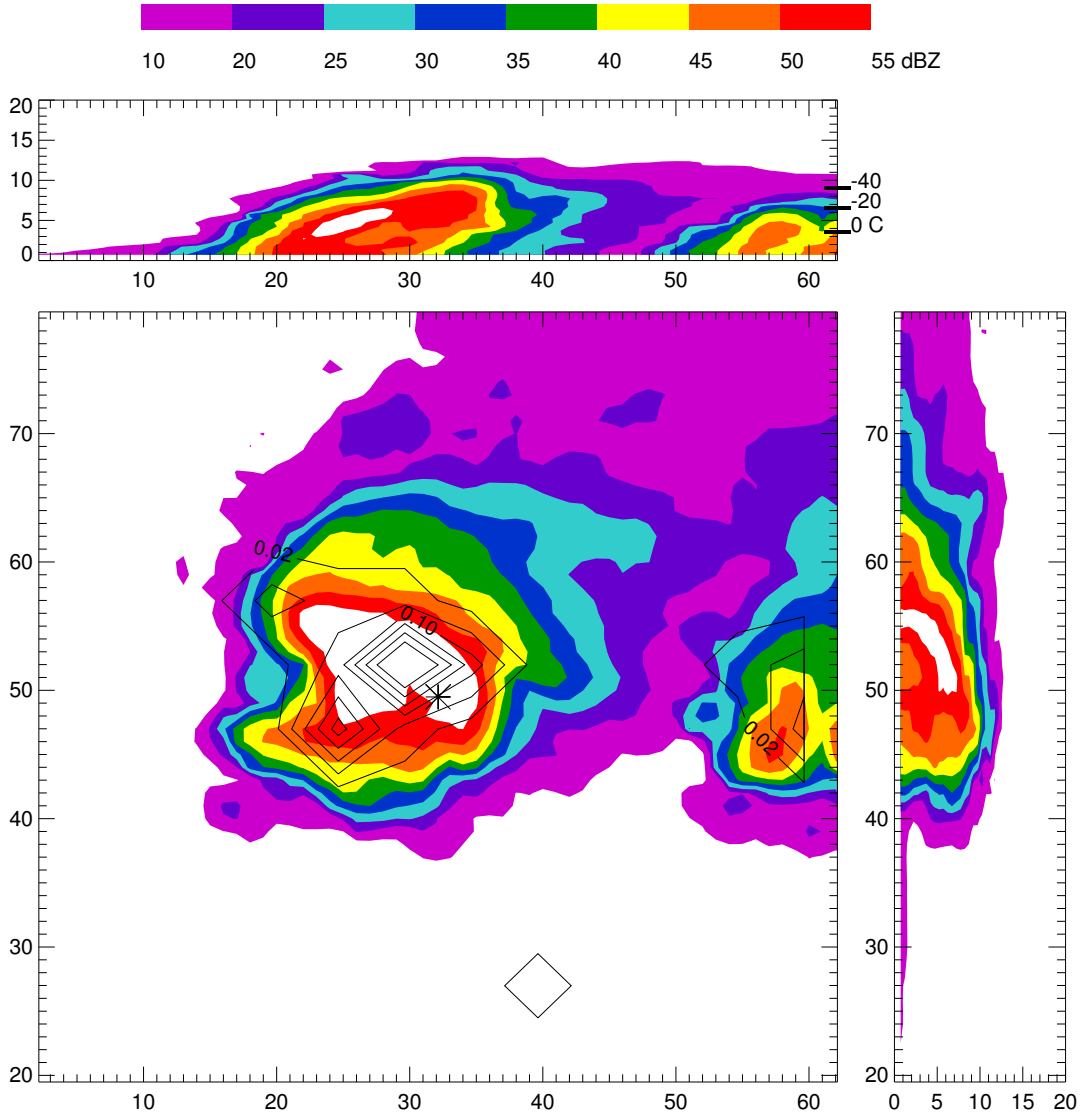

Figure 15. Same as figure 13, except for 035020 to 035517 UTC 6 April 2003. The location of the asterisk indicating the mesocyclone is (32, 49).

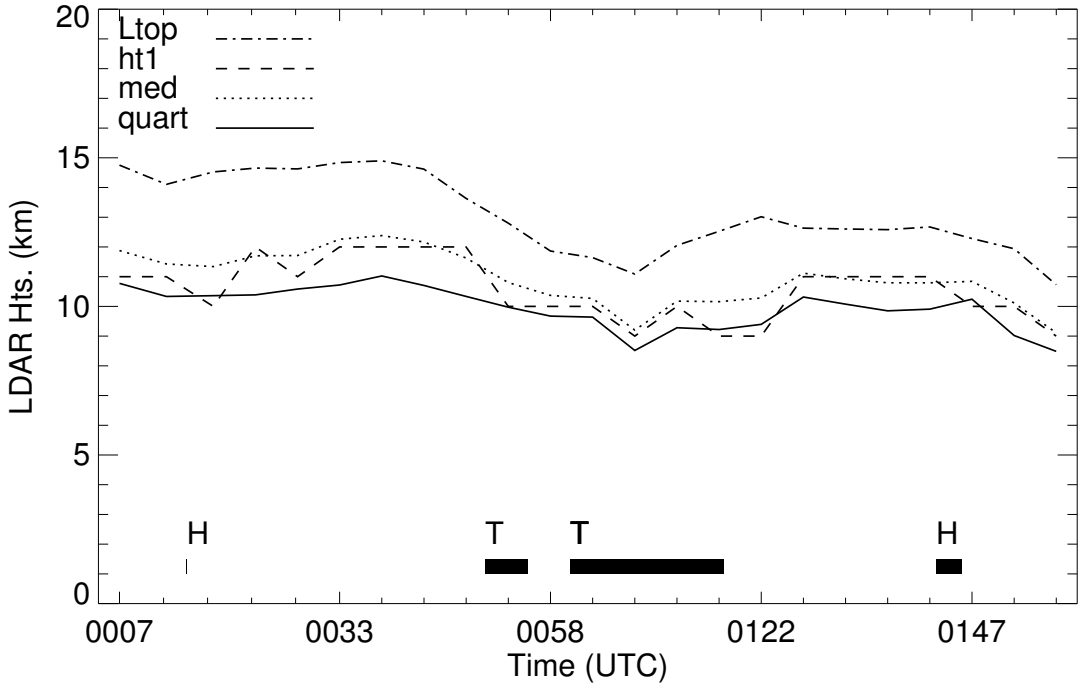

Figure 16. Time history of LDAR II lightning height characteristics for sources within 10 km of a 13 October 2001 mesocyclone: lightning-based storm top (95th percentile height: Ltop), peak (ht1), median (med), and lower quartile heights (quart). The duration of severe hail (H) and tornado (T) events are drawn as bars along the x-axis. Each x-tick mark represents the midpoint of a volume scan. The duration of time between each tick mark is approximately 5 minutes.

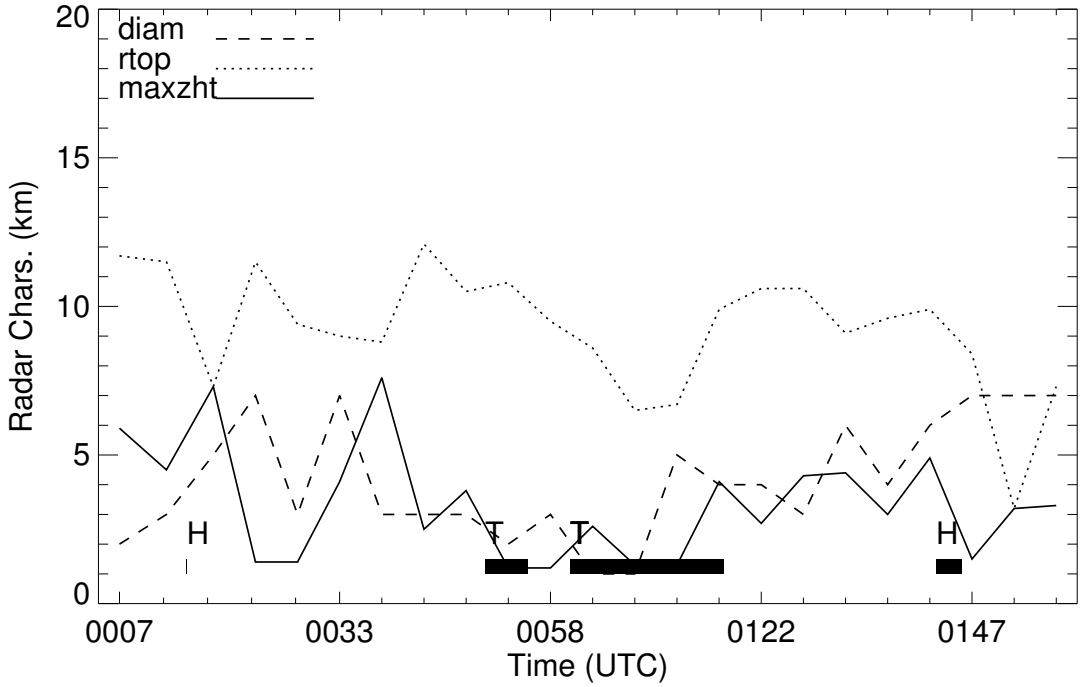

Figure 17. Time history of radar-derived diagnostics for a 13 October 2001 tornadic supercell: low-level mesocyclone diameter (diam), radar top (rtop), and maximum reflectivity height (maxzht). The occurrences of severe hail (H) and tornadoes (T) are also shown. The duration of time between each tick mark is approximately 5 minutes.

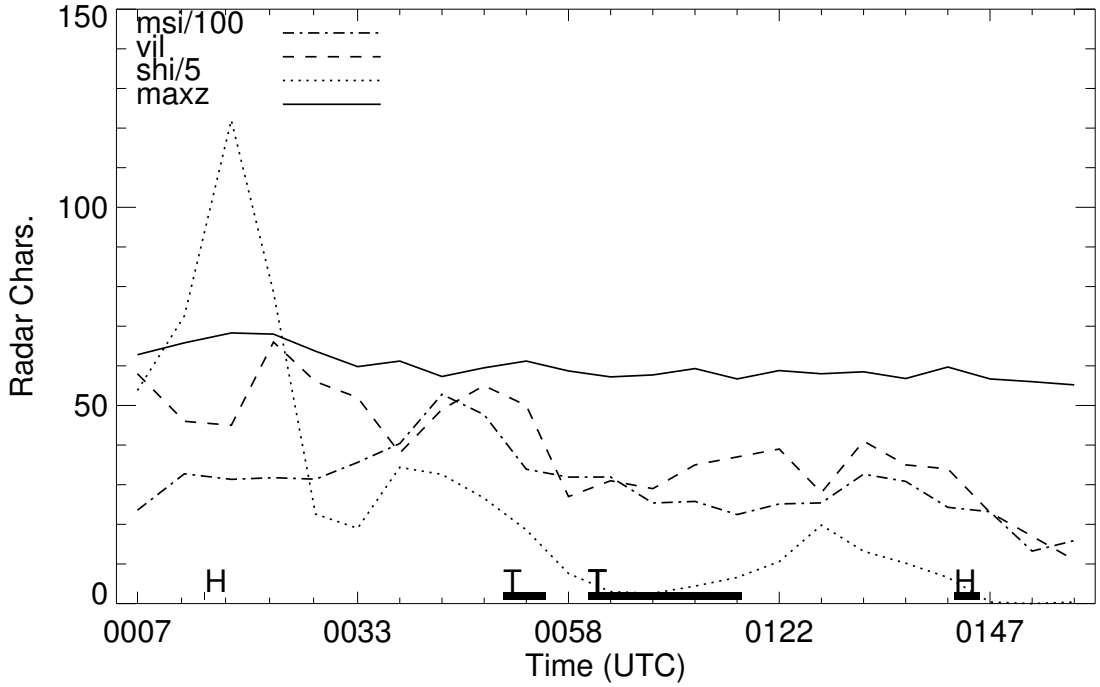

Figure 18. Same as figure 17, but for mesocyclone strength index (msi), vertically integrated liquid water (vil), severe hail index (shi), and maximum reflectivity (maxz, dBZ).

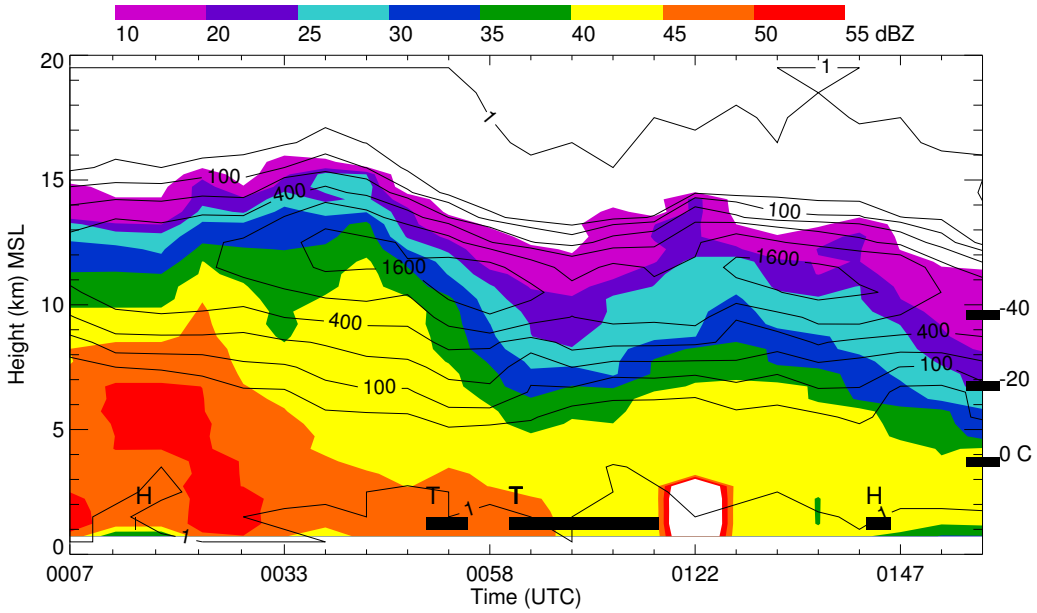

Figure 19. Time-height plot of mean radar reflectivity (see color bar at top) and LDAR II source density (sources km^{-1} (5 minutes)$^{-1}$) for a 13 October 2001 tornadic supercell between 000436 and 015437 UTC. To calculate these values, radar and lightning data were averaged within 20 km of the storm mesocyclone during each volume time interval. Severe hail (H) and tornado (T) reports and the ambient temperature levels are also shown. After 1 source km^{-1} (5 minutes)$^{-1}$, the source density contour intervals proceed as 2x, where x is the previous contour interval, the first value being 50 sources km^{-1} (5 minutes)$^{-1}$. See Data and methodology subsection for more details on the plot construction. The duration of time between each tick mark is approximately 5 minutes.

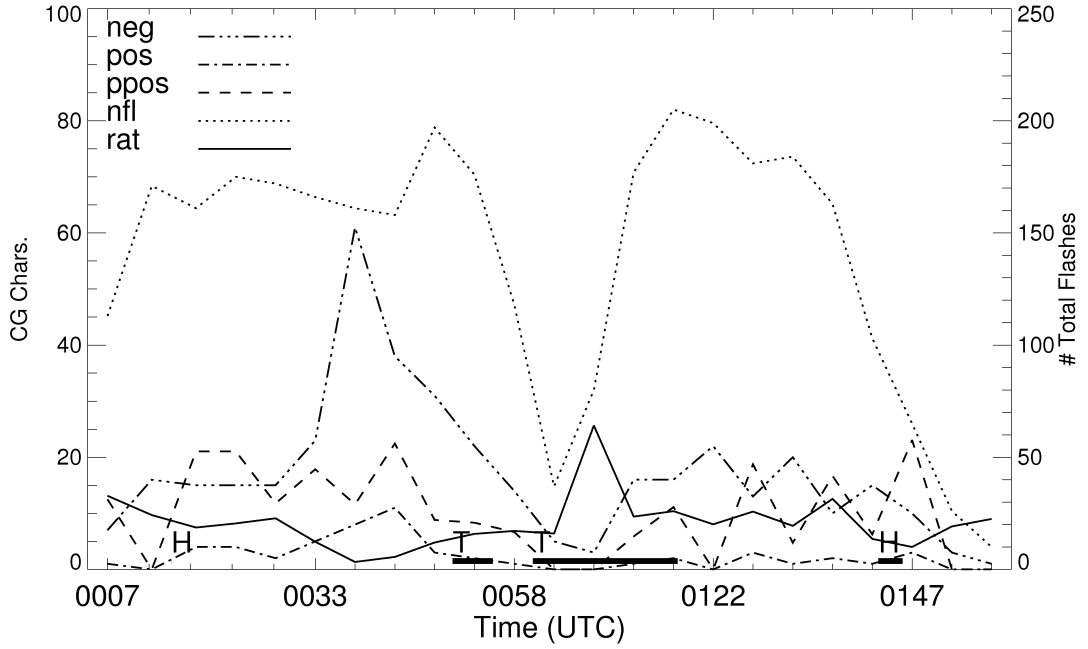

Figure 20. Time history of lightning characteristics calculated within 10 km of a 13 October 2001 mesocyclone for each radar volume scan interval. The -/+ CG flash rate (neg/pos), percent positive CG flashes (ppos), total flash rate (nfl; right y-axis), and IC:CG ratio (rat) are shown. Severe hail (H) and tornado (T) reports are also plotted. The duration of time between each tick mark is approximately 5 minutes.

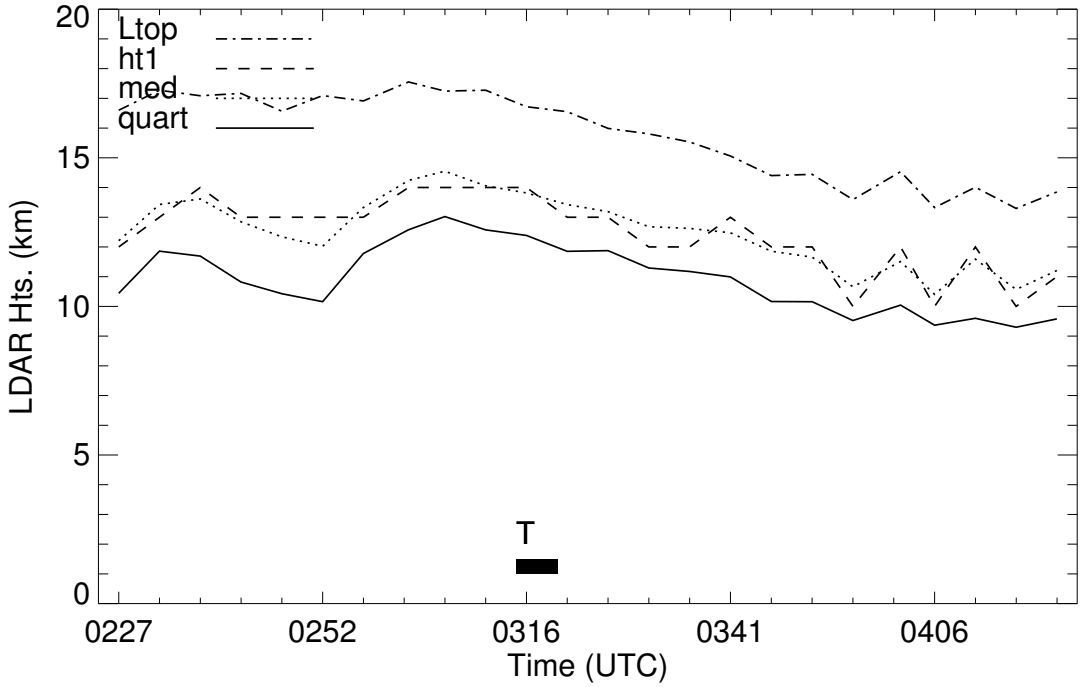

Figure 21. Same as figure 16, except for a different tornadic supercell on 13 October 2001.

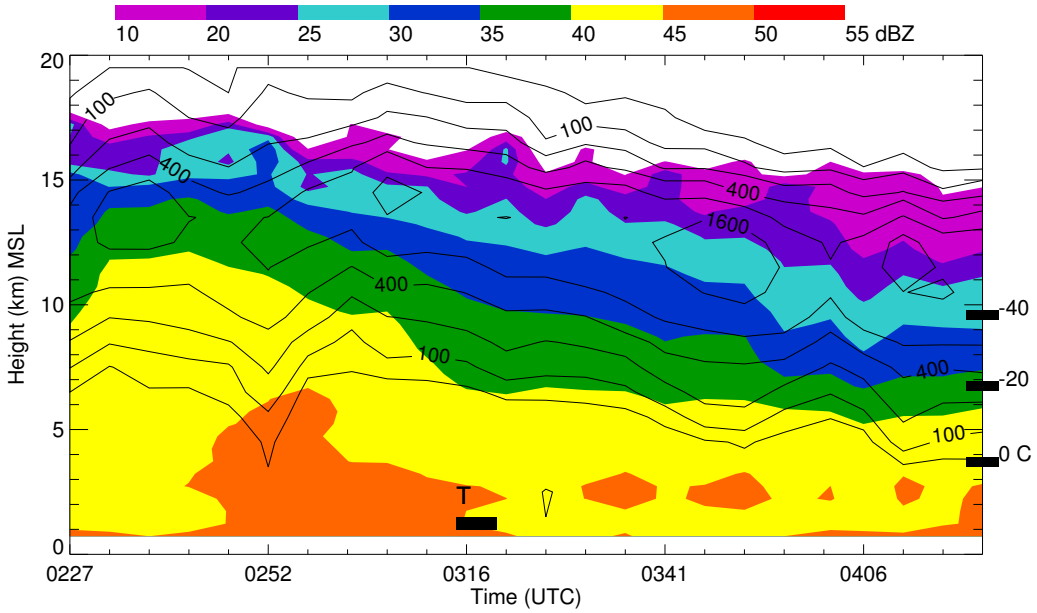

Figure 22. Same as figure 19, except for a different tornadic supercell between 022418 and 042305 UTC 13 October 2001.

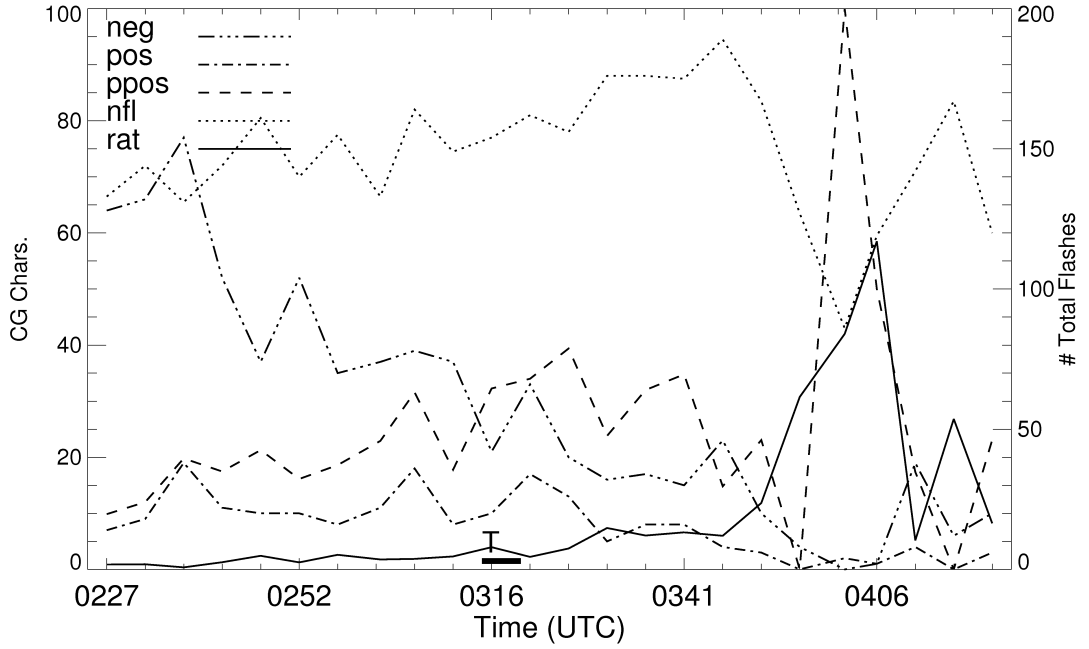

Figure 23. Same as figure 20, except for a different tornadic supercell on 13 October 2001.

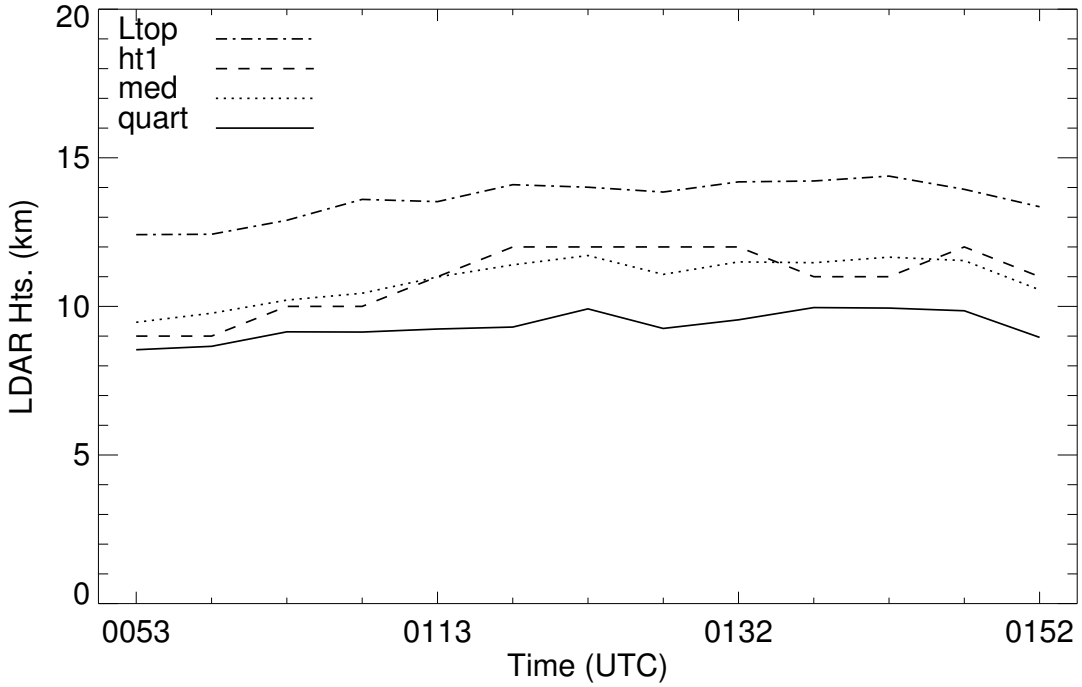

Figure 24. Same as figure 16, but for a non-tornadic supercell on 13 October 2001. There were no severe storm reports associated with this storm.

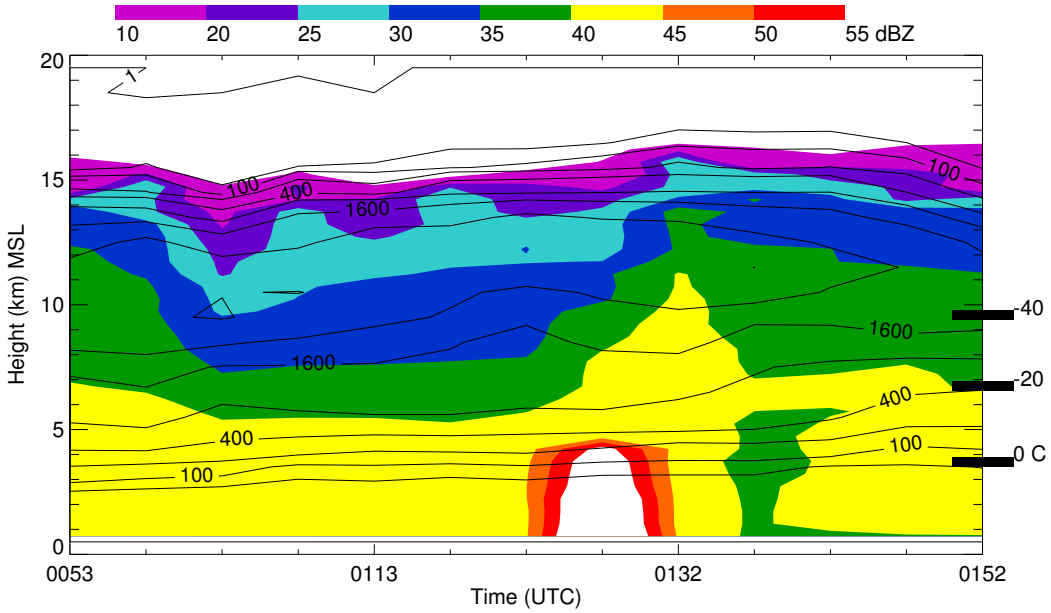

Figure 25. Same as figure 19, except for a non-tornadic supercell on 13 October 2001 between 005015 and 015437 UTC. The area of > 55 dBZ below 5 km at 012700 UTC is a measurement error.

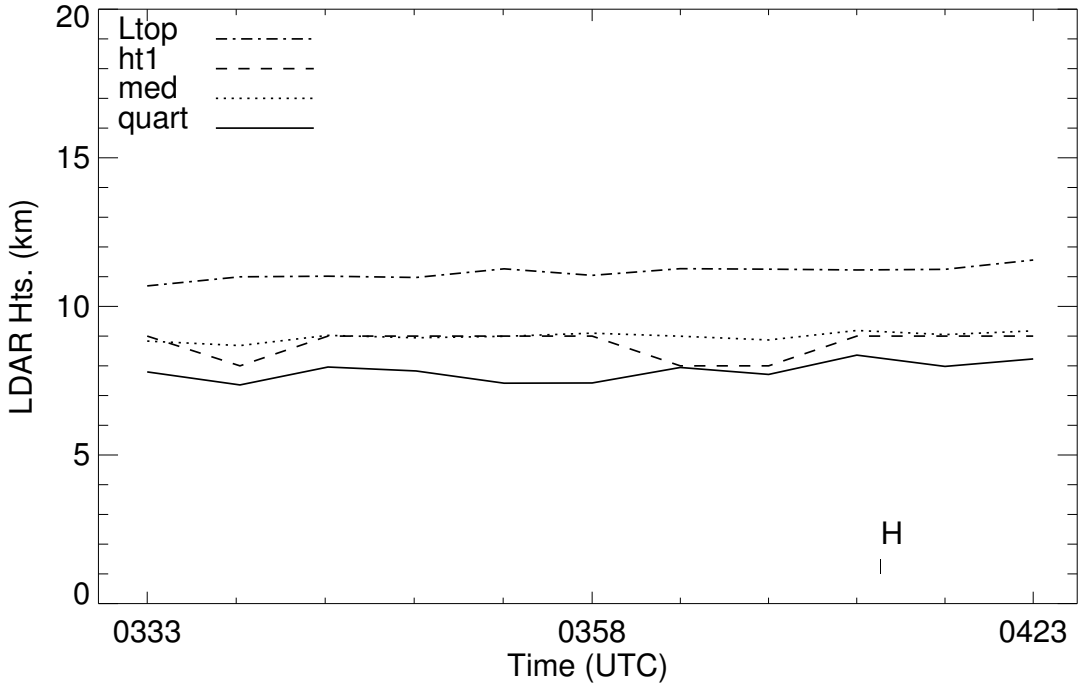

Figure 26. Same as figure 16, but for a hail-producing supercell on 6 April 2003 (hail report indicated with an "H"). These characteristics were calculated using source data within 20 km of the mesocyclone because it was isolated.

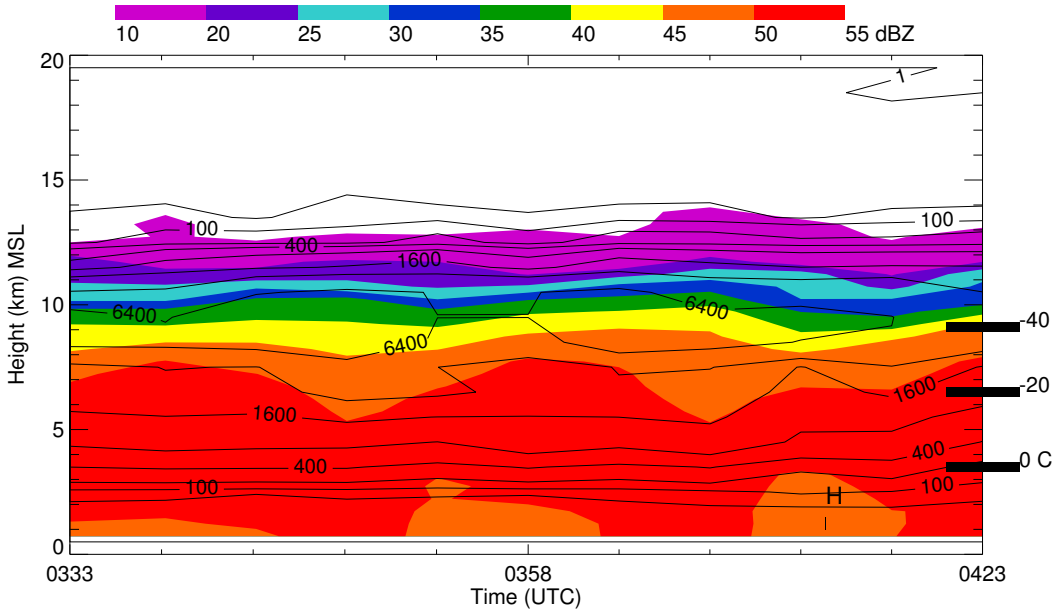

Figure 27. Same as figure 19, except for a hail-producing supercell on 6 April 2003 between 033000 and 042502 UTC. A hail report (H) is also shown.

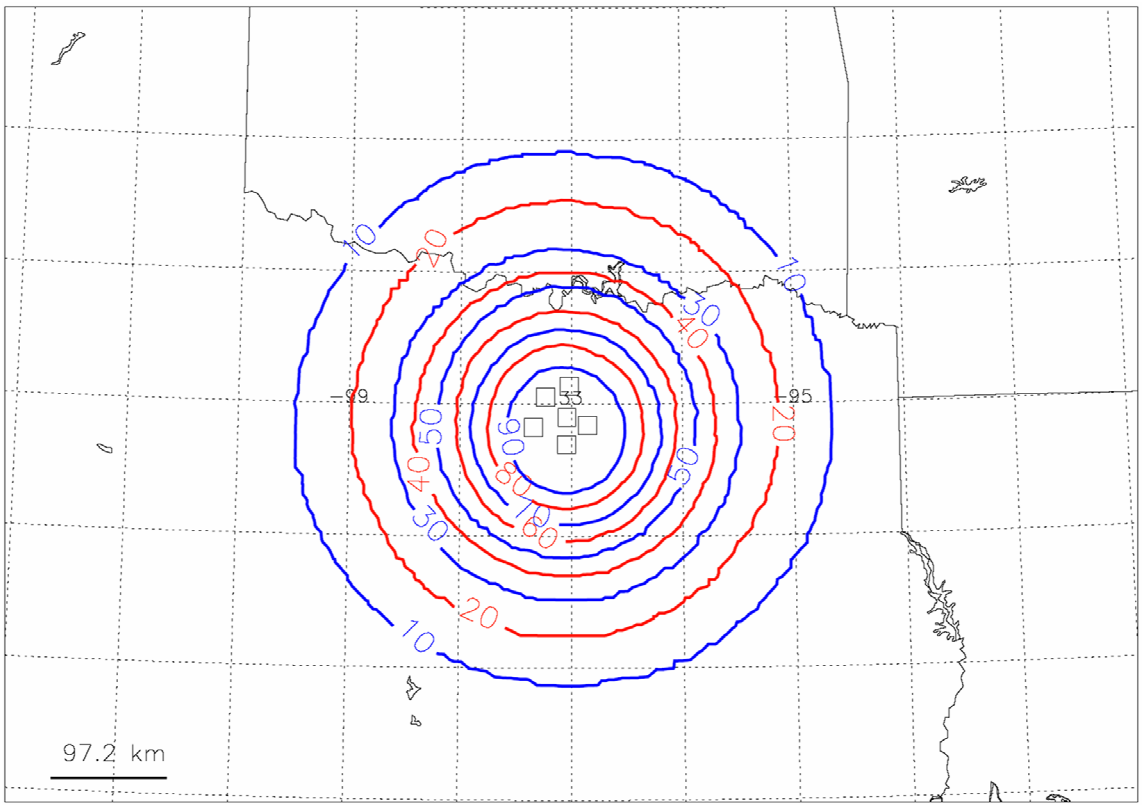

Figure 28. Same as figure 2, except for 27 May 2002.

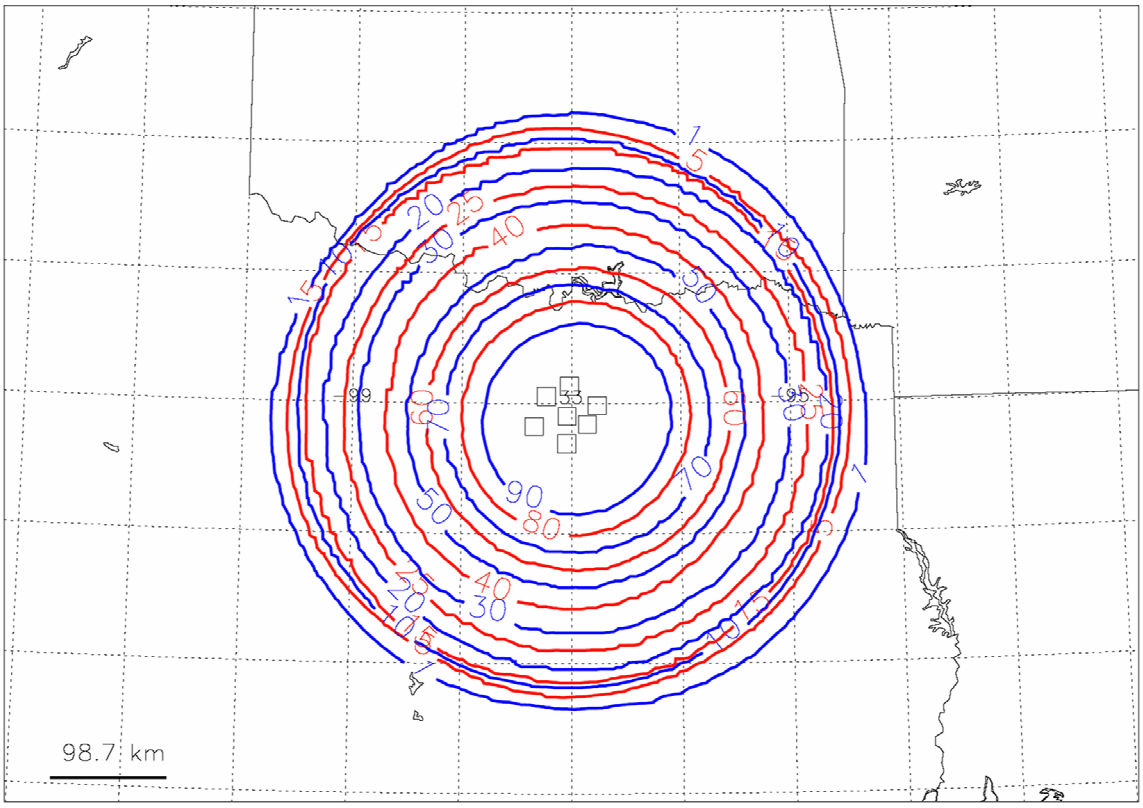

Figure 29. Same as figure 2, except for 16 June 2002.

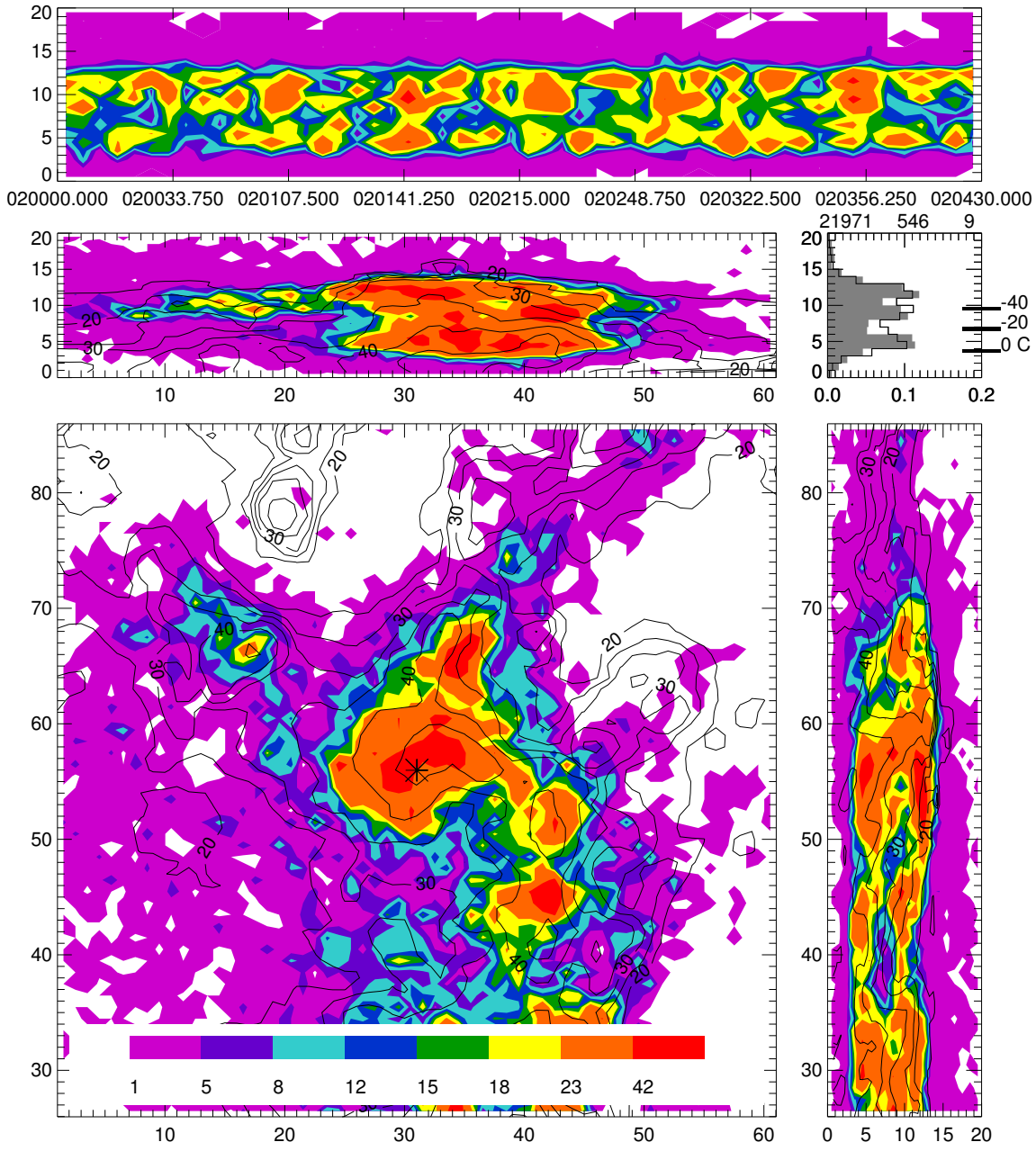

Figure 30. Same as figure 4, except for storm cells within an MCS on 13 October 2001. The asterisk is the location of the cell of interest detected by WDSS-II (at 31, 56 km).

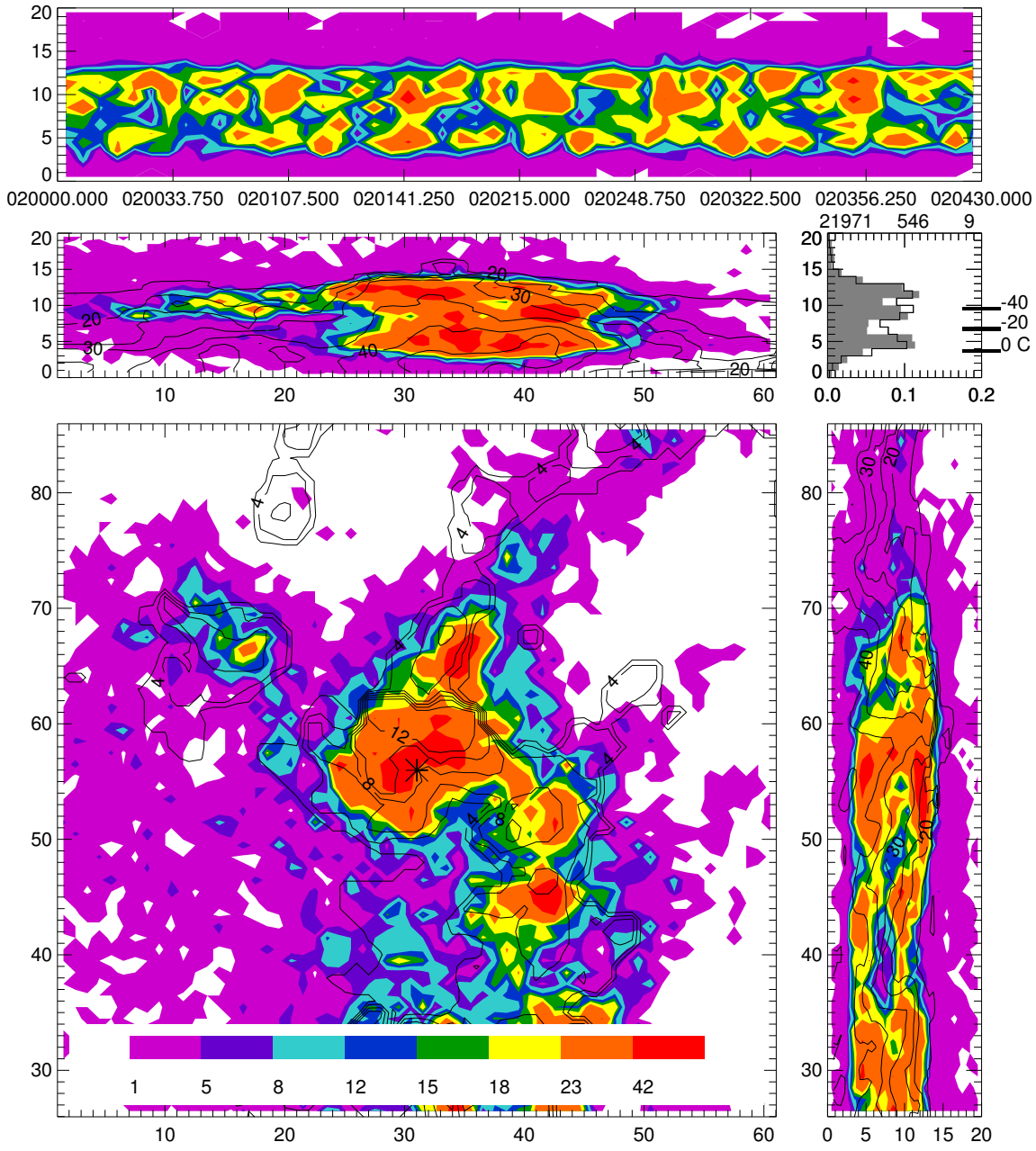

Figure 31. Same as figure 30, except the maximum 40 dBZ echo height (km) is overlaid on the source density in the plan view. The contour interval is 2 km.

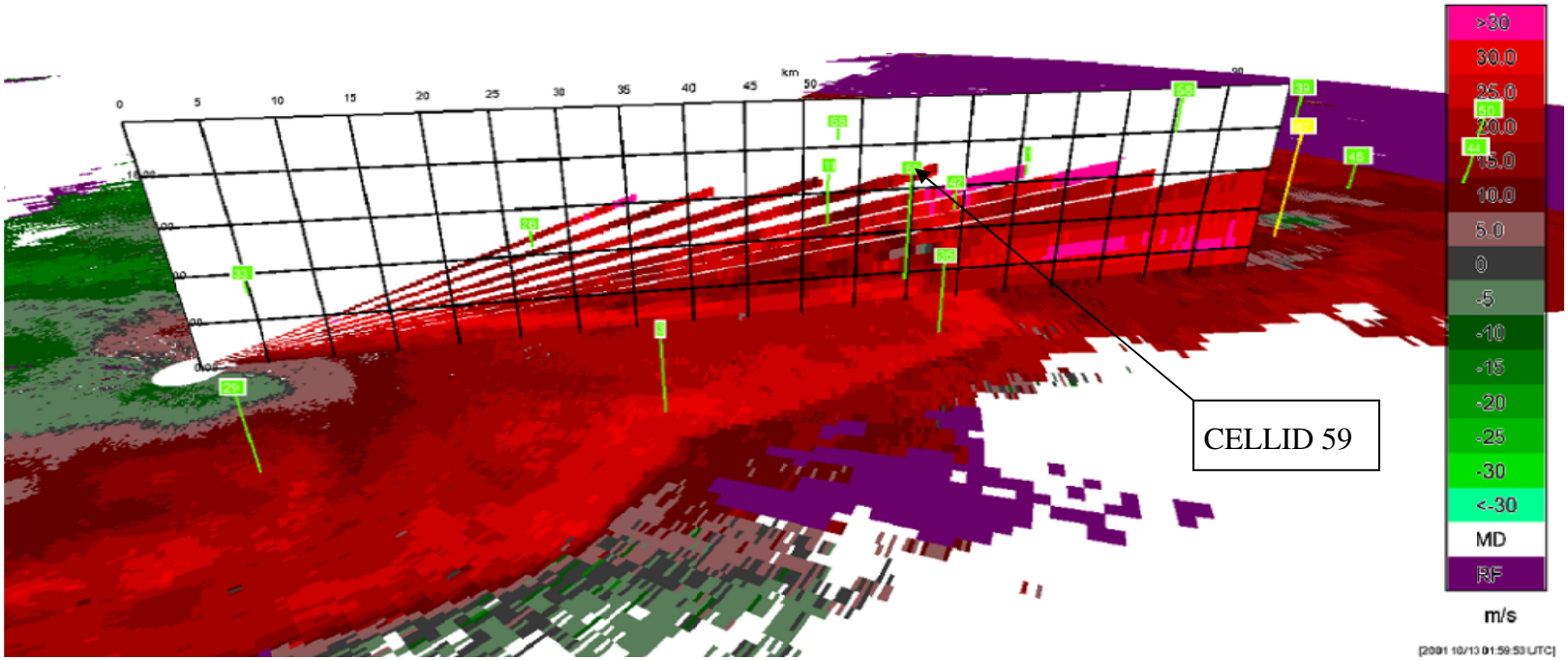

Figure 32. Horizontal and vertical cross sections of Doppler radial velocity measurements of a portion of an MCS obtained from the KFWS radar near 020000 UTC 13 October 2001. The vertical lines with cell identification numbers indicate storm cells. The vertical cross section's lower left corner is approximately at the radar location and extends radially outward to just south of the cell location (cell ID 59 near 60 km range) marked by an asterisk in figure 30; its grid point interval is 4 km (MSL) in the vertical and 5 km in the radial directions. The color bar gives the radial velocity values in m s^{-1}. This figure was created using the WDSS-II software.

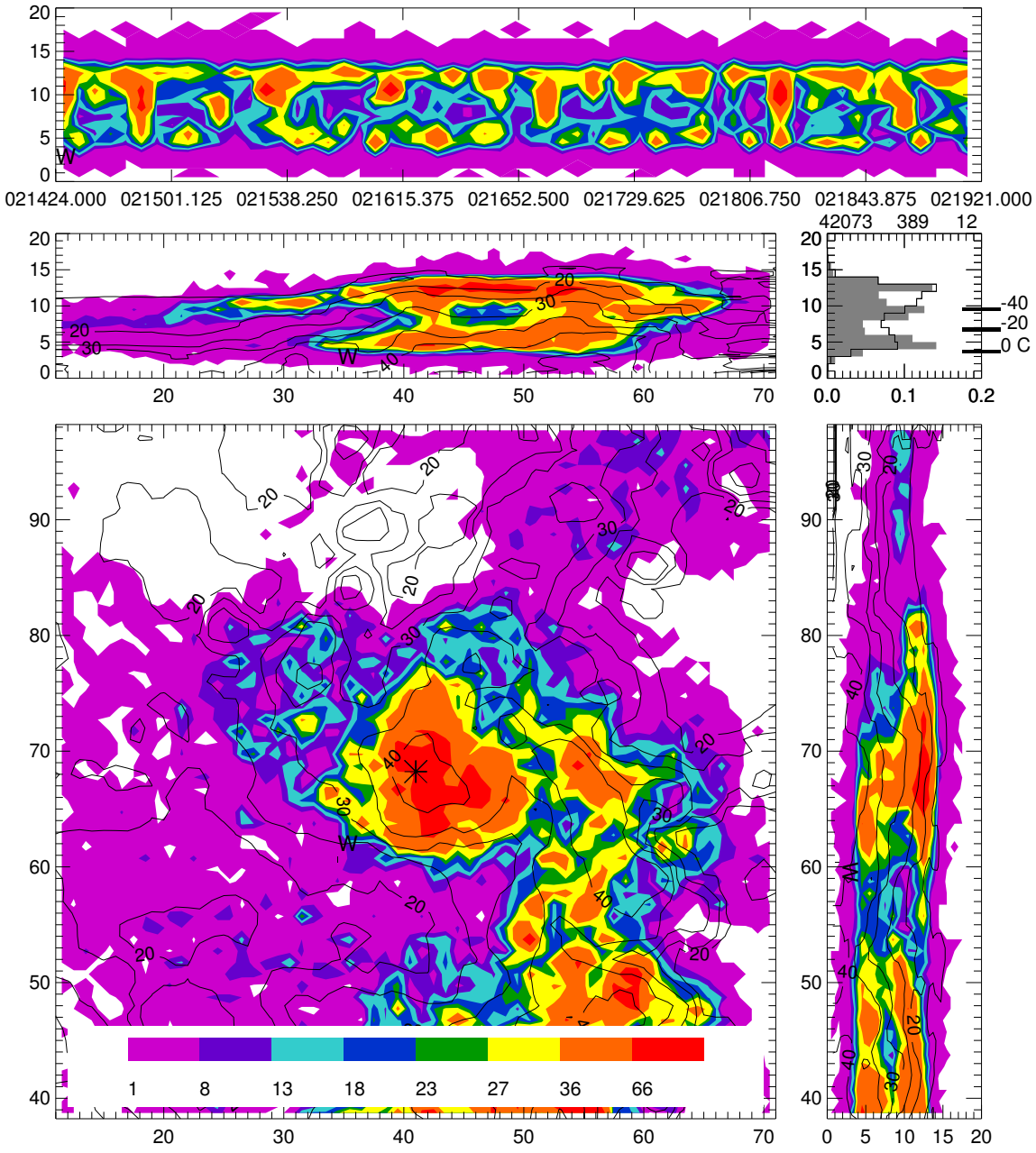

Figure 33. Same as figure 4, except for 021424 to 021921 UTC 13 October 2001. The "W" in each panel represents the time and location of a severe wind report associated with this cell (located at 41, 68 km).

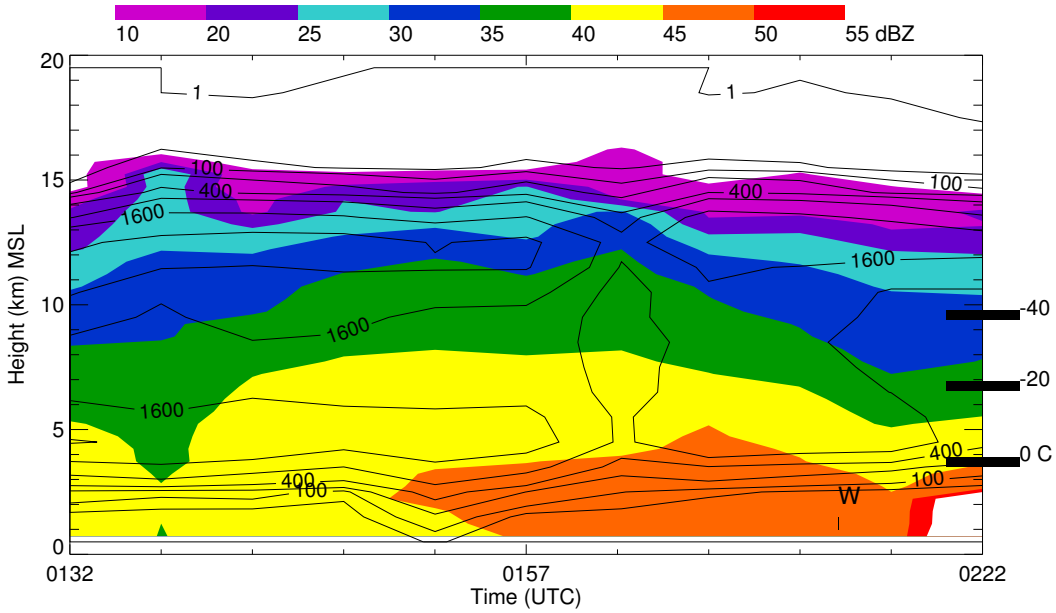

Figure 34. Same as figure 19, except for a 13 October 2001 MCS storm cell between 012952 and 022418 UTC and radar and lightning data were analyzed within only 10 km from the storm. A severe wind (W) report is also shown. The area of reflectivity greater than 55 dBZ below 3 km at 0222 UTC is likely a measurement error.

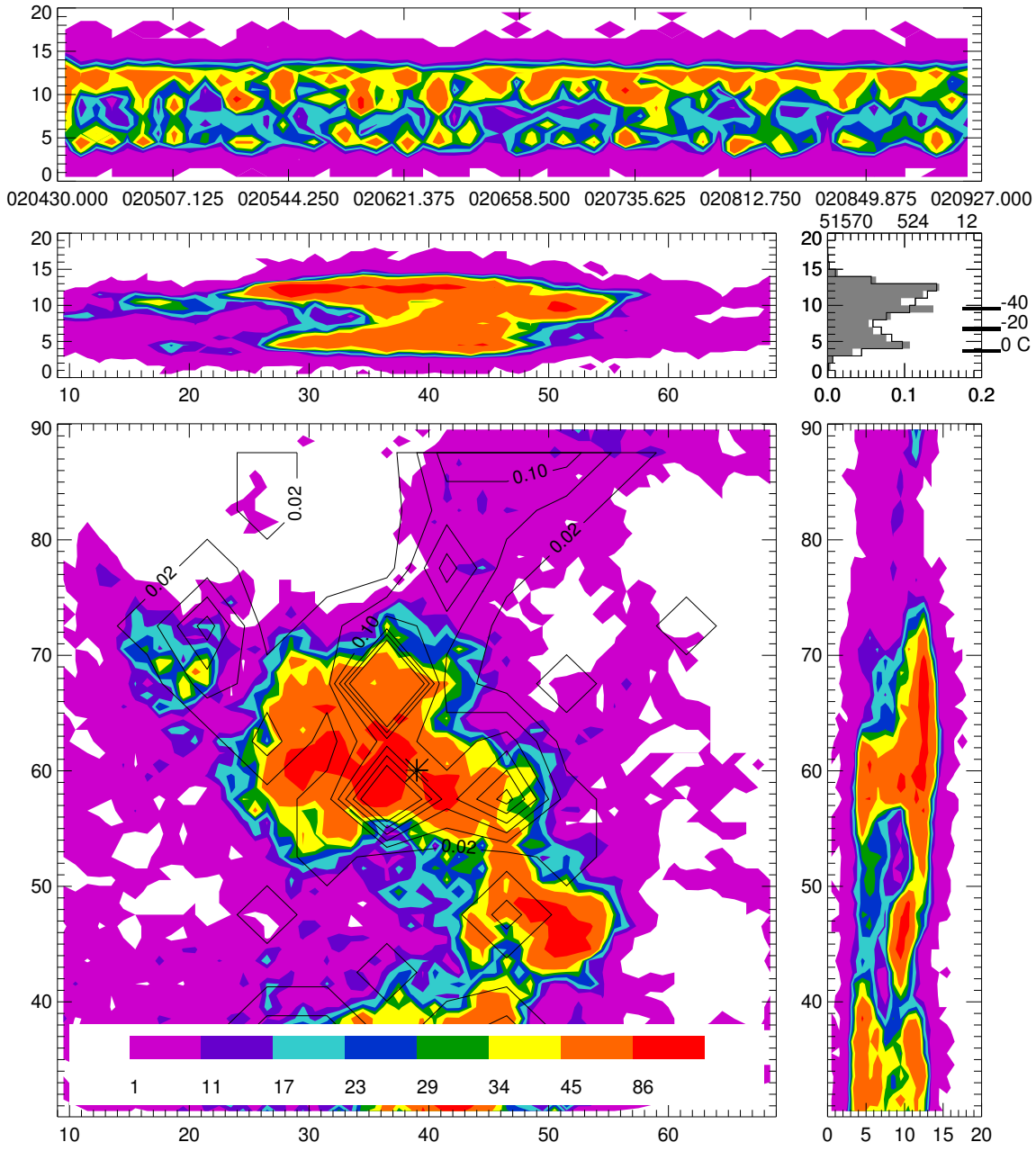

Figure 35. Same as figure 10, except for 020430 to 020927 UTC 13 October 2001. The location of the asterisk indicating the cell is (39, 60).

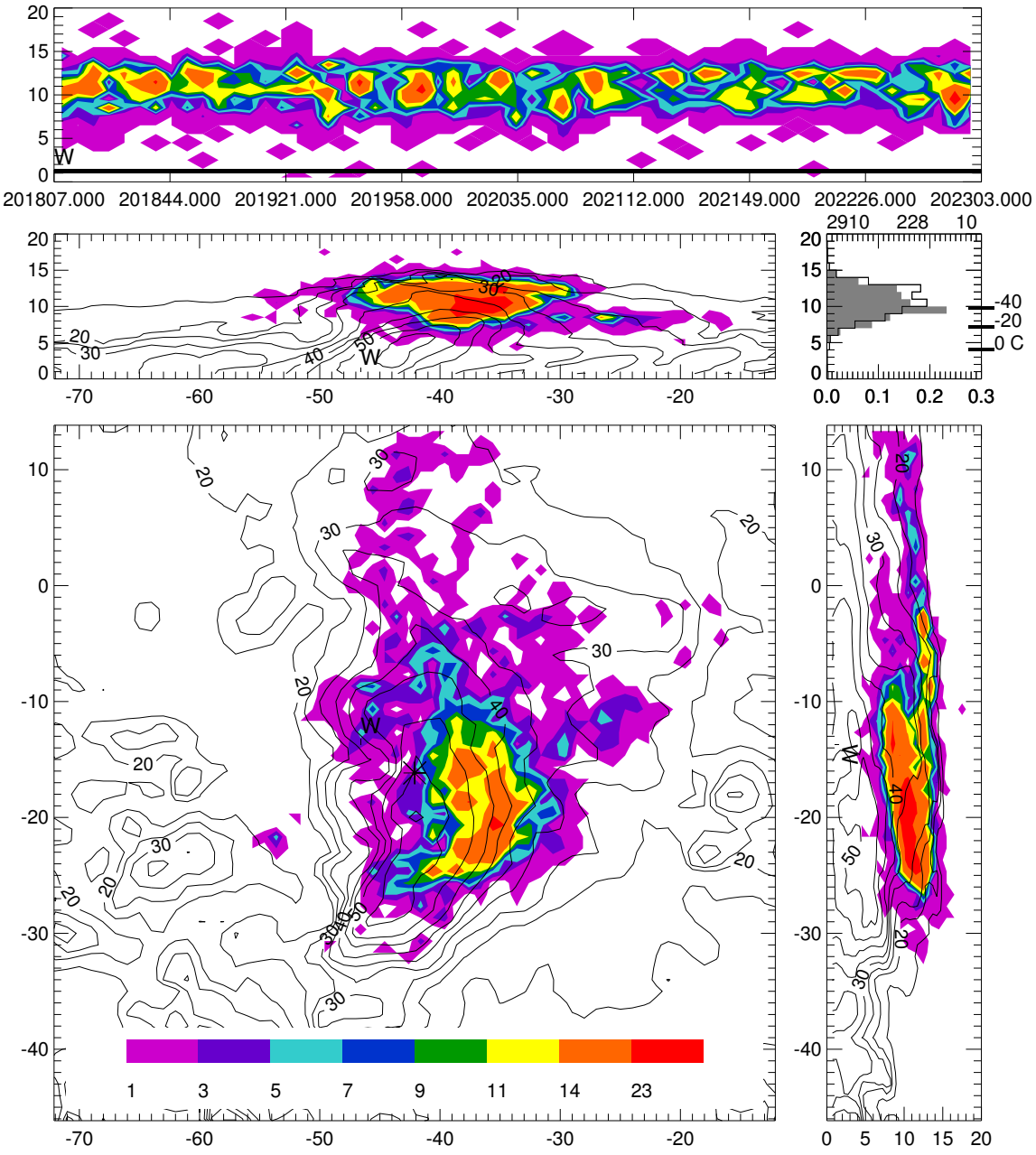

Figure 36. Same as figure 4, except for 201807 to 202303 UTC 27 May 2002. The "W" in each panel represents the time and location of a severe wind report associated with this cell. The cell location (asterisk) is (-42, -16 km).

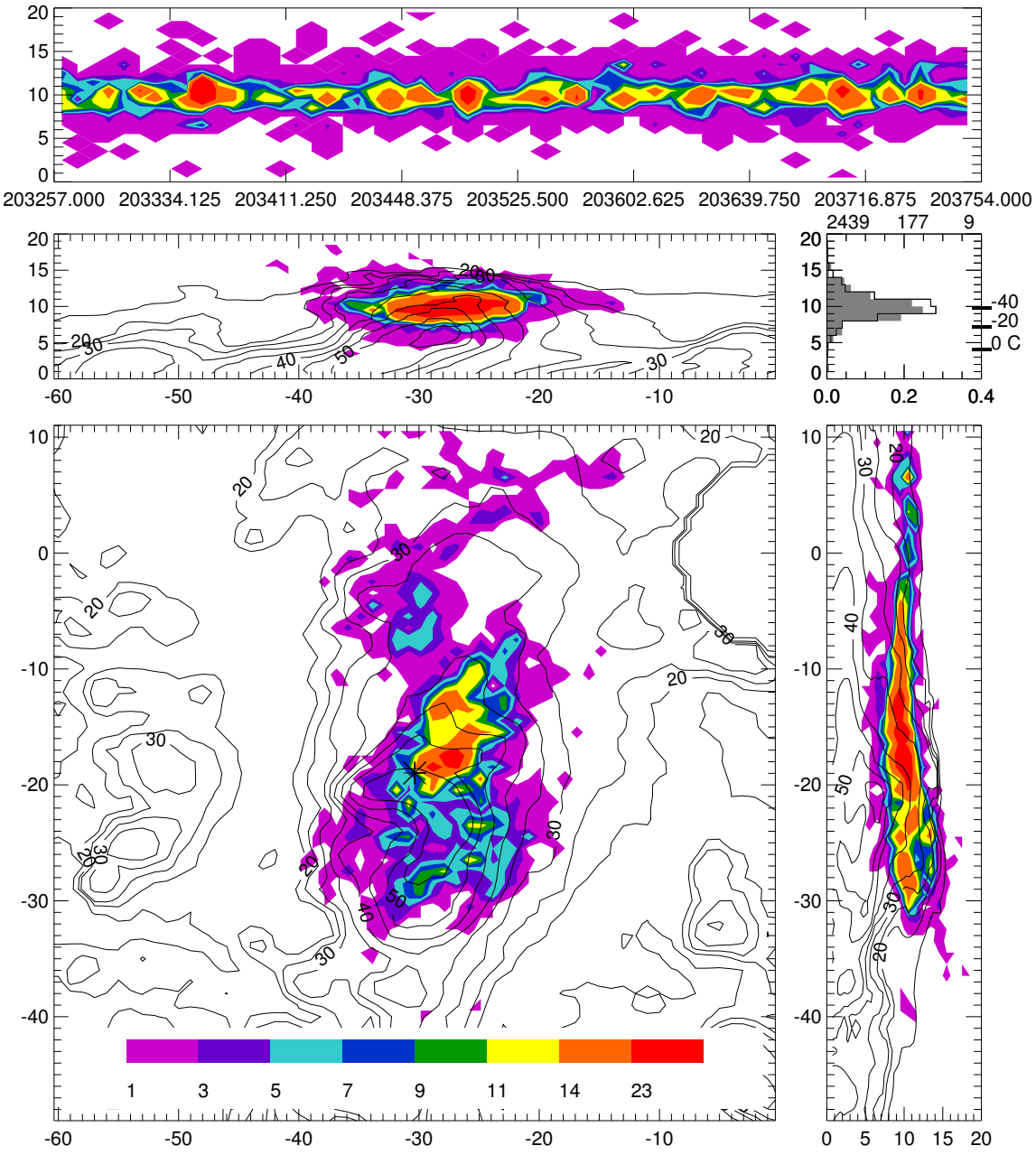

Figure 37. Same as figure 4, except for 203257 to 203754 UTC 27 May 2002. The cell location (asterisk) is (-30, -19 km).

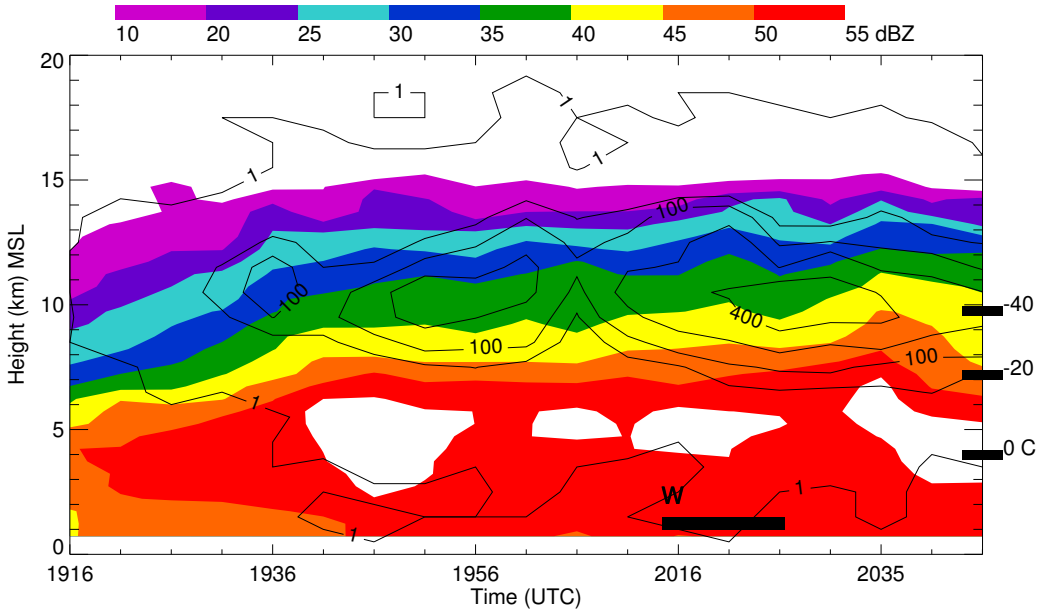

Figure 38. Same as figure 34, except for 191347 to 204748 UTC 27 May 2002.

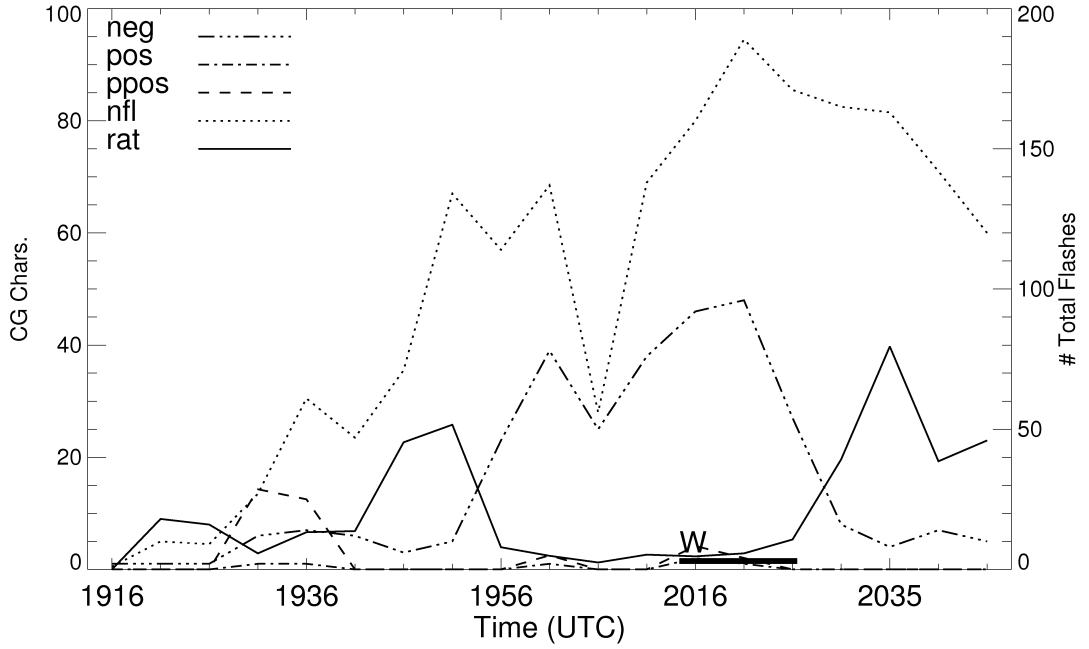

Figure 39. Same as figure 20, except for an MCS storm cell from 191347 to 204748 UTC 27 May 2002. The duration of a severe wind (W) report associated with this storm is also plotted.

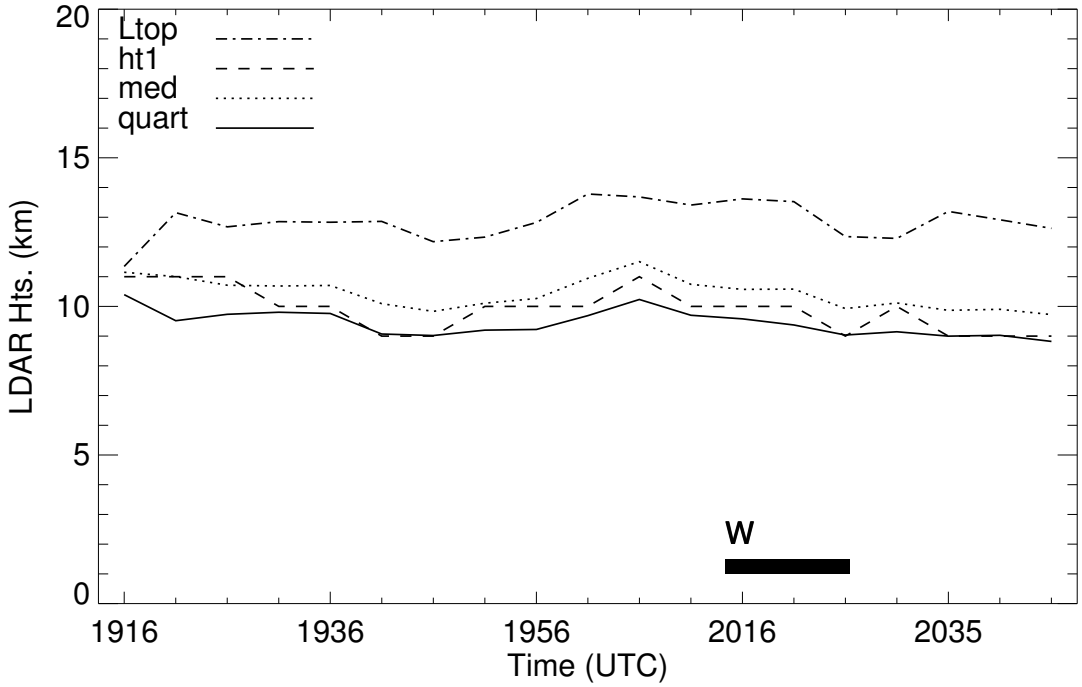

Figure 40. Same as figure 16, except for a 27 May 2002 MCS storm cell. The duration of a severe wind (W) report associated with this storm is also plotted along the x-axis.

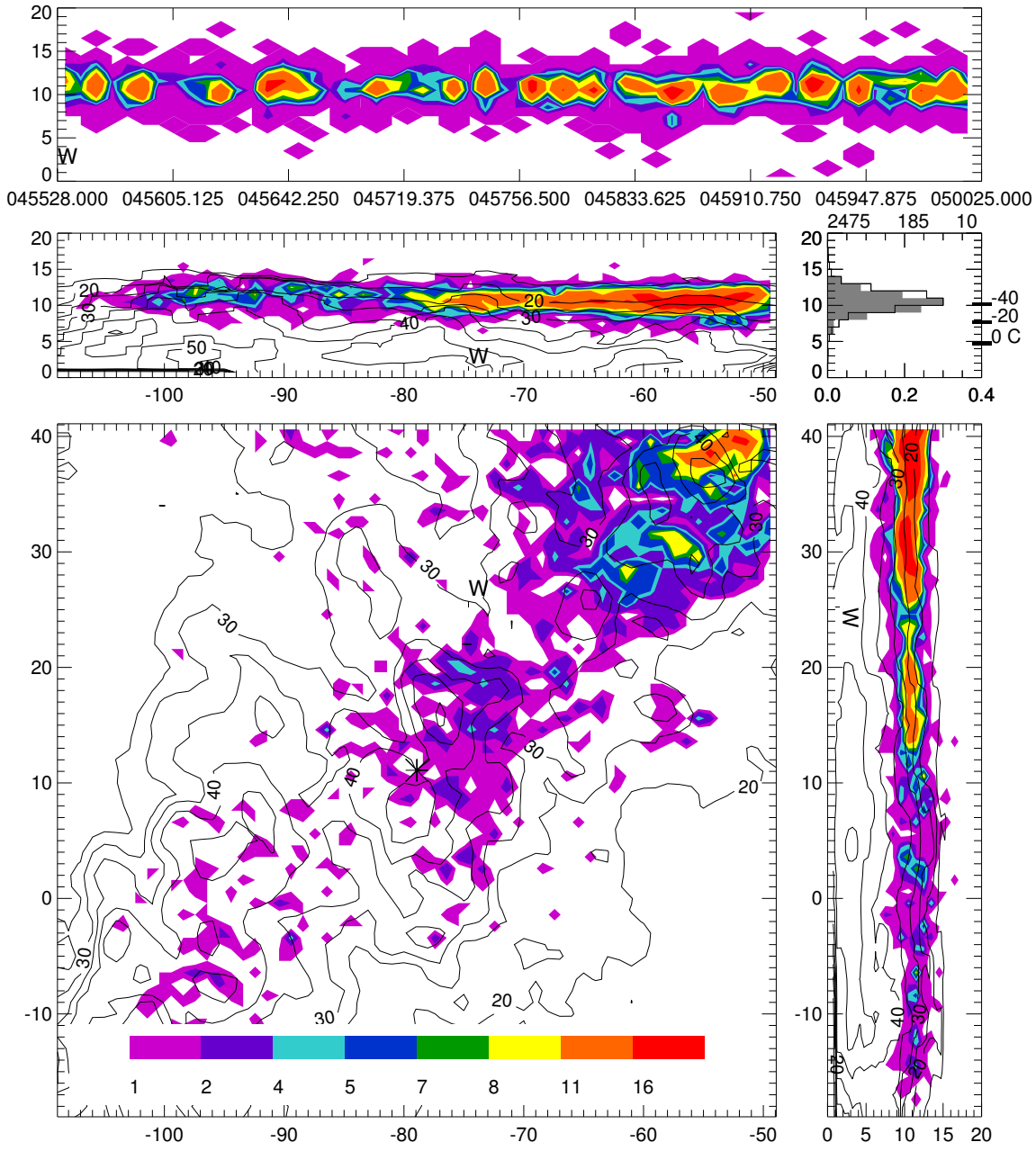

Figure 41. Same as figure 4, except for 045528 to 050025 UTC 16 June 2002. The time and location of a severe wind report is also shown (W). The cell location (asterisk) is (-79, 11 km).

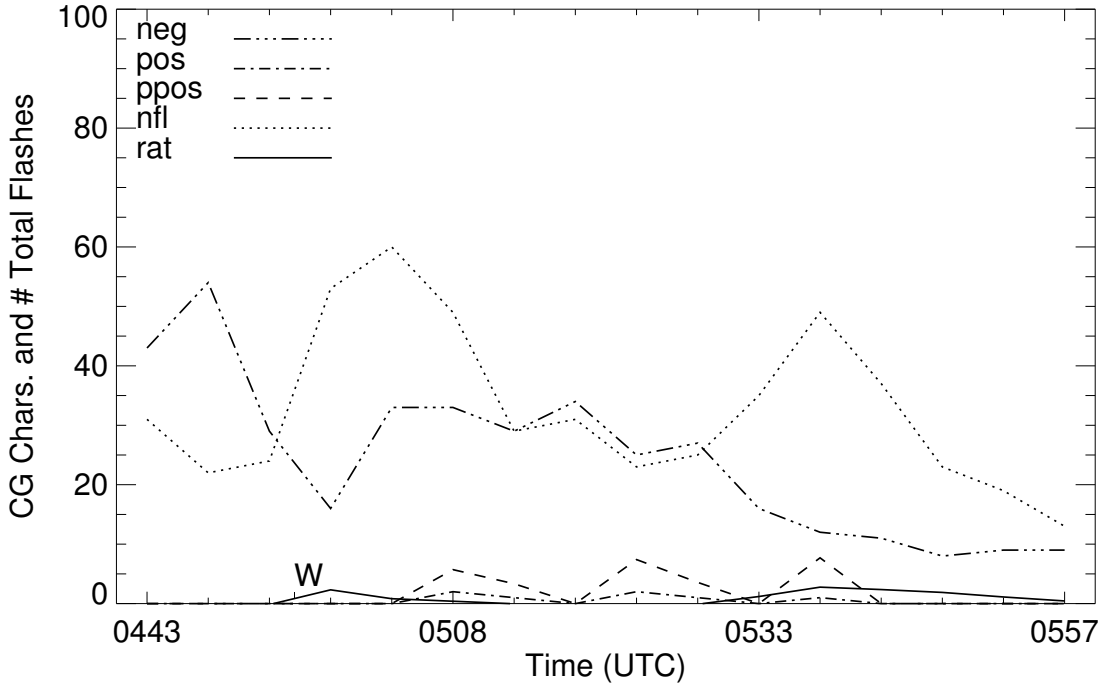

Figure 42. Same as figure 20, except for a different storm cell on 16 June 2002.

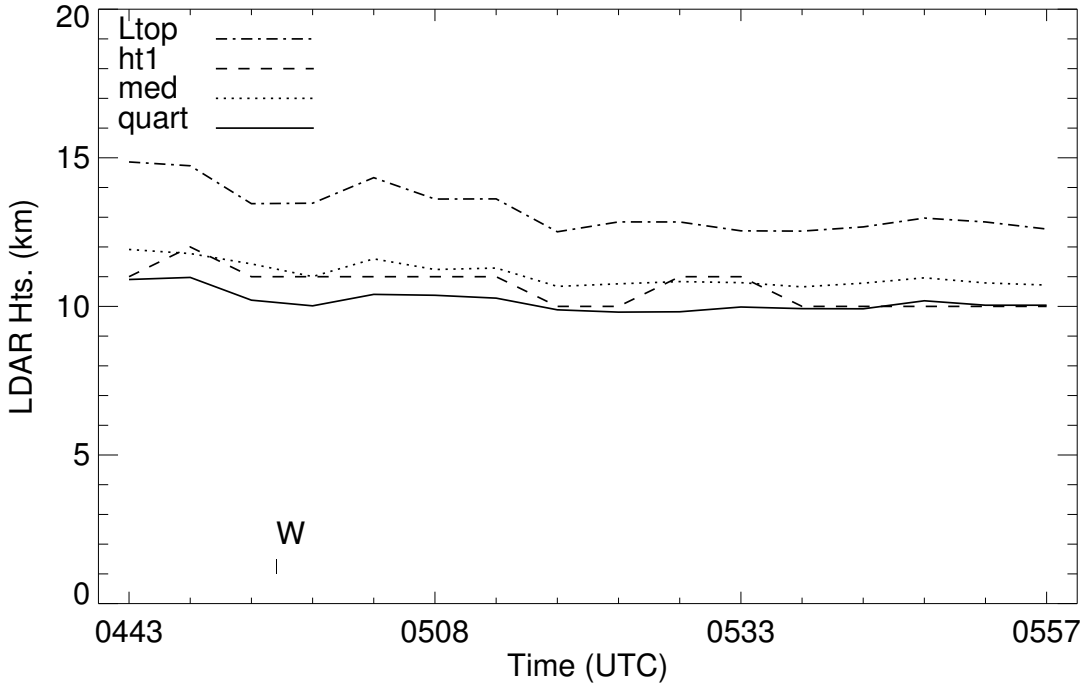

Figure 43. Same as figure 16, except for the 16 June 2002 MCS storm cell.

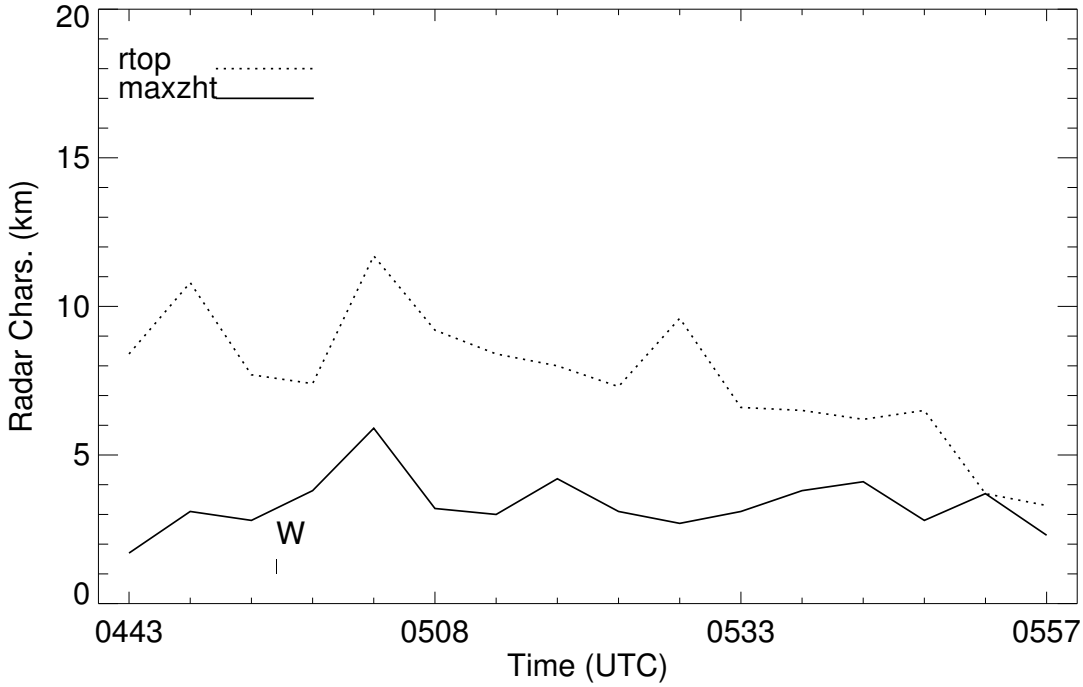

Figure 44. Time history of radar-derived diagnostics for the 16 June 2002 MCS storm cell: radar top (rtop) and maximum reflectivity height (maxzht). The occurrence of a severe wind report (W) is also shown. The duration of time between each tick mark is approximately 5 minutes.

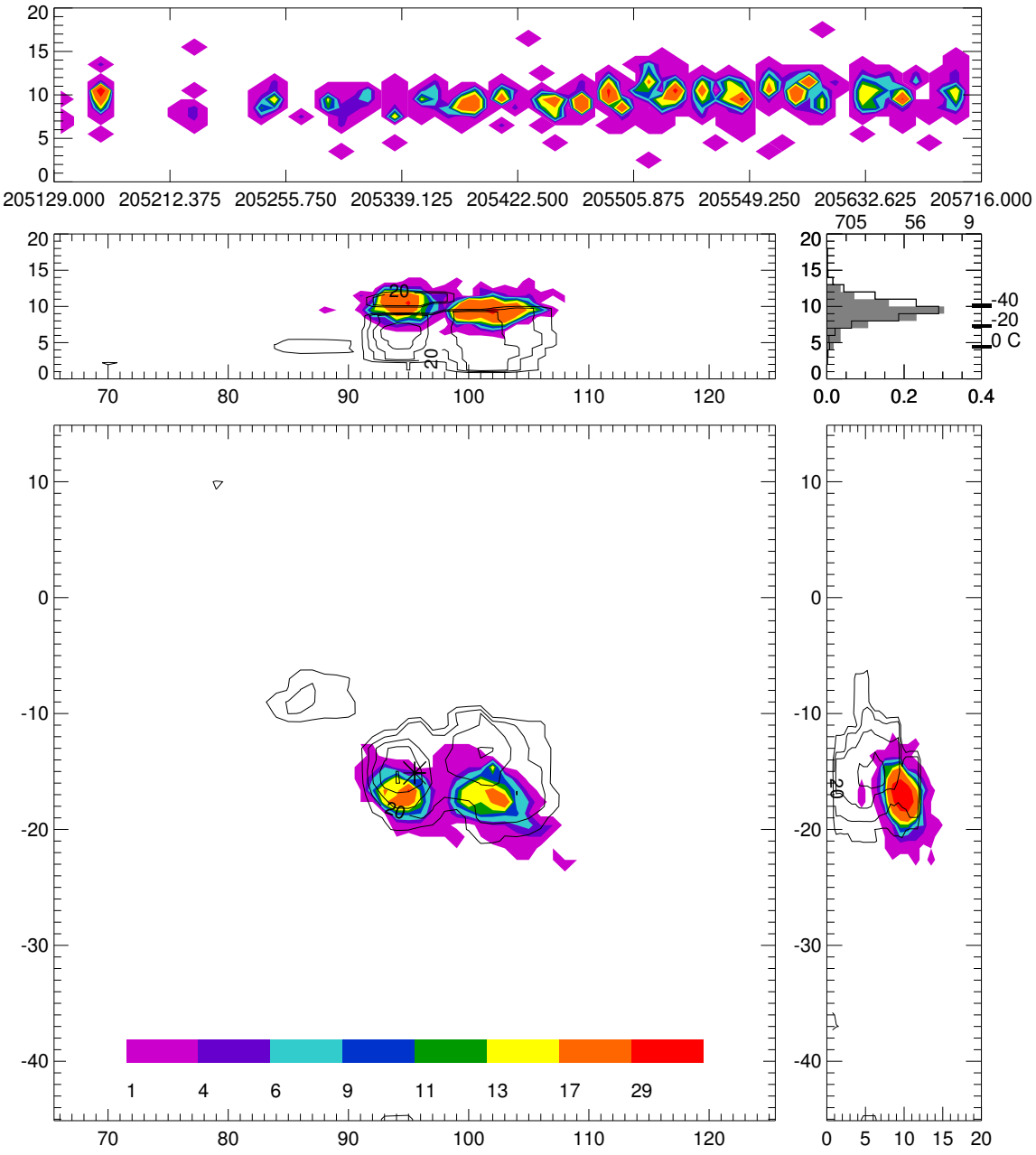

Figure 45. Same as figure 4, except for 205129 to 205716 UTC 27 June 2001. The cell location (asterisk) is (95, -16 km).

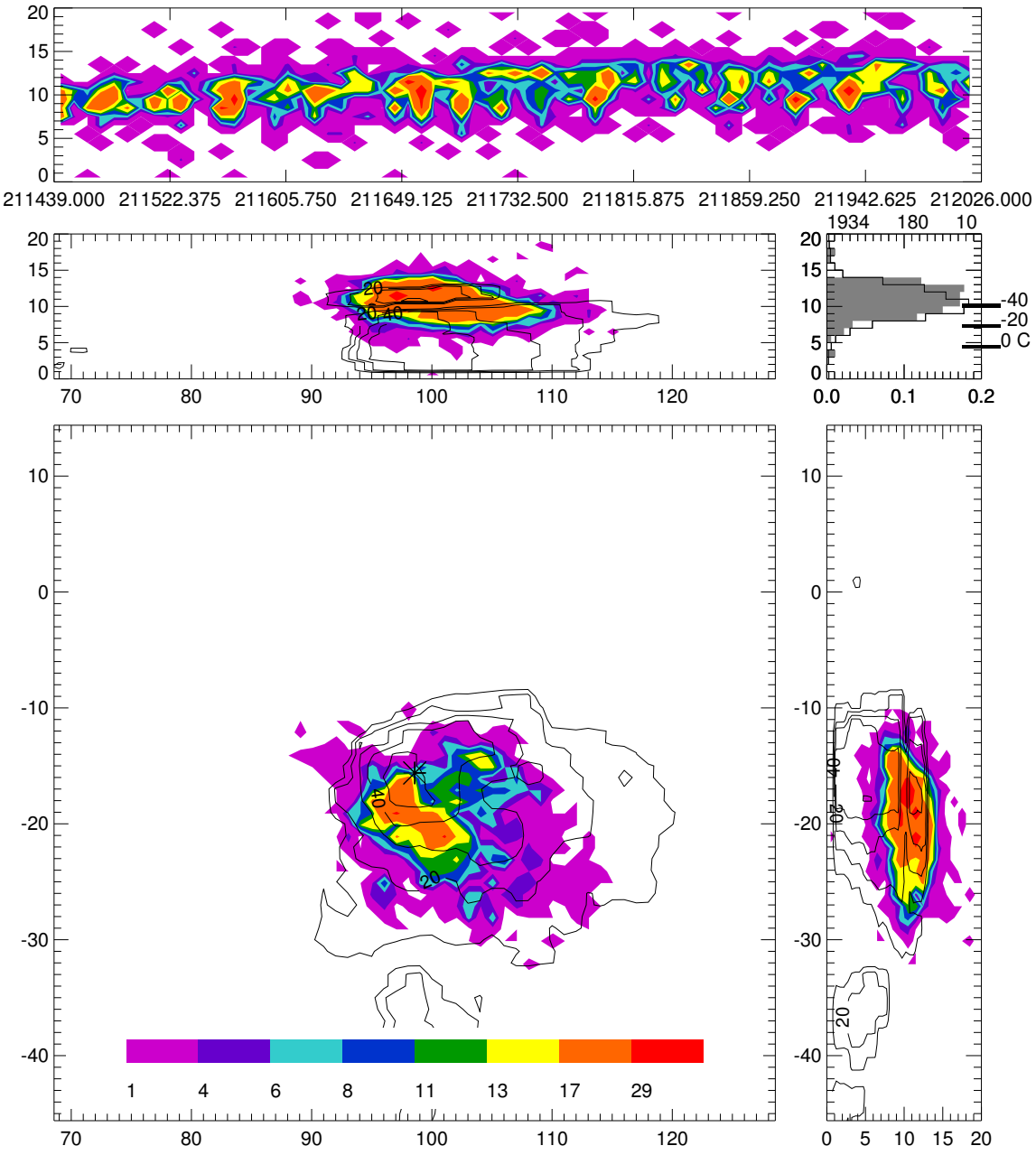

Figure 46. Same as figure 4, except for 211439 to 212026 UTC 27 June 2001. The cell location (asterisk) is (99, -15 km).

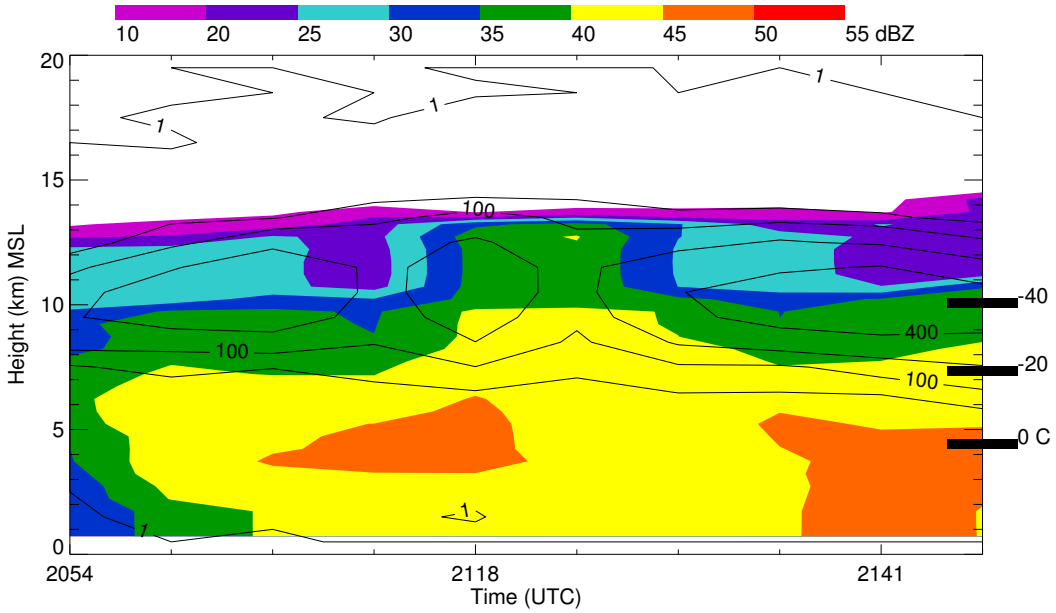

Figure 47. Same as figure 34, except for 205129 to 214924 UTC 27 June 2001. The duration of time between each tick mark is approximately 6 minutes for this case.

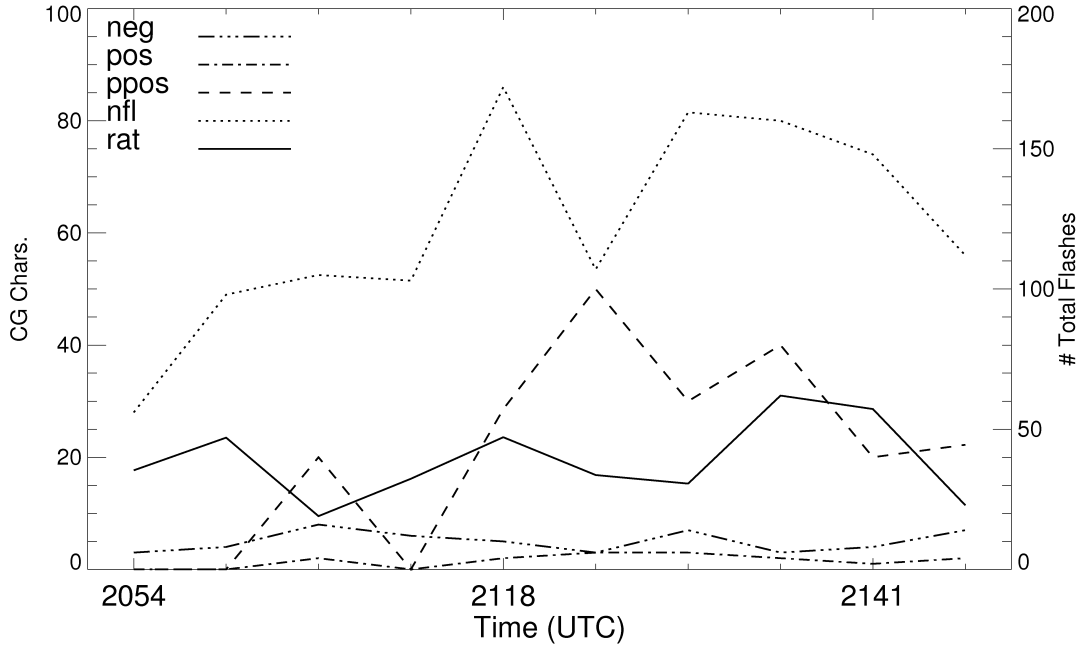

Figure 48. Same as figure 20, except for a different storm cell on 27 June 2001. The time duration between each tick mark is approximately 6 minutes.

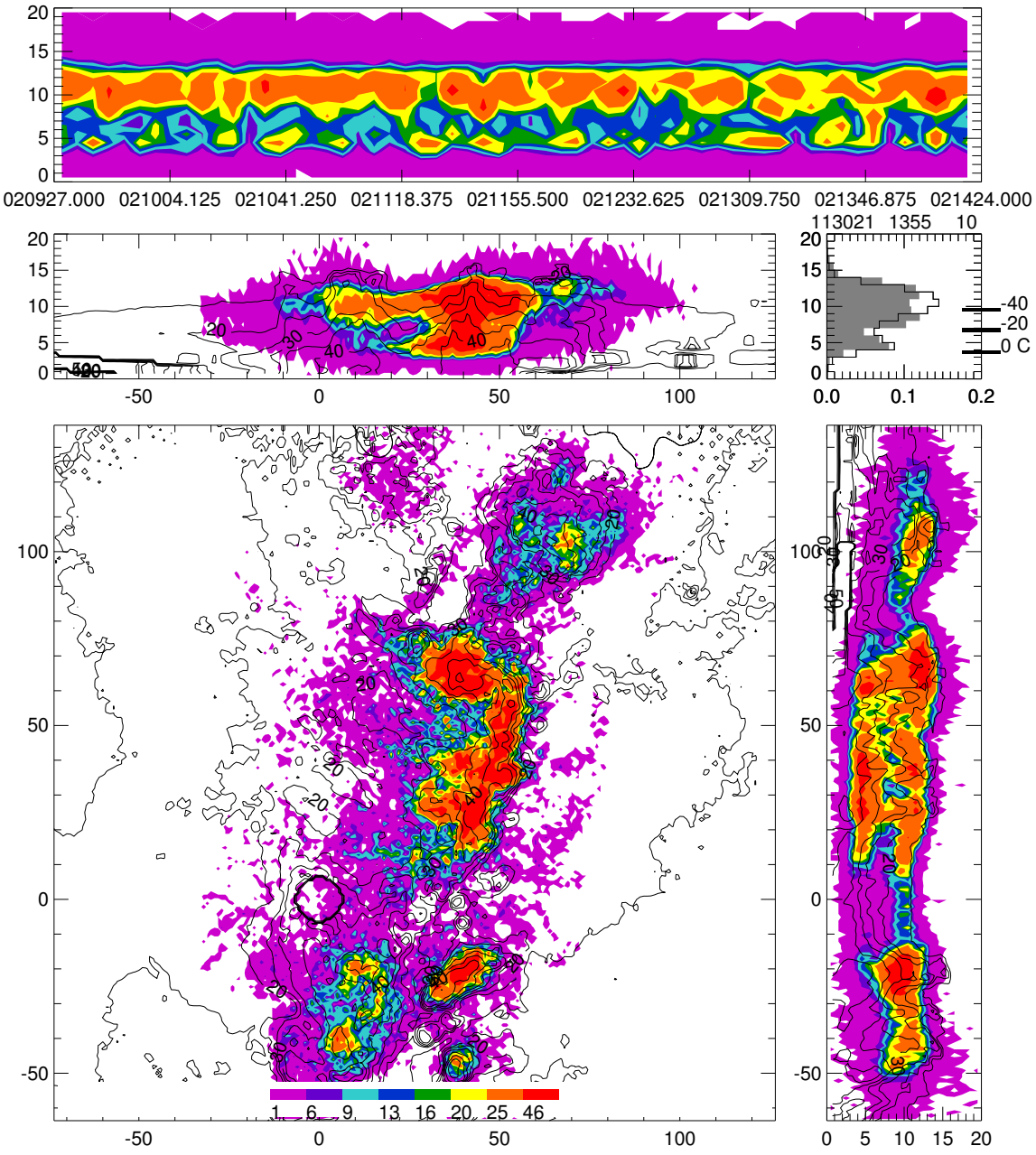

Figure 49. Same as figure 4, except for a total MCS from 020927 to 021424 UTC 13 October 2001. This plot is approximately centered on the LDAR II network located at (25, 35 km).

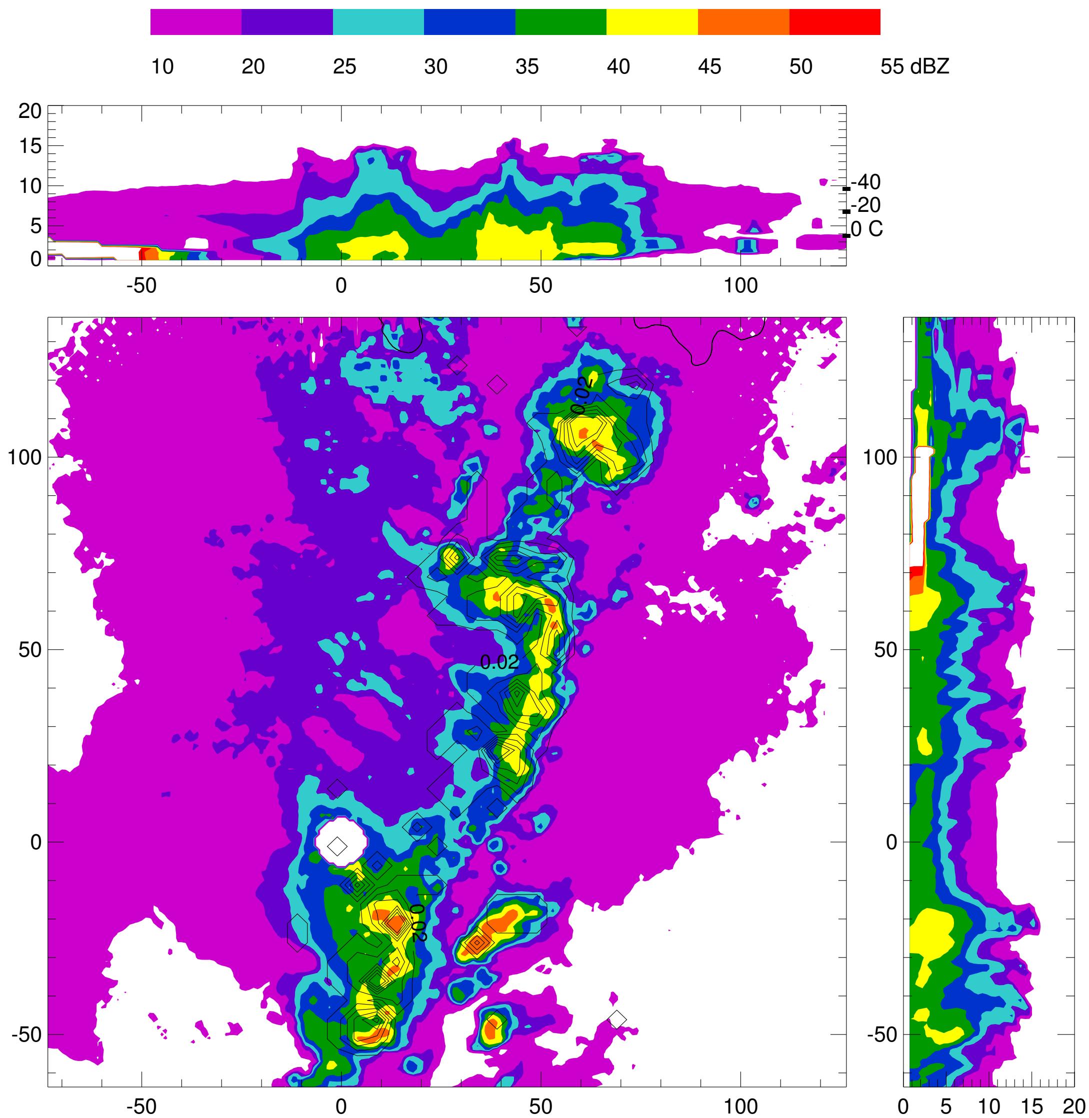

Figure 50. Same as figure 13, except for a total MCS between 020927 and 021424 UTC 13 October 2001. The area of no reflectivity near (0, 0) represents the radar volume scan's cone of silence, while the area of no reflectivity in the south-north vertical projection below 3 km MSL between y = 70 and 100 km is a measurement error (notice the lack of continuity in the contour intervals on the north end). The contour interval is 0.04 flashes km^{-2}, starting with 0.02 flashes km^{-2}.

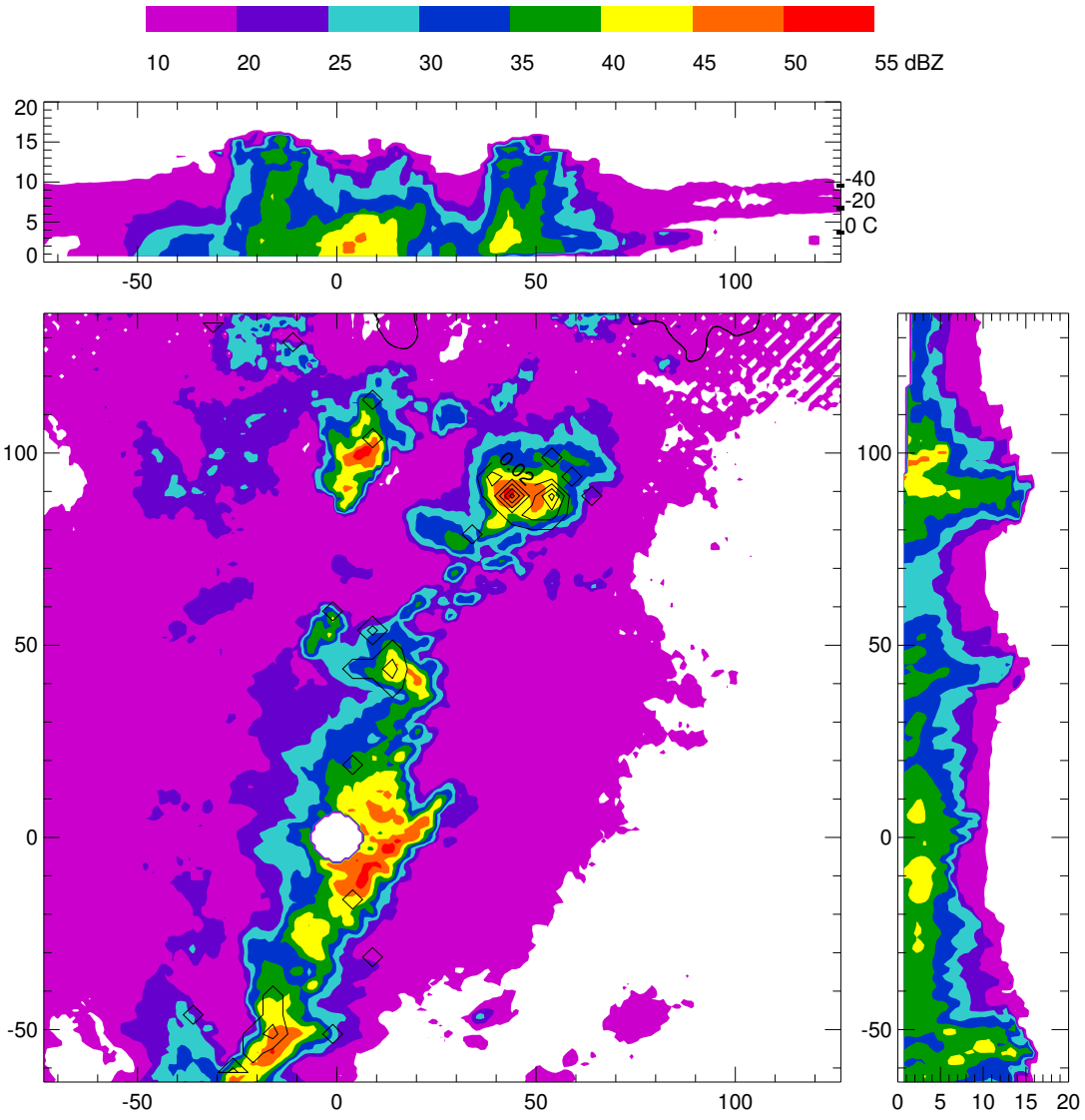

Figure 51. Same as figure 50, except +CG flash density is overlaid on the mean reflectivity in the plan view and this system occurred from 013946 to 014443 UTC 13 October 2001.

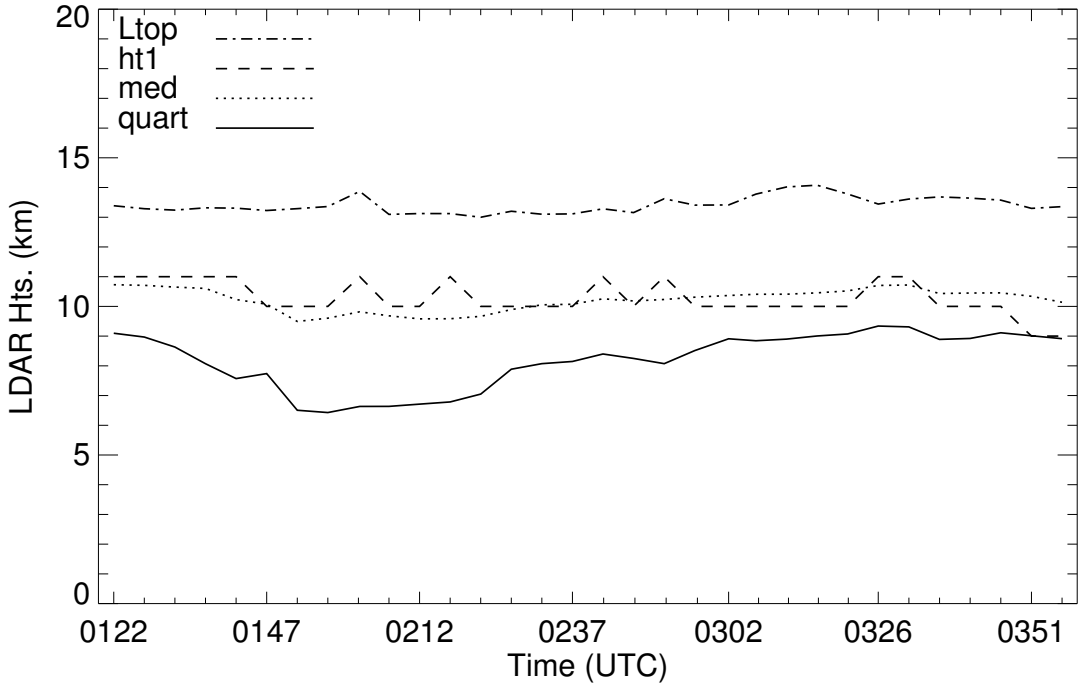

Figure 52. Same as figure 16, except for the entire MCS which occurred on 13 October 2001. These characteristics were calculated using sources within a 200 by 200 km box centered on the LDAR II network for each volume scan.

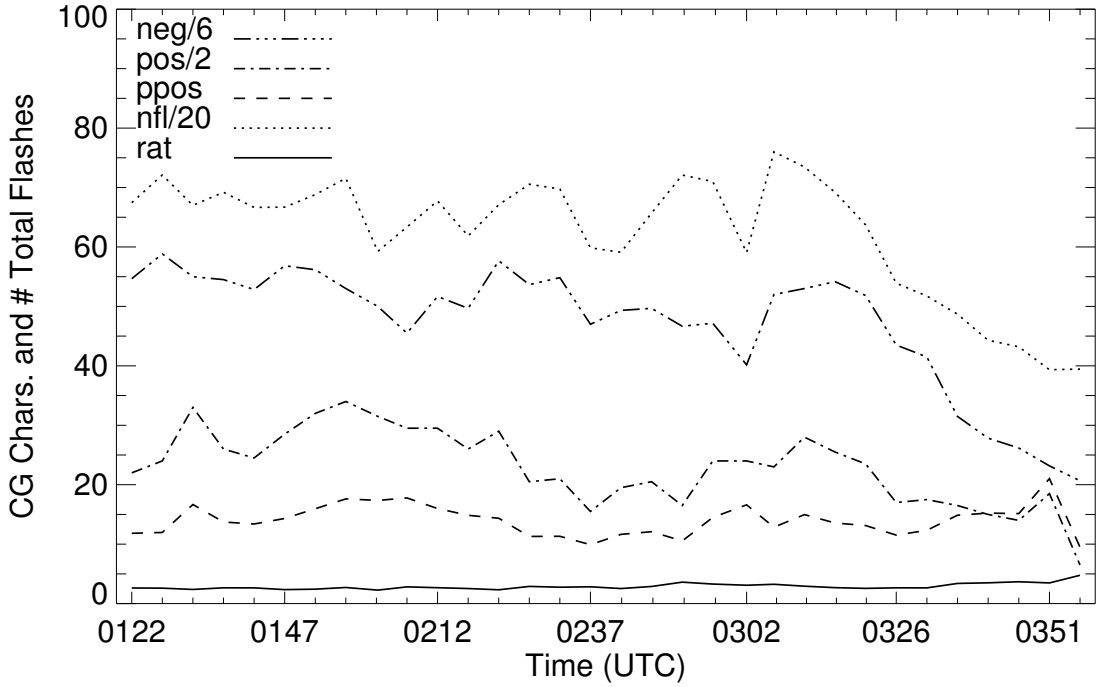

Figure 53. Same as figure 20, except for the entire MCS on 13 October 2001.

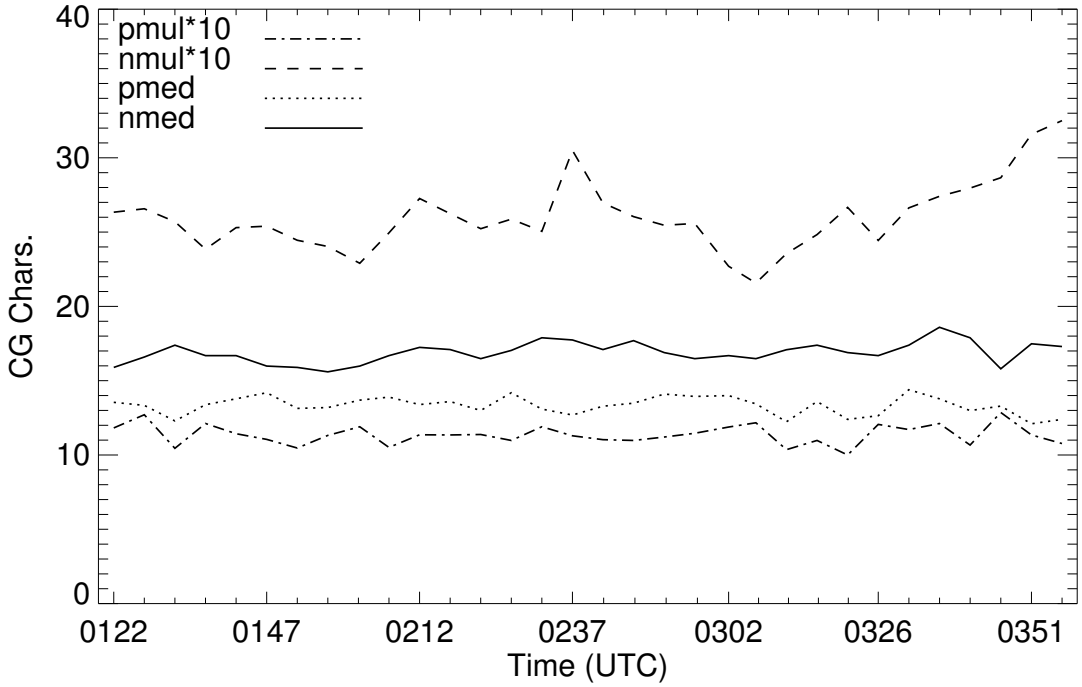

Figure 54. Cloud-to-ground (CG) lightning characteristics for the entire MCS on 13 October 2001: +/-CG mean multiplicity (pmul/nmul) and +/-CG median peak current in kA (pmed/nmed).

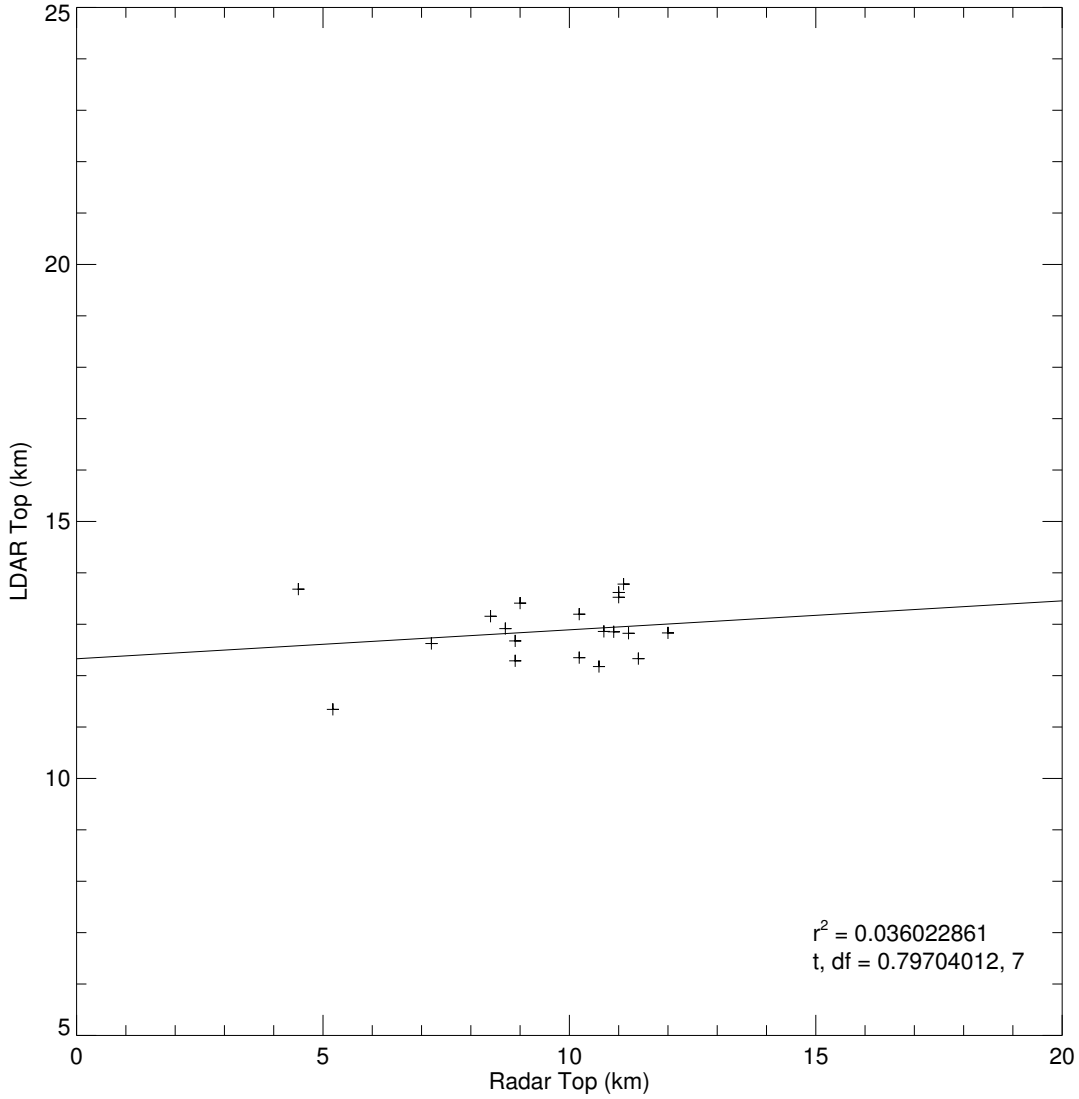

Figure 55. Scatter plot for the 27 May 2002 storm between the LDAR top (95th percentile source height) and radar top (maximum height of the storm's 30 dBZ contour). The best fit line is shown, along with the r-squared value (r is the correlation coefficient), student t-statistic (t), and number of degrees of freedom (df) used to determine statistical significance of the correlation. Each point represents a volume scan measurement.

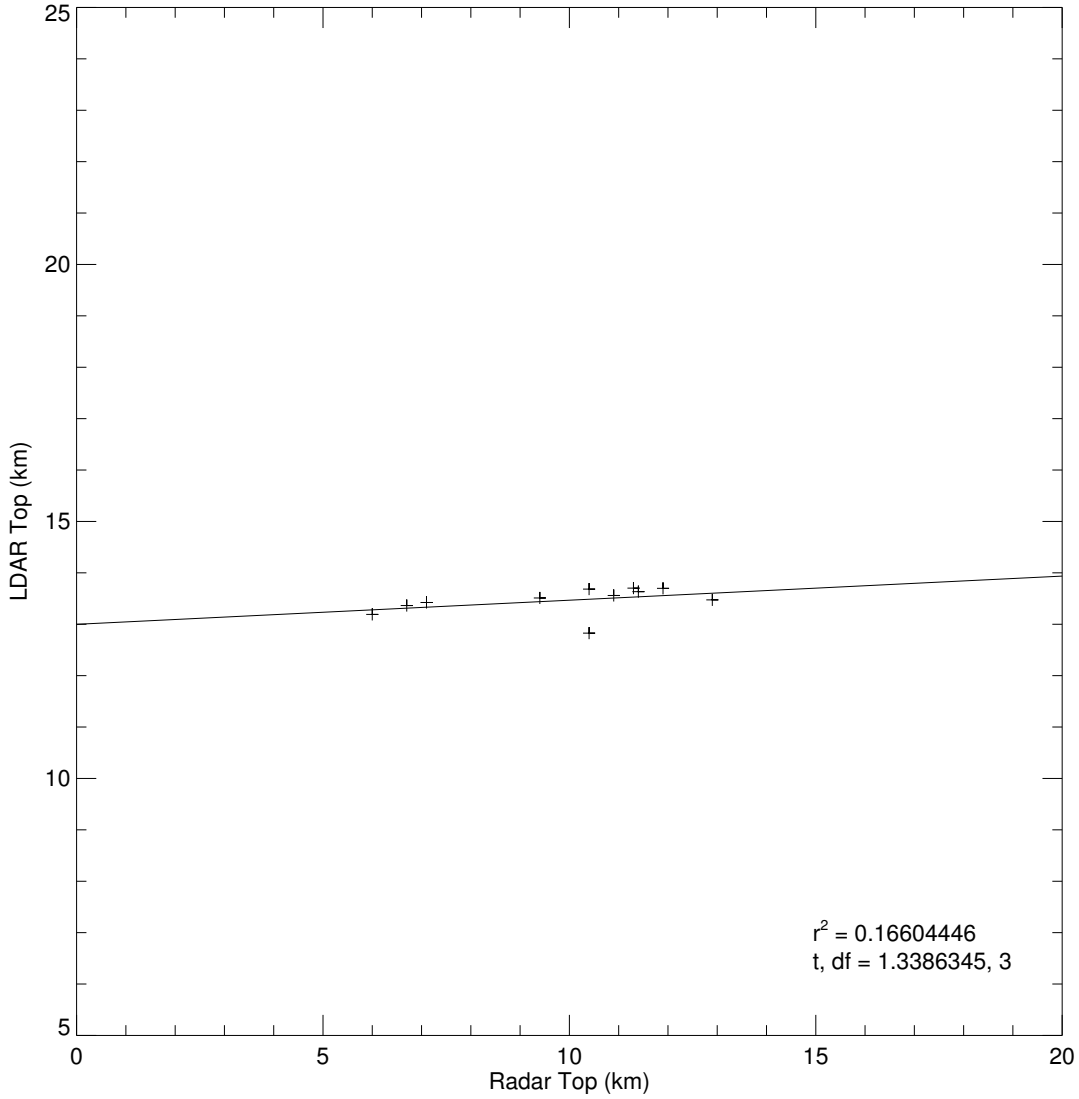

Figure 56. Same as figure 55, but for a 13 October 2001 storm cell.

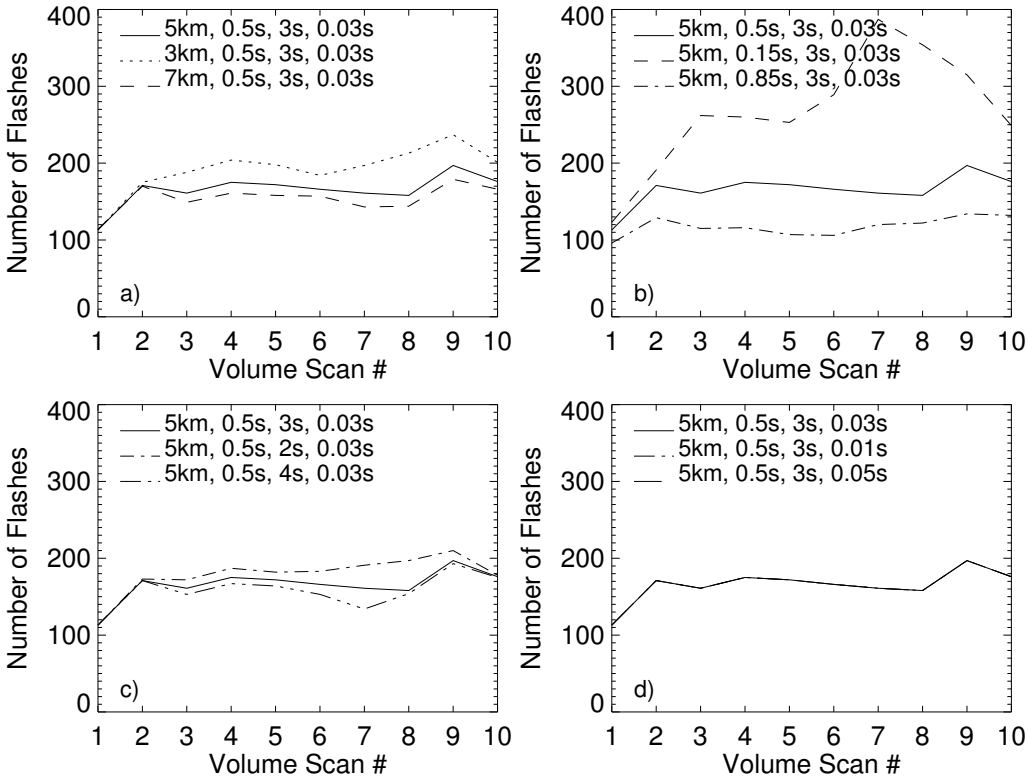

Figure 57. Comparison of flash rates (calculated with sources within 10 km of the mesocyclone) using different constraints within the flash grouping algorithm for the first 10 volume scans of a tornadic supercell which occurred on 13 October 2001. Panel a) shows results when varying the spatial constraint (3, 5, 7 km), b) varies the maximum time interval between sources in a flash (0.15, 0.5, 0.85 s), c) varies the maximum duration of a flash (2, 3, 4 s), and d) varies the time delay between sources in a flash branch (0.01, 0.03, 0.05 s). The baseline algorithm used in this study was the 5 km, 0.5 s, 3 s, 0.03 s algorithm.

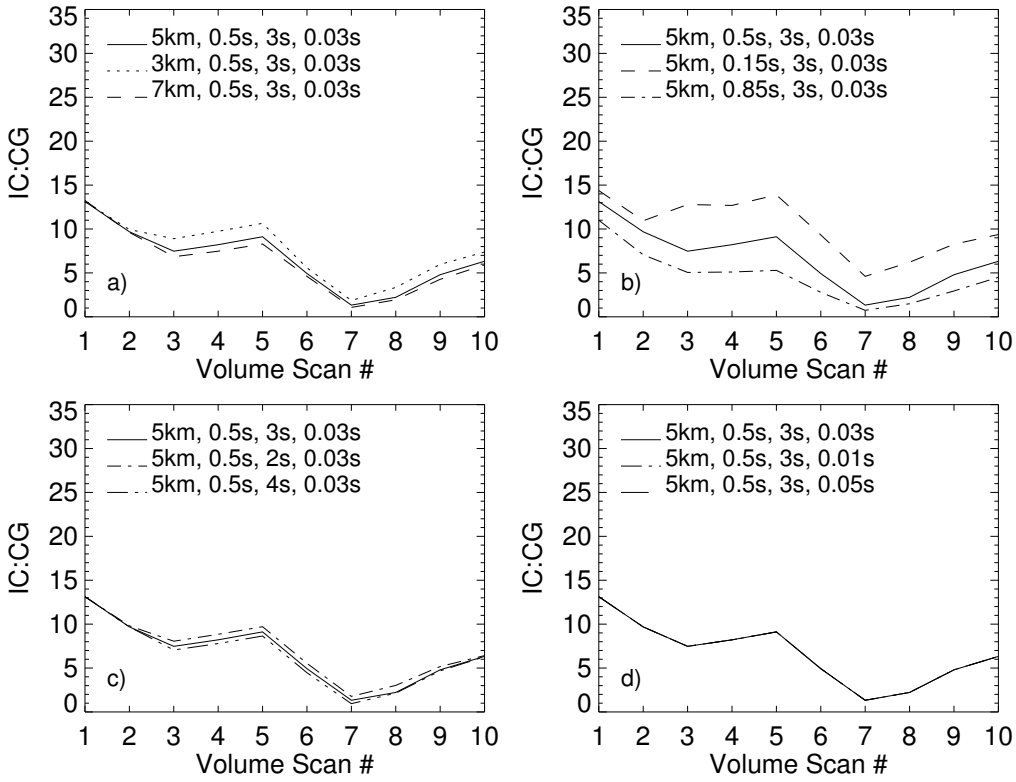

Figure 58. Same as figure 57, but comparing IC:CG ratios.

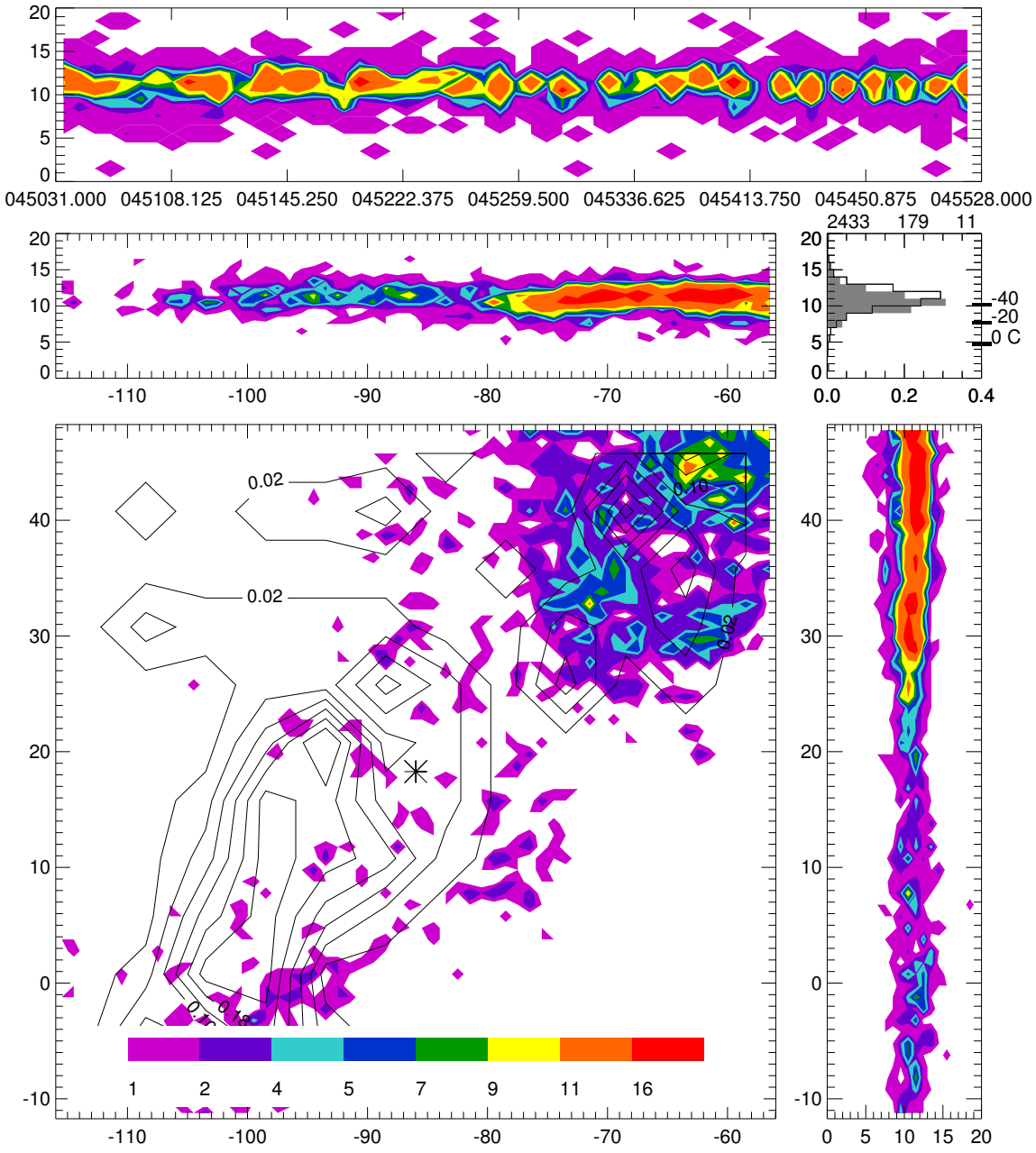

Figure 59. Same as figure 10, except for 045031 to 045528 UTC 16 June 2002 and the asterisk is the location of a radar-detected cell (WDSS-II) the plot is centered on. The –CG flash density has large magnitudes in a southwest-northeast pattern, but the source densities decrease substantially to the southwest due to significantly lower source detection efficiency there.

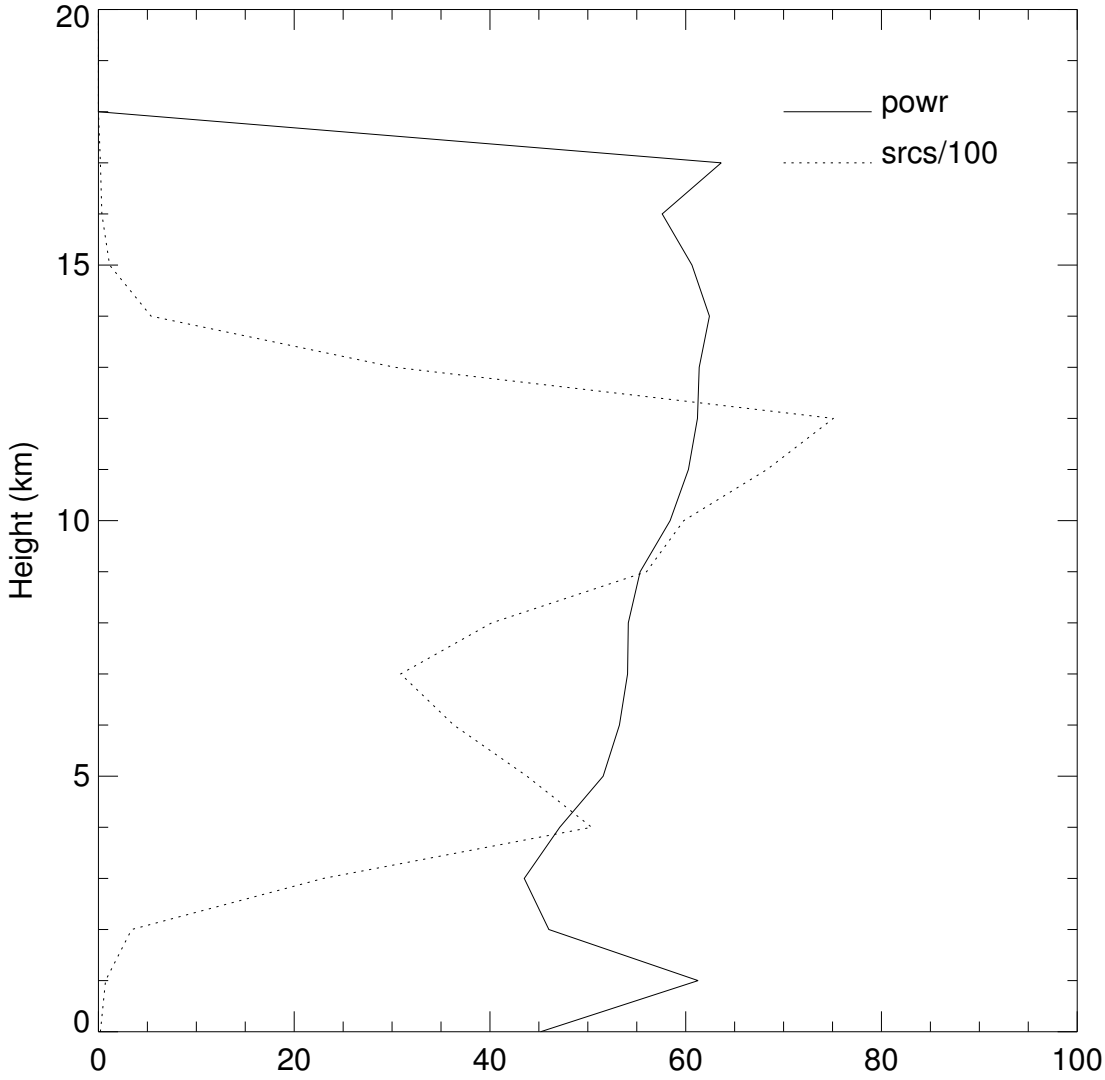

Figure 60. The vertical distribution of the number of sources (srcs) and mean source power (powr, dBm) for the storms shown in figure 35. The vertical resolution is 1 km.

VITA

Scott Michael Steiger was born in Rochester, New York. He graduated from Hilton Central High School (Hilton, NY) in 1995, obtained his Bachelor of Science degree in Meteorology from the State University of New York (SUNY) at Oswego in 1999, and his Master of Science degree in Atmospheric Sciences from Texas A&M University in 2001.

He is an active member of the American Meteorological Society (AMS) and American Geophysical Union (AGU). He was the recipient of the Association of Former Students Distinguished Graduate Student Research Award (2002) and Jeff Montgomery Prize for Leadership (2003) while attending Texas A&M University.

Scott is currently a Visiting Assistant Professor at SUNY Oswego (appointed in August 2003). Since he thoroughly enjoys teaching, Scott plans on continuing being a professor. His professional interests are in electrification of storms, lake-effect snow storms, and many other mesoscale and synoptic weather topics. His dreams of leading a storm chasing class will hopefully be fulfilled in the near future as this is truly the best way to teach and learn about the weather! When his head is not in the clouds, Scott enjoys boating, hiking, and being with his family and friends.

The address Scott may be reached at is:

14 Rolling Meadow Dr.

Hilton, NY 14468

steiger@oswego.edu